Reviews in Mineralogy & Geochemistry
Vol. 61, pp. 7-125, 2006

Crystal Structures of Sulfides and Other Chalcogenides

Emil Makovicky

Geological Institute
University of Copenhagen
Øster Voldgade 10, DK1350 Copenhagen, Denmark
e-mail: emilm@geol.ku.dk

INTRODUCTION

In this chapter, the crystal structures of sulfides and related chalcogenide compounds (involving Se, Te, As and Sb as well as S) are reviewed with emphasis on mineral phases but with some discussion of related synthetic compounds. Before presenting a systematic account of the principal families, relevant crystal chemical concepts are discussed, and structural classification schemes for these phases are reviewed.

Crystal chemical concepts

Chalcogenide ions. Chalcogens differ from oxygen by their moderate electronegativity. The Pauling electronegativity of oxygen is 3.44, whereas that of S is 2.58, Se 2.55, and Te 2.1 (Emsley 1994). The Shannon crystal radius of O^{2-} is 1.40 Å, that of S^{2-} 1.70 Å, Se^{2-} 1.84 Å, and Te^{2-} 2.07 Å (Shannon 1981). We have estimated the radius of As^{3-} as about 1.78 Å, and that of Sb^{3-} as 1.89 Å, based on the structures of selected sulfide-pnictides. The difference in polarizability of chalcogens and oxygen is of great structural importance. The electric polarizability (i.e., the value expressing the displacement of the electron cloud relative to the nucleus) is 3.88×10^{-24} cm^3 for O^{2-}, but it is 10.2×10^{-24} cm^3 for S^{2-}, 10.5×10^{-24} cm^3 for Se^{2-}, and 14.0×10^{-24} cm^3 for Te^{2-} (Pauling 1927). The polarizability values can also be interpreted as expressing covalency trends of anion-cation bonds and anion-anion interactions in the structure.

The difference between oxygen and chalcogens leads to differences in crystal chemistry of oxides and chalcogenides for nearly all element combinations, exceptions being very few. Structural features of certain chalcogenide categories are in common with hydroxides, which have low-charge and polarizable OH^- groups; this is true especially for layer-like structures. There are greater similarities between the above values for S and Se, and a more pronounced difference for Te. However, already the differences between the behaviour of S and Se, and presumably also the possibilities which the larger radius of Se offers for certain cation-cation distances in selenides, lead to important differences between phase diagrams of sulfides and selenides.

With the notable exception of chalcogenides of typical non-metals, a fundamental crystal-chemical division of chalcogenide structures can be based on the difference in electronegativity and bonding schemes between "cations" and "anions," and on Pearson's valence rule,

$$\Sigma/N = 8, \quad \text{where } \Sigma = n_e - b_a - b_c$$

In this expression, n_e is the total number of valence electrons, b_a the number of electrons involved in anion-anion bonds, and b_c number of electrons involved in cation-cation bonds plus those left unshared on cations (i.e., constituting lone electron pairs). In polyanionic

1529-6466/06/0061-0002$15.00 DOI: 10.2138/rmg.2006.61.2

compounds, $n_e/N < 8$, in normal-valence compounds, $n_e/N = 8$, and in polycationic compounds, $n_e/N > 8$. As, Sb, and Bi may play either the role of an anion or that of a cation; details are in the section on structures with dichalcogenide groups X_2. Cation-cation interactions may affect the M:X ratio as, e.g., in pentlandite (M_9S_8), but a range of weaker, although obvious cation-cation interactions occur, especially in the chalcogenides of Cu and Ag, which do not alter their stoichiometry. Typically, the interaction distances in these compounds exceed those in a metal; see discussion by Chevrel (1992).

Packing of anions. Another fundamental crystal-chemical principle relevant to the chalcogenides is that of "close packing of anions" (eutaxy). This is an arrangement in which the shortest distances between pairs of anions are as large as possible (O'Keeffe and Hyde 1996). The result, however, is the densest packing of atoms, corresponding to that seen in metals. To the cubic close packing (*ccp*) and the hexagonal close packing (*hcp*) of anions, and their numerous combinations (O'Keeffe and Hyde 1996), is added a body-centered close packing, which has a lesser space-filling efficiency. It is generated, for example, by the steric requirements of silver cations in Ag_2X, especially at elevated temperatures. The third most efficient mode of packing, the icosahedral configuration, cannot propagate as a 3D periodic structure and can occur only as a cluster in other, especially cubic, structures.

It is not necessary that an entire structure exhibits a continuous pattern of close packing. In a large number of sulfosalts, and in some sulfides, layers, rods or even blocks of a close-packed or a distorted close-packed arrangement occur, joined to the adjacent such layers, rods or blocks, by interfaces on which certain cuts through the close-packed arrangement of anions face quite differently oriented cuts through (mostly) the same arrangement. For example, the pseudotetragonal (100) cuts through a PbS archetype (see below) often face (111) cuts through the same archetype. The keys to this arrangement are suitable cations, or lone electron pair cations, capable of spanning and populating this interface.

Cation coordination. The preferred coordination of a cation in a chalcogenide structure depends on its size, charge and electron configuration. The cations with a "noble gas" (sp^3) configuration have coordinations according to their radius. The appropriate "crystal radii" for sulfides were derived by Shannon (1981) and appear to serve well in most instances. A necessary addition to his table is the tetrahedral radius of Cu^{2+}, equal to ~0.51 Å (Makovicky and Karup-Møller 1994), as opposed to the 0.635 Å given for Cu^+ in sulfides by Shannon (1981). Cations with d^{10} configurations prefer tetrahedral coordinations; the same is true for transition metals with maximum valencies. For spin-paired d^8 configurations, such as in Pd^{2+} and Pt^{2+}, square-planar coordinations occur, whereas for such configurations of Ni^{2+}, a square-pyramidal coordination is typical (Jellinek 1968).

The same picture is obtained using the hybridization concept (e.g., Belov et al. 1982). Tetrahedral coordination is explained by the use of sp^3 hybrid orbitals, octahedral by the use of d^2sp^3 orbitals, square planar is based on dsp^2 orbitals, triangular is based on the sp^2 hybridization (e.g., Cu^+), and the linear coordination of Cu^+ and Ag^+ results from an *sp* hybrid. These concepts are summarized in Table 1. Other crystal chemical concepts relevant to sulfides have been outlined by Prewitt and Rajamani (1974), Vaughan and Craig (1978), and Vaughan and Wright (1998) and are discussed elsewhere in this volume.

Jahn-Teller distortions due to the differential occupancy of individual *d* orbitals are unusual among sulfides because of electron delocalization (Jellinek 1968) but they do explain the configurations found in Cr^{2+}, Pd^{2+} and Pt^{2+} sulfides.

The coordination properties of the cations need to find their counterpart in the anion packing. The majority of the cations in natural chalcogenides have coordination requirements that fit with the filling of tetrahedral, octahedral or other interstices in the anion arrays. Thus, *ccp* and *hcp* offer coordination octahedra and regular tetrahedra, as well as a plethora of

Table 1. Coordination numbers and hybridization types for the cations commonly occurring in chalcogenides.

CN	Type of Hybridization	Category
2	sp; p^2	Cu^+, Cu^{2+}, Ag^+, Hg^{2+}
3	sp^2	Cu^+, Ag^+
3	p^3	As^+, Sb^{3+}, Bi^{3+}, Pb^{2+}
4	sp^3	Cu^+, Ag^+, Au^+; Zn^{2+}, Cd^{2+}, Hg^{2+}; Ga^{3+}, In^{3+}, Tl^{3+}; Ge^{4+}, Sn^{4+}; As^{5+}, Sb^{5+}; $Mn_H{}^{2+}$,$Fe_H{}^{2+}$
4 (sq)	dsp^2	$Fe_H{}^{3+}$, $Co_H{}^{3+}$, $Ni_H{}^{2+}$, $Ni_H{}^{3+}$, Pd^{2+}, Pt^{2+}, Cu^{2+}
5	dsp^3 p^3d^2	$Ni_L{}^{2+}$ Sb^{3+}, Bi^{3+}; Pb^{2+}
6	d^2sp^3 sp^3d^2 p^3; d^2sp^3	$Fe_L{}^{2+}$, $Fe_L{}^{3+}$, $Co_L{}^{3+}$, $Ni_L{}^{4+}$, $Pt_L{}^{4+}$ Sn^{4+} Pb^{2+}; Bi^{3+} (Sb^{3+})

triangular coordinations at different structure sites. They preclude quadratic coordinations, whereas linear coordinations, such as S-Cu-S require a distortion of the anion array. Some coordinations, such as the trigonal prismatic coordination of the early 4*d* or 5*d* elements (Mo, W, Nb, Ta) change anion stacking schemes; the van der Waals intervals of layered structures tend to preserve them. The lone electron pair elements, As^{3+}, Sb^{3+}, Bi^{3+}, Sn^{2+}, Ge^{2+}, and to a lesser extent Tl^+ and Pb^{2+}, require an excessive, usually asymmetrically situated structural space for their non-bonding s^2 pair. This volume is not comparable with that of the anion, which is the case in the oxides, with the relatively smaller O^{2-} (Andersson et al. 1973). The degree of stereochemical activity of the lone pair varies with the species (decreasing with increasing *Z*) and the structure type.

Structural classification

Structural classifications generally employ a combination of the above criteria: the large scale structural configuration (3D/2D/1D character of principal building units), anion packing, bonding characteristics/type of coordination polyhedra of cations, and cation-cation and anion-anion interactions. These factors are used indirectly in the classification of Strunz and Nickel (2001) in which chalcogenides are divided into categories with *M*:S > 1:1, *M*:S = 1:1 (and derivatives), *M*:S = 3:4 and 2:3, and *M*:S < 1:2. Sulfosalts are classified separately, mainly according to their archetypes. Ross (1957) follows similar principles. Kostov and Minčeva-Stefanova (1982) divide sulfide- and sulfosalt structures into axial, planar, pseudoisometric and isometric types, using the axial ratios of their lattices as an expression for the anisotropy of strongest bonds in the structure. The classification of Povarennykh (1972) is similar, although more "classical" in the choice of categories. Takéuchi (1970) and Parthé (1990) divide chalcogenides into polyanionic, polycationic and normal-valence compounds based on Pearson´s valence rule. Belov et al. (1982) discern normal-, cluster-, molecular-, and polyanionic chalcogenides, as well as distinct cation coordinations in the compound. Vaughan and Craig (1978), Robert and Makovicky (1984) and Vaughan and Wright (1998) define chalcogenide groups based on well-known structure types, each of them unifying a number of the above defined structural criteria, in which they include a number of iso-, homeo-, and poly-types as well as interstitial and omission derivatives, eventually even homologues and plesiotypes. An updated overview of the most important groups is given in Table 2.

Table 2. Selection of important sulfide structure families.

Type compound	Principal structural characteristics: Anion array; % of holes filled; stacking; specific properties	Selected isotypes, derivatives and related structures
Sphalerite β-ZnS	*ccp*,½ of tetrahedral holes filled, ABC sequence of corner-connected [ZnS_4] tetrahedra	CdS, HgTe, GaAs, CuAsS, $CuFeS_2$, $Cu_6As_4S_9$, $Cu_4Fe_5S_8$
Wurtzite α-ZnS	*hcp*, ½ of tetrahedral holes filled, ABAB sequence of corner-connected [ZnS_4] tetrahedra	CdS, ZnTe, SiC, Cu_3AsS_4, $ZnA1_2S_4$, $AgInS_2$, $CuFe_2S_3$
Galena PbS	*ccp*, octahedral holes filled, isotypic with NaC1	MgS, CaS, MnS, PbSe, ZrS, $AgSbS_2$, $PbAgAsS_3$
Niccolite NiAs	*hcp*, octahedral holes filled, anion has trigonal prismatic coord., cation omission derivatives	FeSe, FeSb, NiS, PtSn, FeS, $Fe_{1-x}S$: from $Fe_{11}S_{12}$ to Fe_7S_8, $Cr_{1-x}S$
Pyrite FeS_2	S_2 groups instead of anions in *ccp,* octahedral cation coordination	CoS_2, NiS_2, MnS_2,$PtAs_2$, CoAsS, PtAsS, Cu_3FeS_8
Marcasite FeS_2	dimorph of pyrite, S_2 groups and Fe octahedra, distorted *hcp*	$FeSe_2$, $FeAs_2$, $NiSb_2$, $RuSb_2$, FeAsS, CoAsS, CoSbS, OsAsS
Thiospinels $FeNi_2S_4$	*ccp*, 1/8 of tetr. + ½ of oct. holes filled ; sulphur analogues of normal and inverse spinels	Co_3S_4, Ni_3S_4, $FeIn_2S_4$, $CuCo_2S_4$, $ZnA1_2S_4$, $HgCr_2S_4$
Pentlandite $(Fe, Ni)_9S_8$	*ccp*, ½ of tetr. + 1/8 of oct. holes filled;8 edge-sharing tetrahedra with *M-M* bonds	Co_9S_8, Ag $(Fe,Ni)_8S_8$, $K_6Na(Fe, Cu, Ni)_{24}S_{26}C1$
Acanthite – Argentite Ag_2S	(distorted) *bcc* , Ag in oct. + ½ of tetr. holes; above 177 °C ionic conductor: Ag mobile	Ag_2Se, Ag_2Te, ionic conductors Ag_8GeS_6, Cu_2S, Cu_9S_5, Cu_5FeS_4
Mackinawite FeS	*tetragonal layers composed of edge-sharing [FeS_4] tetrahedra; 4 *M-M* bonds per cation	CuTe, T1$FeCu_3S_4$, T1Fe_2S_2, KCu_4S_3, T1 (Cu, Fe) $_{6.35}$ SbS_4, $FeCuS_2$. 1.35 $[Mg_{0.66}A1_{0.33}(OH)_2]$
Berndtite SnS_2	*layers composed of edge-sharing [SnS_6] octahedra; the CdI_2 (i.e. $Cd(OH)_2$) layer type	$NiTe_2$, TiS_2, PtS_2, $LiCrS_2$, $NaCrS_2$, $AgCrS_2$, K_xTiS_2, Ti_5S_8
Molybdenite MoS_2	* layers composed of edge-sharing trigonal [MoS_6] prisms; ABAB and ABCABC variants in layer stacking	WS_2, NbS_2, TaS_2, intercalates $Ta_{1+x}S_2$, Cu_xNbS_2, $K_{0.5}(H_20)_yNbS_2$
Stibnite Sb_2S_3	A chain structure with quadruple ribbons [Sb_4S_6]; Sb in trigonal– and square-pyramidal coordination	Bi_2S_3, Bi_2Se_3, Sb_2S_2O, Sn_2S_3, $CuPbBi_5S_9$, $CuPbBiS_3$
synth. $KFeS_2$	A chain structure; single chains of edge-sharing [FeS_4] tetrahedra are separated by large cations	T1FeS_2, $CsFeS_2$, $Ba_{19}(FeS_2)_{18}$, $Na_3Fe_2S_4$, $NaFeS_2{\cdot}2H_2O$
Lillianite $Pb_3Bi_2S_6$	periodically mirror-twinned slabs of *ccp* array with octahedral holes filled; trigonal prisms on composition planes; several homologous series	$AgPbSbS_3$, $Pb_6Bi_2S_9$, $Ag_5Pb_8Bi_{13}S_{30;}$ $UFeS_3$, Y_5S_7, MnY_2S_4, $Cr_2Er_6S_{11}$, $AgBi_3S_5$, $Cu_{1.6}Bi_{4.6}S_8$
Cosalite $Pb_2Bi_2S_5$	zigzag layers of *ccp* array with oct. holes filled or of SnS-like arrangement; incommensurate interspaces	$Pb_4In_9S_{17}$, $Ce_{1.3}Bi_{3.8}S_8$, $Pb_4Sb_6S_{13}$, $FePb_4Sb_6S_{14}$
Realgar As_4S_4	Molecular structure, As-S and As-As bonds, As-As pairs or, in As_4S_3 also As- triangles	β-As_4S_4, As_4S_3, As_4S_5, $[(As,Sb)_6S_9]$ $[As_4S_5]$
Tetradymite Bi_2Te_2S	* double-octahedral layers, anion-anion contacts may be intercalated by Bi-Bi layers; triple-octahedral layers $M^{2+}BiTe_4$ also present	BiTe, Bi_3Se_2Te, Bi_2Te_3, Bi_2Se_3, Bi_4Se_3, $PbBi_4Te_7$, $PbBi_2Te_4$
Crookesite $TlCu_7Se_4$	a channel structure, Se-Cu and Cu-Cu bonds in channel walls, Tl in channels. Other channel str.: octahedral and square-planar walls	$NH_4Cu_7S_4$, $TeCu_3Se_2$, $Rb_3Cu_8Se_6$, channel structures $K_2Hg_6S_7$; $K_{0.3}Ti_3S_4$, KCr_5Se_8, $CsBi_3S_5$

* A layer structure, layers held together by van der Waals forces. When layers become electrically charged, interstitial or intercalation derivatives are formed.
hcp – hexagonal close packing; *bcc* – body-centered cubic packing; *ccp* - cubic close packing

The approach adopted in this contribution will highlight a prominent structural principle for each category, sometimes splitting some of the classical description groups, such as sulfosalts. The following divisions are adopted:

Fibrous sulfides:
-with FeS_4 tetrahedra
-other cases

Layer-like structures:
Monochalcogenides and related
-mackinawite, its intercalates and derivatives
-covellite merotypes
-valleriite
Sesquichalcogenides
Dichalcogenides
Derivatives with two kinds of chalcogenide layers
-cannizzarite and derivatives
-layer misfit structures

Structures with three-dimensional frameworks:
-tetrahedral *ccp, hcp* and combined "adamantane" structures
-pentlandite group and other structures with tetrahedral clusters
-octahedral *ccp* and *hcp* structures and derivatives
-thiospinels
-dichalcogenides with X_2 groups

Channel- and cage structures

Selected cation-specific structures:
-Ni chalcogenides
-Pd and Pt chalcogenides
-ion conductors and other Cu, Ag chalcogenides
-compounds of lone electron pair cations

Selected larger sulfosalt families

A more detailed account of the concepts involved in this classification is given below. At present, often a number of more or less accurate and complete crystal structure determinations have been made on all important sulfide minerals, investigating not only the structure but also specific substitutions, and structural changes under non-ambient conditions.

For example, in the case of tetrahedrite-tennantite, the pioneering structure determination by Machatschki (1928) was followed by Pauling and Neuman (1934) whose results were refined by Wuensch (1964) and Wuensch et al. (1966). Kalbskopf (1971, 1972) determined structures of Hg-rich and Ag-rich tetrahedrite, respectively. Crystal structures of the natural members of the series, with variable types of mixed substitution, were also determined by Kaplunnik et al. (1980), Johnson and Burnham (1985), as well as Peterson and Miller (1986) and Karanović et al. (2003). Structures of the synthetic, pure copper tetrahedrite varieties were studied by Makovicky and Skinner (1979), Pfitzner (1997) and Pfitzner et al. (1997). The crystal structure of a natural copper-rich tennantite was determined by Makovicky et al. (2005), whereas those of the tellurian members of the tetrahedrite-tennantite solid solution by Kalbskopf (1974), Dmitriyeva et al. (1987) and Pohl et al. (1996). These studies were joined by others, in which relationships were determined between element substitutions and unit-cell parameters (e.g., Hall 1972; Johnson et al. 1987; Makovicky and Karup-Møller 1994; Karup-Møller and Makovicky 2003, 2004). Structurally important Mössbauer and other studies of the valence of iron/copper in these minerals were performed as well (e.g., Vaughan and Burns 1972; Charnock et al. 1989; Makovicky et al. 1990, 2003; Di Benedetto et al. 2002, 2005).

As we can see from this example, it is not even remotely possible to treat, or even quote, all the relevant studies in this review. Therefore, preference will be given to recent, accurate structure determinations and, with our deepest apologies to all those other authors, the reader is advised to consult the half-yearly updated Inorganic Crystal Structure Database (ICSD) released by the Fachinformationszentrum Karlsruhe (Germany)/National Institute of Standards and Technology (U.S. Dept. of Commerce) or the chalcogenide file by Matsushita (2005), and similar sources, where a complete picture of structural knowledge can be obtained for a particular compound or family.

PRINCIPLES OF THE DESCRIPTION AND CLASSIFICATION OF CRYSTAL STRUCTURES RELEVANT TO SULFIDES: A BRIEF OUTLINE

The present section gives a brief outline of principal classification criteria used for inorganic structures. Modular and non-modular (i.e., polyhedral) crystal chemistry are interrelated by so-called configuration levels of structure description, to be found in Makovicky (1997b) and Ferraris et al. (2004).

Non-modular categories of similarity

Definition of *isotypy* and *homeotypy* (Lima-de-Faria et al. 1990) is the most important point in non-modular description.

Two structures are *crystal-chemically isotypic* if they (a) are isoconfigurational, i.e., the *entire configurations* of the two structures are similar: axial ratios, unit-cell angles, values of adjustable *x*, *y*, *z* parameters for corresponding atoms and their coordination polyhedra and (b) the corresponding atoms and corresponding bonds (interactions) have similar physical and chemical characteristics (e.g., electronegativities, radius ratios, electronic states, or bond-strength distribution). Without point (b) they are only configurational isotypes. There are no *a priori* limits on geometric, chemical or physical similarity in this definition. These limits will change according to the type of compounds studied, the physical or chemical properties we concentrate upon, and the purpose of study.

Two structures are *homeotypic* if one or more of the following conditions required for isotypism is relaxed:

(a) instead of an identical (or enantiomorphic) space group they can have a subgroup or a supergroup;

(b) limited variation in axial ratios, interaxial angles, *x, y, z* values and coordination properties is allowed;

(c) site occupancy limits are relaxed allowing given sites to be occupied by different atomic species in an ordered fashion (splitting of the original Wyckoff position due to (a)).

Bergerhoff et al. (1999) include interstitial derivatives among homeotypes.

Examples are numerous: among site-ordering variants (and omission and interstitial variants) we can quote C (diamond), ZnS (sphalerite), $CuFeS_2$ (chalcopyrite) or Cu_3SbS_4 (famatinite) and also a variety of "adamantane" structures; among distortion derivatives, $PdSe_2$ vs. parent FeS_2. The structures of bismuthinite-aikinite series are a series of homeotypic structures. The ideal, undistorted structure is called an aristotype and the derived distorted structures hettotypes (Megaw 1973).

Modular categories of structural similarity

Structure building operators. Modular structures are composed of modules/fragments (blocks, rods or layers) of simpler, archetypal structures that are recombined in various

orientations by the action of structure building operators. The structure-building operators are (mostly planar) defects which produce a definite geometric relationship between the structural portions they join; they are connected with localised chemical (crystal-chemical) changes in the structure.

In the majority of cases, they are various types of unit-cell twinning (Andersson and Hyde 1974). Takéuchi (1997) uses the term chemical twinning for this type of operation. The most frequent type is reflection- (i.e., mirror-reflection) twinning that acts either on a full set of atoms (Andersson and Hyde 1974) or only on a partial set of atoms (Takéuchi 1978). Mirror-reflection twinning is usually connected with the creation of a new type of coordination polyhedron straddling the mirror plane. Examples are the capped trigonal coordination prisms of two distinct kinds on composition planes of reflection twinning of ccp and hcp arrays, respectively (illustrated by the lillianite homologues and the wittichenite group). The next types are glide-reflection twinning (Andersson and Hyde 1974) and cyclic twinning (Hyde et al. 1974). For complex sulfides, noncommensurability between adjacent building blocks comes next in order of importance (Makovicky and Hyde 1981, 1992). It means that the substructures in two adjacent blocks meet according to a vernier principle across the block interface (consult cannizzarite and rod-based structures of sulfosalts). Further categories are antiphase and out-of-phase boundaries, crystallographic shear, the *t*/2-shear (or slip) in the structures with a short pronounced *t* period (mostly, $t \sim 4$ Å), and the intergrowth of two different structure types on a unit cell scale (Hyde et al. 1974).

The definition of unit cell twinning implies appreciable configurational and chemical changes on the twin composition planes, unlike that of classical twinning. The coordination states and, often, the chemical species of atoms on the block surfaces or in the interfaces differ from those inside the building blocks. The structure-building operators, especially reflection twinning, can apply either to all the details of the structure, including the chemical species, or only to its general topology (or even only to its anion array), something akin to the difference between isotypes and homeotypes.

Archetypes used in the modular description are those simpler structures that display/encompass all fundamental bonding and geometric properties of the structure portions in the interior of building blocks/moduli. For sulfides they are, for example, PbS, SnS and ZnS. Modular structures can be monoarchetypal or diarchetypal (or even triarchetypal, etc...) with distinct types of blocks based on one, two (three, etc...) different archetypes. Many sulfides are monoarchetypal structures (lillianite homologous series, the jordanite-kirkiite pair, rod-based complex sulfides). Diarchetypal examples include complex sulfides of the kobellite homologous series in which blocks of PbS and SnS archetype combine.

Accretional homologous series/polysomatic series. The accretional series is a series of structures in which the type(s) and general shapes of building blocks (rods, layers) as well as the principles that define their mutual relationships (the recombination operators) remain preserved, but the size of these blocks varies incrementally by varying the number of fundamental coordination polyhedra in them in an exactly defined way. The order *N* of a homologue in this type of series can be defined by the number of coordination polyhedra (polyhedral layers) across a suitably defined diameter of the building block (rod, layer) (see Fig. 1). Every member of the accretional series has its own chemical formula, unit cell parameters and symmetry; a general chemical formula can be devised for the entire series. A given homologue can represent a single compound or a (dis)continuous solid solution which can exsolve into a series of structurally ordered phases with well defined compositions (or compositional ranges) but with the same *N*. The ideal space group can then be reduced to subgroups in the process of (cation) ordering. It should be stressed that all these ordered compounds are members of the homologous series (Ferraris et al. 2004). The best example is the lillianite homologous series of (primarily) sulfosalts.

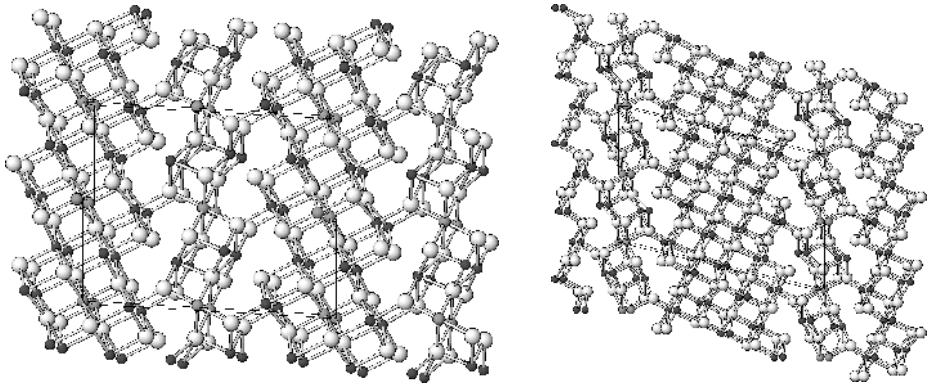

Figure 1. Pavonite (a) and benjaminite (b), the N = 5 and 7 members of the pavonite homologous (accretional) series (Makovicky and Mumme 1979). White spheres: S sites, grey spheres: Ag sites, dark spheres: pure Bi and predominantly Bi sites.

Thompson (1978) described accretional homologous series using a different name, that of a polysomatic series and a different approach: the coordination polyhedra on the surfaces and in the interfaces of the blocks (in his case, layers) are treated as one type of (layer) module whereas the incrementally accreting polyhedral layers in the layer (block) interior as another type of layer modules. Thus, all accretional homologues are treated as ordered intergrowths of (usually) two structure types which occur in different proportions in different homologues (polysomes). The two descriptions are equally valid. Takéuchi (1978) denotes the principle behind homologous series as tropochemical twinning.

Some accretional series, for example the lillianite and the pavonite homologues, are extensive series with N varying over a range of values. Besides the members with equal widths ($N_1 = N_2$) across the unit-cell twinning plane or an interface of another kind, those with unequal widths ($N_1 \neq N_2$) can occur. A number of accretional series are limited to only pairs of homologues (N_1, and $N_2 = N_1 + 1$) because of various local or global crystal chemical reasons (e.g., the pair bertrandite – hutchinsonite of Tl-(Pb)-As sulfosalts). These pairs can be extended into combinatorial series, the members of which represent regular intergrowths of the above two accretional homologues: $N_1N_2N_1N_2$..., $N_1N_1N_2N_1N_1N_2$..., $N_1N_2N_2N_2N_1N_2N_2N_2$..., etc., as in the sartorite homologous series or in the MnS-Y_2S_3 system. In some instances, e.g., for the cuprobismutite homologues, only one intermediate member, $N_1N_2N_1N_2$..., is known (Ferraris et al. 2004).

Chemical-composition series. A series of compositions combining formally two sulfide compositions A_mX_n-B_oX_p usually is not a single homologous (polysomatic) series but it may contain one or two homologous series and/or several structurally unrelated compounds. For example, the Cu_2S-Bi_2S_3 "series" contains wittichenite, as well as (idealized) members of the cuprobismutite and the pavonite homologous series.

Variable-fit homologous series and series with a combined character. Variable fit homologous series occur in crystal structures that are composed of two kinds of alternating, mutually noncommensurate layers (rarely of columns or of a matrix/infilling combination). Each kind of layer has its own short-range (sub)periodicity and it takes m periods of one layer and n periods of the other layer before they meet in the same configuration as at the origin. These are so-called semi-commensurate cases for which the two matching (sub)periodicities of the two layers comprise a ratio of two not very large integers. Besides

them, incommensurate cases exist for which these short-range periodicities comprise irrational fractions or a ratio of very large integers (these two cases are practically indistinguishable) (Fig. 2a). Noncommensurability of layers may occur in one or two interplanar directions. With minor compositional changes in the ratio or type of cations, the *m*/*n* ratio and the *M*/S ratio vary within certain, rather narrow limits, leading to a "variable-fit" series of closely related compounds (Makovicky and Hyde 1981, 1992). Incommensurate layer structures are also known as vernier compounds (Hyde et al. 1974) and layer-misfit compounds. The best examples are cannizzarite, the cylindrite family and the synthetic sulfide layer-misfit structures. The "infinitely adaptive structures" of the $Ba_{1+x}Fe_2S_4$ series belong here as well; the two matching elements in them are structural rods rather than layers.

The cases which represent a combination of the accretional (separately for each layer) and variable-fit (for the interlayer match) *principles* are discussed in connection with the derivatives of cannizzarite (Fig. 2b) and rod-based structures of Pb-Sb(Bi) sulfosalts.

Merotype and plesiotype series express structural relationships that are geometrically less accurate than the relationships between members of a homologous series (Makovicky 1997b; Ferraris et al. 2004). Merotypic and plesiotypic families rank higher than the homeotypic, ordering- or chemical variations between individual real structures.

Merotypic structures (merotypes; meros = part) are composed of alternating layers (blocks). One set of these building layers (blocks) are common to all merotypes (i.e., they are isotypic, homeotypic or they are mutually related via homologous expansion/ contraction) whereas the layers (blocks) of the other set(s) differ for different merotypes. Structures with a layer set missing may exist as well. Examples are the hutchinsonite merotypes, covellite merotypes, and the complete series of layered derivatives of Bi_2Se_3.

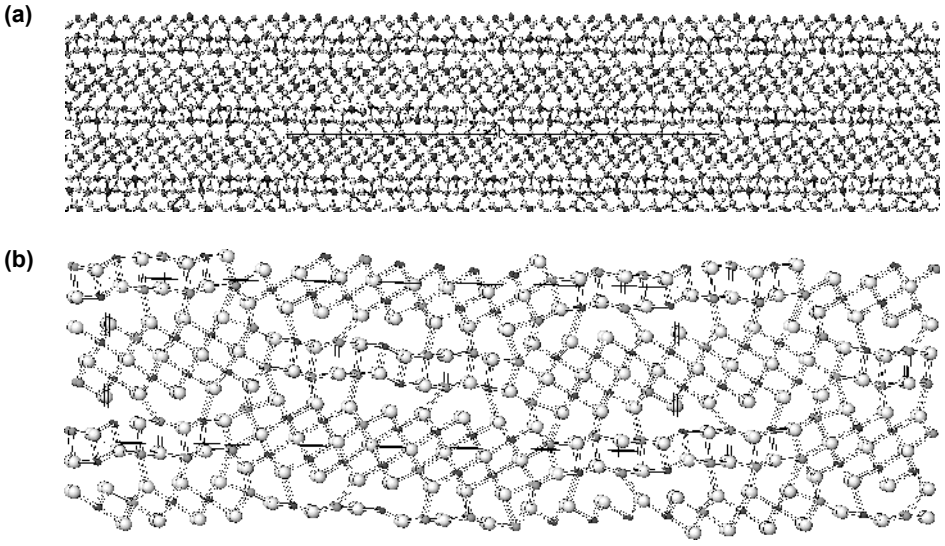

Figure 2. (a) The non-commensurate structure of cannizzarite, $Pb_{46}Bi_{54}S_{127}$ (Matzat 1979) projected upon (010). White circles: S, grey circles: metal atoms (predominant Bi: darker). Double octahedral H layers alternate with two-atoms thick Q, PbS-like layers. A total of 46 primitive Q subcells matches with 27 centered H subcells. (b) Weibullite $Ag_{0.33}Pb_{5.33}Bi_{8.33}(S,Se)_{18}$ (Mumme 1980), a derivative of the cannizzarite structure by means of composition-nonconservative glide planes (100) at x = ¼ and ¾. An example of a structure which combines accretional and variable-fit criteria.

Plesiotypic structures (plesiotypes; plesios = near, close) (a) contain fundamental structural elements (blocks, layers) of the same general type(s), and (b) mutual disposition/ interconnection of these elements in all plesiotypes follows the same general rules. However, unlike the homologous series, (1) the plesiotypic structures may contain additional structural elements that differ from one member of the family to another; and (2) details of fundamental elements, or of their disposition, may differ. For further details, see Ferraris et al. (2004). Rod-layer structures of complex Pb-Sb sulfides and of selected Pb-Bi sulfides belong to this category.

Polytypes and polytype categories. Polytypes are modular structures in which modules (usually layers) are of one or two (in rare cases even more) distinct kinds in strictly regular alternation (Ďurovič 1992). The well-defined geometric relations on the interfaces of two adjacent layers do not determine a unique stacking of modules, i.e., an unambiguously defined three-dimensionally periodic structure.

Ideally, distinct polytypes composed of the same kinds of layers should have the same chemical composition. The strict definition of polytypy stresses the chemical (near) identity of different polytypic modifications. Everyday usage extends these strict criteria. Thus, polytypes will then be defined either on a crystal-chemical or on a configurational level. Polytypes with radically different chemical compositions but with the same layer configurations and layer-stacking principles can be grouped in configurational (= heterochemical) polytypic series (Makovicky 1997).

OD polytypes (order-disorder polytypes) are a family of polytypic structures with a uniquely defined geometric relationship between any two adjacent layers, i.e.,with only one kind of layer pairs for each combination of adjacent layers present (Dornberger-Schiff 1966; Ďurovič 1992; Merlino 1990). From the point of view of symmetry, they belong to one groupoid family (ibid.). Polytypes can be described as OD-polytypes only when the appropriate number and types of layers have been selected.

In a family of non-OD polytypes, different stacking principles of layers are active in different members of the family or these principles combine in the observed sequences of layers in a single compound. It means that more than one kind of layer pairs are present for given type(s) of unit layers. Besides these "proper polytypes," with configurationally unmodified layers, there is a spectrum of polytype-like cases (commonly described as polytypes in the literature), in which configurational modifications occur; these were put in the "improper polytype" category with several subdivisions by Makovicky (1997b) and Ferraris et al. (2004). Among our compounds, e.g., the pair stibnite Sb_2S_3 - pääkkönenite Sb_2S_2As (Bonazzi et al. 1995) (see Fig. 3a,b) belong to this category.

CHALCOGENIDES WITH PRONOUNCED ONE-DIMENSIONAL BUILDING UNITS

Fibrous sulfides with chains of edge-sharing FeS_4 tetrahedra

Crystal structures of this plesiotypic family consist of isolated chains of FeS_4 tetrahedra which share edges perpendicular to the chain extension giving, in principle, a unit cell dimension equal to twice the "tetragonal" height of a tetrahedron. These chains are separated by insertion of large, more complex polyhedra of alkali and alkaline earth cations. Structural water is exceptional, compensating for the small size of interstitial sodium. This family contains several minerals (Table 3).

Stoichiometry of these compounds suggests on the one hand trivalent iron, as in $KFeS_2$, $KFeSe_2$ and $BaFe_2S_4$ (Table 3, Fig. 4a), or, on the other hand, mixed-valence iron: 2.5+ in $K_3Fe_2S_4$ and $K_3Fe_2Se_4$, 2.9+ in $Ba_5Fe_9S_{18}$ (Table 3). The three trivalent cases quoted have

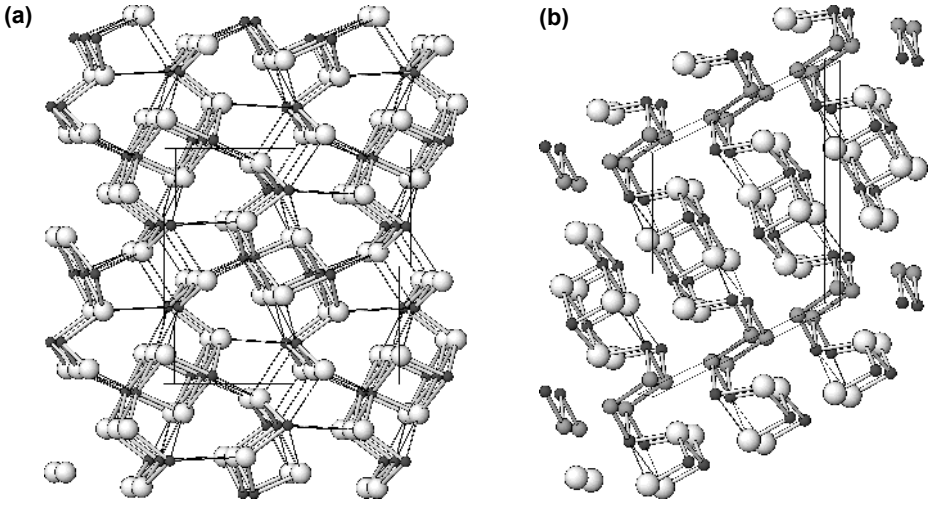

Figure 3. (a) Stibnite Sb_2S_3 in projection along the ribbons Sb_4S_6. Small dark spheres: Sb, large light spheres: S. (b) Pääkkönenite Sb_2S_2As (Bonazzi et al. 1995) with ribbons $Sb_4S_4As_2$; intermediate grey spheres: As-As pairs. (a-b): a pair of pseudopolytypes, with unit layers (100) for stibnite and $(10\bar{1})$ for pääkkönenite. Note the fundamentally different interconnection of unit ribbons in the two structures.

Table 3. Fibrous sulfides with chains of edge-sharing FeS_4 tetrahedra

Compound	Chains	Lattice Parameters				Space Group	Ref.
		a **(Å)**	***b*** **(Å)**	***c*** **(Å)**	**β (°)**		
$Ba_5Fe_9S_{18}$	single	7.776	7.776	49.860		*P4/ncc*	[1]
$Ba_9Fe_{16}S_{32}$	single	7.776	7.776	44.409		*P4/mnc*	[2]
$\alpha BaFe_2S_4$	single	8.111	8.111	5.59		*I4/mcm*	[3]
$BaFe_2Se_3$	double ‖b	11.878	5.447	9.160		*Pnma*	[4]
$Cs_3Fe_2S_4$	single	7.540	11.168	12.923		*Pnma*	[5]
$CsFeS_2$	single	7.126	11.945	5.420		*Immm*	[6]
$K_3Fe_2S_4$	single sinusoidal	7.157	10.989	11.560		*Pnma*	[5]
KFe_2S_4 rasvumite	single	9.049	11.019	5.431		*Cmcm*	[7]
$Na_3Fe_2S_4$	single twisted	6.633	10.675	11.677		*Pnma*	[8]
$NaFeS_2{\cdot}2H_2O$ erdite	single	10.693	9.115	5.507	92.17	*C2/c*	[9]
$Rb_3Fe_2S_4$	single twisted	7.407	11.141	11.997		*Pnma*	[5]
$RbFeS_2$	single	7.223	11.725	5.430	112.0	*C2/c*	[10]
$RbFeSe_2$	single	7.474	12.091	5.662	112.38	*C2/c*	[10]
$KFeSe_2$	single	7.342	11.746	5.629	113.52	*C2/c*	[10]
$Rb_3Fe_2Se_4$	single	7.691	11.403	12.471		*Pnma*	[11]
$K_3Fe_2Se_4$	single sinusoidal	7.433	11.341	12.016		*Pnma*	[12]
$KFeS_2$	single	7.084	11.303	5.394		*C2/c*	[10]
$TlFe_2S_3$ picotpaulite	single	9.083	10.753	5.411		*Cmcm*	[13]

References: [1] Grey 1975; [2] Hoggins and Steinfink 1977; [3] Boller 1978; [4] Hong and Steinfink 1972; [5] Bronger et al. 1995; [6] Bronger and Müller 1980; [7] Clark and Brown 1980; [8] Klepp and Boller 1981; [9] Konnert and Evans 1980; [10] Bronger et al. 1987; [11] Klepp et al. 2000; [12] Bronger et al. 1999; [13] Balić-Žunić, pers. comm.

Fe-S(Se) distances of 2.231 and 2.237 Å, 2.363 Å, and 2.316 Å, respectively. The uniform Fe-Fe distances, 2.700, 2.815, and 2.800 Å, respectively, indicate metal-metal interactions. The cases with mixed valence of iron display (at least) two types of Fe-S and Fe-Fe distances. Thus, $K_3Fe_2S_4$ and $K_3Fe_2Se_4$ display a range of Fe-*X* distances equal to 2.282-2.345 Å (average 2.309 Å) and 2.402-2.465 (aver. 2.428 Å). The Fe-Fe distances are 2.78 and 2.90 Å in the sulfide, 2.865 and 3.015 Å in the selenide, and a string... 2.80-2.67-2.67-2.80-2.77-2.77-2.90-2.77 Å in $Ba_5Fe_9S_{18}$.

The sulfide phases have chain (sub)periodicities typically equal to 5.34-5.59 Å, selenides 5.63-5.67 Å (only exceptionally less, Table 3). The chain-and-cation arrangements lead to a limited choice of tetragonal, orthorhombic and monoclinic space groups. Straight chains predominate; the $A_3Fe_2S_4$ phases have sinusoidal or twisted chains, from $Na_3Fe_2S_4$ with the smallest cation to $Rb_3Fe_2S_4$ with the largest one. A double chain is observed in $BaFe_2Se_3$ (Hong and Steinfink 1972). Coordinations of large cations vary from 8 in α–$BaFe_2S_4$ (Fig. 4a) and 9 in $BaFe_2Se_3$ to 6 for sodium in $Na_3Fe_2S_4$ (Klepp and Boller 1981) and in erdite $NaFeS_2{\cdot}2H_2O$ (Konnert and Evans 1980) (Figs. 4b,c; Table 3). In $NaFeS_2{\cdot}2H_2O$, the coordination octahedra of Na comprise ($4H_2O$ + 2S).

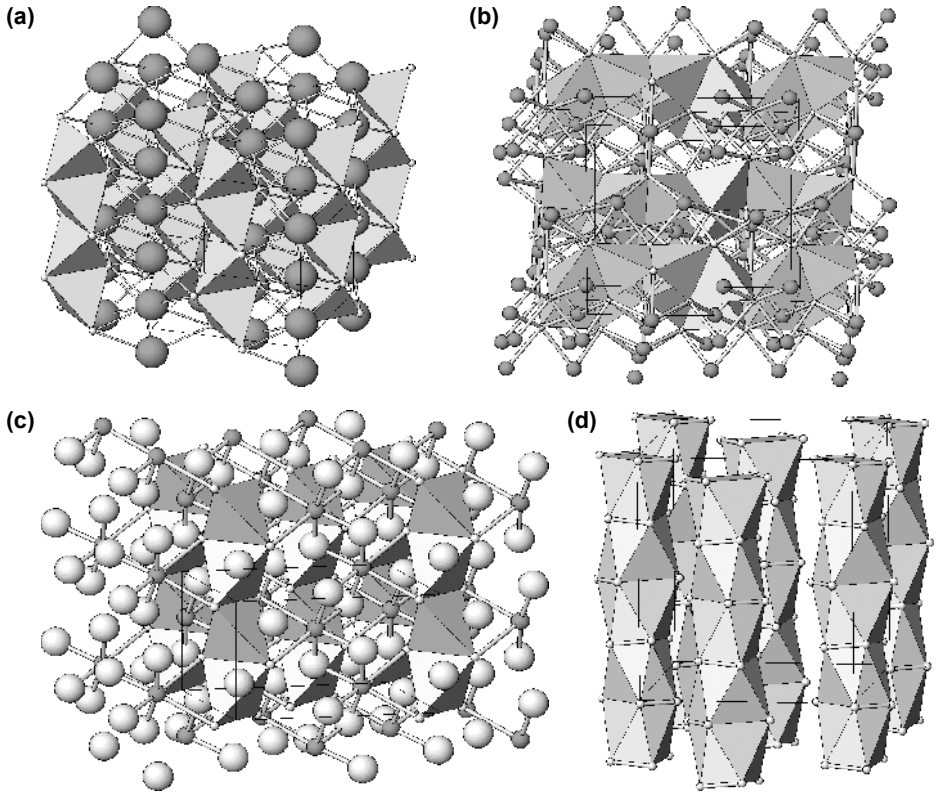

Figure 4. Crystal structures of fibrous sulfides. (a) α–$BaFe_2S_4$ (Boller 1978). Large spheres: Ba; straight chains of edge sharing Fe-S tetrahedra contain Fe^{3+}. (b) $Na_3Fe_2S_4$ (Klepp and Boller 1981). Spheres: Na; folded chains of edge-sharing Fe-S tetrahedra with mixed-valence Fe. (c) $NaFeS_2(H_2O)_2$ (Konnert and Evans 1980) with Na (grey) coordinated by both S (small spheres which participate in tetrahedral chains) and H_2O molecules (large white spheres). (d) Patronite, $V(S_2)_2$ (Kutoglu and Allmann 1972). Chains of "square" VS_8 antiprisms sharing rectangular faces. S-S bonds are indicated by bars.

The variable-fit "infinitely adaptive" structure series, $Ba_{1+x}Fe_2S_4$ (Nakayama et al. 1981), consists of tetrahedral Fe_2S_4 chains and strings of Ba coordination polyhedra which differ in periodicity. It stretches from $Ba_8(Fe_2S_4)_7$ to $Ba_{17}(Fe_2S_4)_{16}$, with a from 7.78 Å to 7.74 Å, and c from 39.03 Å to 82.17 Å (and 104.84 Å for $Ba_{21}(Fe_2S_4)_{19}$, the only phase in which the difference (p-q) in the formula $Ba_p(Fe_2S_4)_q$, in which p,q are believed to be integers, is not one). These phases are rich in Fe^{3+}.

Other fibrous sulfides

An archetypal fibrous structure is that of synthetic SiS_2 (Peters and Krebs 1982) (Table 4), in which single chains of edge-sharing SiS_4 tetrahedra have only van der Waals contacts. Cs_2TiS_3 (Rad and Hoppe 1978) contains yet another type of chain, one composed of square coordination pyramids (TiS_5) sharing two of the edges of the square base with the adjacent pyramids.

The crystal structure of a disulfide of vanadium, patronite $V(S_2)_2$, (Kutoglu and Allmann 1972) consists of isolated chains which are composed of face-sharing distorted (VS_8) tetragonal antiprisms (Fig. 4d). The shared faces are rectangular and not square-shaped, being limited by two parallel S-S covalent pairs each: 2.04 × 3.28 Å and 2.03 × 3.16 Å, respectively. Vanadium – sulfur bonds have the lengths 2.38-2.54 Å. The shortest S-S contacts between chains are 3.24 Å; and along chains are 3.17 Å.

Table 4. Other fibrous structures.

Compound	Space Group	Lattice Parameters				Chain Type	Ref.
		a **(Å)**	***b*** **(Å)**	***c*** **(Å)**	Angle (°)		
SiS_2	*Ibam*	9.545	5.564	5.552		tetrahedral	[1]
$V(S_2)_2$	*I*2/*c*	6.775	10.42	12.11	100.8	antiprisms	[2]
Cs_2TiS_3	$Cmc2_1$	12.51	9.03	6.55		sq.pyramids	[3]

References: [1] Peters and Krebs 1982; [2] Kutoglu and Allmann 1972; [3] Rad and Hoppe 1978

STRUCTURE TYPES COMPOSED OF LAYERS: CHALCOGENIDE LAYERS WITH *M*:S =1:1

Mackinawite and related families

Mackinawite. The crystal structure of mackinawite $Fe_{1+x}S$ (possible metal excess $x \leq 0.07$) consists of sheets of edge-sharing FeS_4 tetrahedra parallel to (100) of the tetragonal cell (Table 5, Fig. 5a). Each cation has short metal-metal contacts with four adjacent cations forming an uninterrupted tetragonal net of metal-metal interactions (Fe-Fe = 2.60 Å). The S atoms are bonded to four Fe atoms on one side only (2.26 Å), their opposite side faces the interlayer space with van der Waals bonds (Evans et al. 1964; Lennie et al. 1995). The interlayer S-S distances are 3.55 Å whereas the intralayer distances are 3.67 Å. Layers are stacked in a tetragonal AAA stacking, so that an S atom from the adjacent layer lies above four Fe atoms from the starting layer. Thus, the Fe atoms form strings parallel to [001] but their distance and screening by S layers preclude interactions.

The "metal surplus" in some samples of mackinawite has been identified as a result of anion vacancies. However, sporadically occupied tetrahedra between adjacent layers may also be envisaged. The mackinawite-type layer is also an anti-litharge (γ-PbO) layer (Dickinson and Friauf 1924), with cations and anions interchanged. The mackinawite-type layer is the fundamental structural element of the thalcusite-rohaite series, and the layer-misfit tochilinite series.

Table 5. Mackinawite and tochilinites.

Mineral/Formula	Comp. Layer	Space Group	Lattice parameters (Å,°)						Ref.
			a	*b*	*c*	α	β	γ	
Mackinawite $Fe_{1+x}S$	Q	*P4/nmm*	3.674	3.674	5.033				[1]
Tochilinite I[(a)]	Q:[(b)]	*A*1	10.72	15.65	5.37	90	95	90	[2]
$6Fe_{0.9}S{\cdot}5[(Mg_{0.7}Fe_{0.3})(OH)_2]$	H:[(b)]	*A*1	10.72	15.65	5.37	90	95	90	
Tochilinite II	Q:[(b)]	*P*1	10.74	8.34	8.54	92	92.7	85.5	[3]
$6Fe_{0.8}S{\cdot}5[(Mg_{0.7}Fe_{0.3})(OH)_2]$	H:[(b)]	*A*1	10.74	15.65	5.42	90	95	90	

Notes: [(a)] Selected semicommensurate cases, for layer match see the text.
[(b)] Q: Pseudotetragonal sulfide component layer. H: Octahedral hydroxide component layer with hexagonal anion patterns on surfaces.
References: [1] Lennie et al. 1995; [2] Organova et al. 1972; [3] Organova et al. 1973

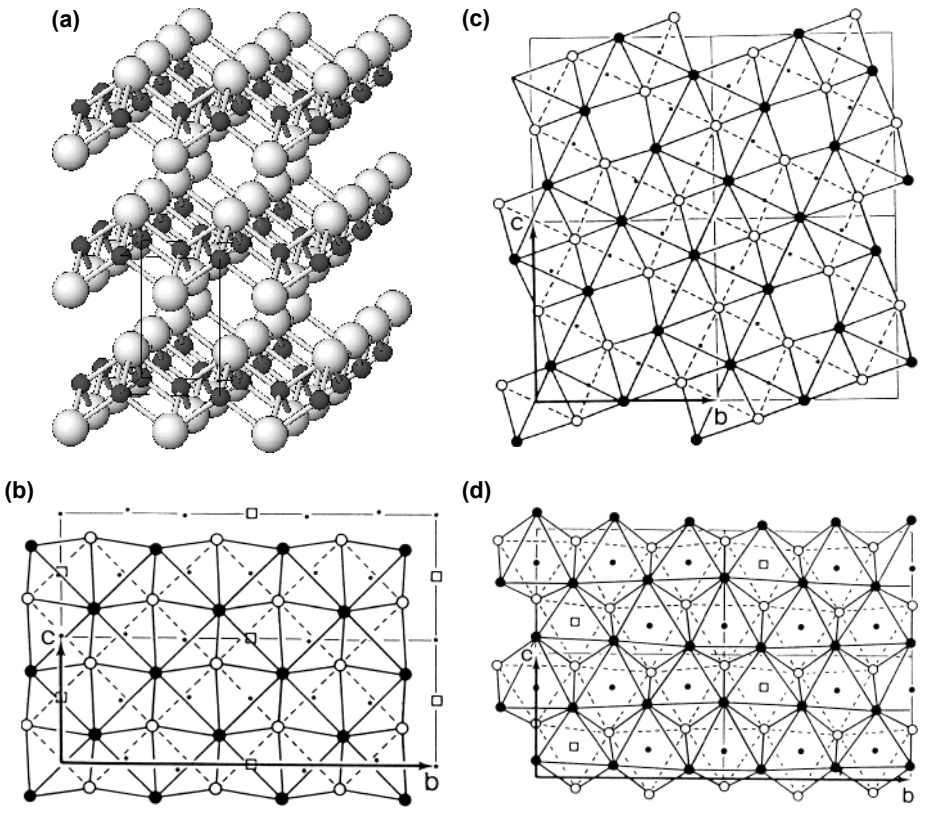

Figure 5. (a) Mackinawite (Lennie et al. 1995). Coordination tetrahedra of Fe share four edges, with four Fe-Fe bonds for each Fe atom. (b-d) Geometry of the sulfide (b, c) and hydroxide (d) layers in tochilinite. Black and white circles: anions at two height levels, dots: cations. Note two different vacancy schemes in the mackinawite-like layers and the Fe^{3+}(Al)-Mg substitution scheme in hydroxide layers; both are indicated by squares.

Mackinawite $Fe_{1-x}S$ is believed to be a metastable polymorph of FeS without a stability field. However, its selenide analog, FeSe, is an important phase in the Fe-Se system, stable up to 457 °C, and equal in importance to the pyrrhotite analog $Fe_{1-x}Se$. Karup-Møller and Makovicky (unpublished) found Cu solubility in mackinawite-like FeSe up to the composition $Cu_{13.6}Fe_{37.2}Se_{49.2}$. This, and the crystal chemistry of thalcusite and its analogs, give credence to the experiments trying to use mackinawite for scavenging metal pollution from reduced sediments.

Tochilinite varieties. Tochilinites (Table 5) are 1:1 intergrowths of tetragonal, mackinawite-like layers with cation vacancies, with a composition between $Fe_{0.91}S$ and $Fe_{0.72}S$, and octahedral "brucite-like" layers $(Mg,Fe)(OH)_2$ or $(Mg,Al)(OH)_2$ (Fig. 5b-d). The initial descriptions of tochilinite (Organova et al. 1972 a,b) concentrated upon exact crystallography with respect to layer match, the later descriptions only relied upon these results and were less detailed in character. The tochilinite problem has been summarized in detail by Organova (1989) as well as by Makovicky and Hyde (1981, 1992).

The two-layer sandwich of tochilinite has a repeat period of 10.7 Å. The sulfide layer has a mackinawite-like 5.2 × 5.4 Å substructure perturbed by diverse patterns of cation vacancies: centered orthorhombic for tochilinite I, tetragonal with a large supercell for tochilinite II (Fig. 5b-d) and tetragonal with 1:1 distribution of partial vacancies in "tochilinites III-VII," or disordered for other samples (including those studied after long standing in water).

The periodicity of the hydroxide layer, i.e., its superstructure, is created by a centered orthorhombic distribution of Fe^{3+}(Al) among the essentially Mg-occupied octahedra of the trioctahedral layer (Fig. 5b-d). If the vacancies are disregarded, stacking of both layer types is monoclinic ($\beta = 95°$); varieties with a two-layer sequence of hydroxide layers mutually rotated by 22° ("Phase 1" of Organova et al. 1974), or with extensive layer orientation disorder, and with twinning of the hydroxide sequence by 90° rotation (the Mg-Al case) have also been observed.

The layers can be denoted according to the anion patterns on their surfaces as the tetragonal (Q) sulfide layers and the hexagonal (H) hydroxide layers. The layer match between the non-commensurate Q and H layers is complex and variable. The commensurate, semicommensurate or incommensurate, approximate matches observed are apparently connected with the distribution of trivalent cations in the hydroxide layer, which interact with the distribution of fractional cation vacancies in the sulfide layer.

In tochilinite I, the semi-commensurate:commensurate match $3b_Q = 5b_H$ and $c_Q = c_H$ indicates the same A1 supercell for the two layers; in tochilinite II, the coincidence mesh is in a complicated relationship to the subcells. The layers undergo a common compositional modulation either based on centered subcells (in tochilinite I) or along the *b* direction (tochilinite II). Further tochilinite types (Organova 1989) have mutually incommensurate layers, in one or both directions, mostly with $5b_H < 3b_Q$ but with variable c_H:c_Q ratios. This situation appears connected with a detailed chess-board pattern of fractional vacancies.

The composition of this remarkable mineral varies with the concentration of vacancies, reflected in the subcell-area match:

$$2Fe_{1-x}S{\cdot}k(Mg,Fe,Al)(OH)_2$$

where $0.08 < x < 0.28$ and $1.58 < k < 1.75$, based on crystallographic evidence. Hydroxide layers vary from $(Mg_{0.9}Fe_{0.1})(OH)_2$ to $(Mg_{0.7}Al_{0.3})(OH)_2$. Chemical analyses indicate a surplus of hydroxide layers, not observed in the structure; Cu and Ni substitutions in the sulfide layers have been observed (Muramatsu and Nambu 1980). Terrestrial occurrences of tochilinite have been followed by discoveries in carbonaceous chondrites (Zolensky 1984; Tomeoka and Busek 1985) making it an important component in cosmic mineralogy. Both platy and cylindrical varieties of tochilinite are known.

Thalcusite-rohaite series. The thalcusite-rohaite series (Makovicky et al. 1980) with only one known intermediate member, chalcothallite, is a merotypic series. Its structures are composed of regularly occurring layers of coordination cubes of thallium, or of other large cations, which alternate either with quadratic, tetrahedral sulfide layers of mackinawite type (Fig. 6a), fully occupied by (Cu, Fe) in $Tl_2Cu_3FeS_4$ (thalcusite), or with thicker, complex sulfide-antimonide layers in $Tl_2Cu_{8.67}Sb_2S_4$ (rohaite). In chalcothallite, $Tl_2(Cu,Fe)_{6.35}SbS_4$, these two layer types alternate regularly (Fig. 6b). Only Tl and minor K have been found in association with the sulfide-antimonide layers.

In $TlCu_4Se_3$ and $TlCu_6S_4$, the single-tetrahedral, Cu-filled layers between two consecutive Tl layers undergo homologous expansion giving double- and triple-tetrahedral layers (Berger 1987). Other large cations occur in these phases (Table 6) but the multiple tetrahedral layers are known only for Cu. The chemical formulae and the plethora of short Cu-Cu (in one-layer varieties also Fe-Fe and Fe-Cu) contacts imply a complex bonding/valence scheme. Natural compounds exhibit a combination of Cu and Fe close to the 3:1 ratio. Ordered vacancies are present in tetrahedral layers of, e.g., $Rb_2Mn_3S_4$ (Bronger and Böttcher 1972) (Table 6).

Other M:S=1:1 layer types

Covellite merotypes. Covellite, CuS, is a sulfide with a layer structure that is composed of consecutive sheets (0001) of tetrahedrally coordinated copper, trigonally coordinated copper and of covalent S-S dimers that are parallel to the hexagonal *c*-axis (Fig. 7a). The same structure is adopted by CuSe (klockmannite).

For the sake of comparison with other structures of this small merotypic series, the covellite structure can be divided into composite layers that are limited on both surfaces by the sulfurs of the trigonal planar sheet, and include the tetrahedral sheets adjacent to them, and the central S-S layer. In covellite, these layers share the bounding S atoms; the "exchangeable interlayer" is formed in this case only by the trigonal planar Cu atoms connected to these sulfur atoms.

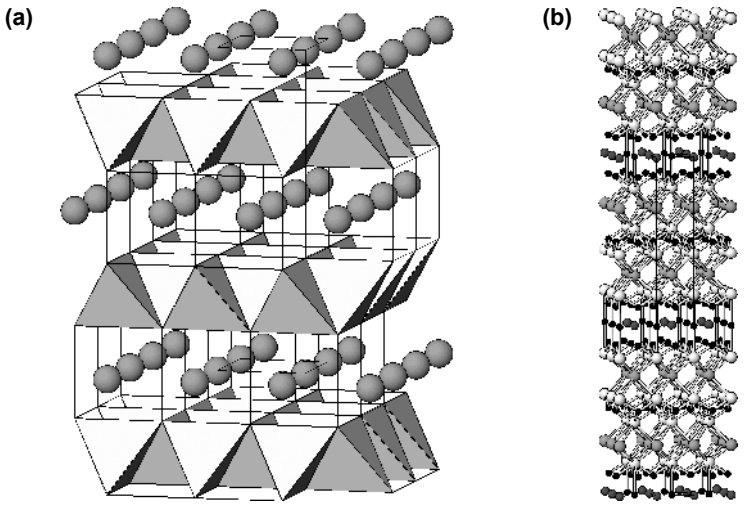

Figure 6. (a) $TlFe_2Se_2$ (Klepp and Boller 1978), a typical structure of the thalcusite family. Large circles: Tl in a cube-like coordination; Fe is in tetrahedral coordination with short Fe-Fe contacts. (b) Chalcothallite $Tl_{1.7}K_{0.2}Cu_{5.5}Fe_{0.7}Ag_{0.1}SbS_4$ (Makovicky et al. 1980). Tl (grey) in 8-fold coordination; Cu (black) in tetrahedral mackinawite-like layers. Cu also participates in triple "antimonide" layers with a partial, 1/3 Cu site (black) and Sb (dark grey) in their central row.

Table 6. Mackinawite and the thalcusite family

Mineral	Formula	Space Group	Lattice Parameters (Å)		Ref.
			a	*c*	
Mackinawite	FeS	*P*4/*nmm*	3.674	5.033	[1]
Thalcusite	$Tl_2Cu_3FeS_4$	*I*4/*mmm*	3.88	13.25	[2]
Murunskite	$K_2Cu_3FeS_4$	*I*4/*mmm*	3.88	13.10	[3]
Bukovite	$Tl_2Cu_3FeSe_4$	*I*4/*mmm*	3.98	13.70	[4], [5]
Rohaite	$Tl_2Cu_{8.7}Sb_2S_4$	*Pmmm* or *P*222	*a* 7.60 *b* 3.80	*c* 20.99	[5]
Chalcothalllite	$Tl_2Cu_{5.7}Fe_{0.7}SbS_4$	*I*4/*mmm*	*a* 3.827	*c* 34.280	[5]
Synthetic	$TlCu_4Se_3$	*P*4/*mmm*	3.894	9.33	[6]
Synthetic	$TlCu_6S_4$	*I*4/*mmm*	3.936	24.183	[7]
Synthetic	$Rb_2Mn_3S_4$	*Ibam*	*	6.295	[8]
Synthetic	KCu_4S_3	*P*4/*mmm*	3.899	9.262	[9], [10]
Synthetic	KCu_4Se_3	*P*4/*mmm*	4.019	9.720	[11]
Synthetic	$TlFe_2Se_2$	*I*4/*mmm*	3.890	14.00	[12]
Synthetic	$KCuFeS_2$	*P*4/*mmm*	3.837	13.384	[13]
Synthetic	$NH_4Cu_4S_3$	*P*4/*mmm*	3.907	9.453	[14]
Synthetic	$RbCu_4S_3$	*P*4/*mmm*	3.928	9.43	[10]
Synthetic	$CsCu_4S_3$	*P*4/*mmm*	3.975	9.689	[15]
Synthetic	$CsCoCuS_2$	*I*4/*mmm*	3.967	13.833	[16]
Synthetic	$CsCuFeS_2$	*I*4/*mmm*	3.942	14.238	[17]
Synthetic	$TlCo_2S_2$	*I*4/*mmm*	3.741	12.956	[18]
Synthetic	$TlCu_2Se_2$	*I*4/*mmm*	3.80	13.77	[19]
Synthetic	$TlCu_2S_2$	*I*4/*mmm*	3.777	13.379	[20]

* $a = 7.119$, $b = 13.140$

References: [1] Lennie et al. 1995; [2] Kovalenker et al. 1976; [3] Dobrovolskaya et al. 1981; [4] Johan and Kvaček 1971; [5] Makovicky et al. 1980; [6] Klepp et al. 1980, Berger 1987; [7] Berger and Eriksson 1990; [8] Bronger and Böttcher 1972; [9] Brown et al. 1980, [10] Ruedorff et al. 1952; [11] Stoll et al. 1999; [12] Klepp and Boller 1978; [13] Ramirez et al. 2001; [14] Boller and Sing 1997; [15] Burschka 1980; [16] Oledzka et al. 1996; [17] Llanos et al. 1996; [18] Huan and Greenblatt 1989; [19] Avilov et al. 1971; [20] Berger 1989

In the first of the known merotypes of covellite (Table 7), $Cu_{3.39}Fe_{0.61}S_4$, nukundamite (Sugaki et al. 1981), the "exchangeable interlayer" consists of edge-sharing tetrahedra, all of which are filled with (Cu, Fe) in a valleriite-like arrangement (for valleriite see the next section) (Fig. 7b). The "exchangeable interlayer" in Cu_4SnS_6 (Chen et al. 1999) (Fig. 7c) and in synthetic $NaCu_4S_4$ (Zhang et al. 1996) contains trigonal planar copper on both surfaces, and octahedrally coordinated Sn^{4+} inside the sandwich.

Valleriite is a two-layer misfit structure composed of two trigonal layers—a sulfide and a hydroxide layer in an incommensurate match (Evans and Allmann 1968). The sulfide component represents a trigonal layer of edge-sharing MS_4 tetrahedra, with the stoichiometry MS (M = Cu and Fe) (Fig. 8). The boundary S layers are 3^6 nets. In the original valleriite (Evans and Allmann 1968), a three-layer rhombohedral sequence of sulfide layers was observed, with $a = 3.792$ Å, $c = 34.10$ Å, component space group $R\bar{3}m$.

The hydroxide component of the original valleriite is a brucite-like trioctahedral layer with Mg^{2+} and Al^{3+}. These layers form a one-layer sequence with $a = 3.070$ Å, $c = 11.37$ Å and a different space group, $P\bar{3}m1$. The a and c axes of the two components coincide, giving an approximate match of 17 a (sulph) = 21 a (brucite), without a visible common modulation.

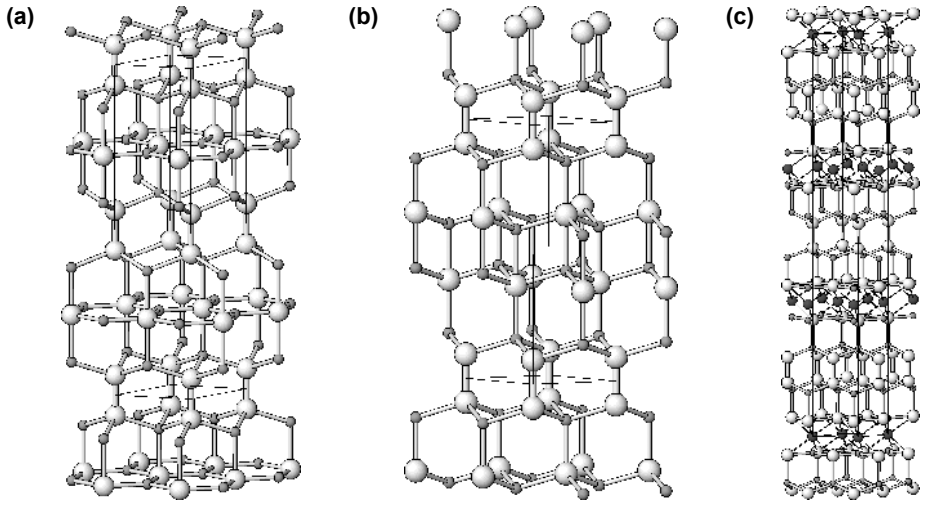

Figure 7. (a) Covellite CuS (Evans and Konnert 1976). Large spheres: S; small grey spheres: Cu. Alternating layers of CuS_3 coordination triangles and CuS_4 coordination tetrahedra. S_2 groups are parallel to [001]. (b) Nukundamite $Cu_{3.4}Fe_{0.6}S_4$ with alternating layers of tetrahedrally coordinated Cu, of edge-sharing (Cu,Fe) tetrahedra and of S_2 groups. (c) Cu_4SnS_6 (Chen et al. 1999). Grey small spheres: Cu; white spheres: S; dark spheres: partly occupied Sn^{4+} positions. These are flanked by partly occupied triangular Cu sites, fully occupied Cu tetrahedra and S_2 groups.

Table 7. Covellite merotypes.

Mineral	Formula	Space Group	Lattice Parameters (Å)		Interlayer	Ref.
			a	*c*		
Covellite	CuS	$P6_3/mmc$	3.79	16.34	Cu[3]	(1)
Klockmannite	CuSe	$P6_3/mmc$	3.94	17.25	Cu[3]	(2)
Nukundamite	$Cu_{3.39}Fe_{0.61}S_4$	$P\bar{3}m$	3.78	11.2	(Cu,Fe)[4]	(3)
Synthetic	Cu_4SnS_6	$R\bar{3}m$	3.74	32.94	Cu[3], Sn[6]	(4)
Synthetic	$NaCu_4S_4$	$P\bar{3}m1$	3.83	12.07	Cu[3], Na[6]	(5)

References: (1) Evans and Konnert 1976; (2) Effenberger and Pertlik 1981; (3) Sugaki et al. 1981; (4) Chen et al. 1999; (5) Zhang et al. 1996

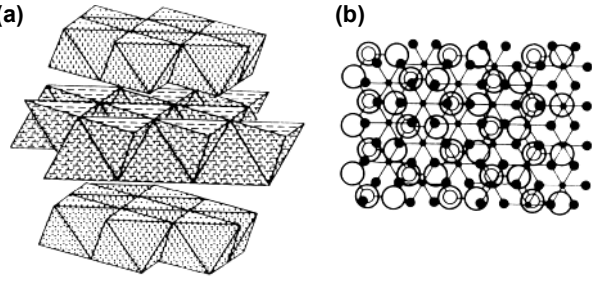

Figure 8. Structural scheme of valleriite. (a) Tetrahedral sulfide layers alternate with octahedral hydroxide layers. (b) In the projection on (0001), the sulfide layer is indicated by large circles, the hydroxide layer by smaller, filled circles.

For valleriite with Mg and Fe^{3+} in brucite-like layers, a one-layer stacking sequence was found for both components by Organova et al. (1973), with ordered Mg and Fe^{3+} in the brucite layer, resulting in $a_{brucite}$ = 5.34 Å, at 30° to the a_{sulph} = 3.79 Å. This appears to be a unique case. In her compilation, Organova (1989) quotes all other known valleriites as having a three-layered sequence of sulfide layers, with an almost constant composition, with Cu:Fe about 1:1. The hydroxide components vary from $Mg_{0.68}Al_{0.32}$ to Mg-Fe combinations (0.1-1.0 Fe), with a increasing from 3.07 Å to 3.20 Å in this process. These changes result in the formula $2MS{\cdot}1.53\text{-}1.37M(OH)_2$. Chemical analyses indicate a surplus of hydroxide component, not explained by the structure investigations. The brucite-like layers display negative charge; compensation by sulfide layers is assumed although less obvious because of the dense net of metal-metal interactions.

Wang and Buseck (1990) suggest that valleriite is triclinic, the 11.47 Å layer pair being quadrupled and with occasional wavy modulation similar to antigorite. This reminds us that Organova (1989) found a regularly interstratified valleriite-serpentinite phase. For the Ni-analog, haapalaite (Huhma et al. 1973), $Fe_{1.26}Ni_{0..74}S_2{\cdot}1.61$ $[Mg_{0.84}Fe_{0.16}(OH)_2]$, only limited crystallographic data exist. The vanadium analog, yushkinite, $V_{1-x}S{\cdot}0.53\text{-}0.61$ $[(Mg,Al)(OH)_2]$ (Makeyev et al. 1984) with x = 0.38-0.47 has a_{sulph} = 3.21 Å, $a_{brucite}$ =3.06 Å, the stacking axis c = 11.3 Å. The structural scheme by Organova (1989) suggests a slight surplus of metal in the sulfide layer and the above layer ratio equal to 0.55.

STRUCTURES COMPOSED OF SESQUICHALCOGENIDE LAYERS

Tetradymite series (selenides and tellurides of bismuth). Under ambient conditions, the orthorhombic structure of bismuthinite (Bi_2S_3) type is limited to the sulfide of bismuth. At high pressures, however, it is also assumed by the selenide of bismuth. Otherwise, with the polarizable anions Se and Te, bismuth forms a series of layer-like selenide/telluride or more complex structures. On the one hand, these can be extended to subselenides and subtellurides with a portion of Bi-Bi bonds present and, on the other hand, layers of this series may be modified to incorporate suitable divalent cations, originating yet another, parallel structural series (Table 8). The works on the structural classification of this series include Bayliss (1991), Strunz and Nickel (2001), and Cook et al. (in press).

The fundamental unit layer of this series is an octahedral double layer Bi_2X_3, consisting of three hexagonal anion sheets in an ABC stacking sequence, with intermediate Bi atoms in slightly eccentric octahedral coordination (Fig. 9a). A complete sheet- and layer-stacking sequence is AcBaC-BaCbA-CbAcB, with anion sheets symbolized by capitals, cation sheets by lower-case letters, and anion-anion contacts without cation interlayer by hyphenation.

Bismuth-anion bonds to the median sheet of anions are longer than those to the marginal sheets. In Bi_2Se_3 these distances are 3.30 Å and 2.89 Å, respectively; in Bi_2Te_3 they are 3.26 Å and 3.07 Å, in the same sequence (Fig. 9b). Tetradymite, Bi_2Te_2S, accommodates sulfur in the median plane (central anion sheet, with Bi-S equal to 3.06 Å) and tellurium in the outer sheets (Bi-Te 3.13 Å) (Fig. 10a); here the difference between anion radii comes into play. On the other hand, in skippenite, Bi_2Se_2Te, with 10% sulfur substituting for Te, tellurium fills the central plane of the slab (Bi-(Te,S) 3.06 Å), and Se forms its boundary sheets (Bi-Se 2.93 Å).

The anion surfaces of two adjacent double-layers show a eutactic relationship, with the interlayer *X-X* distance of 3.70–3.65 Å for Te and 3.51 Å for Se. These are van der Waals contacts across planes of excellent cleavage. The Se-Se distances are 4.14 Å and 4.23 Å in the marginal sheets and the interior of a double layer of Bi_2S_3, obviously as a result of the coordination requirements of Bi. This fundamental Bi_2X_3 structure has symmetry $R\bar{3}m$ (Table 8).

At lower anion fugacities (native bismuth is not a rare constituent of ore deposits with

Table 8. Selected structures of the tetradymite family

Mineral	Formula	Space Group	Lattice Parameters (Å,°)			Ref.
			a	*c*	γ	
tsumoite	BiTe	$P\bar{3}m1$	4.422	24.050	120	[1]
nevskite	BiSe	$P\bar{3}m1$	4.212	22.942	120	[2]
telluronevskite	Bi_3Se_2Te	$P\bar{3}m1$	4.264	23.25	120	[3]
paraguanajuatite	Bi_2Se_3	$R\bar{3}m$	4.143	28.636	120	[4]
kawazulite	Bi_2Te_2Se	$R\bar{3}m$	4.298	29.774	120	[4]
tellurobismutite	Bi_2Te_3	$R\bar{3}m$	4.395	30.440	120	[5]
tetradymite	Bi_2Te_2S	$R\bar{3}$	10.33	—	24.17	[6]
skippenite	Bi_2Se_2Te	$R\bar{3}m$	4.183	29.137	120	[7]
laitakarite	Bi_4Se_3	$R\bar{3}m$	4.27	40.0	120	[8]
rucklidgeite	$PbBi_2Te_4$	$R\bar{3}m$	4.452	41.531	120	[9]
kochkarite	$PbBi_4Te_7$	$P\bar{3}m$	4.44	71.7	120	[10]*

* Shelimova et al. (2004) indicate $P\bar{3}m1$, a = 4.426 Å, c = 23.892 Å

References: [1] Shimazaki and Ozawa 1978; [2] Gaudin et al. 1995; [3] Řídkošil et al. 2001; [4] Nakajima 1963; [5] Feutelais et al. 1993; [6] Harker 1934; [7]Bindi and Cipriani 2004; [8] Stasova 1968; [9] Zhukova and Zaslavskii 1972; [10] Talybov and Vainshtein 1962

bismuth sulfides and sulfosalts), the Bi_2X_3 layers can be intercalated by trigonal double-layers of covalently bonded bismuth. Such an intercalate in essence is a tightly-bonded double layer from the rhombohedral structure of native bismuth. In Bi_4Se_3, the Bi-Bi bonds in this double-layer are 3.04 Å long, whereas the Bi-Se distances to the surfaces of the Bi_2Se_3 layers are 3.46 Å. Bi_4Se_3 (laitakarite) is the limiting case of the series, in which the Bi_2 interlayer is intercalated at every *X*–*X* contact (Fig. 10b). Its presence has a pronounced influence on layer stacking, and it results in a partial sequence...B-a-c-B..., i.e., the lowermost and the uppermost anions of the two adjacent Bi_2X_3 double-layers are situated above one another. The Bi-Se distances in the interior of double-layers do not appear to be modified by this intercalation.

An ordered derivative with a Bi_2 interlayer in every second interlayer space is nevskite, BiSe (Gaudin et al. 1995) (Fig. 10c). Here, the intercalation appears to influence the distortion of the scheme of shorter and longer Bi-Se bonds in the octahedra adjacent to the intercalated double-layer of pure Bi. In telluronevskite, Bi_3Se_2Te (Řídkošil et al. 2001), tellurium forms anion sheets lining the interfaces between the telluroselenide double-layers, whereas the corresponding interspaces, which are occupied by the intercalated bismuth, are lined by selenium.

Incorporation of large divalent cations leads to MBi_2X_4 triple-octahedral layers (Fig. 10d). In the structure of $PbBi_4Te_7$, they alternate regularly with the double layers described above; in $PbBi_2Te_4$ they stand alone. Both structures (Table 8), however, were not sufficiently refined.

At present, at least 26 minerals of this series have been defined; caution should be exercised in the cases when the definition is based on powder data only: the visible reflections are usually limited to relatively low *d* values when compared to the unit cell *c* parameter derived from them. Based on inspection of the ranges of different published microprobe investigations, it is this author's opinion that many intermediate, disordered layer sequences may exist, both in the subselenide/subtelluride series and among the M^{2+} containing tellurides.

Both the subchalcogenide and the M^{2+}-containing series can be understood as individual homologous (polysomatic) series. Among the subsulfides, the Bi_2 layers are the unit-size

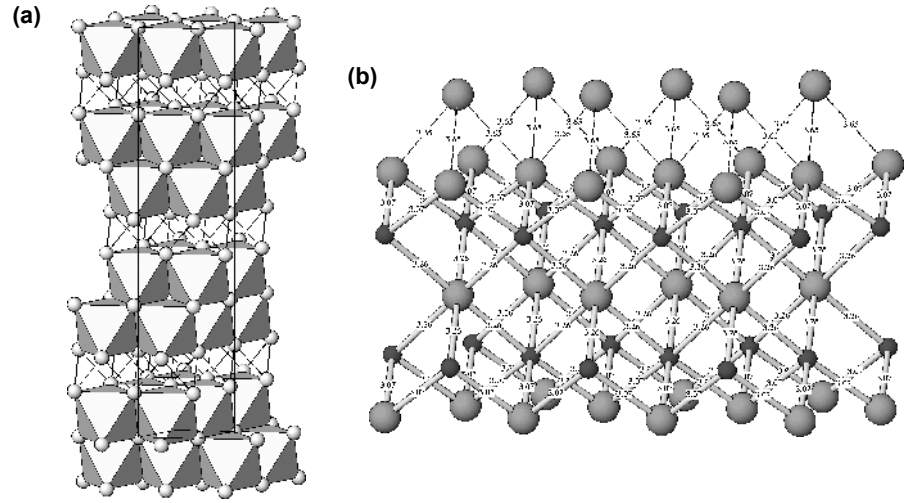

Figure 9. (a) Paraguanajuatite Bi_2Se_3 (Nakajima 1963). Double layers of coordination octahedra of bismuth are separated by long van der Waals Se-Se interactions. ABC packing of double layers. (b) Configuration details for Bi (black spheres) and Te (large spheres) in tellurobismutite, Bi_2Te_3 (Feutelais et al. 1993). One double-layer and a contact to an adjacent layer are shown.

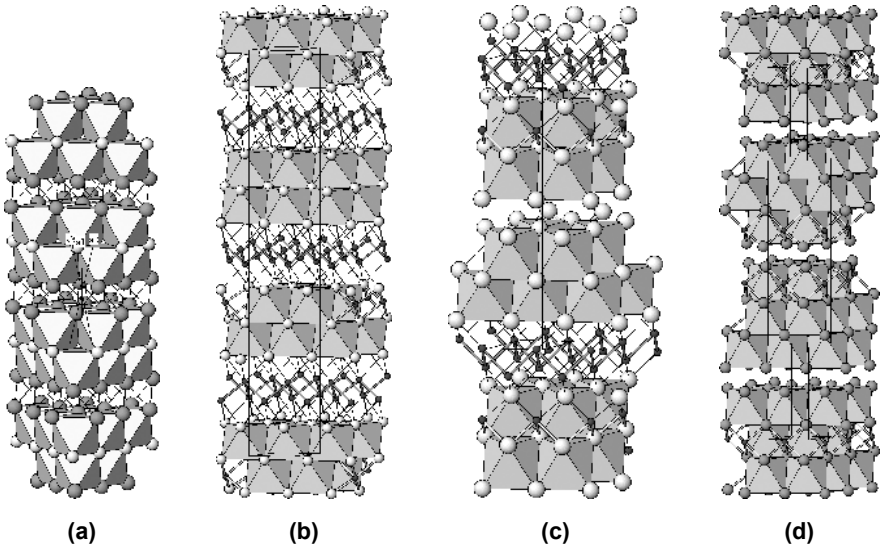

Figure 10. (a) Distribution of sulfur (light spheres) and tellurium (dark spheres) in double-octahedral layers of tetradymite Bi_2Te_2S (Harker 1934). (b) Laitakarite Bi_4Se_3 (Stasova 1968). Double-octahedral layers Bi_2Se_3 alternate with corrugated Bi_2 layers. The latter Bi atoms are coordinated to 3 Bi at 3.04 Å and 3 Se at 3.46 Å. (c) Nevskite BiSe (Gaudin et al. 1995). Bi_2Se_3 double layers are alternately in van der Waals Se-Se contact and intercalated by corrugated Bi_2 layers. Tsumoite BiTe is isotypic. (d) $PbBi_2Te_4$ (Zhukova and Zaslavskii 1972). Pb is concentrated in the central octahedral layer, Bi in the marginal octahedral layers of a three-layer packet. ABC stacking of layer packets.

portions of one end-member (rhombohedral Bi) and they are combined with one, two or more Bi_2X_3 layers separating them in consecutive polysomes. Pure Bi_2X_3 structures are the other pole of the series. An analogous scheme can be constructed for the combination of Bi_2X_3 and MBi_2S_4 layers. Layers thicker than the triple-octahedral MBi_2X_4 appear largely hypothetical at present (Cook et al. in press).

STRUCTURES COMPOSED OF DICHALCOGENIDE LAYERS

Layer-like MS_2 structures. The layer-like MS_2 structures consist of MS_2 layers in which a sheet of central cations is sandwiched between sheets of anions (S, Se, Te). Adjacent layers adhere via van der Waals contacts between their marginal anion sheets. The electrostatic repulsion of anions on these contacts is reduced by the strongly covalent character of *M-X* bonds, which limits the extent of electron transfer onto anions. Long *M-X* interactions, across the interlayer space, contribute to the stacking modes; each anion resides above three anions of the previous layer.

Besides the structure of berndtite, SnS_2 (Table 9), layer MS_2 structures are typical for transition metals on the left-hand side of each transition series: up to d^1 (Ti^{4+}), d^2 (Mo^{4+}) and d^3(Re^{4+}), respectively. In these cases, the *d* energy levels are high above the valence band. When we move along the transition series to the right, their energy decreases, until they start overlapping with the S-based valence band and draw electrons from it, giving disulfides such as pyrite instead of layer structures (Rouxel 1991; see also Vaughan and Rosso 2006, this volume).

In their basic form, these layer sulfides have very simple structures—regular stacking of either octahedral (Sn, Ti, high-temperature TaS_2 and $TaSe_2$, ReS_2) or trigonal-prismatic (Nb, Ta, Mo, W, Hf) layers (Figs. 11a-c). Compounds and solid solutions with one type of layer strongly predominate, layer sequences in which octahedral and prismatic layers mix are rare.

The schemes used to describe layer stacking include the standard polytype notation, e.g., 2H- or 3R-TaS_2; sheet stacking notations which are based on the prismatic layers denoted as AbA and octahedral ones as AbC, and the standard sections $(11\bar{2}0)$ in which both the layer type and the layer stacking are visible (Figs. 12a,b).

The two fundamental stacking modes of trigonal prismatic layers are 2H and 3R. Their stability differs; e.g., for MoS_2 the 2H polytype (Fig. 11c) is widespread whereas the 3R polytype (Fig. 13a) is assumed to have formed at lower temperatures. For octahedral layers, the 1T stacking (isotypic with CdI_2) or the 3R stacking (isotypic with $CdCl_2$) is present (Table 9).

Dependence on the conditions of formation has been investigated thoroughly for chalcogenides of the d^1 metals Nb and Ta. The octahedral 1T form of $TaSe_2$ is a stable high-temperature form whereas the intermediate, 4H and 6R polytypes with a mixed-layer character, in which there are sequences of regularly alternating octahedral and trigonal-prismatic layers (Fig. 13b), are secured by quenching from about 950 K. The trigonal prismatic 2H form is stable at room temperature (Wilson et al. 1975). Below a transition temperature, the simple structures of the layered polytypes of Ta and Nb become complicated by charge-density waves connected with a formation of superlattices and/or strong diffuse scattering (Wilson et al. 1975). Thus, at room temperature, the $4H_b$ polytype of $TaSe_2$ (a structure with alternating octahedral and trigonal-prismatic layers), forms an $a\sqrt{13} \times a\sqrt{13} \times c$ superstructure by the action of charge density waves in the octahedral layers.

These lamellar structures are eminently suited for intercalation of various cations (Fig. 13d). Besides the large, low-charge alkali cations, many other cations such as Cu or Bi, even H^+ and different organic cations, have been successfully intercalated (Table 9). The intercalated element *A* contributes an electron to the MX_2 layer, changing primarily the valence of the metal in the layer. It is a low-energy process and it is reversible, a subject of "soft chemistry" of practical

Table 9. Selected dichalcogenides with layer structures.

Mineral	Formula	Space group	Lattice Parameters (Å,°)				Ref.
			a	***b***	***c***	***Angle***	
Synth.	NbS_2	$R\bar{3}m$	3.330	3.330	17.918	γ 120	[1]
Synth.	NbS_2	$P6_3/mmc$	3.31	3.31	11.89	γ 120	[2]
Synth.	TaS_2-1T	$P\bar{3}m1$	3.365	3.365	5.897	γ 120	[3]
Synth.	TaS_2-2H	$P6_3/mmc$	3.314	3.314	12.097	γ 120	[4]
Synth.	TaS_2-6R	$R\bar{3}m$	3.335	3.335	35.85	γ 120	[5]
Synth.	$Ti_{1-x}S_2$	$P\bar{3}m1$	3.407	3.407	5.695	γ 120	[6]
Synth.	$Ti_{0.5}Nb_{0.5}S_2$	$P\bar{3}m1$	3.387	3.387	5.784	γ 120	[6]
Synth.	$Cu_{0.7}TiS_2$	$R\bar{3}m$	3.439	3.439	18.900	γ 120	[7]
Synth.	$Cu_{0.375}TiS_2$	$P\bar{3}m1$	3.415	3.415	5.855	γ 120	[8]
Synth.	$Li_{0.33}TiS_2$	$P\bar{3}m1$	3.444	3.444	14.0	γ 120	[9]
Synth.	$Ag_{0.167}TiS_2$	$P\bar{3}m1$	3.413	3.413	12.092	γ 120	[10]
Synth.	$[NH_4]_{0.22}TiS_2$	$R\bar{3}m$	3.418	3.418	41.81	γ 120	[11]
Synth.	$RbTiS_2$	$R\bar{3}m$	3.43	3.43	24.2	γ 120	[12]
Synth.	$Na_{0.3}TiS_2$	$R\bar{3}m$	3.406	3.406	38.20	γ 120	[13]
Synth.	$LiNbS_2$	$P6_3/mmc$	3.331	3.331	12.90	γ 120	[14]
Synth.	$NaNbS_2$	$P6_3/mmc$	3.336	3.336	14.52	γ 120	[14]
Synth.	$KNbS_2$	$P6_3/mmc$	3.345	3.345	16.22	γ 120	[14]
Synth.	$Nb_{1.09}S_2$	$R3m$	3.330	3.330	17.869	γ 120	[15]
Synth.	$Cs_{0.6}NbS_2$	$P6_3/mmc$	3.354	3.354	18.324	γ 120	[16]
Synth.	$Bi_{0.64}NbS_2$	$P6_3/mmc$	3.313	3.313	17.350	γ 120	[17]
Synth.	$H_{0.76}NbS_2$	$P6_3/mmc$	3.34	3.34	12.39	γ 120	[18]
Synth.	$Ge_{0.33}NbS_2$	$P6_3/mmc$	5.767	5.767	13.518	γ 120	[19]
Molybdenite 3R	MoS_2-3R	$R3m$	3.163	3.163	18.37	γ 120	[20]
Molybdenite 2H	MoS_2-2H	$P6_3/mmc$	3.161	3.161	12.295	γ 120	[20]
Drysdallite 2H	$MoSe_2$-2H	$P6_3/mmc$	3.289	3.289	12.927	γ 120	[21]
Synth.	$MoSe_2$-3R	$R3m$	3.292	3.292	19.392	γ 120	[22]
Tungstenite 2H	WS_2-2H	$P6_3/mmc$	3.153	3.153	12.323	γ 120	[23]
Tungstenite 3R	WS_2-3R	$R3m$	3.158	3.158	18.490	γ 120	[23]
Synth.*	$Mo_{0.5}Ta_{0.5}S_2$	$R3m$	3.252	3.252	18.138	γ 120	[24]
Synth.	$Mo_{0.2}TaS_2$	$P6_3/mmc$	3.29	3.29	12.30	γ 120	[25]
Synth.	$FeMo_2S_4$	$C\bar{1}c1$	11.815	6.550	13.014		[26]
Synth.	$LiMoS_2$	$P1$	6.963	6.386	6.250	α 88.60, β 89.07, γ 120.06	[27]
Synth.	$In_{0.25}MoSe_2$	$P6_3/mmc$	3.291	3.291	12.929		[28]
Berndtite 4H	SnS_2-4H	$P6_3/mc$	3.645	3.645	11.802	γ 120	[29]
Berndtite 2T	SnS_2-2T	$P\bar{3}m1$	3.638	3.638	5.88	γ 120	[30]
Synth.	$SnSe_2$-2T	$P\bar{3}m1$	3.811	3.811	6.137	γ 120	[31]
Synth.	$SnTaS_2$	$P6_3/mmc$	3.307	3.307	17.442	γ 120	[32]
Synth.	$SnNbS_2$	$P6_3/mmc$	3.324	3.324	17.37	γ 120	[32]
Synth.	$LiSnS_2$	$P\bar{3}m1$	3.67	3.67	7.90	γ 120	[33]
Synth.	$NaSnS_2$	$P\bar{1}$	3.69	3.69	25.54	γ 120	[33]
Synth.	$KSnS_2$	$R3m$	3.67	3.67	25.61	γ 120	[33]
Calaverite	$AuTe_2$	$C2/m$**	7.189	4.407	5.069	β 89.96	[34]
High P	$AuTe_2$	$P\bar{3}m1$	4.078	4.078	5.000	β 120	[34]
Sylvanite	$AuAgTe_4$	$P2/c$	8.95	4.478	14.62	β 145.35	[35]
Krennerite$^+$	$(Au,Ag)Te_2$	$Pma2$	16.58	8.849	4.464		[35]

Notes: *An example for the phases of the series $Mo_{0.05}Ta_{0.95}S_2$-$Mo_{0.9}Ta_{0.1}S_2$. $^+$ Unit-cell twinned octahedral layer stack. ** A subcell for a non-commensurately modulated structure

References: [1] Morosin 1974; [2] Jellinek et al. 1960; [3] Spijkerman et al. 1997; [4] Meetsma et al. 1990; [5] Jellinek 1962; [6] Furuseth 1992; [7] le Nagard et al. 1974; [8] Kusawake et al. 2000; [9] Hallak and Lee 1983; [10] Burr et al. 1990; [11] McKelvy et al. 1990; [12] Bichon et al. 1973; [13] Bouwmeester et al. 1982; [14] Omloo and Jellinek 1970; [15] Meerschaut and Deudon 2001; [16] Chen et al. 1993; [17] Eppinga and Wiegers 1980; [18] Riekel et al. 1979; [19] Pocha and Johrendt 2002; [20] Schoenfeld et al. 1983; [21] Bronsema et al. 1986; [22] Towle et al. 1966; [23] Schutte et al. 1987; [24] Remmert et al. 1994; [25] Saeki and Onoda 1987; [26] Vaqueiro et al. 2002; [27] Petkov et al. 2002; [28] Shamrai et al. 1986; [29] Guenter and Oswald 1968; [30] Hazen and Finger 1978; [31] Busch et al. 1961; [32] Eppinga and Wiegers 1977; [33] le Blanc and Rouxel 1972; [34] Reithmayer et al. 1993; [35] Pertlik 1984

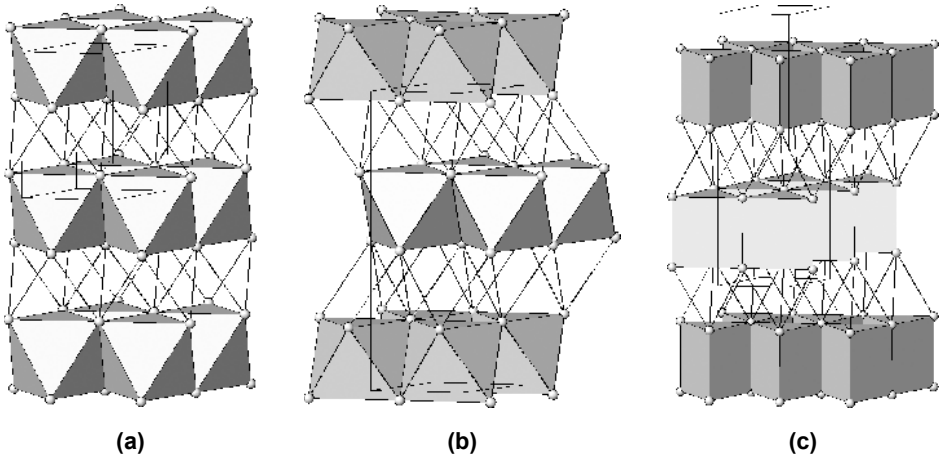

Figure 11. (a) 2H and (b) 4H polytypes of SnS_2, respectively, with octahedrally coordinated Sn^{4+}. Thin S-S connections help to outline the configuration of the interlayer space. (c) hexagonal 2H polytype of MoS_2 with a trigonal prismatic coordination of molybdenum.

importance as, e.g., in the $TiS_2 \leftrightarrow LiTiS_2$ cathode in lithium batteries (Rouxel 1991). The influence of selected substitutions on unit cell parameters and stacking of these phases can also be seen in Table 9. This table also contains examples of layer structures slightly "pillared" by their own (or a very similar) cations, e.g., $Mo_{0.2}TaS_2$ (Saeki and Onoda 1987). Intercalated forms should be expected in nature.

The crystal structures of gold and gold-silver tellurides (Table 9) are layered MX_2 structures as well. Calaverite, $AuTe_2$, (space group $C2/m$, β 89.96°) consists of octahedral layers which display a non-commensurate modulation in one direction (Reithmayer et al. 1993). In the averaged structure, the octahedrally coordinated Au has two shorter Au-Te bonds (2.67 Å) in a trans-configuration and four longer distances, 2.97 Å. The average Te-Te distances are: one at 3.46 Å, in a trans position to the above Au-Te distance of 2.67 Å, and two at 3.20 Å, opposing the Au-Te distances of 2.97 Å. Apparently the latter distances are the sites of the majority of Te-Te bonds in the real, modulated structure. These bonds solve the problem created by the presence of Au^{3+} (instead of M^{4+}) in a layered MTe_2 structure. In the high-pressure form of $AuTe_2$, the layered structure becomes a regular, unmodulated $P\bar{3}m1$ MX_2 structure, which at the pressure of 5130 MPa has Au-Te bonds of 2.77 Å and uniform Te-Te distances of 3.13 Å (Reithmayer et al. 1993).

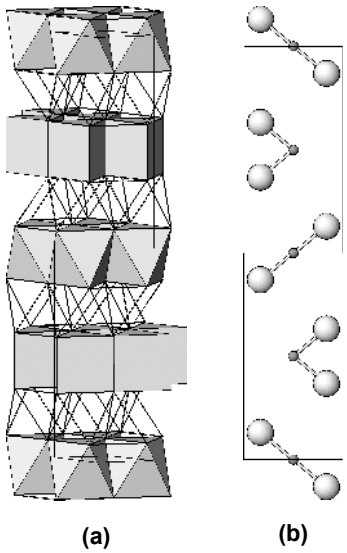

Figure 12. Example of the graphical shorthand used in the literature for the layered structures composed of octahedral and trigonal prismatic layers: (a) the crystal structure of $TaSe_2$ composed of alternating layer types, and (b) its illustration as cation and anion sites in a $(11\bar{2}0)$ section of the hexagonal cell.

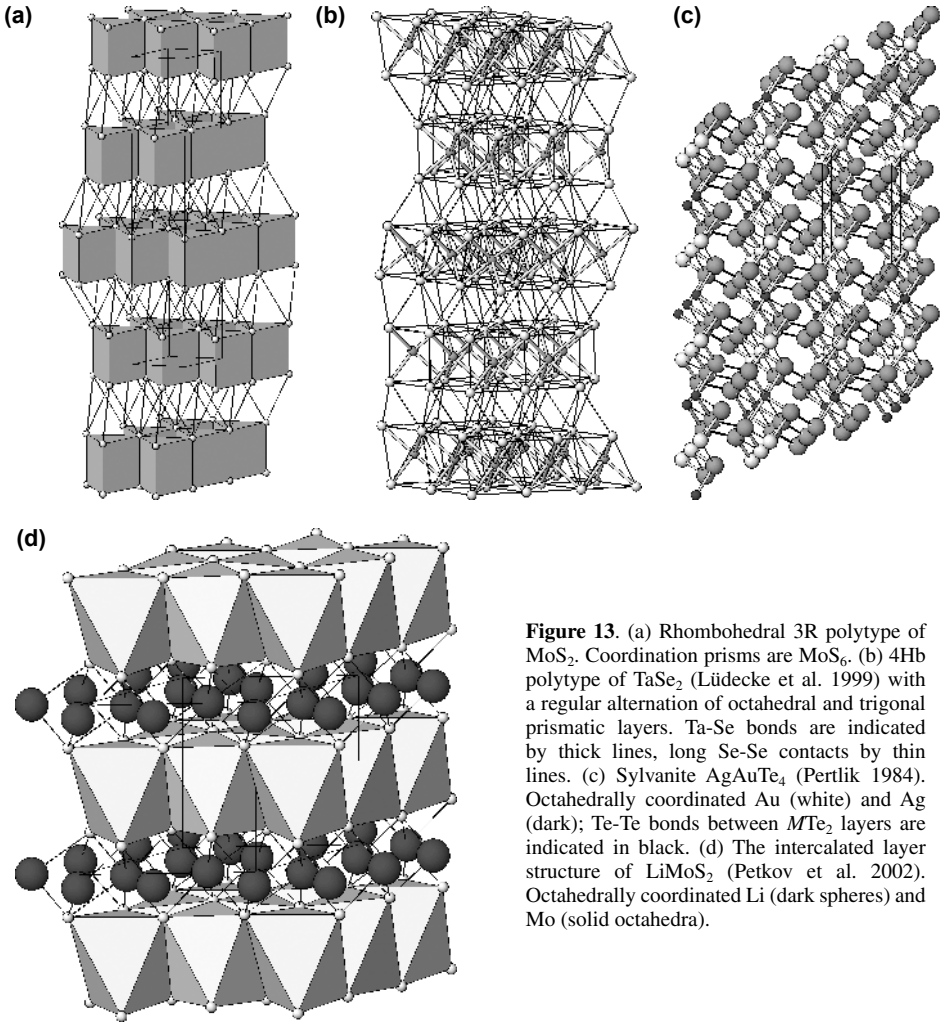

Figure 13. (a) Rhombohedral 3R polytype of MoS_2. Coordination prisms are MoS_6. (b) 4Hb polytype of $TaSe_2$ (Lüdecke et al. 1999) with a regular alternation of octahedral and trigonal prismatic layers. Ta-Se bonds are indicated by thick lines, long Se-Se contacts by thin lines. (c) Sylvanite $AgAuTe_4$ (Pertlik 1984). Octahedrally coordinated Au (white) and Ag (dark); Te-Te bonds between MTe$_2$ layers are indicated in black. (d) The intercalated layer structure of $LiMoS_2$ (Petkov et al. 2002). Octahedrally coordinated Li (dark spheres) and Mo (solid octahedra).

The mutual shift of MX_2 layers out of the close-packed situation, observed in calaverite, is even more pronounced in sylvanite, $AuAgTe_2$ (Pertlik 1984) (Fig. 13c). The interlayer Te-Te bond is 2.82 Å long. The cation octahedra are asymmetric, 2 × 2.74 Å, 2 × 2.93 Å, and 2 × 3.23 Å for Ag, and close to a square coordination for Au: 2 × 2.68 Å, 2 × 2.69 Å, and 2 × 3.33 Å. The short distances are in a *trans* configuration for both cations. The dimorph of $AuTe_2$, krennerite $(Au_{0.81}Ag_{0.12})Te_2$ (space group *Pma*2) is a unit-cell twinned version of a layered MX_2 structure, twinned on every fourth octahedron of the sequence.

LAYER-LIKE STRUCTURES WITH TWO TYPES OF CHALCOGENIDE LAYERS

Cannizzarite and related structures

Cannizzarite, ~$Pb_{48}Bi_{54}S_{127}$, (Fig. 2a) is believed to form a true variable-fit series. The

structure consists of a regular alternation of (two atomic sheets) thick pseudotetragonal layers and of double-octahedral layers. Both layers are occupied by a mixture of Pb and Bi. The pyramidal sites of the Q layer form distorted capped trigonal prismatic sites and, in some cases, distorted octahedral sites by extending across the interlayer space. The two layers are mutually non-commensurate, $b_H = b_{Qprimitive}$ and $c_H > c_{Qprimitive}$ (e.g., $17c_Q$ approximately corresponds to $10c_H$).

Matzat (1969) found a match of 46 subcells of the pseudotetragonal (Q) layer with 27 centered orthohexagonal subcells of the pseudohexagonal (H) layer (Fig. 3), i.e., practically a non-commensurate structure. There are a number of near-matches between the two layer sets in this model. Should these be fully materialized, the match of the two layer components, expressed as the match coefficient k in the reduced chemical formula $MS{\cdot}kM_2S_3$ (0.587 for the above case) will alter as follows: for 12Q/7H, the composition would be $Pb_{12}Bi_{14}S_{33}$, i.e., $k = 0.583$; for 17Q/10H, i.e., $Pb_{17}Bi_{20}S_{47}$, $k = 0.588$. For the very simple match, perhaps not attainable by the structure, 5Q/3H, i.e., the composition is $Pb_5Bi_6S_{14}$, and $k = 0.600$. This scheme suggests that very small changes in chemical composition, requiring greater accuracy than provided by microprobe measurements, will lead to a change in the match ratio.

The cannizzarite interlayer match is typical for about equally large average cations in the Q and H layers (a mixture of Pb and Bi in both layer types). The $LaCrS_3$-like match, typical for the layer misfit compounds discussed elsewhere, occurs for the largest Q/H cation radius ratio. The Q layers in these "ABX_3 compounds" are turned by 45° compared with cannizzarite and the match ratios in them differ from cannizzarite (Makovicky and Hyde 1992). The cannizzarite interlayer match is the point of reference for interlayer matches in a number of Cu(or Ag)-Pb-Bi sulfosalts and Pb-Sb sulfosalts, in which different segments of this match occur in the interspaces with Q/H contacts.

In cannizzarite, the H layer is two octahedra thick, in the synthetic phase of Graham et al. (1953) it is presumably three octahedra thick, whereas in the $Cr_2Sn_3Se_7$ polymorph (Jobic et al. 1994) it is a single-octahedral layer, i.e, an accretional homologous relationship. A Q layer of the same thickness occurs in all these phases (Table 10).

Derivatives of cannizzarite: combinations of accretion with variable-fit

Cannizzarite (Fig. 2a) acts as a parent structure for the majority of layer-like structures of sulfosalts with non-commensurate layer contacts (Makovicky and Hyde 1981; Makovicky 1981, 1992; Ferraris et al. 2004) (Table 11). They represent stacks of alternating Q- and H-type layers with different thicknesses (not always the layer thicknesses observed in cannizzarite itself); they have similar match modes to cannizzarite and similar average cation radii. The layers, however, are periodically broken up into strips by different structural adjustments, avoiding the poor fit problems periodically encountered along the non-commensurate direction.

The structure of weibullite $Ag_{0.33}Pb_{5.33}Bi_{8.33}(S,Se)_{18}$ (Mumme 1980) is the most obvious derivative of cannizzarite, obtained by shearing its layers by means of composition non-conservative glide planes (Fig. 2b). Due to the necessity to satisfy both the accretional and the variable-fit principles, the nearest lower homologue of weibullite is structurally very distant from it. It is the short-range structure of galenobismutite, $PbBi_2S_4$. This structure combines pairs of distorted octahedra of Bi, those of "lying" monocapped trigonal prisms of Bi and "standing" bicapped trigonal prisms of Pb; it shows affinity to that of $CaFe_2O_4$ (Mumme 1980). For the second and third cation site, Pinto et al. (in press) indicate mixed (Bi, Pb) and (Pb, Bi) occupancies. In the "weibullite-like" expansion (parallel to a of galenobismutite) the ½ subcell broad Q module in galenobismutite expands to 5½ subcells in weibullite, whereas the ½ H subcell (i.e., 1 octahedron) broad pseudohexagonal module expands to a 3½ H subcells long layer fragment (compare Figs. 14a and 2b).

Table 10. Selected cannizzarite homologues.

Mineral	Formula	Cell Type	Lattice Parameters [Å,°]				Space Group	Ref.
			a	*b*	*c*	β		
Cannizzarite	$Pb_{46}Bi_{54}S_{127}$ [a]	Unit cell	189.8	4.09	74.06	11.9	$P2_1/m$	[1]
		Q subcell	4.13	4.09	15.48	98.6	$P2_1/m$	
		H subcell	7.03	4.09	15.46	98.0	$C2/m$	
Synth.	$Pb_{38}Bi_{28}S_{80}$ [a]	Q subcell	4.11	4.08	18.58	93.6	$P2/m$ [b]	[2]
		H subcell	7.03	4.08	27.16	93.6	$F2/m$	
		unit cell n.d.						
Synth.	$Cr_2Sn_3Se_7$	Unit cell	12.77	3.84	11.79	105.2	$P2_1/m$	[3]

Notes: n.d. = not determined; [a] The compositions are derived from the crystal structure; [b] Probably $P2_1/m$ [Matzat 1979].
References: [1] Matzat 1979; [2] Graham et al. 1953; [3] Jobic et al. 1994

Table 11. Selected plesiotypes based on a cannizzarite structure type.

Mineral	Formula	Lattice Parameters (Å)			β (°)	S.G.	Ref.
Galenobismutite	$PbBi_2S_4$	*a* 11.81	*b* 14.59	*c* 4.08	—	*Pnam*	[1]
Weibullite	$Ag_{0.33}Pb_{5.33}Bi_{8.33}(S,Se)_{18}$	*a* 53.68	*c* 15.42	*b* 4.11	—	*Pnma*	[2]
Synth.	$Pb_4In_3Bi_7S_{18}$	*a* 21.02	*b* 4.01	*c* 18.90	971	$P2_1/m$	[3]
Junoite[b]	$Cu_2Pb_3Bi_8(S,Se)_{16}$	26.66	4.06	17.03	127.2	$C2/m$	[4]
Felbertalite[b]	$Cu_2Pb_6Bi_8S_{19}$	27.64	4.05	20.74	131.3	$C2/m$	[5]
Proudite	$Cu_4Bi_{40}Pb_{32}(Se,S)_{94}$	31.81	4.10	36.56	109.3	$C2/m$	[6]
Nordströmite	$CuPb_3Bi_7(S.Se)_{14}$	17.98	4.11	17.62	94.3	$P2_1/m$	[7]
Neyite	$Ag_2Cu_6Pb_{25}Bi_{26}S_{68}$	3753	407	4370	1088	$C2/m$	[8]
Synth.	$Pb_3In_{6.67}S_{13}$[a]	*a* 38.13	*c* 3.87	*b* 13.81	γ 91.3	$B2/m$	[9]
Synth.	$Bi_3In_5S_{12}$	33.13	3.87	14.41	91.2	$C2/m$	[10]

Notes: [a] 1/3 *M* is vacant in one metal site. [b] Homologues $N = 1$ and $N = 2$, respectively, of the junoite homologous series.
References: [1] Pinto et al. submitted; [2] Mumme 1980; [3] Krämer and Reis 1986; [4] Mumme 1975; [5] Topa et al. 2000; [6] Mumme, oral comm.; [7] Mumme 1980; [8] Makovicky et al. 2001; [9] Ginderow 1978; [10] Krämer 1980

A simple solution to the mismatch problem occurs when the pseudotetragonal layer fragment A continues laterally as a pseudohexagonal layer fragment B and vice versa. The misfit problems of the pseudotetragonal and pseudohexagonal layers facing one another are solved and compensated for by this periodical reversal (Makovicky and Hyde, 1992; Ferraris et al. 2004). A simple example of this phenomenon is the orthorhombic polymorph of $Cr_2Sn_3Se_7$ (Jobic et al.1995)(Fig. 16a) in which the interior match is identical to that of the above mentioned layer-like polymorph, but it is periodically reversed after a width of three peudotetragonal polyhedra.

Other derivatives of cannizzarite are members of the pair junoite $Cu_2Pb_3Bi_8(S,Se)_{16}$ - felbertalite $Cu_2Pb_6Bi_8S_{19}$ (Mumme 1975 and Topa et al. 2000). These structures are composed of fragments of $(100)_{PbS}$ layer, 2 atomic sheets thick and 3 coordination polyhedra broad (stippled in Figs. 14b,c), alternating with en échelon fragments of $(111)_{PbS}$ octahedral layers which have a thickness of one octahedron (Fig. 14b) or two octahedra (Fig. 14c).

Owing to the differences in the thickness of their octahedral layers, these two compounds were recognized as the first and second homologue of an accretional homologous series (Topa

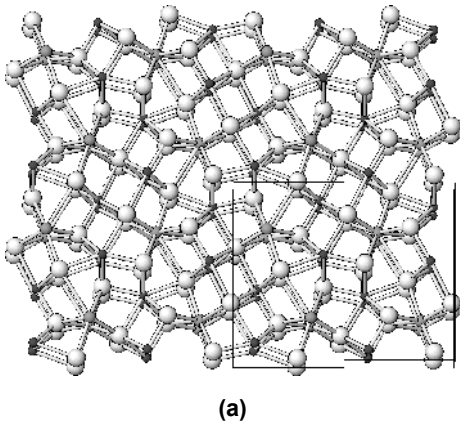

Figure 14. Structures derived from the structural principles observed in cannizzarite. (a) Galenobismutite $PbBi_2S_4$. S: light spheres, Pb: light grey; Bi: dark grey. (b) Junoite $CuPb_3Bi_7(S,Se)_{14}$ (Mumme 1980), the $N = 1$ member of the junoite-felbertalite homologous pair. (c) Felbertalite $Cu_2Pb_6Bi_8S_{19}$ (Topa et al. 2000), the $N = 2$ homologue of this pair. In (b) and (c), in order of increasing size, circles indicate Cu, Bi, Pb and S. Sheared pseudohexagonal slabs are ruled, pseudotetragonal ribbon-like fragments with pairs of Cu tetrahedra in the step regions are stippled. Shading of all circles indicates two levels of the 4 Å structure, 2 Å apart. (d) Neyite $Ag_2Cu_6Pb_{25}Bi_{26}S_{68}$ (Makovicky et al. 2001), with two types of blocks indicated by different shades of grey, and with the subvertical layers left unshaded. In order of decreasing size, circles describe S, Pb, Bi, Ag (linear coordination) and Cu.

et al. 2000). The next member of the accretional sequence, with triple octahedral layers and (two atomic sheets thick) pseudotetragonal slab fragments was not found as an independent phase but forms a substantial part of the box-work structure of neyite $Ag_2Cu_6Pb_{25}Bi_{26}S_{68}$ (Makovicky et al. 2001) (Fig. 14d). Junoite participates in another homologous series, in which the layer thicknesses are preserved but the length of straight layer portions between two adjacent kinks varies. The shortest member of this series is the pavonite homologue $N = 3$ (Tomeoka et al.1980), the longest one is proudite (Mumme, pers. comm.).

Zero mutual shift of octahedral fragments in the case of felbertalite and the plus-one-octahedron shift for junoite (compare Figs. 14b,c) were both adopted by these sulfosalts in order to create a lone electron pair micelle*,* i.e., an extended common space for lone electron pairs of bismuth in the overlapped, kinked portions of the $(111)_{PbS}$ layer. For octahedral elements without active lone electron pairs, other shift geometries might be formed instead. This, and other examples (e.g.*,* the pairs $Pb_4Sb_6S_{11}$ (robinsonite)–$Pb_5Sb_6S_{14}$ (synthetic) and $Pb_5Sb_4S_{11}$ (boulangerite)–$Pb_7Sb_4S_{13}$ (synthetic), led to a definition of a "sliding series of structures" described in Ferraris et al. (2004), in which complex structural slabs slide past one another by increments, gradually creating new coordination sites at their stepped interface.

Selected synthetic and natural chalcogenides with layer-misfit structures

The family of synthetic sulfides known as layer-misfit structures or alternatively as "ABX_3" sulfides (or sulfides with alternating incommensurate layers) is composed of pseudotetragonal *MX* layers which can be described as (100) slices of NaCl/PbS type, interleaved with MX_2 octahedral layers which are (111) slices of NaCl type or, alternatively, with trigonal-prismatic layers (0001) of NbS_2 (Figs. 15a,b). The A cation in the pseudotetragonal layers can be a lanthanide ion, Pb, Sn^{2+}, Bi,.... whereas the B cation is Ti, V, Cr,...in the octahedral layers, and Nb or Ta in the trigonal prismatic layers (Table 12). Crystallography of these compounds implies non-integral valence of (presumably) cations. This may be a real situation (compare with the intercalates of NbS_2 etc.) or it may be an idealized situation in other cases (e.g., Rouxel et al. 1994; Moëlo et al. 1995). Detailed reviews of these topics have been written by Makovicky and Hyde (1992), Wiegers and Meerschaut (1992) and van Smaalen (1995).

The interlayer interactions of the "ABX_3" layer-like structures are weak, van der Waals and charge-transfer in nature, resulting in a weak modulation of the component layers. Still, the resulting mutual adjustment of the two layer sets preserves a high degree of order in the layer stacking (Kuypers et al. 1990) and the equality $b_Q = b_H$.

The bulk of these compounds are composed of two atomic sheets thick pseudotetragonal layers and single octahedral or trigonal-prismatic layers. Examples are $(LaS)_{1.14}NbS_2$ and $(PbS)_{1.14}NbS_2$ with trigonal-prismatic layers and $(PbS)_{1.13}VS_2$ with octahedral layers. Rarely, two trigonal prismatic layers are found sandwiched between adjacent pseudotetragonal layers, e.g.*,* in $PbNb_2S_5$ (Table 12) and three such layers, partly pillared by additional Nb in their van der Waals interspaces, in $(Gd_xSn_{1-x}S)_{1.16}(NbS_2)_3$ (Hoistad et al. 1995). Another complication of the simple basic scheme is observed in the structure of $(Pb_2FeS_3)_{0.58}NbS_2$ (Lafond et al. 1999), with three atomic sheets thick pseudotetragonal layers in which Pb assumes the exterior, half-octahedral positions and iron, split into a five-fold cluster of sub-sites, the interior, octahedral positions (Figs. 15a,b). As well as these non-commensurate cases, commensurate or, semi-commensurate cases exist, with the ratio of periodicities represented by a fairly simple ratio of small values. The 3Q:2H match is observed in the structures of $(SnS)_6(InS_2)_4$ (Adenis et al. 1986) and $Sn_{3.04}Cr_{1.9}Se_7$ (Jobic et al. 1994) (Fig. 15c). Here the interlayer space contains portions of two bicapped trigonal coordination prisms and an octahedron of (primarily) Sn.

Buckhornite, $(Pb_2BiS_3)(AuTe_2)$ (Effenberger et al. 2000) and nagyagite, $Pb(Sb,Pb)S_2(Au,Te)$ (Effenberger et al. 1999) are semi-commensurate composite structures.

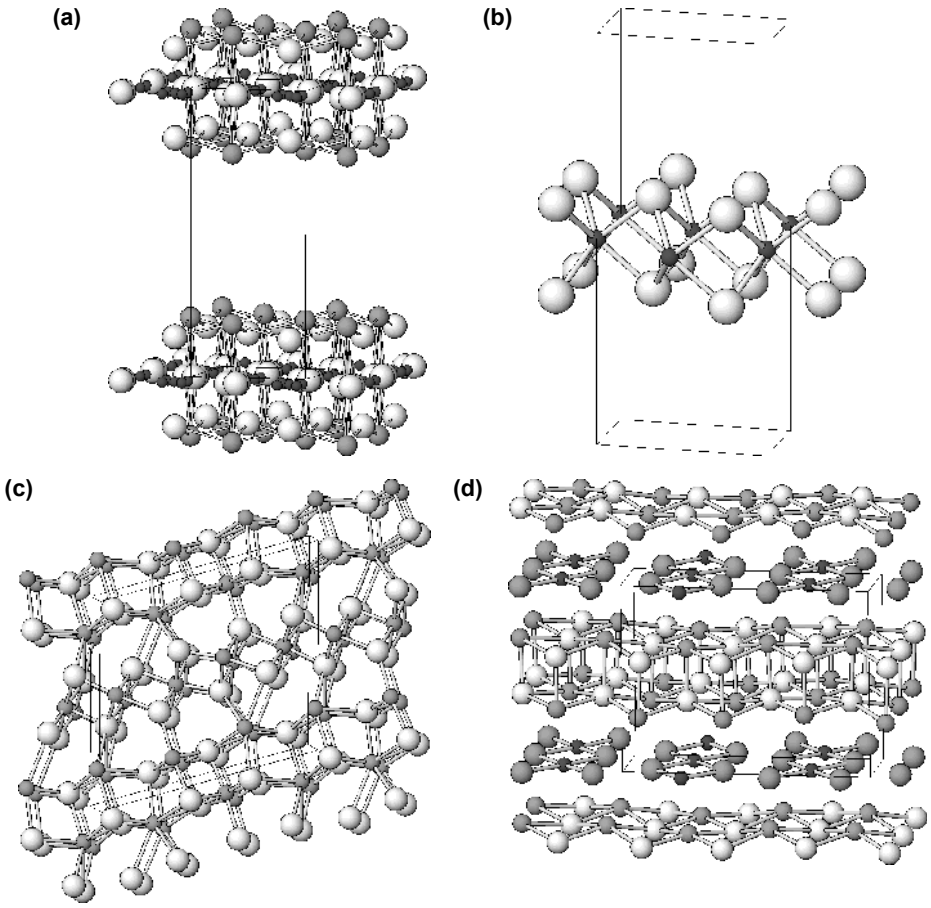

Figure 15. (a, b) Components of the layer-misfit structure of $(Pb_2FeS_3)_{0.58}NbS_2$ (Lafond et al. 1999). (a) The pseudotetragonal layer with Pb on the outside and statistical Fe sites in the interior, and (b) the intervening pseudohexagonal NbS_2 layer of trigonal prisms. (c) $Cr_3Sn_2S_7$ (Jobic et al. 1994). Pseudotetragonal layers are two atomic sheets thick and host primarily Sn^{2+}; pseudohexagonal (octahedral) layers contain primarily Cr^{3+}. Note the semi-commensurate match of the respective subperiodicities. (d) Buckhornite (Effenberger et al. 2000). Pseudotetragonal layers with Pb and Bi (undifferentiated, grey) in a square-pyramidal coordination are intercalated by telluride sheets with square planar Au (dark) coordination in $AuTe_2$ ribbons.

They consist of a combination of: (a) pseudotetragonal sulfide layers, respectively 2 atomic sheets thick and composed of Pb and Bi in the case of buckhornite, and 4 atomic sheets thick in an SnS like arrangement and composed of Pb and Sb in the case of nagyagite, with (b) single-atom thick sheets of tellurium involved in square planar coordination to the atoms of gold. In buckhornite, 3 subcells of the pseudotetragonal layer match with two subperiods of the telluride layer. The latter consist of ribbons of edge-sharing coordination squares of Au (Au-S = 2.70 Å), separated by strips of van der Waals Te-Te interactions (Te-Te = 3.34 Å) (Fig. 15d). Both the four atomic sheets thick sulfide layers of nagyagite, with Sb situated in their interiors, and the intervening Te coordinations, are asymmetric causing the structure to be polar. Both layers,or at least the telluride sheet, are positionally disordered. All the positions observed in the telluride sheet are mixed Te and Au sites.

Table 12. Selected non-commensurate, two-layer "ABX_3" structures

Compound	Comp. Layer	Space Group	Lattice Parameters (Å,°)			Match Q/H	Ref.*
			a, α	b, β	c, γ		
OCTAHEDRAL H LAYERS							
$(LaS)_{1.20}CrS_2$	Q: LaS	$C\bar{1}$	5.936	5.752	11.040	1.675	[1]
			α 90.33	β 95.30	γ 90.02		
	H: CrS_2		5.936	3.435	11.045		
			α 93.29	β 95.30	γ 90.02		
$(PbS)_{1.12}VS_2$	Q: PbS	$C121$	5.728	5.789	23.939	1.778	[2]
				β 98.95			
	H: VS_2		5.728	3.256	23.939		
				β 98.95			
$(SmS)_{1.25}TiS_2$	Q: SmS	$C211$	5.494	5.818	10.991	1.593	[3]
			α 95.38				
	H: TiS_2	$C2/m11$	3.448	5.821	21.990		
			α 95.40				
$(SnS)_{1.20}TiS_2$	Q: SnS	*tricl.*	5.833	5.683	11.680	1.666	[4]
			α 94.78	β 95.85	γ 90.03		
	H: TiS_2		5.835	3.412	23.288		
			α 90.30	β 95.86	γ 90.01		
$(SnS)_6(InS_2)_4$	Q: SnS	$P12_1/m1$	11.643	3.784	12.628	1.5	[5]
				β105.81			
	H: InS_2						
$(Sn_3Se_3)(Cr_{1.9}Sn_{0.04}Se_4)$		$P12_1/m1$	12.765	3.835	11.785	1.5	[6]
				β105.21			
	H:$CrSe_2$						
TRIGONAL PRISMATIC H LAYERS							
$(LaS)_{1.15}NbS_2$	Q: LaS	$Cm2a$	5.828	5.797	11.512	1.761	[7]
	H: NbS_2	$Fm2m$	3.310	5.797	23.043		
$(CeS)_{1.14}TaS_2$	Q: CeS	$Cm2a$	5.737	5.749	11.444	1.742	[8]
	H: TaS2	$Fm2m$	3.293	5.752	22.892		
$(PbS)_{1.14}NbS_2$	Q: PbS	$Cm2a$	5.834	5.801	11.902	1.761	[7]
	H: NbS_2	$Cm2m$	3.313	5.801	23.807		
$(PbS)_{1.14}(NbS_2)_2$	Q: PbS	$Cmc2_1$	5.829	5.775	35.861	1.752	[9]
	$H_{1,2}$: NbS_2	$Cmc2_1$	3.326	5.776	35.876		
$(SmS)_{1.19}TaS_2$	Q: SmS	$Fm2m$	5.562	5.648	22.56	1.690	[7]
	H: TaS_2	$Fm2m$	3.293	5.679	22.50		
$(YS)_{1.23}NbS_2$	Q: YS	$Fm2m$	5.393	5.658	22.284	1.623	[10]
	H: NbS_2	$C2$	3.322	5.662	11.13		
				β 92.62			
$(BiS)_{1.11}NbS_2$	Q: BiS	$F2mm$	5.752	36.156	23.001	1.809	[11]
	H: NbS_2	$F2mm$	5.750	3.331	23.000		
$(Pb_3FeS_3)_{0.58}NbS_2$	Q: Pb_2FeS_3	$Cmmm$	5.763	5.795	14.081	1.732	[12]
	H: NbS_2	$Cm2m$	3.328	5.795	14.081		
$(BiS)_{1.09}TaS_2$	Q: BiS	$Pm2m$	3.135	2.984	12.174	1.833	[13]
	H: TaS_2	$Fm2m$	3.421	5.970	24.341		

References: [1] Kato 1990; [2] Onoda et al. 1990; [3] Cario et al. 1997; [4] Wiegers et al. 1992; [5] Adenis et al. 1986; [6] Jobic et al. 1994; [7] Wiegers et al.1990; [8] de Boer et al 1991; [9] Meerschaut et al. 1990; [10] Rabu et al. 1990; [11] Gotoh et al. 1995; [12] Lafond et al. 1999; [13] Petříček et al. 1993

Cylindrite family: a doubly-noncommensurate example

Noncommensurability in two dimensions is typical for the chemically complex structures of the cylindrite-franckeite family of Pb-Sn^{2+}-Sn^{4+}-Sb-Fe sulfides, rather recently broadened to include similar compounds with Bi (and Cu) or As as well as synthetic selenides (Table 13). In this family, layers which are two or four atomic layers thick and based on the SnS archetype, alternate regularly with octahedral, essentially SnS_2 layers. Minor elements, Sb (Bi,As), and Fe (Cu) are believed to be distributed over both layer types.

The type compound, cylindrite, with average composition $FePb_3Sn_4Sb_2S_{14}$, has the coincidence mesh in terms of *b* and *c* parameters of pseudotetragonal subcells 19,0/0,13, or in terms of orthohexagonal subcells 30,0/0,12 (see below). Layer stacking proceeds in the *a* direction (Fig. 16b). Common geometrical and compositional modulation occurs along [001], resulting in the semi-commensurate match 13Q/12H. Along [010], there is incommensurate match, expressed as the empirical ratio 19Q/30H without a manifest modulation, i.e., the layers only have the repetition periods 5.79 Å and 3.67 Å, respectively (Makovicky 1976).

Pseudotetragonal layers are essentially (Pb,Sn^{2+})S with substitutions of minor elements; with the change in the Pb:Sn^{2+} ratio in these layers, a change in the c_Q/c_H ratio occurs, giving matches from 12Q/11H to 16Q/15H; variation in the ratio of *b* parameters was not systematized. The synthetic, all-Sn selenide cylindrite has a c_Q/c_H ratio of 11.5Q/10.5H, apparently as a result of containing selenium instead of sulfur (Makovicky et al. in prep.; Fig. 16b).

If the ratio of *b* axes is fixed in a simple way as $7b_Q = 11b_H$, the 12/11 ratio means a composition $(12\times7)M_4S_4 + (11\times11)M_2S_4$, resulting in an M_Q/M_H ratio of 1.388 and *M*/S ratio of 0.7048. In the same way, the ratio 16/15 gives an M_Q/M_H ratio equal to 1.358 but an *M*/S ratio of 0.7022, i.e., a very small change in the resulting valence distribution in this variable-fit series (Makovicky and Hyde 1992). Levyclaudite is a Pb rich, Cu-Bi containing analog of cylindrite.

Franckeite (Table 13) is closely related to cylindrite and displays all the above variations and a similar variable-fit series (Henriksen et al. 2002). It is an accretion homologue of cylindrite: the Q layers are 2 atomic layers thick in the latter, whereas they are 4 such layers thick in franckeite, stacked in a SnS-like fashion. Lengenbachite, approximating $Pb_{182}Ag_{45}Cu_{20}As_{117}S_{390}$ is a closely related structure with the semi-commensurate match fixed

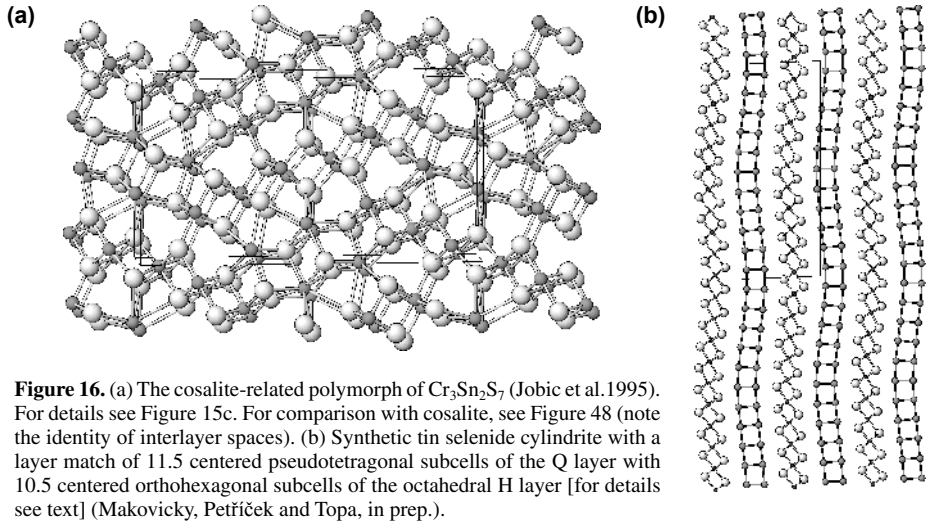

Figure 16. (a) The cosalite-related polymorph of $Cr_3Sn_2S_7$ (Jobic et al.1995). For details see Figure 15c. For comparison with cosalite, see Figure 48 (note the identity of interlayer spaces). (b) Synthetic tin selenide cylindrite with a layer match of 11.5 centered pseudotetragonal subcells of the Q layer with 10.5 centered orthohexagonal subcells of the octahedral H layer [for details see text] (Makovicky, Petříček and Topa, in prep.).

Table 13. Selected crystallographic data on the members of the cylindrite-franckeite series.

Compound		Q component		H component		Coin. data	Ref.
		Subcell	**Unit cell**	**Subcell**	**Unit cell**		
Cylindrite	*a*	11.73 Å	11.73 Å	11.71 Å	11.71 Å	13Q/12H	[1]
~$FePb_3Sn_4Sb_2S_{14}$	*b*	5.79 Å	5.79 Å	3.67 Å	3.67 Å		
	c	5.81 Å	75.53 Å	6.32 Å	37.92 Å		
	α	90°	90°	90°	90°		
	β	92.38°	92.38°	92.58°	92.58°		
	γ	93.87°	93.88°	90.85°	90.85°		
	S.gr.	A1	A1	A1	P1		
Potosiite	*a*	17.28 Å	17.28 Å	17.28 Å	17.28 Å	16Q/15H	[2]
~$Pb_{24}Ag_{0.2}Sn_{8.8}$	*b*	5.84 Å	5.84 Å	3.70 Å	3.70 Å		
$Sb_{7.8}Fe_{3.74}S_{55.6}$	*c*	5.88 Å	188.06 Å	6.26 Å	188.06 Å		
	α	90°	90°	90°	90°		
	β	92.2°	92.2°	92.2°	92.2°		
	γ	90°	90°	90°	90°		
	S.gr.	*A*1 or $A\bar{1}$	*P*1 or $P\bar{1}$	*A*1 or $A\bar{1}$	*A*1 or $A\bar{1}$		
Franckeite	*a*	17.3 Å		17.3 Å		16Q/15H	[3]
natural	*b*	5.84 Å		3.68 Å			
	c	5.90 Å		6.32 Å			
	α	91°		91°			
	β	95°		96°			
	γ	88°		88°			
	S.gr	$A\bar{1}$		$A\bar{1}$			
Lévyclaudite	*a*	11.84 Å		11.84 Å		13Q/12H	[4]
subcell	*b*	5.83 Å		3.67 Å			
	c	5.83 Å		6.31 Å			
	α	90°		90°			
	β	92.6°		92.6°			
	γ	90°		90°			
	S.gr.	*A*2/*m*, *A*2 or *Am*		*A*2/*m*, *A*2 or *Am*			
Langenbachite	*a*	36.89 Å	36.89 Å	36.89 Å	36.89 Å	12Q/11H	[5]*
	b	5.84 Å	11.68 Å	3.90 Å	11.68 Å		
	c	5.85 Å	70.16 Å	6.38 Å	70.16 Å		
	α	90°	90°	90°	90°		
	β	90°	90°	90°	90°		
	γ	91°	91°	91°	91°		
		A centered	*A* centered	*A* centered	*A* centered		

*Also other variants and stacking disorder of the H component are reported.
References: [1] Makovicky 1976; [2] Wolf et al. 1981; [3] Wang 1989; [4] Moëlo et al. 1990; [5] Makovicky et al. 1994

at 12Q/11H subcells in the *c* direction and at exactly 2Q/3H subcells in the *b* direction.

The match of the 13Q subcells tall A-centered "Q" cell with two 6H subcells tall, primitive orthohexagonal cells in cylindrite, and the corresponding 11.5Q/10.5H match in its synthetic Sn selenide analog, results in its OD character with 2 positions of the Q layer, ½ b_Q apart. The OD character becomes dominant in lengenbachite. It is caused by coincidences due to the combination of the $12c_Q/11c_H$ match with the exact $2b_Q/3b_H$ match. These coincidencies result in complete disorder of the H layer in lengenbachite (Makovicky et al. 1994).

STRUCTURES WITH 3D-FRAMEWORKS

Adamantane structures

The structures treated in this section can be considered as homeotypes of the structures of (cubic) diamond and lonsdaleite, the hexagonal diamond polymorph. Consequently, they have been named the adamantane structures by Parthé (1990). The common feature of adamantane structures is tetrahedral coordination of cations and anions. Simple adamantane structures are normal compounds, i.e., when all sites are occupied (C_nA_n) the valence electron concentration (VEC) on cations is four and that on anions, VEC_A is 8 (Parthé 1990). In defect adamantane structures (C_{n-p} vacancy$_p$ A_n), VEC_A is still 8 but VEC has to be larger than four. The anions surrounding the cation vacancy have non-bonding orbitals present. Experience shows that the defect adamantane structures exist for $4 \leq VEC \leq 4.923$, or the maximum number of vacancies are three out of eight potential tetrahedral cation sites (Parthé 1990). Cases with anion vacancies are rather rare and are connected with the presence of non-bonding "lone" electron pairs on some cations (such as Sb and As).

The adamantane compounds (Table 14) can be classified according to several criteria. The universally accepted fundamental categories are: (a) the homeotypes of cubic sphalerite; (b) those of hexagonal wurtzite, and (c) a few structures with combined hexagonal and cubic stacking sequences of cation tetrahedra. The site symmetries for cation tetrahedra in the ZnS aristotypes are $\bar{4}3m$ and $3m$, respectively, imposing different constraints on the occupying cations; these are transferred to a different degree onto cations in the homeotypes.

Across the boundaries of this classification, the adamantane compounds can be divided into:

(i) normal compounds C_nA_n, with both the cation and anion sites fully occupied;
(ii) compounds (omission derivatives) with vacancies in certain tetrahedral sites:
  (a) cation vacancies (e.g., Ga_4GeS_8);
  (b) anion vacancies (e.g., sinnerite $Cu_6As_4S_9$);
(iii) compounds ("stuffed derivatives") with additional cation tetrahedra occupied, in excess of the aristotype composition C_nA_n (e.g., talnakhite, $Cu_{18}Fe_{16}S_{32}$);
(iv) compounds with excess cation tetrahedra and cation vacancies present in one structure;
(v) structures with more complex modifications of certain parts (e.g., tetrahedrite, $Cu_{10}(Fe,Zn)_2Sb_4S_{13}$).

The third classificational principle divides the tetrahedral structures into binary, ternary, quaternary, etc., according to the number of distinct cations present in ordered substitution for the Zn of the aristotypes. This replacement results in a "tree" of sub- and supergroup relationships between the ZnS aristotypes and the homeotypes of various compositions. Ordered vacancies enter these relationships as well. Recently, Pfitzner and Reiser (2002), Pfitzner and Bernert (2004), and Bernert and Pfitzner (2005) have stressed the importance of the variability in volumes of different tetrahedra in the tetrahedral compounds (i.e.,in atomic radii of the species occupying these sites) for the preference of the structure for a wurtzite or sphalerite stacking principle.

Sphalerite–wurtzite. The two fundamental polytypes, cubic sphalerite and hexagonal wurtzite, differ by possessing *ccp* and *hcp* arrays of anions, respectively. Occupancy of a half of the tetrahedral positions in them, with the coordination tetrahedra of cations sharing only their corners, gives respective stackings of tetrahedral layers which have layer symmetry $P3m1$. When the tetrahedral positions in the initial layer are denoted as A, tetrahedra of the next layer can alternatively be positioned above the triangular voids of the first layer or above the S atoms joining three adjacent tetrahedra in this layer. Stacking according to the first principle results in

Table 14. Adamantane structures and their derivatives.

Mineral	Chemical Formula	Space Group	Lattice Parameters (Å,°)				Ref.
			a	*b*	*c*	Angle	
Chalcopyrite	$CuFeS_2$	$I\bar{4}2d$	5.289	5.289	10.423		[1]
Wurtzite	ZnS	$P6_3mc$	3.811	3.811	6.234	γ 120	[2]
Enargite	Cu_3AsS_4	$Pmn2_1$	7.413	6.440	6.158	—	[3]
Synth.	Cu_2MnGeS_4	$Pmn2_1$	7.635	6.527	6.244	—	[4]
Nowackiite	$Cu_6Zn_3As_4S_{12}$	$R3$	13.440	13.440	9.17	γ 120	[5]
Sinnerite	$Cu_6As_4S_9$	$P1$	9.064	9.830	9.078	α 90.00 β 109.50 γ 107.80	[6]
Talnakhite	$Cu_{18.3}Fe_{15.9}S_{32}$	$I\bar{4}3m$	10.593	10.593	10.593	—	[7]
Haycockite	$Cu_4Fe_5S_8$	$P222$	10.705	10.734	31.630	—	[8]
Mooihoekite	$Cu_9Fe_9S_{16}$	$P\bar{4}2m$	10.585	10.585	5.383	—	[9]
Colusite	$Cu_{24}As_6V_2S_{32}$	$P\bar{4}3n$	10.538	10.538	10.538	—	[10]
Arsenosulvanite	$Cu_{25.1}As_{5.6}V_{2.2}S_{32}$	$P\bar{4}3n$	10.527	10.527	10.527	—	[11]
Germanite	$Cu_{26}Ge_4Fe_4S_{32}$	$P\bar{4}3n$	10.586	10.586	10.586	—	[12]
Renierite	$Cu_{9.6}Fe_{3.6}Zn_{0.8}Ge_{1.5}As_{0.2}S_{16}$	$P\bar{4}2c$	10.623	10.623	10.551	—	[13]
Mawsonite	$Cu_6Fe_2SnS_8$	$P\bar{4}2m$	7.603	7.603	5.358	—	[14]
Sphalerite	ZnS	$F\bar{4}3m$	5.417	5.417	5.417	—	[15]
Stannite	$Cu_2Fe_{0.8}Zn_{0.2}SnS_4$	$I\bar{4}2m$	5.449	5.449	10.757	—	[16]
Kesterite	$Cu_2Zn_{0.7}Fe_{0.3}SnS_4$	$I\bar{4}$	5.427	5.427	10.871	—	[16]
Briartite	Cu_2FeGeS_4	$I\bar{4}2m$	5.325	5.325	10.51	—	[17]
Černyite	Cu_2CdSnS_4	$I\bar{4}2m$	5.487	5.487	10.848	—	[18]
Lenaite	$AgFeS_2$	$I\bar{4}2d$	5.66	5.66	10.3	—	[19]
Gallite	$CuGaS_2$	$I\bar{4}2d$	5.347	5.347	10.474	—	[20]
Synth.	$CuGaSe_2$	$I\bar{4}2d$	5.596	5.596	11.004	—	[20]
Synth.	$CuGaTe_2$	$I\bar{4}2d$	6.023	6.023	11.940	—	[21]
Famatinite	Cu_3SbS_4	$I\bar{4}2m$	5.385	5.385	10.754	—	[22]
Luzonite	Cu_3AsS_4	$I\bar{4}2m$	5.332	5.332	10.57	—	[23]
Stannoidite	$Cu_{16}Fe_{4.3}Zn_{1.7}Sn_4S_{24}$	$I222$	10.767	5.411	16.118	—	[24]
Sulvanite	Cu_3VS_4	$P\bar{4}3m$	5.393	5.393	5.393	—	[25]
Lautite	CuAsS	$Pna2_1$	11.35	5.546	3.749	—	[26]
Synth.	CuAsSe	$Pbcn$	11.75	6.79	19.21	—	[27]
Cubanite	$CuFe_2S_3$	$Pcmn$	6.457	11.093	6.223	—	[28]
Catamarcaite	Cu_6GeWS_8	$P6_3mc$	7.524	7.524	12.390	—	[29]
Kiddcreekite	Cu_6SnWS_8	$F***$	10.856	10.856	10.856	—	[30]
Synth.	$CdGa_2S_4$	$I\bar{4}$	5.553	5.553	10.172	—	[31]

References: [1] Hall and Stewart 1973; [2] Xu and Ching 1993; [3] Karanovic et al. 2002; [4] Bernert and Pfitzner 2005; [5] Marumo 1967; [6] Makovicky and Skinner 1975; [7] Hall and Gabe 1975; [8] Rowland and Hall 1975; [9] Hall and Rowland 1973; [10] Spry et al. 1994; [11] Frank-Kamenetskaya et al. 2002; [12] Tettenhorst and Corbato 1984; [13] Bernstein et al. 1989; [14] Szymanski 1976; [15] Agrawal et al. 1994; [16] Hall et al. 1978; [17] Wintenberger 1979; [18] Szymanski 1978; [19] Zhuze et al. 1958; [20] Abrahams and Bernstein 1973; [21] Leon et al. 1992; [22] Garin et al. 1972; [23] Marumo and Nowacki 1967; [24] Kudoh and Takeuchi 1976; [25] Mujica et al. 1998; [26] Craig and Stephenson 1965; [27] Whitfield 1981; [28] McCammon et al. 1992; [29] Putz et al. 2005; [30] Harris et al. 1984; [31] Gastaldi et al. 1985

layers with parallel orientation and a cubic stacking ABCABC... whereas stacking according to the second principle results in every other layer being in antiparallel orientation (its tetrahedra "reversed" in respect to the preceding layer) and the stacking sequence becomes AB′AB′. We choose to denote the "reversed" layers by priming. These situations are shown in Figs. 17a-b and 17c-d, respectively. Natural representatives are almost always these two polytypes, 3C (3-

layer repeat, cubic sphalerite) and 2H (2-layer repeat, hexagonal wurtzite). In a parallel notation used for polytypes (O'Keeffe and Hyde 1996), they possess stacking schemes *ccc* and *hh* where each symbol *c* signifies formation of a layer pair according to the cubic stacking principle and *h* a corresponding layer pair according to the hexagonal stacking principle. The reader is invited to consider these two notations using the examples given below. Cation site symmetry differs in these two structures, being $\bar{4}3m$ and $3m$, respectively. Thus, the Zn-S distances are 4×2.35 Å in sphalerite, and 3×2.31 Å plus 1×2.32 Å in wurtzite.

At present, 60 structure determinations on ZnS polytypes have been published (ICSD), not counting the repeated investigations on certain polytypes under non-ambient conditions. All these data fall into three categories:

1. Polytypes 2,4,6,8,10,12,14-, and 16H, as well as 20H, which have space group $P6_3mc$. The layer multiplicities are divisible by two, i.e., their layer stacks consist of two equal portions, always joined by an *h* stacking event. Thus, 4H has the stacking sequence *hchc*, 8H is *ccchccch*, 10H (Fig. 18a) is *cccchcccch*, and 20H is $(ccccccccch)_2$. In terms of tetrahedral layers 4H is ABC′B′, 8H is ABCAB′A′C′B′, and 20H is $C(ABC)_3A'(C'B'A')_3$.
2. Polytypes 15,18,24,30,36,42,48,54,60,66,72,78,84-, and 114R with the space group $R3m$. This group includes the cubic 3C polytype, in the structure of which a rhombohedral cell can be outlined as well. Their layer multiplicities are divisible by 3 and above 15H, also by six. Divisibility by three predicts a structure composed of three equivalent layer stacks in a rhombohedral arrangement which does not explain the additional divisibility by two. The lowest polytype, 3C, represents a *ccc* sequence (ABC) whereas the 15H polytype is an exceptional structure, *hhhhchhhhchhhhc*, i.e.,

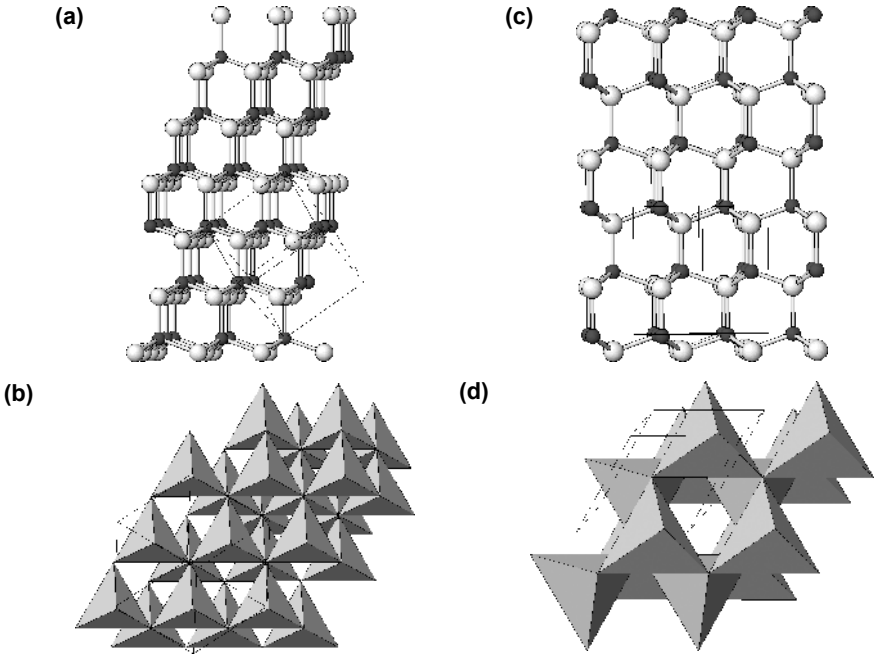

Figure 17. (a, b) Cubic 3C polytype of ZnS, sphalerite (Agrawal et al. 1994). Zn (dark) in tetrahedral coordination; ABC stacking of corner-sharing ZnS_4 tetrahedra. (c, d) Hexagonal 2H polytype of ZnS, wurtzite (Xu and Ching 1993). AB′AB′ stacking of ZnS_4 tetrahedra.

AB′ABC′BC′BCA′CA′CAB′, not known from the next higher homologue, 18H. This latter structure and the higher polytypes are actually composed of two alternating layer stacks with cubic sequences, always separated by a single *h* stacking event. Their multiplicities are in the ratio *n:*(*n*+*2*). Thus, 18R has the stacking sequence *hccchchccchchccchc,*and 24R is $(ccchcch)_3$. In the alternative notation these sequences are AB′A′C′B′ABC′B′A′C′BCA′C′B′A′C, and ABC′B′A′C′B′ABCA′C′B′A′C′BCAB′A′C′B′A′C. Finally, 36R has the stacking $(ccccchccccch)_3$, starting as ABCABC′B′A′C′B′A′C′, and followed by the rhombohedrally displaced variations of this sequence. As a result of the above-defined difference in layer multiplicities, each of the two cubic subsets is arranged in a rhombohedral stacking sequence (Fig. 18b); this difference also explains the divisibility by two.

3. Polytypes 10,12,14,16,18,20,22,24,26,28-, and 44H, with layer multiplicities again divisible by two, but with the terms below the 10-fold stack missing. The multiplicities combined with the space group *P*3*m* indicate that these structures ought to be composed of two alternating *c*-type layer stacks with generally different multiplicities, always separated by a single *h* event. Indeed, the *P*3*m*-10H structure (Fig. 18c; BAC′A′B′C′A′B′C′A′) is *hchccccccch* and *P*3*m*-20H is *hchccccchccccccchcc,*as two examples. Both these cases have $P6_3mc$ analogs which were quoted above.

Formation of the short-period polytypes obviously is a result of crystal-chemical factors. A lot of literature deals with the models for long-period polytypes. The ANNNI model, for example (Angel et al. 1985), and others have been summarized by Baronnet (1997). However, when amalgamated, the ZnS polytypes listed here amount to a fairly random incidence of combinations of two different or equal layer-stack thicknesses which, whenever they happen to satisfy a particular multiplicity ratio, produce a certain type of space group symmetry. There might be a human factor enhancing the frequency of observation of the first two categories from the above list in comparison to the last one, for which the structure determination is more difficult. The reader may have noticed the presence of "sphalerite-like blocks" of different thicknesses in the above polytype sequences. Mardix (1986) suggests that these thicknesses are a function of formation temperature. Propagation of these long-period sequences would be a result of growth mechanisms, such as screw dislocations perpendicular to the layer stacks.

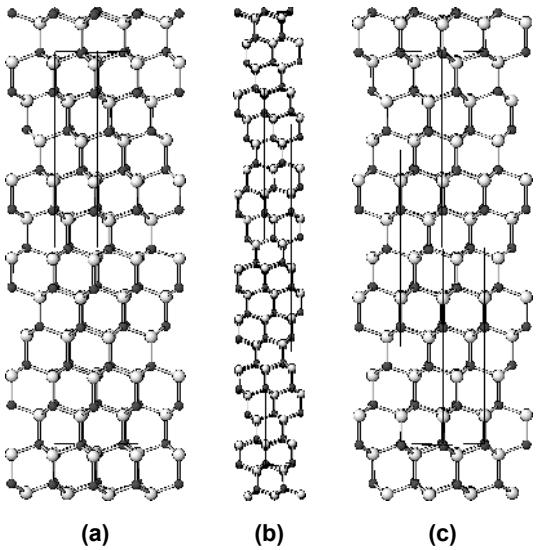

Figure 18. (a) The hexagonal 10H polytype of ZnS, space group $P6_3mc$. Zn: small black spheres. Projection on $(11\bar{2}0)$. The *h* stacking preserves orientation of ZnS_4 tetrahedra, *c* stacking (2 events) reverses it. (b) The rhombohedral 18R polytype of ZnS, space group *R*3*m*. A regular, repeating combination of *h* and *c* stacking principles. (c) The hexagonal 10H polytype of ZnS with the space group *P*3*m*1. Only two closely spaced events of *c* stacking (close to the top of the figure) occur in the *h* sequence. Compare this stacking sequence with that in (a); for discussion of all three sequences see the text.

Structures based on the sphalerite stacking principle

Chalcopyrite. The aristotype structure for ternary sulfides $C(1)C(2)A$ is that of chalcopyrite ($CuFeS_2$) (Fig. 19a). The tetragonal unit cell has $a_1 = a_2$ equal to that of the sphalerite aristotype, whereas the c parameter is twice the a parameter of sphalerite. The space group of this structure type is $I\bar{4}2d$. The structure consists of identical layers (001), with alternative cation sites (e.g., 000 and ½½0) occupied by the two cations (Cu and Fe, respectively in chalcopyrite). In the c direction, four such layers follow one another, with origin shifts $½a_1$, $½a_2$, $–½a_1$, $–½a_2$, producing the familiar Fe/Cu distribution in the unit cell of chalcopyrite. Neutron diffraction studies (Donnay et al. 1958) and Mössbauer investigations (summarized by DiGiuseppe et al. 1974) suggest that Cu in chalcopyrite is univalent whereas iron is trivalent. The Fe tetrahedron is very regular (Fe-S= 2.256 Å; tetrahedral angles 109.4°-109.6°), that of Cu is somewhat distorted (Cu-S=2.299 Å; 108.68°-111.06°). Lenaite $AgFeS_2$ (Zhuze et al. 1958) and gallite $CuGaS_2$ (Abrahams and Bernstein 1973) are isostructural, as also are $CuGaSe_2$ (Abrahams and Bernstein 1974), the technologically important $CuInS_2$ (Abrahams and Bernstein 1973), and $CuGaTe_2$ (Leon et al. 1992) (Table 14).

Kesterite and stannite. According to Hall et al. (1978), the normal quaternary adamantanes fall into two categories: the kesterite Cu_2ZnSnS_4 structure type, with the space group $I\bar{4}$, and the stannite Cu_2FeSnS_4 structure type, space group $I\bar{4}2m$. In terms of (001) tetrahedral layers, these are 2-layer structures, with two such layer pairs in one c period.

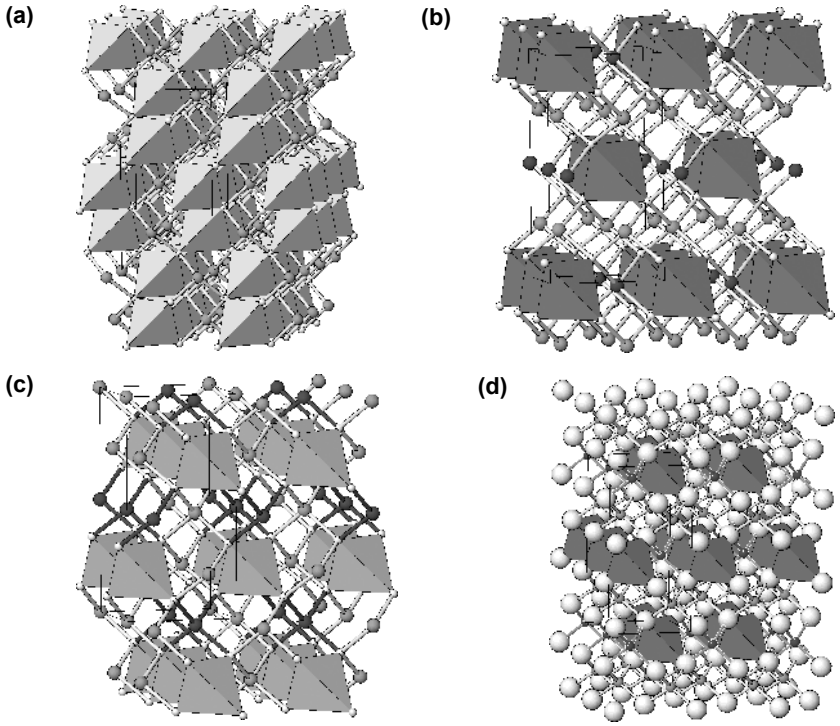

Figure 19. (a) Chalcopyrite $CuFeS_2$ (Hall and Stewart 1973). Fe coordination tetrahedra are shown as solid tetrahedra, the coordination of Cu (medium grey) by Cu-S bonds. (b) Stannite $Cu_2Fe_{0.8}Zn_{0.2}SnS_4$ (Hall et al. 1978). Solid tetrahedra: Fe, grey cations: Cu, black cations: Sn. (c) Kesterite $Cu_2Zn_{0.7}Fe_{0.3}SnS_4$ (Hall et al. 1978). Solid tetrahedra: Zn, grey and black cations: Cu and Sn, respectively. (d) Černyite Cu_2CdSnS_4 (Szymanski 1978). Solid tetrahedra: Sn, black cations: Cd, grey cations: Cu.

In stannite ($Cu_2Fe_{0.8}Zn_{0.2}SnS_4$, Hall et al. 1978), a layer of Fe and Sn tetrahedra (at $z = 0$ and ½; note *I* centration), occupied in a chess-board fashion by these two cations, alternates with a layer of copper tetrahedra (at $z = ¼$ and ¾)(Fig. 19b). According to Hall et al. (1978), in kesterite, $Cu_2Fe_{0.3}Zn_{0.7}SnS_4$, both layers have a chess-board occupation scheme: the tetrahedral layer at $z = 0$ and ½ is occupied by Sn and Cu whereas that at ¼ and ¾ by Zn and Cu. Hall et al. suggest that not only the Cu-Sn layer but also the Cu-Zn layer is ordered (Fig. 19c); the latter ordering reduces the space group to $I\bar{4}$.

Bonazzi et al. (2003) examined six crystal structures along the join stannite–kesterite quenched from 750 °C. They confirmed the structure scheme for stannite but found that the space group symmetry $I\bar{4}2m$ is valid for all compositions. As the Zn content increases, Zn moves progressively into the layer which was occupied by pure Cu in stannite and Cu moves into the Fe sites of stannite. For 70 mol% of stannite component, Cu is dominant in the latter site, which is marked by a break in the trend of unit cell parameters. The *c* parameter is rising whereas the *a* parameter is slightly decreasing until they "meet" at this point, as $2a \approx c$. The structure becomes and stays pseudocubic, with the above value approximately equal to 10.86 Å. Bonazzi et al.(2003) found that Cu and Zn are statistically distributed in the layers at $z = ¼$ and ¾, giving the space group $I\bar{4}2m$. The question whether there is a difference in the state of ordering between natural, hydrothermal samples and the synthetic products from 750 °C remains open. The same holds for the existence of a synthetic cubic stannite described by several investigators using powder diffraction, and recently refined by Rietveld method by Evstigneeva et al. (2001). For a complete list of stannite-kesterite related investigations see Bonazzi et al. (2003).

Other representatives. Briartite, Cu_2FeGeS_4 (Winterberger 1979) and černyite $Cu(Cd,In,Fe)SnS_4$ (Szymanski 1978) are isostructural with stannite, $I\bar{4}2m$. The alternation of the structural layers with larger cations (Cd and Sn) and those with smaller cations (Cu) leads to a marked flattening of Cu tetrahedra in černyite in the direction along the four-fold inversion axis (Fig. 19d). Famatinite Cu_3SbS_4 (Garin et al. 1972), with the same symmetry, $I\bar{4}2m$, has layers in which Sb tetrahedra alternate with tetrahedra of Cu; these layers are sandwiched by the tetrahedral layers which contain only copper (Fig. 20a). Thus, in spite of its 3:1 cation composition, it follows the same structural principles as the quaternary sulfides. Luzonite, Cu_3AsS_4 (Marumo and Nowacki 1967) has the same structure.

Structures based on the wurtzite stacking principle

Enargite (the latest one of several structure determinations is by Karanović et al. 2002), is a substitution derivative of wurtzite. The mutually identical tetrahedral (Cu_3AsS_4) (0001) layers have tetrahedra pointing in the $[00\bar{1}]$ direction. They are trigonal nets of Cu tetrahedra, one quarter of which are periodically replaced by As tetrahedra (Fig. 20b). The latter tetrahedra lie on lines that are one lattice *a* spacing (or one *b* spacing) apart; the resulting layer symmetry is *Pm*.

A more complicated substitution scheme is found in Cu_2MnGeS_4 (Bernert and Pfitzner 2005), also based on a wurtzite-like stacking. A single layer again has symmetry *Pm*, with [100] rows of pure Cu tetrahedra alternating with the combined Ge-Mn-Ge-Mn rows. The cited authors use this compound as an example of how the large differences in the volumes of component tetrahedra favour the wurtzite-type of layer stacking.

Adamantane structures with additional, interstitial tetrahedra

Colusite, $Cu_{24}As_6V_2S_{32}$ (Spry et al. 1994), space group, $P\bar{4}3n$, is an example of a compound with an additional tetrahedron, interstitial to the simple tetrahedral motif, and occupied by vanadium (Fig. 21a). It shares edges—and short metal-metal (Cu-V) contacts—with 6 surrounding copper tetrahedra. In a two-layer (001) representation (here in all three directions <100>), the VAs_2Cu_6 layer with symmetry $P\bar{4}2m$, alternates with a Cu_7As_2 layer,

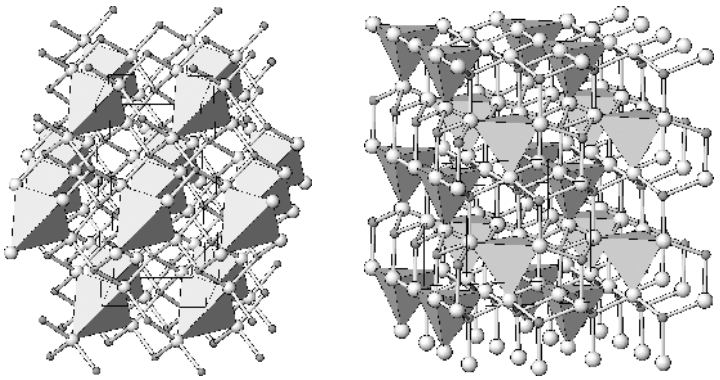

Figure 20. (a) Famatinite Cu_3SbS_4 (Garin et al. 1972). Solid tetrahedra: Sb^{5+}, grey cations: Cu^+. (b) Enargite Cu_3AsS_4 (Karanovic et al. 2002). Solid tetrahedra: As^{5+}, grey cations: Cu^+.

with the same layer group but with the origin shifted ; in both layer types the cations other than copper are much "diluted" against the 1:1 situation observed in the chalcopyrite group. In a 3D description, the As tetrahedra form an icosahedron around every V tetrahedron, with edge lengths of 5.33 and 6.52 Å; it also encloses nine Cu atoms (Fig. 21b). The interstitial position of vanadium is best appreciated in the edge-on view of tetrahedral (111) layers. The octahedral metal clusters (VCu_6) are widely dispersed, and represent flat-lying octahedra between adjacent sulfur (111) layers in this view (Fig. 21c).

Colusite is a mineral with a rather flexible composition; the number of (Cu+Fe+Zn) atoms in a formula unit with 32 S atoms varies from 24 (the above described structure scheme) to 28, whereas the number of V atoms stays at about two and the sum of As+Sb+Sn+Ge replacing one another stays equal to 6. Spry et al. (1994), Wagner and Monecke (2005) and Frank-Kamenetskaya et al. (2002) propose substitution mechanisms $(As,Sb)^{5+} \leftrightarrow (Sn,Ge)^{4+} + Cu^+$, $(As,Sb)^{5+} + Cu^+ \leftrightarrow (Sn,Ge)^{4+} + (Fe,Zn,Cu)^{2+}$, and, with some differences in interpretation, $V^{5+} \leftrightarrow V^{4+} + Cu^+$. Two of these mechanisms involve filling of the tetrahedra not occupied in the structure model described here.

Arsenosulvanite is $Cu_{25.1}V_{2.2}As_{5.6}S_{32}$, space group $P\bar{4}3n$ (Frank-Kamenetskaya et al. 2002). Its structure is composed of non-intersecting <100> rods of edge-sharing, alternating V and As tetrahedra, immersed in a matrix of Cu tetrahedra (Fig. 21d). In a description by means of (100) layers, Cu-rich Cu_7As layers of corner-connected tetrahedra alternate with $V_3As_2Cu_7$ layers which display a number of shared tetrahedral edges. Similar to colusite, As tetrahedra form an icosahedron (edges of 5.26 and 6.45 Å). It is centered upon Cu1, which is the Cu atom with 6 close Cu neighbours (Cu-Cu = 2.74 Å). The As-icosahedron has an octahedron of vanadium atoms inscribed, vanadium being positioned on 6 edges of the icosahedron. The metal coordinations around Cu1 and V, respectively, form a perovskite-like framework of corner-connected octahedra (only Cu surrounds Cu1 whereas 2As + 4Cu is situated around V). The unit cell *a* parameter is twice that of perovskite, and the configuration is *I*-centered, with Cu1 at 0,0,0. Sulfur decorates every second octahedral face, forming a tetrahedron interstitial to the perovskite-like motif.

The structure contains little cube-like subunits defined by metal-metal contacts along their edges: V-As-V (2 × 2.63 Å), V-Cu-V (2 × 2.63 Å), and V-Cu-Cu (2.52 & 2.74 Å); these contacts are present (the last one twice) in each of the <100> *M-M* rows.The entire scheme of edge-sharing tetrahedra, leaving only Cu4 as a corner-sharing tetrahedron, is analogous to that

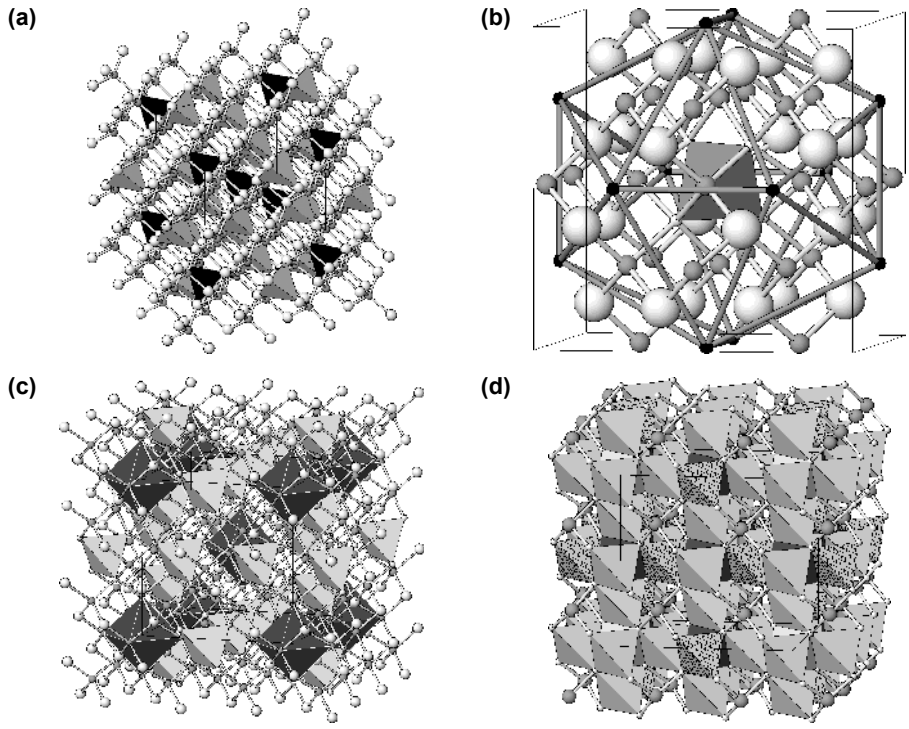

Figure 21. (a) Colusite $Cu_{24}As_6V_2S_{32}$ (Spry et al. 1994). Tetrahedral stacking (As: grey tetrahedra) with interstitial vanadium tetrahedra shown in black. (b) Icosahedral configuration of arsenic (black) around a central coordination tetrahedron of V in colusite; Cu atoms in grey. (c) Octahedral VCu_6 metal clusters (black) in the crystal structure of colusite. Coordination tetrahedra of As are grey. (d) Arsenosulvanite (Frank-Kamenetskaya et al. 2002). Edge-sharing solid tetrahedra form a "scaffolding": grey tetrahedra contain Cu, cross-hatched As, and black V. Interstitial, corner-sharing tetrahedrally coordinated cations: Cu (grey spheres).

observed in sulvanite but is populated by a complex combination of 3 elements. Cu1 and V are the nodes of this 3D framework. Furthermore, the positions of Cu4 are empty in sulvanite; these two phases are therefore quite distinct minerals.

Talnakhite, mooihoekite and haycockite. The crystal structure of talnakhite $Cu_{18.3}Fe_{15.9}S_{32}$, space group $I\bar{4}3m$ (Hall and Gabe 1972), contains eight interstitial tetrahedra in a unit cell of an otherwise regular 3D tetrahedral array with a sphalerite-like stacking. Only one such site is classified as Fe (at 000 and ½½½), the remaining 6 interstitial tetrahedra are Cu. The framework of edge-sharing tetrahedra (i.e., of *M-M* contacts) is three-dimensional, every such tetrahedron sharing edges with two interstitial tetrahedra (Fig. 22a). This results in a perovskite-like framework of corner-sharing cation octahedra (there are 6 Cu-ligands around each interstitial Fe or Cu atom), with S and additional tetrahedral Cu in the cuboctahedral cavities of this framework (Fig. 22b). The latter tetrahedra share only corners with the edge-sharing set of tetrahedra; one such tetrahedron occurs in every large cavity.

The tetragonal structure of mooihoekite $Cu_9Fe_9S_{16}$ ($P\bar{4}2m$) contains interstitial Fe atoms at 000 and ½½0 (Hall and Rowland 1973). There are infinite chains of metal-metal contacts parallel to [001], alternately Fe-Fe-Fe-Fe and Fe-Cu-Fe-Cu. However, the $Fe_{interstitial}Fe_2Cu_4$ and $Fe_{interstitial}Cu_2Fe_4$ clusters share only corners and not edges of common tetrahedra as in talnakh-

ite (Fig. 22c). Octahedral metal-metal clusters share metal atoms along [001] but are isolated in the (001) plane; chains of octahedra result (Fig. 22d). In a layer description, the "defect mackinawite-type (001) layer," with some tetrahedra missing, alternates with a layer which contains only a few tetrahedra. These share their edges with the tetrahedra in the top and bottom layers; the bulk of tetrahedra in this layer are only corner-sharing tetrahedra of Fe and Cu.

Haycockite, $Cu_4Fe_5S_8$, space group *P*222 (Rowland and Hall 1975), is the most complicated of these "stuffed derivatives of chalcopyrite" (Fig. 23). Along [001], planes with interstitial Fe arranged in a chess-board pattern alternate with those arranged in a primitive square mesh. The former yield isolated octahedral clusters $Fe_{interstitial}Fe_4Cu_2$, with additional, corner-sharing tetrahedra (both Cu and Fe) capping the net openings in this layer; the latter are analogous to the (100) layer from talnakhite. However, the cluster composition is identical with the previous layer. The clusters in adjacent layers are shifted by one half of an octahedron height, so that the "wings," i.e., tetrahedra protruding from the two layer types towards the layer of the opposite kind meet only via common S atoms and no 3D pattern of metal-metal contacts is present (Fig. 23).

Stannoidite. In order to compare it with the 2-layer structures, such as those of stannite-kesterite groups, the crystal structure of stannoidite, $Cu_{16}Fe_{4.3}Zn_{1.7}Sn_4S_{24}$, space group *I*222, (Kudoh and Takeuchi 1976), should be considered in terms of tetrahedral (100) layers. In this

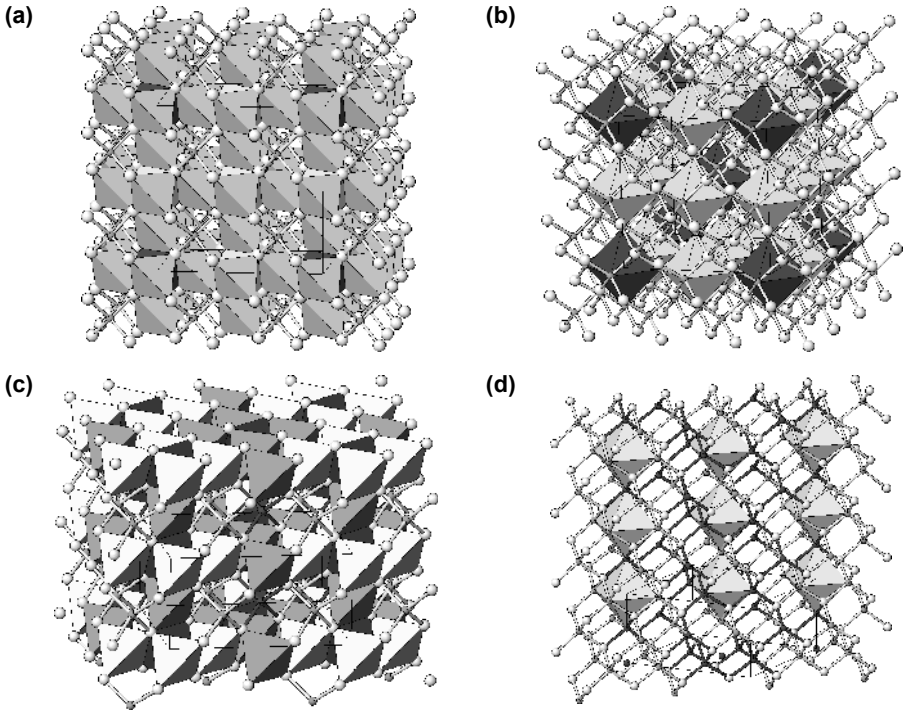

Figure 22. (a) Talnakhite $Cu_{18.3}Fe_{15.9}S_{32}$ (Hall and Gabe 1975). "Scaffolding" of edge-sharing tetrahedra; grey tetrahedra: Cu, black tetrahedra: Fe. Tetrahedral Cu sharing only tetrahedron corners: grey spheres. (b) The "perovskite-like" configuration of octahedral metal clusters in talnakhite. Light octahedra are Cu-centered, dark octahedra are Fe-centered. (c) Mooihoekite $Cu_9Fe_9S_{16}$ (Hall and Rowland 1973). Edge-sharing tetrahedra: solid light-coloured: Cu, solid dark-coloured: Fe. Interstitial, corner-sharing tetrahedra: ball-and-stick representation, Cu grey, Fe black. (d) A layer of the crystal structure of mooihoekite with chains [001] of Fe-centered octahedral metal clusters. Dark cations: Fe, light cations: Cu.

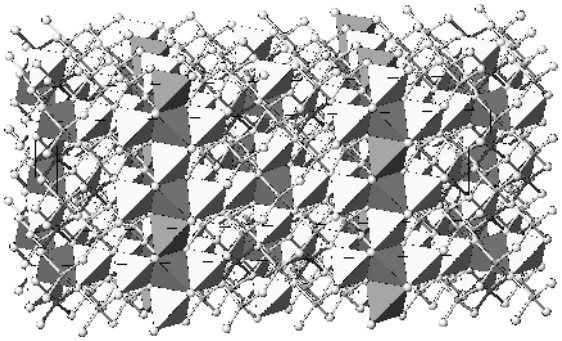

Figure. 23. The structure of haycockite $Cu_4Fe_5S_8$ (Rowland and Hall 1975). Fe: dark atoms and all-grey tetrahedra; Cu: light cations and light tetrahedra. Solid tetrahedra represent groups of edge-sharing tetrahedra (octahedral metal clusters). *c* axis is horizontal, *b* axis vertical; note the differences between the (001) layers at $z = 0$ and those at $z = ¼$.

interpretation, the layer at $x = 0$ and ½ contains Fe, Zn, Sn and both "normal" and "interstitial" Cu whereas the layer at $x = ¼$ and ¾ only "normal" tetrahedral Cu (Fig. 24a). In the layer at $x = 0$, Zn and "normal" Cu are surrounded by Sn and Fe. The interstitial tetrahedral Cu has two close Cu neighbours and two Fe neighbours in the $x = 0$ layer (at 2.71 Å and 2.74 Å, respectively) as well as two Cu neighbours in the adjacent Cu layers (at 2.70 Å), forming octahedral clusters interconnected along [010]. The intra-layer configuration of this layer along the [001] direction can be described as a cation sequence Zn-Sn-Fe-(Cu and Cu interstitial)-Fe-Sn-Zn. The layer at $x = ¼$ is a regular net of corner-connected coordination tetrahedra of Cu, positioned over vacant tetrahedra, as well as over the interstitial Cu atom, of the $x = 0$ layer.

Germanite, $Cu_{13}Fe_2Ge_2S_{16}$, space group $P\bar{4}3n$ (Tettenhorst and Corbato 1984) can again be described by means of two alternating <100> layers: (1) a pure Cu layer of corner-connected tetrahedra, with an additional, interstitial Cu tetrahedron inserted in a primitive (2a, 2a) pattern, and (2) a chalcopyrite-like Fe-Cu layer with a chess-board ordering of Fe and Cu. Interstitial Cu has 6 Cu neighbours at 2.72 Å, the resulting Cu_7 octahedral clusters are isolated, in an I-centered motif. Ge and other cations are not differentiated in the extant structure refinements. Each Cu_7 octahedron is surrounded by 8 Fe tetrahedra arranged as corners of a cube; the tetrahedra of Cu are positioned in the cube faces (Fig. 24b).

***Renierite*,** $Cu_{9.56}Fe_{3.56}Zn_{0.8}Ge_{1.46}As_{0.16}S_{16}$ (Bernstein et al. 1989), a tetragonal structure with the space group $P\bar{4}2c$ and a pseudocubic cell is a structure with additional tetrahedral Fe forming octahedral clusters with four Cu and two Fe atoms as ligands (Fig. 24c). The framework of edge-sharing tetrahedra in renierite looks very much like that in arsenosulvanite but only Fe2 forms a tetrahedron present in the intersection of the rods of edge-sharing tetrahedra. As mentioned, it has four Cu and two Fe as close contacts. The corresponding tetrahedron in the other half of rod intersections, surrounded by 2 Zn, 2 Cu and 2 Ge tetrahedra is void, destroying the expected scheme of *M-M* contacts in these intersections. Out of these surrounding tetrahedra, only 2 copper-containing ones share edges with (i.e., form a part of a cluster around) the Fe2 tetrahedron. The tetrahedra of Zn and Ge do not share edges with any other tetrahedra, always being sandwiched between two empty tetrahedra.

In the (001) layer description, similar to arsenosulvanite, layers densely populated in an open-grid pattern by Fe, Zn, Ge and Cu, alternate with layers that contain corner-sharing Cu and Ge, as well as edge-sharing Cu and Fe.

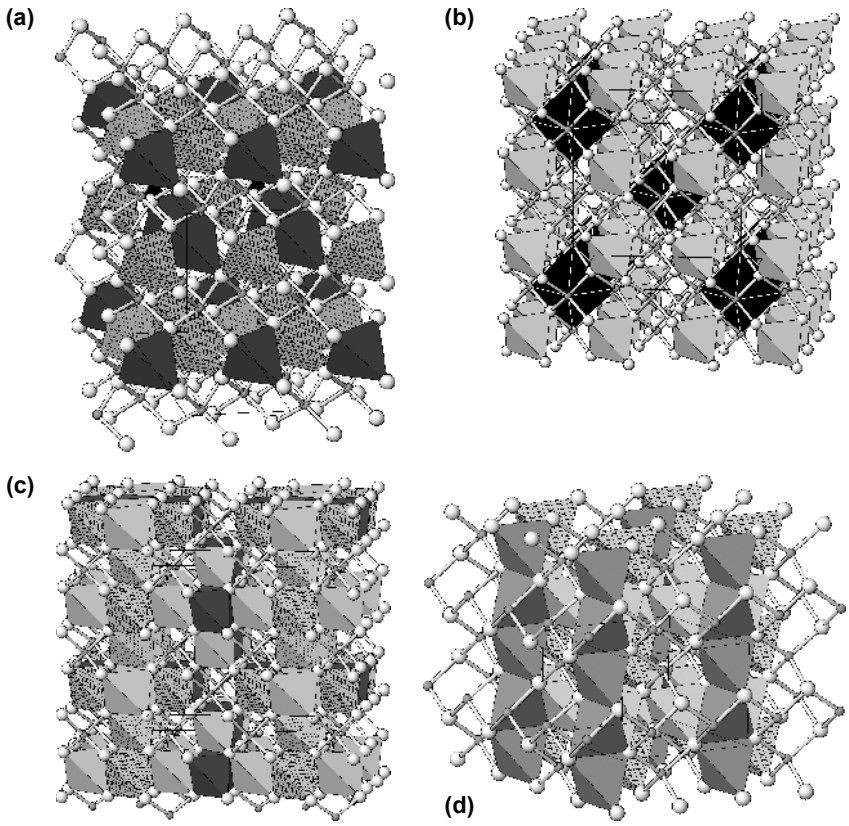

Figure 24. (a) Stannoidite $Cu_{16}Fe_{4.3}Zn_{1.7}Sn_4S_{24}$ (Kudoh and Takeuchi 1976). Fe: black tetrahedra, Sn: cross-hatched tetrahedra, Zn: stippled tetrahedra, Cu: grey spheres. (b) Germanite $Cu_{26}Ge_4Fe_4S_{32}$ (Tettenhorst and Corbato 1984). Copper-centered Cu_7 cation octahedra are black, Fe tetrahedra are solid grey; Cu atoms are grey spheres. (c) Renierite (Bernstein et al. 1989). Edge-sharing coordination tetrahedra: Fe – black, Cu – light grey, Zn – stippled, and Ge – cross-hatched. Corner-sharing tetrahedral cations: Cu –grey spheres. (d) Mawsonite $Cu_6Fe_2SnS_8$ (Szymanski 1976). Fe tetrahedra: dark, cross-hatched tetrahedra: Sn, grey cations: Cu.

***Mawsonite*,** $Cu_6Fe_2SnS_8$, space group $P\bar{4}2m$ (Szymanski 1976) is based on a sphalerite-like packing of tetrahedra, with additional Fe forming interstitial tetrahedra. Columns of edge sharing tetrahedra of Fe define the $a \times a$ mesh, one set "normal," the other interstitial. The central row is built by corner-sharing Sn tetrahedra (Fig. 24d).

The interstitial tetrahedra share edges with four Cu tetrahedra in the (001) layer but these Cu tetrahedra from adjacent Fe-centered clusters share only corners with one another and with the Sn tetrahedra above and below. The remaining Cu tetrahedron shares only corners with adjacent tetrahedra. The octahedral clusters ($FeCu_4Fe_2$) form corner-connected chains parallel to [001], separated by columns of Cu tetrahedra.

The problem of interstitial cations in *hcp* and related stackings

Insertion of an interstitial tetrahedron is not possible in the adamantane structures with a hexagonal packing of anions. The interstitial tetrahedron would share a face with a regular tetrahedron of the wurtzite packing scheme, giving in fact a trigonal bipyramidal coordination. Two ways which nature has used to circumvent these problems are as follows.

In cubanite, $CuFe_2S_3$ (McCammon et al. 1992), a hexagonal close packing of sulfurs is maintained but the wurtzite-like structure is limited to two-octahedra wide (010) slabs, with Cu tetrahedra situated in the central portions and Fe tetrahedra being marginal (Fig. 25a). Adjacent slabs are related by two-fold rotations about [010] and the zig-zag surfaces of slabs are characterized by short Fe-Fe contacts (2.799 Å) across slab boundaries. This is expressed by edge-sharing of two adjacent Fe tetrahedra. The reversal of an entire wurtzite-like slab instead of an individual tetrahedron avoids the above mentioned problem of exceedingly close cation-cation contacts via a common face of two tetrahedra. Above 200-210 °C, cubanite transforms into "isocubanite," a cubic $F\bar{4}3m$ phase with a = 5.296 Å and disordered Cu and Fe, i.e., into an isotype of sphalerite (Cabri et al. 1973).

In catamarcaite Cu_6GeWS_8 (Putz et al. in press), the collision of a "regular" and an "inserted" cation is avoided by the presence of *hchc* stacking instead of the *hh* stacking of wurtzite type. The excess tetrahedron of tungsten is inserted into the bottom layer of a pair of upward-pointing layers stacked according to the sphalerite principle (Fig. 25b). It shares edges, and 2.73 Å contacts, with six surrounding Cu sites, forming an isolated regular metal octahedron. Tungsten is hexavalent; germanium in the structure is tetravalent, and is situated in corner-sharing tetrahedra with no short *M-M* contacts. There is a vacant Cu tetrahedron in

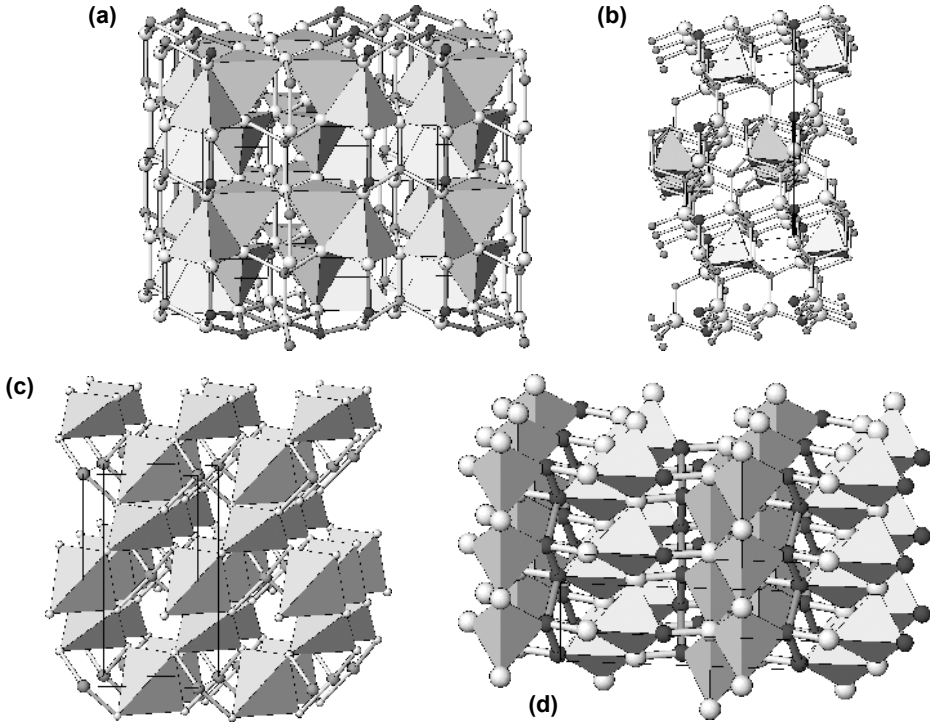

Figure 25. (a) Cubanite $CuFe_2S_3$ (McCammon et al. 1992). small spheres: Cu (light) and Fe (dark), solid tetrahedra: Fe. Note the edge-sharing of Fe tetrahedra. *b* axis is horizontal, *c* axis vertical. Slabs (010) of wurtzite-like arrangement are centered on the planes of Cu tetrahedra. (b) Catamarcaite Cu_6GeWS_8 (Putz et al. 2005). Grey tetrahedrally coordinated cations: Cu, black ones: Ge. Solid interstitial tetrahedra: W. (c) $CdGa_2S_4$ (Gastaldi et al. 1985). Gallium – solid tetrahedra of two kinds; Cd – grey spheres. (d) Lautite CuAsS (Craig and Sephenson 1965). Coordination tetrahedra of copper; anions: S - white spheres, As – black spheres. Covalent As-As bonds (dark).

the structure, below the WS_4 tetrahedron, along the $[00\bar{1}]$ direction. However, it shares only a corner with the WS_4 tetrahedron and the obvious reason for its existence is the bond saturation of the sulfur atom forming this corner. It is bound to one tungsten and three adjacent Cu atoms; a lone electron pair of this sulfur points into the empty tetrahedral cavity. This part of the structure is stacked according to the wurtzite principle.

An alternative stacking of these "sphalerite-like" double-layers in a cubic *cc* fashion leads to a cubic structure with the same type of cation clusters but arranged in such a way as to form an F-centered cubic structure. This obviously is the structure of kiddcreekite Cu_6SnWS_8 (Harris et al. 1984). The difference in stacking is apparently caused by the much larger tetrahedral radius of Sn^{4+} than that of Ge^{4+}.

Defect adamantane structures and more complicated cases

$CdGa_2S_4$. An often quoted example of a defect (omission-) tetrahedral structure is that of $CdGa_2S_4$ (Gastaldi et al. 1985). It displays a "chalcopyrite-like" cell but the symmetry is reduced to $I\bar{4}$. Fully occupied layers with a chess-board pattern of Cd- and Ga-occupied regular tetrahedra (at $z = 0$ and ½) alternate with half-empty layers of flattened Ga tetrahedra in a primitive $a \times a$ arrangement (Fig. 25c). These tetrahedra lie under one half of the empty tetrahedral spaces in the former layer and above such spaces in the next Cd-Ga layer which is displaced by (½*a*, ½*a*). The empty space is an irregular, flattened octahedron.

Sulvanite Cu_3VS_4, space group $P\bar{4}3m$ (Mujica et al. 1998) is a combined "interstitial and vacancy structure." In the (001) layer description, "defect mackinawite" $VCu_2^{\square}$ layers alternate with $Cu_3^{\square}$ layers (which are portions of the former layers in the (010) and (100) orientations). The six Cu-V contacts are 2.70 Å and the corner-connected VCu_6 octahedra outline a 3D perovskite-like motif, with S atoms at the vertices of flat three-fold pyramids above every second triangular Cu_3 face.

Lautite. The crystal structure of lautite CuAsS (Craig and Stephenson 1965) is often described as an ordered homeotype of the crystal structure of diamond, because no sphalerite-like distinction into the subsets of anion and cation sites, respectively, can be seen. Copper is coordinated tetrahedrally to three S and one As, whereas each As has two As, one S and one Cu as ligands, and each S is surrounded by three Cu and one As in a tetrahedral coordination. The As-As distances are 2.51 Å, the S-As distance 2.26 Å, whereas the Cu-S bonds vary between 2.25 and 2.36 Å, plus an additional Cu-As distance of 2.43 Å.

In a modular description, (100) slabs of tetrahedral S-Cu arrangement, two atomic layers thick are separated by corrugated (100) layers consisting of parallel zig-zag [001] chains of covalently bound arsenic atoms (Fig. 25d). The Cu-As and Cu-S bonds complete the tetrahedral coordination of all three elements involved. Orientation of Cu-centered tetrahedra in the adjacent (100) slabs reminds one of that in cubanite, i.e., they are oppositely oriented in the [012] and $[01\bar{2}]$ directions. Nearly the same structure type is found for CuAsSe (Whitfield 1981). It is a superstructure of lautite in which, in each of the above (100) slabs, the orientation of CuS_3As tetrahedra along [010] is reversed after a period of three tetrahedra. Thus, each slab exhibits a *cch* stacking.

Summary of cation-cluster configurations

Talnakhite and arsenosulvanite are the phases with the largest concentration of (MM_6) octahedra; these form perovskite-like frameworks, with two species of central metals alternating in both phases. Sulvanite has a similar framework, populated only by clusters with central vanadium. Haycockite contains $(100)_{perovskite}$-type planes of interconnected cation octahedra, interleaved by layers of isolated M_7 octahedra between them. Parallel chains of metal octahedral clusters occur in mooihoekite, stannoidite and mawsonite, whereas isolated octahedra occur in colusite, germanite and renierite.

All "octahedral clusters" are clusters of seven edge-sharing tetrahedra; in the perovskite-like frameworks each "ligand" also belongs to an adjacent cluster. Perovskite-like structures can also be presented as 3D openworks composed of these edge-sharing tetrahedra, with corner-sharing tetrahedra filling the interstices. In all these structures we have to rely upon the author's own idea of Cu/Fe distribution among the cation sites; this might be problematic in some larger structures. Edge-sharing involves Cu, Fe, V, W, and (exceptionally) As. Although of fundamental importance for some minerals, Zn, Sn and Ge avoid edge-sharing clusters and their coordination tetrahedra are corner-sharing, as also is a portion of Cu in the structure. The Cu-Fe phases—talnakhite, mooihoekite and haycockite—transform above 165-185 °C into a cubic $F\bar{4}3m$ "intermediate solid solution" with $a \sim 5.36$ Å in which the interstitial cations are statistically distributed.

Tetrahedrite-tennantite

The crystal structure of $(Cu,Ag)_{10}(Fe,Zn,Hg,Cu,....)_2(Sb,As)_4S_{13}$, known in the literature as the tetrahedrite-tennantite isomorphous series (Wuensch 1964, Wuensch et al. 1966 and numerous other works quoted in the introduction), has habitually been interpreted as a derivative of the sphalerite structure with extensive omission, substitution and insertion of new sites. Voids in the tetrahedral framework have the shape of truncated tetrahedra, called also "Laves polyhedra," and are separated by single-tetrahedral walls (Fig. 26a). Each wall consists of a wreath of six tetrahedra around an originally tetrahedral position MS_4, which is always replaced by a trigonal coordination pyramid $(As,Sb)S_3$. Four such pyramids point into the cavity, filling it partly with the lone electron pairs of the metalloids. A further six copper sites of the original framework are altered into trigonal planar sites by coordinating to a new sulfur site placed in the centre of the cavity. Thus, the Laves polyhedron accommodates a "spinner" of six Cu coordination triangles, as well as the lone electron pairs of four metalloids in its walls (Fig. 26b). A pronounced anisotropic displacement ellipsoid of the trigonal planar Cu2 site has been found in all structure determinations. The Cu-S interatomic distances become more credible when a slightly displaced, flat-pyramidal copper position is assumed. The Rietveld refinements of powder neutron diffraction data on Fe-bearing tennantite and tetrahedrite (Andreasen et al. in prep.) suggest that this copper site is indeed flat pyramidal, statistical around the ideal triangular position.

An alternative picture of the structure of tetrahedrite-tennantite (Belov 1976; Johnson et al. 1987) postulates that the tetrahedral framework is a maximally collapsed sodalite-type framework. The large cage openings, hexagonal in sodalite, became reduced, and nearly perfectly trigonalized by clasping of the trigonal coordination pyramids of (As,Sb) by surrounding tetrahedra. This dual image is useful when considering the pure-copper tetrahedrite-tennantite with additional copper atoms in the unit cell (up to the ideal composition $Cu_{14}(Sb,As)_4S_{13}$; Makovicky and Skinner 1979; Pfitzner 1997; Makovicky et al. 2005). These atoms move inside (for As), or between, the cages, assuming new tetrahedral or trigonal-planar positions, respectively, which were not occupied in the basic structure. In the case of Sb, the original tetrahedral Cu sites appear to be involved in copper mobility.

The tetrahedrite-tennantite structure type $Cu_6^{[3]}(Cu,....)_6^{[4]}(Sb,As)_4^{[3]}S_{12}^{[4]}S^{[6]}$ allows extensive substitutions. Nature tries to avoid the presence of formally divalent Cu (i.e., the composition $Cu_{10}^{+}Cu_2^{2+}Sb_4S_{13}$) by substituting Zn, Fe, Hg, Cd, rarely also Mn, etc., in the tetrahedral sites (up to 2 sites out of 6). Synthetic tetrahedrites can also accommodate up to two atoms p.f.u. of Co, Ni, Mn, as well as partial substitutions by Sn, Ge, Pb, Ga and In (Hall 1972; Makovicky and Karup-Møller 1994; Klünder et al. 2003a,b; Karup-Møller and Makovicky 2004). Bismuth can partly substitute for As and Sb (Breskovska and Tarkian 1994; Klünder et al. 2003) whereas tellurium does so in full, following a substitution principle $Cu_{10}M_2^{2+}(Sb,As)_4S_{13} \rightarrow Cu_{12}Te_2(Sb,As)_2S_{13} \rightarrow Cu_{10}Te_4S_{13}$ (Trudu and Kittel 1998 and references therein; Karup-Møller and Makovicky in prep.). Here, copper vacancies occur in the triangular copper sites

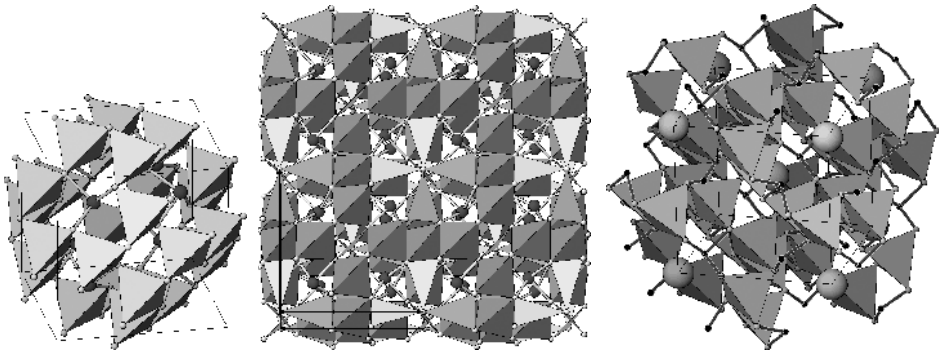

Figure 26. (a) A void Laves polyhedron in the structure of tetrahedrite $Cu_{10}(Zn,Fe)_2Sb_4S_{13}$ (Wuensch 1964). Tetrahedra containing (Cu,Zn,Fe) form the walls of a truncated tetrahedral cavity. Ball-and-stick SbS_3 pyramids close the openings in them. Four Sb atoms have lone electron pairs pointing into the cavity. (b) Tetrahedrite (Wuensch 1964), a complete structure. A sphalerite-like framework of (Cu, Zn, Fe) tetrahedra, with large truncated-tetrahedral cavities in an I-centered cubic arrangement, filled by "spinners" of six triangularly coordinated Cu atoms around a central S atom. A part of the framework tetrahedra are replaced by trigonal pyramidal coordinated Sb. (c) Galkhaite $(Cs,Tl)(Hg,Cu,Zn)_6As_4S_{12}$ (Chen and Szymanski 1981). Oblique projection upon (100). Tetrahedral openwork, with $(Hg,Cu,Zn)S_4$ tetrahedra and (AsS_3) pyramids (As: black small spheres) forming large cages which contain (Cs,Tl) (large spheres).

(Kalbskopf 1974). Electronic processes act as well, e.g., the selenium analog of tetrahedrite exists only as a fully substituted form, $Cu_{10}(Fe,Zn)_2Sb_4Se_{13}$, whereas the partly substituted, as well as the unsubstituted compound, $Cu_{\sim 12}Sb_4Se_{13}$, known for the sulfur analog, is not stable (Karup-Møller and Makovicky 1999).

All these substitutions influence the unit cell parameter *a*. For example, the substitution by zinc leads to *a* (Å) = 0.0293 Zn (atoms p.f.u.) + 10.324 for the substitution line $Cu_{12}Sb_4S_{13}$-$Cu_{10}Zn_2Sb_4S_{13}$ and *a* (Å) = 0.319 Zn (atoms p.f.u.) + 10.448 for the line $Cu_{14}Sb_4S_{13}$-$Cu_{10}Zn_2Sb_4S_{13}$ (Karup-Møller and Makovicky 2004).

For $Cu_{12}Sb_4S_{13}$, copper acts as a mixture of 10 Cu^+ with the Shannon crystal radius of 0.635 Å (Shannon 1981) with two Cu^{2+} with a radius ~0.51 Å (Makovicky and Karup-Møller 1994). Although the mixed valence of Cu appears to be a collective property, this scheme works perfectly for the unit cell size calculations. Some of the older equations (especially Johnson et al. 1987) fail for partly substituted tetrahedrite-tennantite compositions because they do not address this phenomenon. Substitution by Ag is universally assumed to start in the triangular sites and spill over into tetrahedral sites only when the former are (nearly) filled. The presence or absence of the central S atom in the Laves polyhedra of the varieties heavily substituted by Ag is still contested.

Incorporation of iron into tetrahedrite-tennantite starts, at low concentrations, in the form of Fe^{3+}, ideally up to the composition of $Cu^+_{11}Fe^{3+}Sb_4S_{13}$. Afterwards, additional incorporation of Fe proceeds parallel to the conversion of the already incorporated Fe into Fe^{2+}, until the final composition $Cu^+_{10}Fe^{2+}_2Sb_4S_{13}$ is reached (Charnock et al. 1989; Makovicky et al. 1990). For broad compositions about Cu:Fe = 1:1, in tennantite (As) but to some extent also in tetrahedrite (Sb) iron with intermediate valence is observed, indicating strong electron delocalization/charge-transfer via intervening S (and Cu) atoms (Makovicky et al. 2003). The position of Fe in the structure has been contested. Charnock et al. (1989), working with EXAFS, place Fe^{3+} preferentially into trigonal planar sites and Fe^{2+} into tetrahedral sites.

Makovicky et al. (1990, 2003) place all Fe into tetrahedral sites, based on their Mössbauer studies. Finally, Andreasen, Lebech, Makovicky and Karup-Møller (in prep.) place Fe into tetrahedra at all stages of substitution, based on the Rietveld refinements of neutron diffraction data on synthetic tetrahedrite.

Galkhaite: a cage-like sulfide. In galkhaite (Cs,Tl)(Hg,Cu,Zn)$_6$As$_4$S$_{12}$ (Chen and Szymanski 1981) the Laves polyhedron of the tetrahedrite-tennantite structure is occupied by a single (rattling) Cs(+Tl) atom, and the size and a charge balance in the structure is achieved by a heavy substitution of tetrahedral Cu^+ by divalent metals, especially Hg^{2+}. It is cubic, a = 10.365(3) Å and the space group is $I\bar{4}3m$. Nearly regular (Hg, Cu, Zn)S$_4$ tetrahedra have M-S = 2.496 Å and the trigonal pyramids AsS$_3$ have As-S = 2.265 Å. (Cs,Tl) in the cavity centre (Fig. 26c) is 12-coordinated, with Cs-S distances equal to 3.863 Å. There are 19% vacancies in the position of the large cation. Chen and Szymanski (1981) suggest the exchange of 2 Tl for 3 Cs but we interpret their plot as the exchange of 0.8 Tl for 0.8 Cs, with the exception of the case with Cs ≈ 1.0.

Structures with anion vacancies

Nowackiite and sinnerite. A plesiotypic pair of anion-deficient structures consists of nowackiite, Cu$_6$Zn$_3$As$_4$S$_{12}$ (Marumo 1967) (as well as the isostructural aktashite Cu$_6$Hg$_3$As$_4$S$_{12}$) and sinnerite Cu$_6$As$_4$S$_9$ (Makovicky and Skinner 1975). Both structures are based on a sphalerite-like cubic stacking of tetrahedral layers. Selected clusters of four adjacent tetrahedra are replaced in them by four AsS$_3$ pyramids, with lone electron pairs of As^{3+} directed into a common volume with a missing anion (an octet of lone pair electrons). In nowackiite, a rhombohedral structure with a polar c axis (space group $R3$), the (Cu,Zn):As ratio guarantees that the As$_4$S$_{12}$ clusters are isolated (Fig. 27a). A part of the Cu is replaced by Zn in order to maintain charge balance. In sinnerite, with a lower Cu:As ratio, the As$_4$S$_{12}$ groups are partly condensed via common S atoms and the resulting As-S configurations are kinked chain fragments As$_3$S$_7$ and As$_5$S$_9$ (Fig. 27b). The larger, branched fragment is just an extension of the shorter one. Mistakes in the fragment growth, i.e., formation of a larger fragment instead of the smaller one and vice versa in the growing layer, lead to OD phenomena and ubiquitous twinning: the $P1$ structure of sinnerite forms up to 24 twin orientations, restoring the $F\bar{4}3m$ symmetry of the underlying sphalerite-like substructure.

Structures with tetrahedral clusters

Pentlandite and its derivatives. The crystal structure of the parent compound, pentlandite (Ni,Fe)$_9$S$_8$ or Co$_9$S$_8$ (Rajamani and Prewitt 1975) contains isolated cubic clusters of eight metal-sulfur tetrahedra. Tetrahedra in a cluster share edges, yielding 3 direct short metal-metal interactions (2.505 Å for Co-Co, 2.549 Å for Fe-Ni, and 2.670 for argentopentlandite, Table 15) for each cation. Clusters are hinged via common apical S atoms and the cubic space between 6 adjacent clusters is occupied by a cation (Co, Fe and Ni, Ag or PGE in different pentlandites) in octahedral coordination (Fig. 28a). Cages in the pentlandite structure are closed, preventing movement and exchange of atoms between cages.

Djerfisherite is a complex sulfide of iron and copper, containing large cations, K and lesser amounts of Na, as well chlorine in an independent site. Its structure was determined by Dmitrieva et al. (1979) and refined on a synthetic analog K$_6$LiFe$_{23}$S$_{26}$Cl by Tani et al. (1986). Natural djerfisherite, K$_6$Na$_{0.81}$(Fe$_{0.84}$Cu$_{0.16}$)$_{24}$S$_{26}$Cl, is an iron-copper sulfide but its synthetic analog and the related bartonite K$_{5.68}$Fe$_{20.37}$S$_{26.93}$ (Evans and Clark 1981) indicate that copper can be fully exchanged by Fe and, in bartonite and owensite, even Cl is replaced by S. A nickel-barium analog of djerfisherite, Ba$_6$Ni$_{25}$S$_{27}$, with S instead of Cl, has been synthetized (Gelabert et al. 1997) (Table 15).

In cubic djerfisherite, pentlandite-like units—cubic cages with 6 surrounding clusters—are interconnected into a loose framework with a channel system <100>, i.e., these channels run

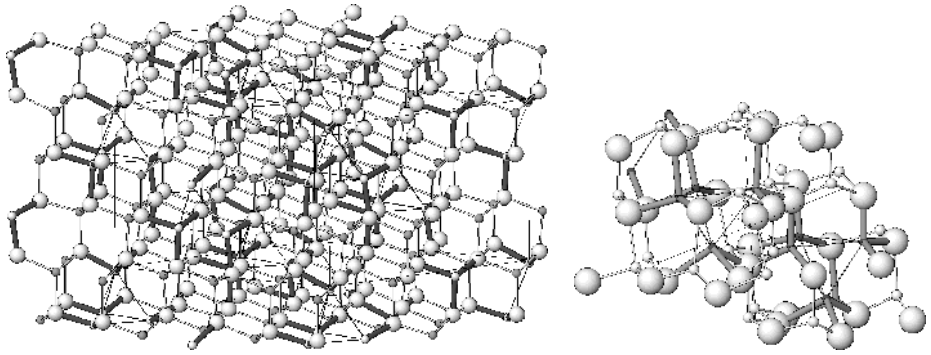

(a) **(b)**

Figure 27. (a) Nowackiite $Cu_6Zn_3As_4S_{12}$ (Marumo 1967). A 3D framework of $(Cu,Zn)S_4$ tetrahedra (Cu-S bonds as thin lines) with clusters composed of four AsS_3 pyramids (As-S bonds as thick lines) concentrated around a sulfur vacancy. Imaginary tetrahedra, outlined in thin lines, indicate the S vacant sites. (b) A fragment of the crystal structure of sinnerite $Cu_6As_4S_9$ (Makovicky and Skinner 1975). Two adjacent clusters, with four AsS_3 coordination pyramids each, situated around S vacancies of the sphalerite-like framework of Cu tetrahedra. Amalgamation of adjacent AsS_3 groups into larger groups (note an $(As_3S_7)^{5-}$ group in foreground) proceeds via common S atoms. The anion vacancies are outlined as in (a).

Table 15. Pentlandite, djerfisherite and related phases.

Mineral	Formula	Lattice parameters (Å)			Space Group	Ref.
		a	*b*	*c*		
Bartonite	$K_{5.68}Fe_{20.368}S_{26.925}$	10.424(1)	—	20.626(2)	*I*4/*mmm*	[1]
Chlorbartonite	$K_6(Fe,Cu)_{24}S_{26}(Cl,S)$	10.381(8)	—	20.614(2)	*I*4/*mmm*	[2]
Djerfisherite	$K_6LiFe_{23}S_{26}Cl$	10.353(1)			$Pm\bar{3}m$	[3]
Synthetic	$Ba_6Ni_{25}S_{27}$	10.057(1)			$Pm\bar{3}m$	[4]
Thalfenisite	$Tl_6Fe(Fe,Ni)_{24}S_{26}Cl$	10.92			$Pm\bar{3}m$	[5]
Owensite	$(Ba,Pb)_6(Cu,Fe,Ni)_{25}S_{27}$	10.349(1)			$Pm\bar{3}m$	[6]
Argentopentlandite	$AgFe_8S_8$	10.521(3)			$Fm\bar{3}m$	[7]
Co-pentlandite	Co_9S_8	9.923(1)			$Fm\bar{3}m$	[8]

References: [1] Evans and Clark 1981; [2] Yakovenchuk et al. 2003; [3] Tani et al. 1986; [4] Gelabert et al. 1997; [5] Rudashevskyi et al. 1979; [6] Szymanski 1995; [7] Hall and Stewart 1973; [8] Rajamani and Prewitt 1975

along all edges of the cubic unit cell when the cubic cage, occupied by Na(Li), is situated at ½ ½ ½ (Fig. 28b). Chlorine atoms lie at intersections of the channel systems and are octahedrally surrounded by K atoms; these occur as two cations per each [100] channel interval (Fig. 28b). No constrictions are found in the channels. The Fe-Fe distance in the clusters is 2.731 Å. In thalfenisite (Table 15), K is replaced by Tl and Na (Li) by a divalent octahedrally coordinated metal (as in pentlandite). In owensite the univalent metals in the channels are replaced by Ba and, in the ratio 1:9, also by Pb with an active lone electron pair. Chlorine is replaced by S and Na by octahedrally coordinated metal with the *M*-S distance equal to 2.50 Å.

Tetragonal bartonite (Fig. 28c) contains intersecting channels [100] and [010] but lacks continuous channels in the [001] direction. The "nuclei" of vertical channels reach only

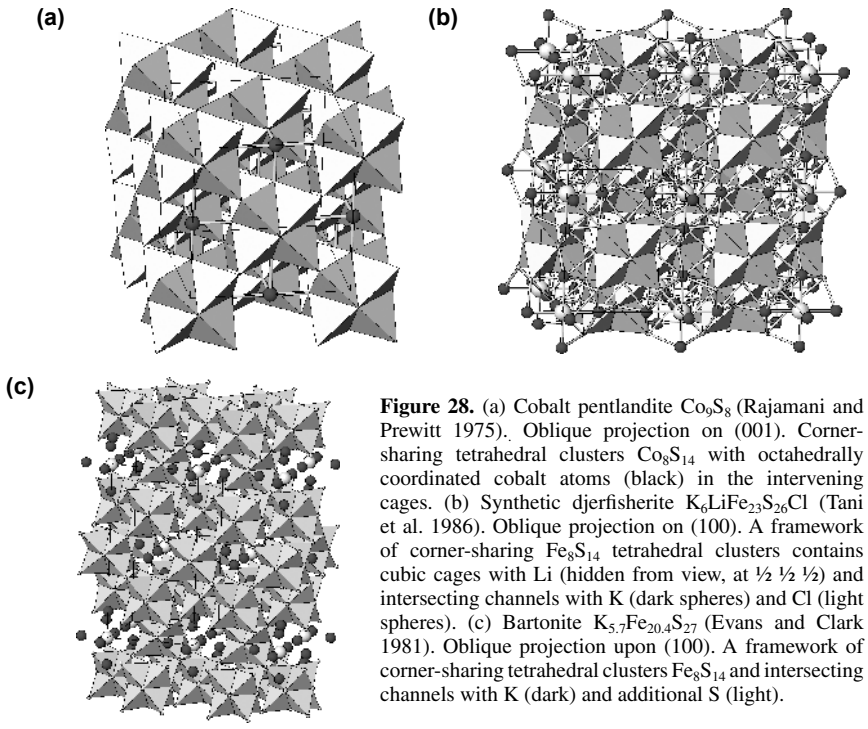

Figure 28. (a) Cobalt pentlandite Co_9S_8 (Rajamani and Prewitt 1975). Oblique projection on (001). Corner-sharing tetrahedral clusters Co_8S_{14} with octahedrally coordinated cobalt atoms (black) in the intervening cages. (b) Synthetic djerfisherite $K_6LiFe_{23}S_{26}Cl$ (Tani et al. 1986). Oblique projection on (100). A framework of corner-sharing Fe_8S_{14} tetrahedral clusters contains cubic cages with Li (hidden from view, at ½ ½ ½) and intersecting channels with K (dark spheres) and Cl (light spheres). (c) Bartonite $K_{5.7}Fe_{20.4}S_{27}$ (Evans and Clark 1981). Oblique projection upon (100). A framework of corner-sharing tetrahedral clusters Fe_8S_{14} and intersecting channels with K (dark) and additional S (light).

one cage up and one cage down from each intersection, with appropriate K atoms again completing an octahedron around the non-framework S atoms in the channel intersection. Lacking enclosed cages, bartonite lacks the smaller cation (Na or Fe, Ni, Cu). The Fe-Fe distance in the clusters is 2.708-2.737 Å.

Djerfisherite and bartonite can be considered two polytypes, where the channel-containing (in terms of cluster interconnection "loosely built") (001) layers are stacked in the AAAA sequence in djerfisherite whereas in bartonite they follow the ABAB stacking sequence. Thus, any occurrence of the "bartonite sequence" in djerfisherite will block the [001] channels. Eight K-S bonds in djerfisherite (constituting a square antiprism) are 4 × 3.31 and 4 × 3.44 Å, the single K-Cl bond is 3.10 Å long. The corresponding Ba-S bonds in owensite are 4 × 3.24 and 4 × 3.30 Å, plus a single Ba-S bond equal to 3.15 Å.

Bornite. Crystallographic investigations on bornite, ideally Cu_5FeS_4, by means of X-ray diffraction and High Resolution Transmission Electron Microscopy (HRTEM) have been the topic of a series of publications, twenty-five or more, since the first one by Frueh (1950). A complete listing can be found in Ding et al. (2005a,b).

Bornite occurs in three different polymorphs, respectively known under the names of high-, intermediate and low-temperature bornite in the literature (Table 16). The high-temperature form of Cu_5FeS_4 is stable above 265 °C (Pierce and Buseck 1978). It is cubic, with sulfur atoms in an *fcc* arrangement, and six cations in a unit cell distributed over eight tetrahedral sites (Morimoto 1964). Its quenched structure (Fig. 29a) alters only slowly to a low form on standing. This polymorph forms a complete solid solution with high-temperature digenite, $Cu_{7.2+x}S_4$, and also in the direction of excess iron, up to the composition of $Cu_{36.7}Fe_{21.9}S_{41.4}$ at 900 °C (Karup-Møller and Makovicky, unpublished). At room temperature, however, only the

composition Cu_5FeS_4 is stable, and all excess Cu or Fe, as well as the contents of minor metals dissolved in bornite-digenite at high temperatures and sulfur fugacities, are exsolved again as metal and/or sulfides.

According to Morimoto and Kullerud (1961), the intermediate form, stable between 265 °C and 200 °C, has the tetrahedral cation vacancies ordered, and the cubic unit cell has a cell edge doubled against that of the *F*-centered high form (i.e., it is known as a 2*a* form). Its structure was described as an alternation of 1*a*1*a*1*a* cubes with antifluorite- and zincblende structure, respectively (see below). On cooling below 200 °C, further ordering of tetrahedral atoms and empty tetrahedra was postulated, leading to the 2*a*4*a*2*a* superstructure of the low, stoichiometric bornite (Koto and Morimoto 1975).

Figure 29b shows that the antifluorite cubes actually represent clusters of eight edge-sharing tetrahedra, like those observed in pentlandite and its more complex derivatives. The *M*-*M* distances in these clusters vary from 2.76 to 2.97 Å; they are supposed to host a mixture of Cu and Fe. Those cube-like spaces between six clusters, which host *M* octahedra in pentlandite, host four Cu atoms in slightly convex, three-fold planar coordination in bornite. These copper atoms are strongly eccentric in four corner-sharing tetrahedra of the "sphalerite-like" cube. They have moved into four faces of the empty octahedron which was filled in pentlandite by a cation. Their separation (≥ 3.05 Å) exceeds the distances typical for Cu-Cu interactions. Alternative orientations of these Cu configurations are the basis of the 2*a*4*a*2*a* superstructure of the low form.

These observations are in accordance with the refinement of the 2*a* superstructure of the intermediate form by Kanazawa et al. (1978), who described it as an alternation of cubes with half-filled sites, occupied by Cu, and of those with fully occupied sites, hosting Cu and Fe (Fig. 29c). There is, however, ambiguity in the space group of the cubic symmetry; $Fm\bar{3}m$ was chosen. Ding et al. (2005) express a number of doubts about this model, including the questionable homogeneity of bornite at this temperature.

Other compositions of the intermediate-temperature bornite-digenite solid solution produce *Na* superstructures, with $N = 6$ for the compositions close to digenite, and the value of *N* decreasing gradually through 5, 4, and 3, to reach 2 for stoichiometric bornite. Samples may present peculiar diffraction patterns: in the $[10\bar{1}]$ axis patterns, only those reciprocal lattice rows which are parallel to [*NNN*] and pass through the 1*a*-substructure reflections are present. In order to explain these, twinning or antiphase domains were invoked but Pierce and Buseck (1978) did not find them. Instead, they suggested, as did Van Dyck (1979,1980) and Conde et al. (1978), vacancy or cation ordering. The corresponding 3D structure models were calculated for

Table 16. Crystallographic data for polymorphs of bornite.

Polymorph	Space Group	Lattice parameters (Å, °)				Temp.	Refs.
		a	*b*	*c*	Angle		
High-*T* bornite	$Fm\bar{3}m$	5.5	5.5	5.5	—	Quenched	[1]
High-*T* bornite*	*R*3*m*	6.7	6.7	6.7	rhomb. 33.53°	Quenched	[1]
High-*T* bornite	*R*3*m*	3.862	3.862	19.975	hexag. axes 120°	Quenched	[2]
Intermediate bornite	$Fm\bar{3}m$	10.981	10.981	10.981	—	458 K	[3]
Low-*T* bornite*	*Pbca*	10.950	21.862	10.950	—	Room *T*	[4]

Notes: * For details of interpretation see the text. Further interpretation/existence problems are discussed in Ding et al. (2005a,b)
References: [1] Morimoto 1964; [2] Daams and Villars 1993; [3] Kanazawa et al. 1978; [4] Koto and Morimoto 1975

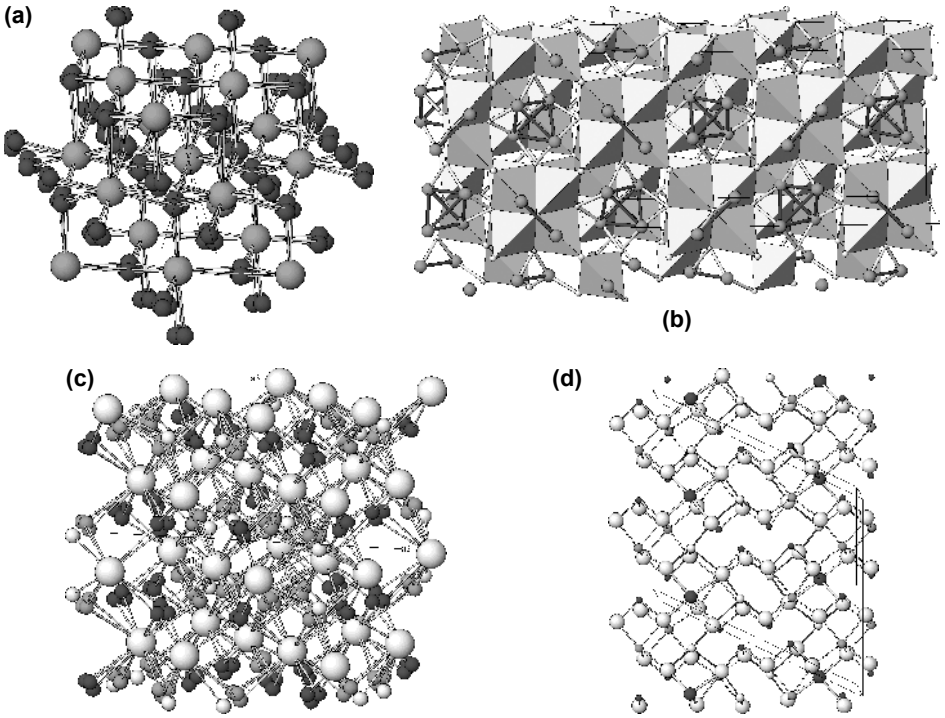

Figure 29. (a) High-temperature bornite (Morimoto 1964). Large spheres: S, dark spheres: disordered Cu sites, refined as clusters of split, statistically distributed atoms. All coordination tetrahedra are occupied. (b) Low-temperature polymorph of bornite according to Koto and Morimoto (1975). Pentlandite-like clusters ("antifluorite cubes") of eight (Cu,Fe) edge-sharing coordination tetrahedra alternating with clusters ("zincblende cubes") of four quasi-planar CuS_3 groups surrounding an empty octahedron. Dark outlined Cu-Cu connections help to define this space. Compare with Ding et al. (2005). (c) Intermediate bornite (Kanazawa et al. 1978). Two distinct, statistically occupied tetrahedral (Cu,Fe) sites (indicated by shades of grey) alternate with clusters of eight statistically occupied trigonal planar sites (white spheres), analogous to the triangular sites in (b). (d) Diaphorite projected along [001]. Large white spheres: S; small white spheres with bonds rendered in dark: Ag; small dark spheres: Sb; large dark spheres: Pb; intermediate grey spheres: positions in which Ag and Pb are mixed due to disorder caused by the OD character of diaphorite.

the cubic 4*a* and 6*a* superstructures (unit cell edges equal to 21.88 Å and 32.82 Å, respectively) by Ding et al. (2005), fitting them to the electron-diffraction and HRTEM data. The space group $Fm\bar{3}m$ was assumed. Calculated occupancies of cation sites (Cu and Fe could not be distinguished) vary from 0.67 to 1.0 for the 4*a* model and from 0.81 to 1.0 for the 6*a* model.

Ding et al. (2005) note that only Pierce and Buseck (1978) claim to have observed the 2*a*4*a*2*a* polymorph of bornite by HRTEM whereas Ding et al. (2005) only observed intergrowths of 1*a*, 2*a*, 4*a*, and 6*a* domains in different proportions. Based on these observations and on a number of inconsistencies observed in structural and magnetic studies of bornite (e.g., a changing ratio of Fe^{2+} and Fe^{3+}; summarized in Ding et al. 2005a,b), they propose that the 2*a*4*a*2*a* polymorph might actually be a mixture of 2*a* and 4*a* superstructures, simulating the orthorhombic structure. For the 2*a* polymorph, Ding et al. (2005) derived a new structure model, with the space group $F\bar{4}3m$, with (preferentially) Cu and Fe concentrated in the clusters of tetrahedra and Cu in the "zincblende cubes." The resulting chemistry is $Cu_8Fe_4S_8$, however, so it obviously can be only one of the components present in low-

temperature bornite. All these models were tested by comparing the calculated and observed HRTEM images. The temperatures of the two polymorphic transformations were refined for the digenite-bornite series by Grguric and Putnis (1998).

Monosulfides with octahedral cations: *ccp* vs. *hcp* stacking of anions

The fundamental difference between the *ccp* and *hcp* variants of the structures with octahedrally coordinated cations is the absence or presence of direct cation-cation interactions. Candidate cations for these two general structure types sharply differ. Occupation of all octahedral positions precludes occupation of tetrahedral voids. Partial vacancies in the *hcp* category, if frequent, can also be considered "pillared" versions of the layered MX_2 structure type, although a smooth transition is virtually unknown (but it is assumed for NiTe – $NiTe_2$ at elevated temperatures).

Phases derived from cubic close packing. The fundamental *ccp* type is represented by galena PbS and its isotypes PbSe, PbTe, as well as the series CaS-MgS-MnS. It goes virtually unnoticed that the octahedral coordination of Pb (Pb-S 2.966 Å) in galena is an exception and not a rule for this lone electron pair element in chalcogenides; its coordination becomes less symmetrical or its coordination number increases whenever possible, i.e., in a less symmetrical environment. Of interest are the homeotypes of PbS, obtained by means of coupled substitutions, such as Ag + Bi = 2Pb, Ag + Sb = 2Pb, which at elevated temperatures work for all substitution proportions. Cubic $AgBiS_2$ and $AgSbS_2$ are limited to higher temperatures (about 200 °C for $AgBiS_2$) and have disordered distribution of cations. Of particular interest are the two monoclinic room-temperature ordered homeotypes which occur on the PbS-$AgSbS_2$ join, the sulfosalts freieslebenite $PbAgSbS_3$ (Ito and Nowacki 1974) and diaphorite $Pb_2Ag_3Sb_3S_8$ (Armbruster et al. 2003). In these structures, Pb forms the largest, trapezoidally deformed octahedra, Ag polyhedra have rhomb-like cross-sections whereas Sb forms distorted square coordination pyramids. Diaphorite (Fig. 29d) appears to be an OD structure (Armbruster et al. 2003). An analog of sinnerite and nowackiite amongst the adamantane structures is the structure of $Tl_4Bi_2S_5$ (Julien-Pouzol et al. 1979). It displays a missing anion, replaced by a lone electron pair micelle of four Tl atoms.

Phases derived from hexagonal close packing. Among the *MX* compounds with octahedral cation coordination, the NiAs structure type occurs for the transition metals which favour the presence of direct metal-metal interactions, especially via the shared octahedral faces in the (0001) planes (Table 17). This is connected with high electrical conductivity, sometimes with variable stoichiometry and the dependence of lattice parameters on electron configuration. For example, for selenides, the *c*/*a* ratio changes as follows: TiSe (1.68), VSe (1.67), CrSe (1.64), $Fe_{1-x}Se$ (1.64), CoSe (1.46), and NiSe (1.46). For the arsenides and antimonides, rich in valence electrons, the *c*/*a* ratio is even lower (e.g., 1.39 for NiAs). The ideal *c*/*a* ratio of hexagonal close packing being 1.633, this substantial reduction of the *c* parameter corresponds to intense *d* orbital metal-metal interaction in this direction (Müller 1996). The anion is surrounded by six cations forming a trigonal coordination prism (Fig. 30a).

The room-temperature modification of stoichiometric FeS, troilite, exhibits triangular Fe_3 clusters parallel to (001) (the Fe-Fe distance being 2.93 Å). They are interconnected by Fe-Fe interactions at 2.99 Å between the Fe_3 triangles stacked above one another, and 2.95 Å for those in different [001] stacks of octahedra (Fig. 30b). The Fe-S bonds range from 2.36 Å to 2.72 Å in length. At 453 K, the high-temperature modification of FeS (Keller-Besrest and Collin 1990) is hexagonal, space group $P6_3mc$. Octahedral bond distances vary between 2.43 Å and 2.54 Å, and there is a continuous string [001] of Fe-Fe interactions, 2.91-2.92 Å long, via the shared octahedral faces. The intermediate modification of FeS (King and Prewitt 1982) has an orthorhombic structure, described as the MnP structure type, with distorted octahedra and a zig-zag pattern of short Fe-Fe interactions parallel to [001]. The Fe-S bonds

Table 17. Selected homeotypes of NiAs.

Mineral	Formula	Space Group	Lattice Parameters (Å, °)				Ref.
			a	*b*	*c*	Angle	
Pyrrhotite 6c	$Fe_{11}S_{12}$	*F*1*d*1	6.895	11.954	34.518	β 90.0	[1]
Pyrrhotite 3c	Fe_7S_8	$P3_121$	6.866	6.866	17.046	γ 120	[2]
Pyrrhotite 4c	Fe_7S_8	*F*12/*d*1	11.902	6.859	22.787	β 90.4	[3]
Troilite 2H	FeS	$P\bar{6}2c$	5.965	5.965	11.756	γ 120	[4]
Troilite (530 K)*	FeS	$P6_3mc$	6.588	6.588	5.400	γ 120	[5]
Troilite (463 K)$^+$	FeS	*Pnma*	5.825	3.466	6.003	—	[6]
Westerveldite	FeAs	*Pnam*	5.440	6.026	3.371	—	[7]
Modderite	CoAs	*Pnam*	5.286	5.868	3.488	—	[7]
Nickeline	NiAs	$P6_3/mmc$	3.619	3.619	5.025	γ 120	[8]
—	Fe_7Se_8	*P*31	7.21	7.21	17.6	γ 120	[9]
—	Fe_3Se_4	*I*12/*m*1	6.187	3.525	11.290	β 91.98	[10]
—	CrS	*C*12/*c*1	3.826	5.913	6.089	β 101.6	[11]
	Cr_5S_6	$P\bar{3}1c$	5.982	5.982	11.509	γ 120	[12]
Brezinaite	Cr_3S_4	*I*12/*m*1	5.694	3.428	11.272	β 91.50	[11]
—	Cr_2S_3	$P\bar{3}1c$	5.939	5.939	11.192	γ 120	[11]
—	Cr_2S_3	$R\bar{3}$	5.937	5.937	16.698	γ 120	[11]

Notes: * Pressure 9000 MPa; $^+$ Pressure 0.1 MPa; other conditions: Up to 6350 MPa at 294 K
References: [1] Koto et al. 1975; [2] Keller-Besrest and Collin 1983; [3] Tokonami et al. 1972; [4] Keller-Besrest and Collin 1990; [5] Fei et al. 1998; [6] King and Prewitt 1982; [7] Lyman and Prewitt 1984; [8] Yund 1962; [9] Andresen and Leciejewicz 1964; [10] Andresen and van Laar 1970; [11] Jellinek 1957; [12] van Laar 1967

range from 2.44 to 2.50 Å, the Fe-Fe interactions result in a distance of 2.92 Å. All distortions characteristic for the MnP structure type are much more pronounced in westerveldite FeAs (Lyman and Prewitt 1984) (Fig. 30c). The Fe-As distances range from 2.35 to 2.51 Å, and the Fe-Fe interactions along the stacking direction [100] are much shorter than in the sulfide; they are equal to 2.79 Å, in agreement with the *a* parameter of 5.44 Å.

The omission derivatives of FeS, the family of pyrrhotites with a general formula $Fe_{1-x}S$, has been extensively studied. In the intermediate polymorphs, the cation vacancies undergo partial ordering and the occupied, partly ocupied and least occupied cation sites form occupational waves. These are oriented diagonally to (0001) in NA pyrrhotite (between ~209 and 266 °C, Kissin 1974), and parallel to (0001) in NC pyrrhotite (~100-213 °C). In both cases, non-integral periodicities in the *a* and *c* directions result. The low-temperature polymorphs of pyrrhotite (below 100 °C) have ordered cation vacancies in the structure. They occur in every second octahedral (0001) layer, or every second and third layer, and result in unit cells being a multiple of the two-layer cell of high-temperature FeS. The known ordered compositions are: Fe_7S_8 (pyrrhotite 4M, c = 22.88 Å; Fe_9S_{10} (5H, c = 28.67 Å); $Fe_{11}S_{12}$ (6M, c = 34.52 Å); Fe_9S_{10} (7H, c = 40.15 Å); and $Fe_{10}S_{11}$ (11H, c = 63.22 Å). Details of their crystallography, and the structure schemes and phase relations of these phases have been summarized by Scott (1974) and Vaughan and Craig (1978).The structures of the pyrrhotite family can be illustrated using the example of the structure of Fe_7Se_8 obtained from neutron diffraction data by Andresen and Leciejewicz (1964) (Fig. 30d). Every second octahedral layer has 25% of octahedra vacant in a hexagonal pattern; with the adjacent fully occupied layer it gives 7 Fe for every 8 Se atoms. Vacancies in the defect layers are stacked with a shift $^1/_2a_i + {}^1/_3c$, where i = 1, 2 and 3 in the sequence of the layer involved.

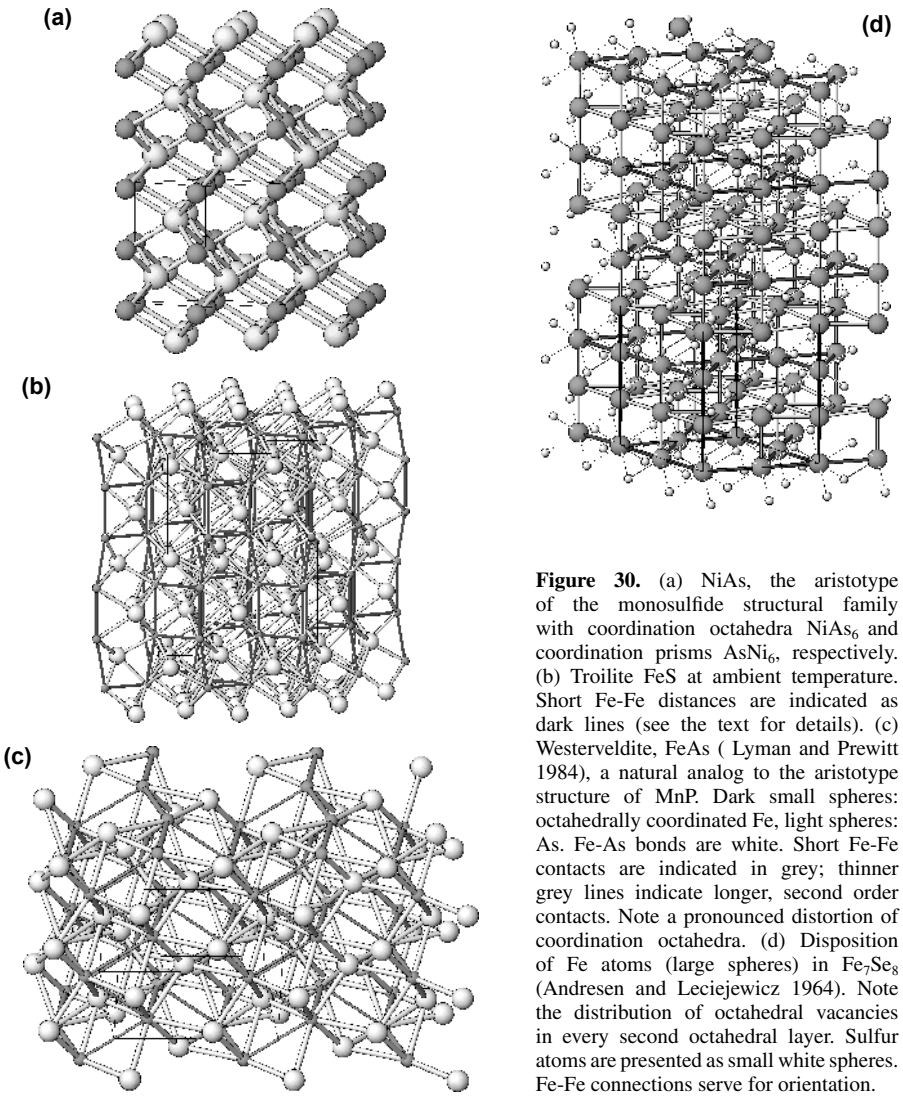

Figure 30. (a) NiAs, the aristotype of the monosulfide structural family with coordination octahedra $NiAs_6$ and coordination prisms $AsNi_6$, respectively. (b) Troilite FeS at ambient temperature. Short Fe-Fe distances are indicated as dark lines (see the text for details). (c) Westerveldite, FeAs (Lyman and Prewitt 1984), a natural analog to the aristotype structure of MnP. Dark small spheres: octahedrally coordinated Fe, light spheres: As. Fe-As bonds are white. Short Fe-Fe contacts are indicated in grey; thinner grey lines indicate longer, second order contacts. Note a pronounced distortion of coordination octahedra. (d) Disposition of Fe atoms (large spheres) in Fe_7Se_8 (Andresen and Leciejewicz 1964). Note the distribution of octahedral vacancies in every second octahedral layer. Sulfur atoms are presented as small white spheres. Fe-Fe connections serve for orientation.

An extreme concentration of vacancies, not attained in the sulfides, is found in the structure of Fe_3Se_4 (Andresen and Laar 1970) where 50% of octahedra in the defect layer are vacant (Fig. 31a). The structure is slightly distorted, with the monoclinic angle $\beta = 91.8°$, and the occupied rows of octahedra run in the [010] direction. Octahedra of the full layer are sizably distorted, the Fe-Se bonds ranging from 2.44 to 2.61 Å. In the Fe-S system, the Fe_3S_4 composition is a thiospinel. The phase closest to this composition, smythite $Fe_{3+x}S_4$ ($0 < x < 0.3$) is rhombohedral, the c parameter is three times that of Fe_3Se_4.

A situation broadly analogous to $Fe_{1-x}S$ exists for the sulfides of chromium. CrS (Jellinek 1957) differs from FeS, however, because the coordination octahedra of the d^4 cation Cr^{2+} undergo Jahn-Teller distortion. Four S atoms at 2.43 Å and two more S atoms at 2.88 Å form an elongated octahedron, and the structure is transitional between NiAs and PtS. Cr_7S_8, Cr_5S_6, Cr_3S_4 and Cr_2S_3 are "defect" structures stable at room temperature (Jellinek 1957). The

vacancies in the metal positions are confined to every second layer of octahedra. For the two compounds with a smaller number of vacancies, ordering disappears at about 320 °C; ordering of vacancy-rich compounds persists up to high temperatures (Jellinek 1968).

Thiospinels

The thiospinels and less common selenospinels (AB_2X_4) are the structural analogs of oxide spinels AB_2O_4. The unit cell edge of the cubic cell, based on cubic close packing of anions, has values from about 9.4 Å to 10.6 Å for sulfur-based spinels, i.e., twice the edge length of the F-centered cell of the anion submotif. The space group of nearly all spinels is $Fd\bar{3}m$, subgroups due to tetrahedral cation ordering or distortion are rare (Table 18).The unit cell contains 32 anion atoms with coordinates (*u,u,u*). This *u* value is equal to 0.25 for the ideal *ccp* structure; it ranges from 0.25 to over 0.26 in thiospinels. This range is narrower than observed in oxide spinels, 0.24-0.27 (Lavina et al. 2002). An increase in *u* produces larger tetrahedral sites at the expense of diminished octahedral sites (Waychunas 1991).

The tetrahedral site has point symmetry $\bar{4}3m$, multiplicity 8, whereas the octahedral site has point symmetry $\bar{3}m$, multiplicity 16. Reduction of symmetry occurs primarily as separation of two distinct kinds of tetrahedral sites. The octahedral *M*-S distance depends on *u* as follows:

$$M\text{-S} = a\sqrt{\left(\tfrac{1}{2} - u\right)^2 + 2\left(\tfrac{1}{4} - u\right)^2}$$

whereas the tetrahedral cation (*T*)-S distance is

$$T\text{-S} = a\sqrt{3\left(\tfrac{1}{8} - u\right)^2}$$

(Lavina et al. 2002).

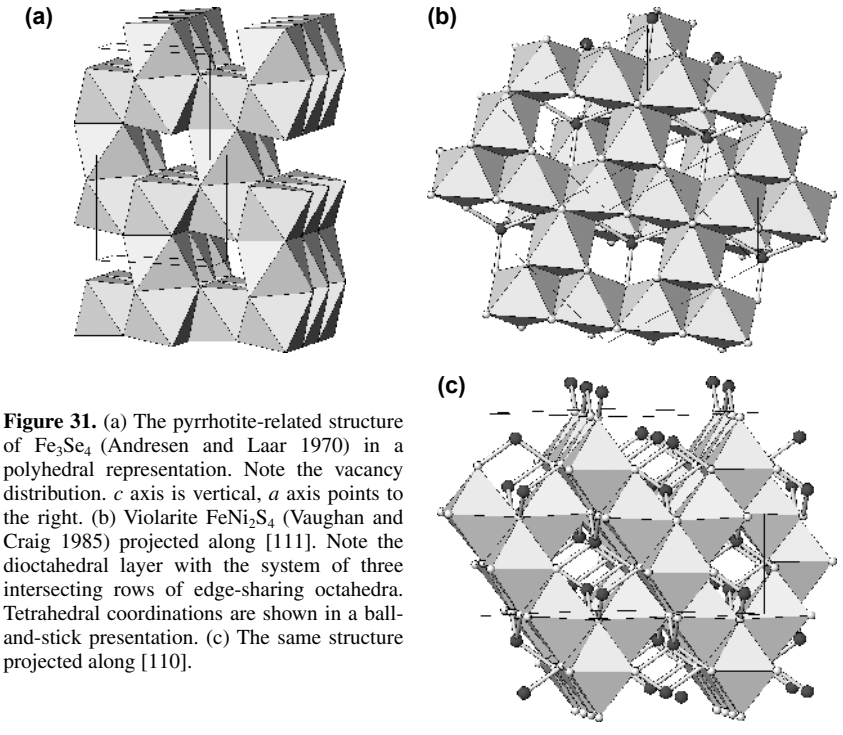

Figure 31. (a) The pyrrhotite-related structure of Fe_3Se_4 (Andresen and Laar 1970) in a polyhedral representation. Note the vacancy distribution. *c* axis is vertical, *a* axis points to the right. (b) Violarite $FeNi_2S_4$ (Vaughan and Craig 1985) projected along [111]. Note the dioctahedral layer with the system of three intersecting rows of edge-sharing octahedra. Tetrahedral coordinations are shown in a ball-and-stick presentation. (c) The same structure projected along [110].

Table 18. Selected thiospinels.

Mineral	Formula	Space Group	Lattice Parameters	*T*-S tetr.	*M*-S oct.	*u*	Refs.
Polydymite	Ni_3S_4	$Fd\bar{3}m$	9.457	2.211	2.274	.260	[1]
Linnaeite	Co_3S_4	$Fd\bar{3}m$	9.406	2.185	2.269	.259	[2]
Greigite	Fe_3S_4	$Fd\bar{3}m$	9.880	2.139	2.470	.250	[3]*
			9.876	2.147	2.464	.2505	[4]*
Violarite	$FeNi_2S_4$	$Fd\bar{3}m$	9.465	2.197	2.284	.259	[5]
Carrollite	$CuCo_2S_4$	$Fd\bar{3}m$	9.478	2.265	2.253	.263	[6]*
Cuproirdsite	$CuIr_2S_4$	$Fd\bar{3}m$	9.847	2.303	2.367	.260	[7]
Cuprorhodsite	$CuRh_2S_4$	$Fd\bar{3}m$	9.788	2.272	2.362	.259	[8]
Indite(disord.)	$FeIn_2S_4$	$Fd\bar{3}m$	10.618	2.466	2.562	.2591	[9]
Indite (ordered)	$FeIn_2S_4$	$F\bar{4}3m$	10.618	2.466	2.562	.2591	[9]
Daubréelite	$FeCr_2S_4$	$Fd\bar{3}m$	9.981	2.322	2.406	.2593	[10]*
Synth.(disord.)	$FeCuCr_4S_8$	$Fd\bar{3}m$	9.904	2.282	2.399	.258	[11]*
Synth.(ordered)	$FeCuCr_4S_8$	$F\bar{4}3m$	9.901	Fe 2.349 Cu 2.178	2.362	.252	[12]*
Synth.	$FeRhCrS_4$	$Fd\bar{3}m$	9.944	2.291	2.409	.258	[13]
Synth.	$ZnCr_2S_4$	$Fd\bar{3}m$	9.974	2.325	2.401	.2596	[14]
Rhodostannite	$Cu_2FeSn_3S_8$	$I4_1/a$	*a* 7.305 *c* 10.330	2.320	2.535	.2593	[15]
Toyohaite	$Ag_2FeSn_3S_8$	$I4_1/a$	*a* 7.46 *c* 10.80	—	—	—	[16]
Synth.	$HgCr_2S_4$	$Fd\bar{3}m$	10.235	2.500	2.406	.266	[17]*

Notes: * powder data (newest ones by using Rietveld refinement)
Hill et al. (1978): parallel refinements as (a) disordered model (mixed In^{3+} and Fe^{2+} in both types of sites) and (b) ordered model with In:Fe about 1:1 in M and one pure In, and one mixed (In,Fe) T site; two distinct T sites in ordered $FeCuCr_4S_8$ as well.

References: [1] Lundqvist 1947; [2] Knop et al. 1968; [3] Uda 1968; [4] Skinner et al.1964; [5] Vaughan and Craig 1985; [6] Williamson and Grimes 1974; [7] Furubayashi et al. 1994; [8] Riedel et al. 1976; [9] Hill et al. 1978; [10] Kim et al. 2002; [11] Riedel et al. 1981; [12] Zaritskii et al. 1986; [13] Riedel and Karl 1980; [14] Wittlinger et al. 1997; [15] Jumas et al. 1979; [16] Yajima et al. 1991; [17] Konopka et al. 1973

Normal spinels have divalent cations in the tetrahedral sites and trivalent cations in the octahedral sites. Inverse spinels have a trivalent cation in the tetrahedral site and a mixture of di-and trivalent cations in the octahedral sites. This division, e.g., $ZnCr_2S_4$ and $CdCr_2S_4$ vs. Fe_3S_4 and $FeIn_2S_4$, is much less obvious in thiospinels than in oxide spinels. Two coexisting valencies are displayed by Fe, Co and Ni; in the case of iron, a temperature dependent gradual transformation of individualized Fe^{2+} and Fe^{3+} in the structure into a completely mixed-valence iron Fe^{n+} was demonstrated for Cu-Fe rhodium and chromium thiospinels by Riedel et al. (1981) using Mössbauer spectroscopy.

Coordination octahedra form dioctahedral layers (111), separated by layers with a set of occupied tetrahedra and "isolated" octahedra (Fig. 31b). This is true for all layers of the {111} set and the "tetrahedral-octahedral" layers of a particular orientation actually contain the octahedra from dioctahedral layers of the other orientations. In this way, each octahedron shares edges with six neighbours. A characteristic result of this is a "pile-up" of octahedral rows [110], and equivalent, separated by interstitial rows containing isolated tetrahedra, in the projection along [001]. Projection of the spinel structure along [110], down the rows of tetrahedra (Fig. 31c), enabled Horiuchi et al. (1981), Navrotsky (1994) and Ferraris et al.(2004) to interpret spinel as a block structure/polytypic structure leading to high-pressure, deep-earth spinelloids in the unary system $(Mg,Fe)_2SiO_4$; we have not (yet) seen a sulfide analog of spinelloids.

In the majority of cases the octahedral cations are transition metals and Al; the choice of tetrahedral cations is wider, including Hg, Cd, Zn, Cu, In and the transition metals. The closest cation-cation distances in the structure are those via the shared edges of two neighbouring octahedra (shared edges are shortened). These Fe-Fe distances in greigite are 3.49 Å, compared with 2.97 Å in magnetite.

Disulfides, sulfarsenides and their analogs

The disulfide S_2^{2-} group with its covalent S-S bond, and the diselenide, sulfarsenide and diarsenide group analogs, are components of a number of highly stable stuctures. The valence of AsS and As_2 groups has been interpreted in a number of ways (e.g., Tossell et al. 1981), often dependent on other assumptions, e.g., that the valence of iron increases along the series FeS_2-FeAsS-$FeAs_2$. Based on the results of Mössbauer spectroscopy and the LCAO calculations, Ioffe et al. (1985) suggest that iron has the same valence state in all three compounds and that the population of the d levels changes little, and never correspons to Fe^{3+}. This is accomplished by back-donation of electrons due to the donor-acceptor interaction between the sp^3 atomic orbitals of the anion and the hybridized d^2sp^3 orbitals of iron. Thus, in FeAsS and $FeAs_2$ the X_2 groups act as divalent anions; they all force Fe into a low-spin state (see Vaughan and Rosso 2006, this volume, for further discussion).

Characteristic *X-X* distances in the dianion pairs in the structures of sulfides and related substances are listed in Table 19. These pairs are an expression of high sulfur fugacity in the formation environment although, in some of these compounds, they also play a space-filling role, enabling the matching of two distinct structure regions. For example, in $HgSb_4S_8$ (livingstonite, Srikrishnan and Nowacki 1975), the S_2^{2-} groups interconnect double-pyramidal Sb_2S_4 rods into layers $Sb_2S_2(S_2)$, extending the repetition period of these layers in order to match that of the alternating $HgSb_2S_4$ layers. The space-filling role is obvious also in $Cu_4Bi_4S_9$ (Takéuchi and Ozawa 1975; Bente and Kupčík 1984) and $Cu_4Bi_4Se_9$ (Makovicky et al. 2002); S_2^{2-} groups join two different structure portions in $Ba_4Sb_4Se_{11}$ (Cordier et al. 1980) and the triselenide Se_3^{2-} and trisulfide S_3^{2-} groups substitute for interlayers in the rod-based structures of $Sr_4Bi_4Se_9(Se_3)$ (Cook and Schäfer 1982) and $Pb_6Sb_6S_{14}(S_3)$ (moëloite, Orlandi et al. 2002). All of these stuctures are confined to the associations with a high activity of the anion in question; the occurrence of diarsenides and sulfarsenides is also limited by a high activity of sulfur, at which As starts acting as a cation. A somewhat different role is played by the S_2 groups in patronite, $V(S_2)_2$,and the Te_2 groups in sylvanite $AgAuTe_4$, mentioned among the fibrous and layered chalcogenides, respectively.

Pyrites. The cubic disulfide of iron, pyrite FeS_2 is the most widespread sulfide in the Earth's crust. In its structure, three coordination octahedra of low-spin divalent iron meet at each end of the S_2 dumbell, with no edge-sharing present. The characteristic configuration of <100> slabs of pyrite structure is shown in Fig. 32a. The pyrite structure type is found in high-spin d^5 transition elements (e.g., MnS_2), low-spin d^6 (e.g., FeS_2, $FeSe_2$, $FeTe_2$, $PtAs_2$, $PdSb_2$, RuS_2, OsS_2), d^7 (CoS_2, $AuSb_2$), high-spin d^8 (NiS_2, $NiSe_2$), and under high pressure even in d^9 and d^{10} elements (CuS_2, ZnS_2) (Hulliger 1968). These compounds are semiconductors or behave as metals (CoS_2, $PdSb_2$). Modifications of the pyrite structure type are a series of rhodium and iridium chalcogenides known as, e.g., $RhS_{\sim 3}$ and $IrSe_{\sim 3}$, because of the cation vacancies in the pyrite-like structure, and an orthorhombic, pseudotetragonal structure of $PdSe_2$ and PdS_2 (Table 22), in which very elongated octahedra with a [4+2] bond scheme, typical for Pd^{2+}, extend one of the unit cell parameters of the "pyrite cube" substantially.

Distinct electron configurations are the cause of miscibility gaps encountered among the isotypes of pyrite: FeS_2 and NiS_2 exhibit only a limited solubility (Clark and Kullerud 1963 and a number of later studies, e.g., 3.6 atomic% Ni in FeS_2 and 9.6 atomic% Fe in coexisitng NiS_2 at 725 °C; Karup-Møller and Makovicky 1995), and the semiconducting Pt pnictides do not form mixed crystals with the metallic Pd pnictides (Hulliger 1963).

Table 19. *X-X* bond distances in the covalent X_2 anion groups in sulfides and related substances.

Compound	*X-X* distance (Å)	Reference
$Cu_4Bi_4S_9$	2.095	Bente and Kupčík 1984
$Cu_4Bi_4Se_9$	2.402	Makovicky et al. 2002
$Ba_4Sb_4Se_{11}$	2.368 2.421	Cordier et al. 1980
FeS_2 cub.	2.140	Will et al. 1984
NiS_2	2.075	Nowack et al. 1991
CoS_2	2.112	Nowack et al. 1991
MnS_2	2.091	Chattopadhyay et al. 1991
$FeSe_2$ orthohomb.	2.550	Pickardt et al. 1975
$HgSb_4S_8$	2.060	Srikrishnan and Nowacki 1975
$Rb_2Sb_8S_{12}(S_2).2H_2O$	2.108	Berlepsch et al. 2001
FeAsS	2.346	Fuess et al. 1987
NiAsS	2.299	Foecker and Jeitschko 2001
CoAsS ($Pca2_1$)	2.292	Fleet and Burns 1990
$FeAs_2$	2.488	Lutz et al. 1987
$PtAs_2$	2.409	Szymanski 1979

The sulfarsenides, sulfantimonides and sulfobismutides (as well as the corresponding seleno- and telluro- varieties) are very important homeotypes of pyrite (Table 20). Some have been described as ordered arrangements of chalcogenide-pnictide dumbels (Figs. 32b,c) such as, for example, ullmanite, NiSbS, $P2_13$, and isotypic PdSbSe (Pratt and Bayliss 1980; Foecker and Jeitschko 2001; Paar et al. 2005). For cobaltite CoAsS, both a disordered and an ordered variety is known, $Pa3$ and $Pca2_1$ (Giese et al. 1965; Scott et al. 1976), the orthorhombic symmetry of the latter causing the weak anisotropy of this mineral in reflected light. For gersdorffite, NiAsS, the disordered, $Pa3$ variety and the ordered $P2_13$ and $Pca2_1$ polymorphs have been found (Bayliss 1986). In both ordered structure types of this family, the cation is coordinated by 3S+3As (or equivalents) in an ordered fashion and the S-As dumbells have ordered orientations. The different disposition of "all-S" and "all-As" faces of octahedra in the two ordering schemes is illlustrated in Figs.32b and 32c. This family is typical for d^6 and d^7 elements (examples are CoAsS and IrAsS, and NiAsS, PdAsS and PdBiTe, respectively). Overgrowths of platinum group element (PGE)-rich MAsS phases on Ni-Co sulfarsenides, typically found in PGE deposits are caused by their isotypism.

Marcasites. In the broad marcasite structure type, the coordination octahedra of cations share edges forming chains parallel to the short crystallographic axis (~3.3 Å for FeS_2). Adjacent chains share vertices and the channels comprised by four adjacent chains are reduced to rhomb-like cross-section by the bridging *X-X* bonds (Fig. 33a). Symmetry constraints are less strict than in pyrite and the variations in octahedron size, elongation and *X-X* distance are easily adjusted by rotating the chains of octahedra around their axes. The marcasite structure type is related to that of rutile, the latter having no anion-anion bond in the channels; this allows the chain rotation until the channels assume a square cross section. Another relative of the marcasite-type is the $CaCl_2$ structure type, in which the $(100)_{CaCl_2}$ boundaries drawn through anions are planar and not warped as in FeS_2. Using this analogy, marcasite can be described as composed of slightly warped $(100)_{FeS_2}$ layers of octahedra, with every second row of octahedra in each layer emptied and substituted by *X-X* bonds.

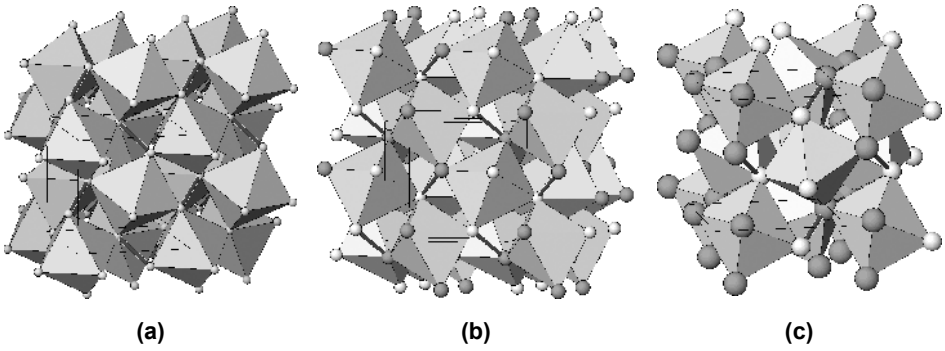

Figure 32. (a) Pyrite FeS_2 in a polyhedral representation. Coordination octahedra (FeS_6) share corners and the covalent S-S bonds (indicated in black). (b) Gersdorfite NiAsS (Foecker and Jeitschko 2001). Light and dark spheres: S and As, respectively. (c) Orthorhombic cobaltite CoAsS (Fleet and Burns 1990). Light and dark spheres: S and As, respectively.

Table 20. Selected disulfides, diarsenides and sulfarsenides.

Mineral	Formula	Space Group	Lattice Parameters (Å,°)				Ref.
			a	*b*	*c*	Angle	
Pyrite	FeS_2	$Pa\bar{3}$	5.418	5.418	5.418		[1]
Marcasite	FeS_2	*Pnnm*	4.443	5.424	3.386		[2]
Ferroselite	$FeSe_2$	*Pnnm*	4.804	5.784	3.586		[3]
Loellingite	$FeAs_2$	*Pnnm*	5.300	5.984	2.882		[4]
Sperrylite	$PtAs_2$	$Pa\bar{3}$	5.968	5.968	5.968		[5]
Vaesite	NiS_2	$Pa\bar{3}$	5.677	5.677	5.677		[6]
Cattierite	CoS_2	$Pa\bar{3}$	5.539	5.539	5.539		[6]
Cobaltite	CoAsS	$Pca2_1$	5.583	5.589	5.581		[7]
Gersdorffite	NiAsS	$P2_13$	5.689	5.689	5.689		[8]
Hauerite	MnS_2	$Pa\bar{3}$	6.104	6.104	6.104		[9]
Arsenopyrite	FeAsS	$C112_1/d$	6.546	9.451	5.649	89.84	[10]
Rammelsbergite	$NiAs_2$	*Pnnm*	5.301	5.986	2.882		[11]
Pararammelsbergite	$NiAs_2$	*Pbca*	5.772	5.834	11.421		[12]
Alloclasite	CoAsS	$P2_1$	4.661	5.501	3.411	90.03	[13]

References: [1] Will et al. 1984; [2] Brostigen et al. 1973; [3] Pickardt et al. 1975; [4] Lutz et al. 1987; [5] Szymanski 1979; [6] Nowack et al. 1991; [7] Fleet and Burns 1990; [8] Foecker and Jeitschko 2001; [9] Chattopadhyay et al. 1992; [10] Fuess et al. 1987; [11] Kjekshus et al. 1979; [12] Kjekshus and Rakke 1979; [13] Scott and Nowacki 1976

This model leads directly to an explanation of the topotactic formation of marcasite by mild oxidation of pyrrhotite. This mechanism was proposed for the pyrrhotite-marcasite pair by Fleet (1978) and for the analogous nickeline (NiAs)-rammelsbergite ($NiAs_2$) pair by Karup-Møller and Makovicky (1979). Every second row in the layer of octahedra (ideally (0001)) of the original FeS or NiAs structure is leached out, creating an overall chess-board pattern of occupied octahedral rows, and the charge balance is maintained by partial oxidation of anions which form X_2 pairs. The orthorhombic products form in three orientations on the (ideally) hexagonal substrate. For both pairs of minerals, misfit of the original periodicities

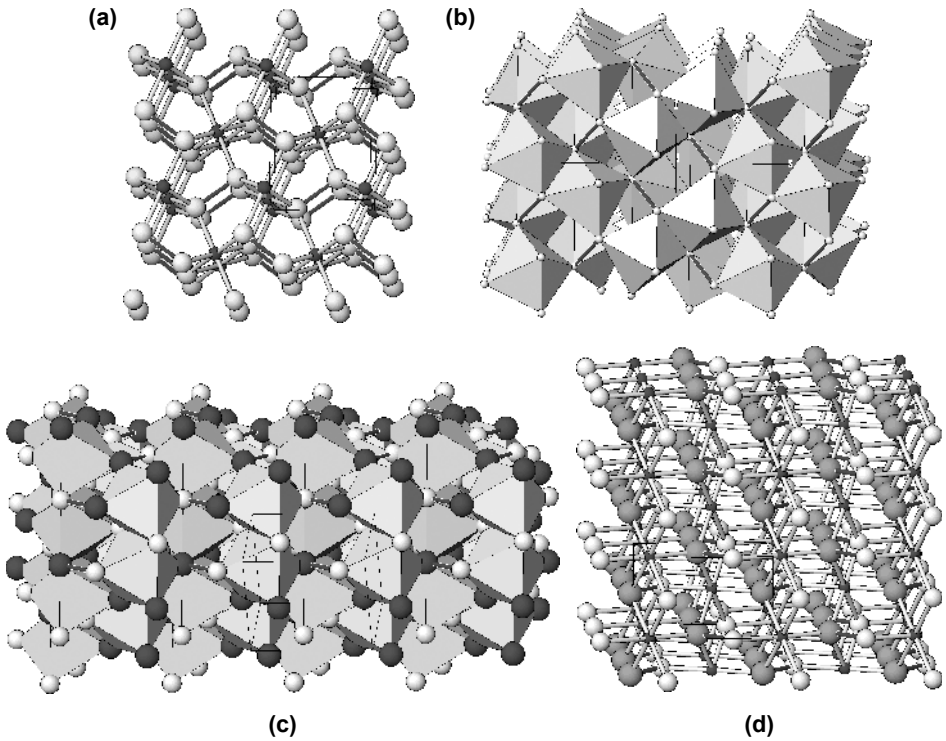

Figure 33. (a) Marcasite FeS_2 (Brostigen et al. 1973) in a ball-and-stick representation. Fe (small dark spheres) is octahedrally coordinated, S-S bonds are accentuated in black. (b) Pararammelsbergite, $NiAs_2$ (Kjekshus and Rakke 1979) projected along [100]. Alternating slabs of a marcasite (i.e., rammelsbergite)-like and pyrite-like arrangement are parallel to (001). As-As bonds are indicated in black. (c) Arsenopyrite, FeAsS (Fuess et al. 1987) in a polyhedral representation. Octahedrally coordinated Fe, S and As: white and grey spheres, respectively, with the covalent As-S bond indicated. (d) Alloclasite CoAsS (Scott and Nowacki 1976). Small spheres: Co, dark spheres: As, light spheres: S. As-S bonds: black.

and those of the products is sizable, leading to extremely fine-grained products, unless further ripening or outward growth (common for marcasite) takes place. It is the present author's opinion that much of the marcasite observed in nature is a result of these topotactic processes. For rammelsbergite, the result of such topotaxy is the formation of rammelsbergite far below its stability limits, in the field of stability of pararammelsbergite.

The relationship of the pyrite structure type to the marcasite structure type has long fascinated crystallographers. Schemes in which a composition plane of a pyrite twin on (110) is the thinnest slab of marcasite or the twin contact of two marcasite individuals on {110} forms a slice of the pyrite {001} configuration, are described by Fleet (1970) and Ramdohr and Strunz (1978).

A compound in which twinning of a marcasite array occurs on a unit cell level with maximum frequency is pararammelsbergite (Fleet 1972), the low-temperature polymorph of $NiAs_2$. Two octahedra thick slabs of rammelsbergite-type arrangement, at $x = 0$ and ½, built by edge-sharing of octahedra in their median planes, are joined in a perfectly pyrite-like fashion at the $z = ¼$ and ¾ planes (Fig. 33b). A single octahedral <100> layer of pyrite configuration (layer symmetry $P2_1/g$) can be stacked with further such layers either by: (1) applying an interlayer glide plane or interlayer two-fold axes, in order to create a pyrite-like

layer pair or, alternatively, (2) the next <100> pyrite-like layer can be attached as a translation equivalent of the original one, displaced by ~(¼ a_1 + ¼ a_2)$_{pyrite}$, giving an arrangement seen in marcasite. In the real structure of pararammelsbergite, those halves of octahedra which are situated along the pyrite-like composition plane are an exact copy of the pyrite motif. However, the "outer" portions of these octahedra, facing the marcasite-like stacking, have to be distorted, in order to fit this stacking. Symmetry of the octahedral layer is reduced to *Pg* and the interlayer symmetry elements are reduced as well (to a parallel glide plane). We do not know of a sulfide equivalent of pararammelsbergite, nor do we know structures with thicker marcasite-like slabs.

The general marcasite type structure is formed by transition metal cations d^2-d^9. In the d^6 (low-spin semiconducting) and metallic d^7-d^9 marcasites (e.g., FeS_2, $FeSe_2$ $CoSe_2$ and $CuSe_2$), the d_{xy} orbitals are fully occupied, acting repulsively and their *c*/*a* ratios are about 0.74. The d^2-d^4 marcasites are Jahn-Teller instable, the d_{xy} orbitals are empty and able to overlap along the *c* axis and result in the *c*/*a* ratios being reduced to 0.47-0.57; these form the loellingites (e.g., $CrSb_2$, $FeAs_2$, $RuAs_2$, and $OsAs_2$) (Hulliger 1967).

Compounds with d^5 lie between these two categories. The half-filled d_{xy} orbitals overlap at every second octahedral contact whereas a non-overlap, i.e., repulsion occurs in the intervening contacts. The resulting structure, the arsenopyrite structure type, has a *c*/*a* ratio intermediate between marcasites and loellingites and a doubled periodicity. Besides $CoAs_2$, $RhAs_2$ and $IrAs_2$, many ternary compounds belong to this structure type, such as FeAsS (arsenopyrite), FeSbS, RuAsS, OsAsS, etc. Note that Hulliger's interpretation of d electron count on cations differs from that of Ioffe et al. (1985) (See also Vaughan and Rosso 2006, this volume)

Arsenopyrite (Fig. 33c) and its isotypes are a superstructure of the marcasite structure type. In each [001] row of dumbells, the two orientations of S-As pairs alternate. Along the *c* axis, the shared edges of octahedra in the rows are alternately S-S and As-As and the [3As+3S] coordinations in the adjacent octahedra of one row are inversion-related. Cation-cation distances along the row are alternately shorter, 2.82 Å, and longer, 3.62 Å for arsenopyrite FeAsS. All this leads to a distorted derivative of marcasite, with the space group $B12_1/d1$ instead of the *Pmnn* of the marcasite aristotype. Results of Fuess et al. (1987) who found partly mixed S and As populations in arsenopyrite $Fe_{0.87}Co_{0.13}As_{0.88}S_{1.12}$ can be interpreted by the presence of antiphase domains in the S-As arrangement, as observed by them using HRTEM. According to Scott and Nowacki (1976), alloclasite CoAsS (Fig. 33d) has a pattern of As and S distribution different from arsenopyrite. The stacks of parallel S-As dumbells along the *c* axis have all dumbells oriented in the same way, i.e., pure S and As [001] stacks are present.

CHANNEL AND CAGE STRUCTURES

Chalcogenides form a range of channel and several cage structures, combining framework-forming cations of various kinds with large cations, in most cases M^+ and M^{2+}. A more complete account of channel structures with octahedral walls, cetineites (Sabelli et al. 1988; Wang and Liebau 1998), channel structures with Cu- and Ag-rich walls, channel-like sulfosalts, and cage-like structures of the skutterudite family is given in Makovicky (2005). Compounds belonging to the mineralogically most important category of channel structures are listed in Table 21.

CATION-SPECIFIC STRUCTURES

Mercury sulfides

Cinnabar. The crystal structure of α-HgS (cinnabar, Schleid et al. 1999) is commonly referred to as a distortion derivative of the PbS archetype. The contents of "octahedra" are

Table 21. Compounds with copper-rich partitions and related structures.

Compound	Lattice Parameters (Å,°)				Space Group	Ref.
	a	*b*	*c*	β		
$TlCu_{3.99}Se_3$	12.431(0)	12.800(0)	3.935(1)	—	*Pnnm*	[1]
$TlCu_5Se_3$	12.900	—	3.968	—	$P4_2/mnm$	[2]
$TlCu_3Se_2$	15.213(1)	4.012(0)	8.394(0)	111.70(1)	*C*2/*m*	[3]
$Tl_5Cu_{14}Se_{10}$	18.097(2)	3.958(0)	18.118(2)	116.09(1)	*C*2/*m*	[4]
$TlCu_7Se_4$	10.448(1)	—	3.968(0)	—	*I*4/*m*	[5]
$TlCu_7S_4$	10.180(0)	—	3.859(0)	—	$I\bar{4}$	[6]
$NH_4Cu_7S_4$	10.25(2)	—	3.84(1)	—	$I\bar{4}$	[7]
$Rb_3Cu_8Se_6$	18.458(6)	4.010(1)	10.212(3)	104.44(2)	*C*2/*m*	[8]
$Cs_3Cu_8Se_6$	19.076(4)	4.078(1)	10.449(3)	106.04(3)	*C*2/*m*	[8]
$K_2Hg_6S_7$	13.805(8)	—	4.080(3)	—	$P42_1m$	[9]
Betekhtinite $Pb_2(Cu,Fe)_{21}S_{15}$	3.86	14.67	22.80		*Immm*	[10]
Miharaite $Cu_4FePbBiS_6$	10.880	12.003	3.874		$Pb2_1m$	[11]
Synthetic $Cu_3Bi_2S_3I_3$	28.056	4.105	10.580	110.57	*C*2/*m*	[12]

Reference: [1] Berger et al. 1995; [2] Berger et al. 1990; [3] Berger 1987; [4] Berger and Meerschaut 1988 [5] Eriksson et al. 1991; [6] Berger and Sobott 1987; [7] Gattow 1957; [8] Schils and Bronger 1979; [9] Kanatzidis 1990; [10] Dornberger-Schiff and Höhne 1959; [11] Petrova et al. 1988; [12] Balić-Žunić et al. 2005

actually covalently bonded S-Hg-S groups (Hg-S = 2.34-2.40 Å), sharing common S atoms. The Hg-S-Hg angle is 173°. Hg coordination is completed by four long Hg-S distances (2 × 3.28 Å and 2 × 3.09 Å) (Fig. 34a). The most interesting view is that along [100] and another along the trigonal axis; they reveal the spiralling system of short Hg-S bonds. Thus, cinnabar is a compound with infinite [001] chains of short Hg-S-Hg-S bonds, with a triple period; these are analogous to the Se-Se-Se chains in native selenium. The dimorph, metacinnabar, is an isotype of sphalerite ($F\bar{4}3m$, a = 5.903 Å).

Nickel sulfides

The sulfides of nickel are distinguished by a number of short metal-metal distances, with lengths comparable to the Ni-Ni distance in the metal. The observed coordinations range from fivefold square-pyramidal to four-fold tetrahedral and flat-tetrahedral or even square planar. At elevated temperatures, NiS has octahedrally coordinated Ni and there is a gradual change in the coordination of nickel from 6- (octahedral) to 5- or 4-fold as the temperature decreases. In addition to the phases described below, pentlandite and a synthetic Ba-Ni sulfide with Ni in tetrahedral coordination and three Ni-Ni bonds belong to this category. The high-temperature phases NiS_2 and Ni_3S_4 with octahedral and tetrahedral nickel coordination are distinct from them.

Heazlewoodite. The rhombohedral, pseudocubic (a = 4.072 Å, α = 89.46°) structure of heazlewoodite, Ni_3S_2, is characterized by four short Ni-Ni distances for each nickel atom (Parise 1980). Two of the interactions are perpendicular to the c axis and form a part of a Ni_3 triangle (Ni-Ni = 2.53 Å). These triangles are stacked in a rhombohedral arrangement, creating Ni spirals parallel to [001] (Ni-Ni = 2.50 Å). Nickel is tetrahedrally coordinated by sulfur at 2 × 2.25 Å and 2 × 2.29 Å. Three tetrahedra share a common edge (cf. the above triangles). Along [001], each of them has two more shared edges (Fig. 34b).

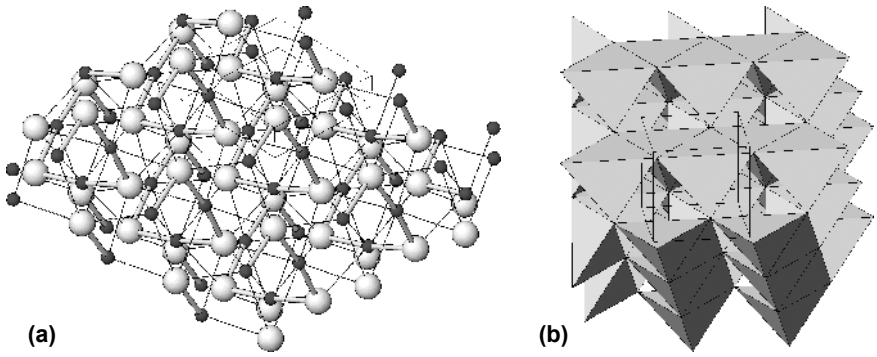

Figure 34. (a) Cinnabar (Schleid et al. 1999). Spirals [001] of short Hg-S bonds are indicated by thick lines, the remaining Hg-S contacts by thin lines. (b) Heazlewoodite, Ni_3S_2 (Parise 1980). Tetrahedrally coordinated nickel with five tetrahedron edges shared with adjacent tetrahedra.

Millerite. The crystal structure of millerite, NiS (Grice and Ferguson 1974) consists of [001] columns of three edge-connected coordination pyramids (NiS_5), with vertices pointing outward and joined to the bases of pyramids in the adjacent columns (Fig. 35a). Pyramidal bases are oriented inward and generate triangles of short Ni-Ni interactions equal to 2.53 Å. In the case of millerite, these triangles do not form a three-dimensional net (Ni-Ni = 3.14 Å along the column direction). Towards the vertex of the NiS_5 coordination pyramid, the Ni-S bond is 2.26 Å long, whereas it is 2.37 Å at the base. Interestingly, the S-centered polyhedra, SNi_5, form the same motif as the NiS_5 polyhedra.

Godlevskite. The structure of orthorhombic godlevskite, Ni_9S_8, space group $C222$ (Fleet 1987), can be described as a sphalerite-like packing of tetrahedra with numerous vacancies in which the tetrahedra are replaced by NiS_5 square pyramids. In the stacking of $(1\,\bar{1}1)$ layers, a two-layer sequence is observed: the more complete one of the two tetrahedral layers has large irregularly-shaped vacancies with interstitial Ni tetrahedra inserted in them ; the less fully occupied, rudimentary tetrahedral layer is filled by square coordination pyramids. In the latter, rows of paired pyramids, parallel to [101] occur, sharing edges with one another and with tetrahedra. Ni-Ni interactions run as infinite chains with some interconnections. The distances are 2.62-2.89 Å; for distinct Ni sites the number of metal-metal contacts varies from zero to five.

Godlevskite (Fig. 35b) is an OD structure composed of two types of (001) layers: (a) layers with a zig-zag arrangement of square pyramids and with a layer group $P2_12(2)$ (the direction perpendicular to the layer indicated by round brackets), and (b) layers with "bisphenoid clusters" of tetragonal pyramids and with edge-sharing tetrahedra, with the layer group $P(\bar{4})2m$. There is only a single position for the $P(\bar{4})2m$ layer after the $P2_12(2)$ layer, but there are two alternative positions for the latter layer after the former one. The zig-zag chains of square pyramids of Ni in these two alternatives run at 90° to one another, suggesting the possibility of a tetragonal polytype. For the planes $(1\,\bar{1}1)$, the OD phenomenon manifests itself by the selected [101] strings of polyhedral configurations sliding past one another, assuming two alternative positions, ½ [101] apart.

Maucherite, $Ni_{11}As_8$, is tetragonal, space group $P4_12_12$, (Fleet 1973). It is a true OD structure although it has not yet been described as such. The layer group of the OD layer is $P(\bar{4})m2_1$. The OD layer consists of two sheets formed by rows of $NiAs_5$ square coordination pyramids; these sheets are related by a four-fold rotoinversion operation. It is limited by the arsenic atoms on planes of glide-reflection (Fig. 35c). The interlayer symmetry is $n_{1/2,1}$, parallel to (001), and 2_1 parallel to [010].

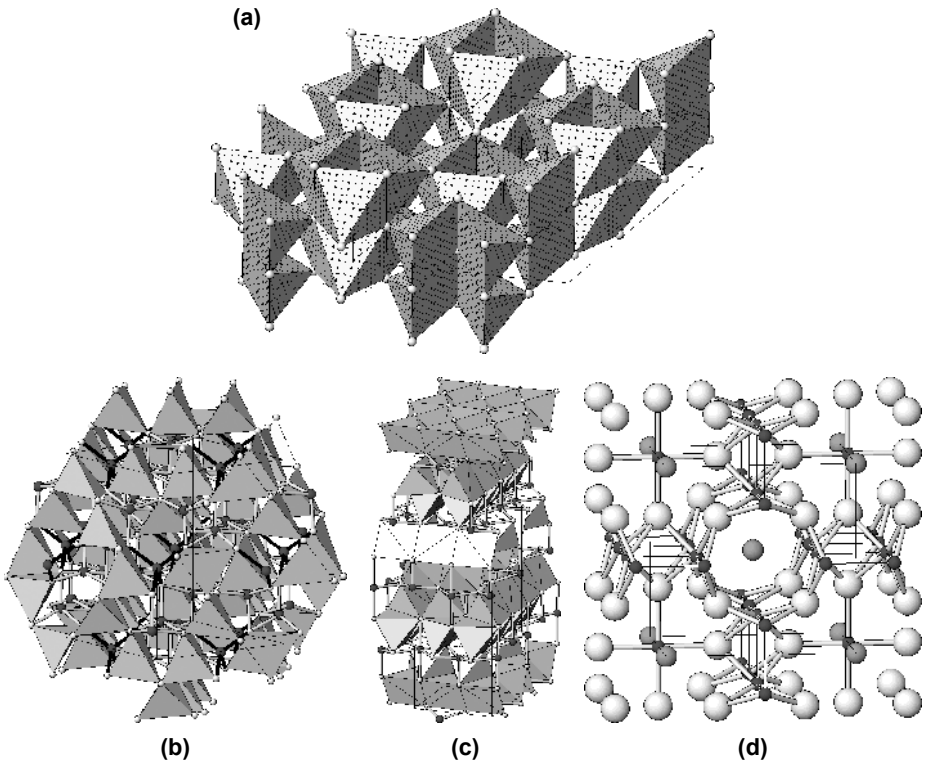

Figure 35. (a) Millerite, NiS (Grice and Ferguson 1994). Columns [001] of square pyramids (NiS_5) sharing edges. Nickel forms triangles of short Ni-Ni contacts inside the columns. (b) Godlevskite, Ni_9S_8 (Fleet 1987). Combination of NiS_4 coordination tetrahedra and NiS_5 square coordination pyramids. Note the layers (001) (horizontal) with edge-sharing tetrahedra (central tetrahedra of clusters are rendered in a black, ball-and-stick presentation) which alternate with layers rich in square coordination pyramids (bonds outlined in light). OD character: see text. (c) The OD structure of maucherite, $Ni_{11}As_8$ (Fleet 1973). Edge- and face sharing coordination pyramids ($NiAs_5$) and a coordination octahedron $NiAs_6$. The OD layer (see text) is composed of the two top layers of pyramids in the figure. (d) Hauchecornite (Kocman and Nuffield 1974). Coordination squares of Ni (shown as small dark spheres), with Ni-Ni interactions as thin black lines; medium grey: Bi, large white spheres: S.

Hauchecornite group. Hauchecornite, $Ni_9(Bi_{1.3}Sb_{0.7})S_8$, (Kocman and Nuffield 1974) and arsenohauchecornite, $Ni_{18}AsBi_3S_{16}$ (Grice and Ferguson 1989) are sulfide-bismuthides. Their structures (Fig. 35d) can be understood as a channel structure, with double-columns of accordion-arranged coordination squares of nickel, sharing edges, and forming a very regular ladder-like motif of longitudinal- and cross- Ni-Ni bonds, 2.68 and 2.73 Å for the former, and 2.64 Å for the latter. Ni-S distances lie between 2.26 and 2.32 Å. Square channels created by the accordion-like walls contain Bi in $BiNi_8$ and Ni-Bi-Ni coordinations, respectively. Bi-Ni distances are 2.69 and 2.70 Å, Bi-S only 2.78 Å.

Sulfides of palladium and platinum

Fairly complete structural knowledge exists for the numerous sulfides of palladium (Table 22).

Cation-based polyhedra. In sub-sulfides of Pd, the coordination polyhedra of palladium are very complex. The number of direct Pd-Pd contacts is a function of the Pd:S ratio. In

Pd_4S (an unnamed mineral), palladium atoms are 12-coordinated, by 10 palladium atoms up to a distance of 3.12 Å and two S ligands at 2.34 and 2.48 Å, respectively, in an irregular polyhedron. The sulfur atoms are in a near-trans configuration (Fig. 36a). In Pd_3S, different Pd sites are surrounded by 7 and 8 Pd atoms, at 2.78-2.95 Å, and again coordinated only to two sulfur ligands (at 2.28 and 2.46 Å) in an approximate trans-configuration.

Vasilite, $Pd_{16}S_7$, contains two distinct palladium sites. Pd1 has a five-fold ring of Pd atoms at 2.74-2.79 Å and, in the orientation perpendicular to this ring, a pair of S ligands in a trans-configuration, at 2.27 and 2.32 Å, respectively. Pd2 has six Pd ligands at 2.74-2.95 Å, and three S ligands forming a triangular configuration, all situated at 2.45 Å from Pd2. For comparison, in the cubic F-centered palladium, the Pd-Pd distance is 2.749 Å.

In the crystal structure of its 1:1 sulfide vysotskite, PdS, palladium assumes a square-planar coordination, with S ligands at 2.32-2.35 Å (Fig. 36b). Each Pd atom has zero, one or two very long Pd-Pd distances (minimum value is 3.30 Å). In the projection on (001), the tetragonal stucture imitates a $3^2.4.3.4$ net. One of the [001] square channels is filled by a stack of mutually parallel, horizontal PdS_4 coordination squares, whereas the other has walls lined by alternating, vertical PdS_4 square configurations. The latter is also true for the triangular channels separating the square ones. This configuration lowers the symmetry to $P4_2/m$.

The structure of PdSe (Fig. 36c) is an $N = 2$ homologue of the structure of PdS. The square piles of "horizontal" coordination $PdSe_4$ squares are doubled, the paired squares being inserted in a network of square- and triangular channels with walls lined by alternating vertical $PdSe_4$ squares. The structure is still tetragonal, space group $P4_2/mbc$, the Pd-Se distances are 2.427-2.468 Å and the closest Pd-Pd distances, in the interior of vertically lined square channels, are 3.20 Å.

A different stacking of square coordination units occurs in PtS (Fig. 37a,b). In this simple tetragonal structure, space group $P4_2/mmc$, only square channels parallel to [001] are present;

Table 22. Palladium and platinum chalcogenides.

Mineral	Formula	Space Group	Lattice Parameters (Å,°)				Ref.
			a	*b*	*c*	β	
Vysotskite	PdS	$P4_2/m$	6.429		6.611		[1]
Synthetic	PdS_2	*Pbca*	5.460	5.541	7.531		[2]
Synthetic	PdSe	$P4_2/mbc$	11.565		6.998		[3]
Cooperite	PtS	$P4_2/mmc$	3.47		6.110		[4]
Synthetic	PtS_2	$P\bar{3}m1$	3.543		5.039		[5]
Synthetic	Pd_4S	$P\bar{4}2_1c$	5.115		5.590		[6]
Synthetic	Pd_3S	*Ama*2	6.088	5.374	7.453		[7]
Vasilite	$Pd_{16}S_7$	$I\bar{4}3m$	8.93				[8]
Palladseite	$Pd_{17}Se_{15}$	$Pm\bar{3}m$	10.606				[9]
Prassoite	$Rh_{17}S_{15}$	$Pm\bar{3}m$	9.911				[9]
Synthetic	$Ni_{10}Pd_7S_{15}$	$Pm\bar{3}m$	9.872				[10]
synthetic	$Tl_2Pt_5S_6$	$P2_1/n$	6.971	6.941	11.088	97.83	[11]
Jaguéite	$Cu_2Pd_3Se_4$	$P2_1/c$	5.672	9.909	6.264	115.40	[12]
Chrisstanleyite	$Ag_2Pd_3Se_4$	$P2_1/c$	5.676	10.342	6.341	115.00	[12]

References: [1] Brese et al. 1985; [2] Grønvold and Rost 1957; [3] Ijjaali and Ibers 2001; [4] Grønvold et al. 1960; [5] Furuseth et al. 1965; [6] Grønvold and Rost 1962; [7] Rost and Vestersjö 1968; [8] Matković et al. 1976; [9] Geller 1962; [10] Dubost et al. in press; [11] Klepp 1993; [12] Topa et al. in press

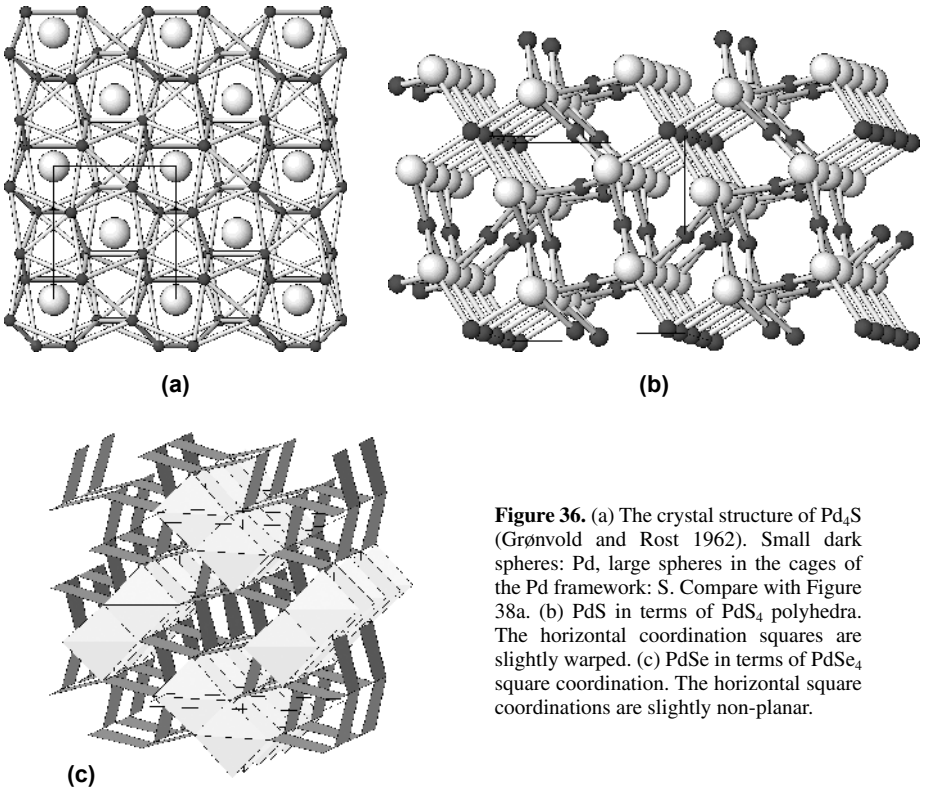

Figure 36. (a) The crystal structure of Pd_4S (Grønvold and Rost 1962). Small dark spheres: Pd, large spheres in the cages of the Pd framework: S. Compare with Figure 38a. (b) PdS in terms of PdS_4 polyhedra. The horizontal coordination squares are slightly warped. (c) PdSe in terms of $PdSe_4$ square coordination. The horizontal square coordinations are slightly non-planar.

all are lined by vertical coordination PtS_4 squares. The alternation of these configurations results in bands <100> of edge-sharing PtS_4 squares. Along [001], the [100] and [010] strips alternate, meeting in common S atoms (Fig. 37b).

PtSe is not known. The structure of palladseite, $Pd_{17}Se_{15}$, stoichiometrically close to the above described PdSe, is one of the most complicated structures in this category. Isotypic are prassoite, $Rh_{17}S_{15}$ and synthetic $Ni_{10}Pd_7S_{15}$ (Table 22), whereas $Pd_{17}S_{15}$ has never been encountered. This complicated cubic structure has four distinct cation sites of widely different type. It contains: (a) a "scallop" consisting of two "shells," i.e., cup-like configurations of four edge-sharing, flattened tetrahedra (Fig. 37c); (b) a coordination octahedron sandwiched between the dorsal portions of six "scallops," and (c) two distinct types of square coordination situated in a <100> system of channels between the above elements. The first type of coordination square occupies all faces of a cube formed in each channel intersection, whereas the second one halves the channels between two intersections (Fig. 37d).

In the ternary sulfide, $Ni_{10}Pd_7S_{15}$, nickel shows preference for the octahedral site (90% Ni, *M*-S = 2.41 Å), and the flat-tetrahedral site (60% Ni, *M*-S = 2.25-2.33 Å), whereas the square coordinations forming the cube have 50% Ni and *M*-S distance equal to 2.27 Å. The other square site is 90% Pd, here *M*-S = 2.41 Å. The flattened tetrahedra are a hallmark of this structure type. In these sites, the *M*-S distance varies from 2.26 Å to 2.35 Å in $Rh_{17}S_{15}$; this corresponds to 2.43-2.51 Å in $Pd_{17}Se_{15}$. The trans-configuration angle, which would be 180° for the planar coordination and 109.47° for a regular tetrahedron, is $2 \times 163.9°$ and $2 \times 166.5°$ in the flat tetrahedra of the ternary compound. The only short cation-cation distance

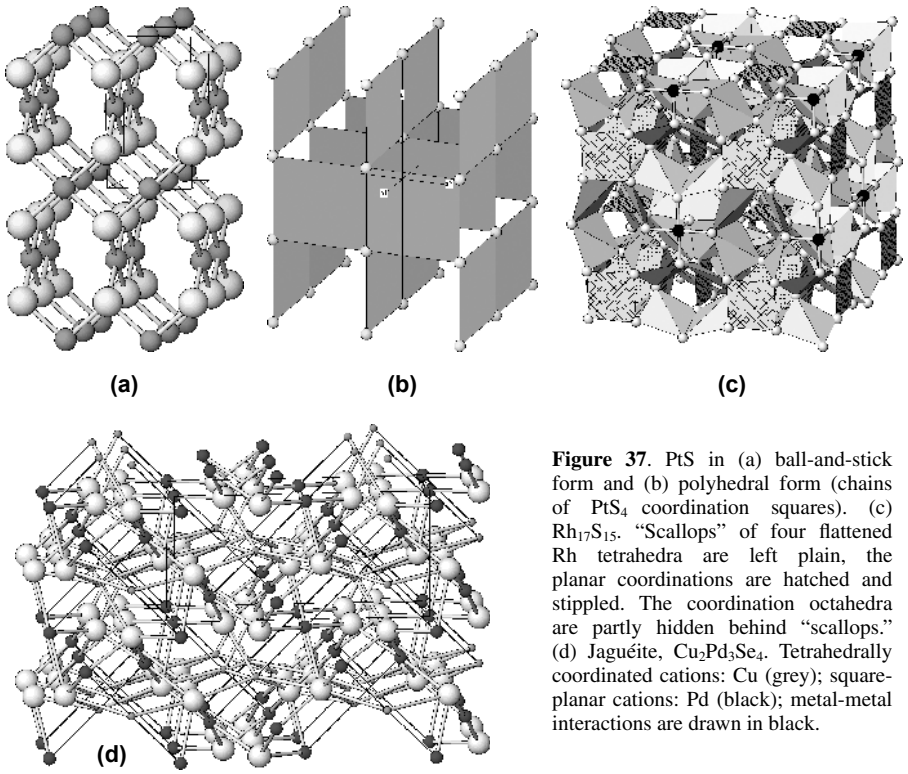

Figure 37. PtS in (a) ball-and-stick form and (b) polyhedral form (chains of PtS_4 coordination squares). (c) $Rh_{17}S_{15}$. "Scallops" of four flattened Rh tetrahedra are left plain, the planar coordinations are hatched and stippled. The coordination octahedra are partly hidden behind "scallops." (d) Jaguéite, $Cu_2Pd_3Se_4$. Tetrahedrally coordinated cations: Cu (grey); square-planar cations: Pd (black); metal-metal interactions are drawn in black.

is found between the two square coordinations outside the cube, equal to 2.63 Å in the case of $Ni_{10}Pd_7S_{15}$, and commensurate with distances in pure metals also for both remaining compounds. Differences in electronic configurations in the four distinct cation sites (metal-metal bonds in the latter case) are solved by the distribution of Ni *vs.* Pd in $Ni_{10}Pd_7S_{15}$ but must be resolved using the same cation in the two binary compounds.

Square-planar configurations occur also in ternary sulfides/selenides of Pd and Pt. Staggered, variously folded and in one direction also cut-up strips of PtS_4 squares occur, e.g., in $Tl_2Pt_5S_6$ (Klepp 1993), in which their interspaces are occupied by Tl. Another interesting structure with planar coordinations is that of jaguéite, $Cu_2Pd_3Se_4$, and of the isotypic chrisstanleyite, $Ag_2Pd_3Se_4$ (Topa et al. in press). In these structures, Pd1 forms isolated square coordinated $PdSe_4$, whereas Pd2 occurs as coordination squares paired via a common edge (Fig. 37d). The Pd-Se distances are 2.49-2.50 Å, and 2.47-2.49 Å, respectively. The $Pd1Se_4$ coordination is perfectly square, whereas that of paired Pd2 squares is slightly puckered (their planarity expressed by the trans-configuration Se-Pd-Se angles of 180.0° and 175.2° ± 0.3°, respectively). The openwork structure created by corner-connection of these square coordinations is stabilized by the presence of elongated $CuSe_4$ (resp. $AgSe_4$) tetrahedra, occuring as edge-sharing pairs, and by linear cation-cation interactions Pd2-Cu(Ag)-Pd1-Cu(Ag)-Pd2, with Cu-Pd distances equal to 2.86 Å for Pd1 and 2.75 Å (plus additional 2.90 Å) for Pd2 (Fig. 37d).

Anion-based coordination polyhedra. The complex structures of lower sulfides of Pd are easier to comprehend when they are presented in terms of S-centered coordination polyhedra, with cations as ligands. In the structure of Pd_4S, the anion-based polyhedra are bisdisphenoids (SPd_8) which share all eight corners with adjacent bisdisphenoids (Fig. 38a). In Pd_3S, the

coordination number of sulfur is 6 (Makovicky 2002). Completely different coordinations are observed in vasilite, $Pd_{16}S_7$: tetrahedral clusters of trigonal coordination prisms (SPd_6), radiating from a common Pd_4 tetrahedron, are interspersed by disphenoids (SPd_4) which interconnect free vertices of the trigonal coordination prisms (Fig. 38b). The shortest Pd-S bonds (2.28 Å) occur in these disphenoids.

In both 1:1 sulfides and the selenide, the central anion is tetrahedrally coordinated by the cation. In PdS, there are (S_2Pd_6) clusters composed of two edge-sharing tetrahedra, strung along [001] and interconnected with adjacent strings of such groups, one at the same height, whereas the others are displaced by ½ [001]. The structure can be described as stacking of $\bar{4}2m$ propellers of four tetrahedra along [001] by means of horizontal, inter-propeller *m* planes and only corner-sharing with adjacent stacks (Fig. 38c). Similar strings of tetrahedra that alternatively share and do not share edges along [001] occur in PdSe. However, the "propeller scheme" is modified compared with that in PdS. In PtS, the S-centered tetrahedra form strings of edge-sharing tetrahedra along [001]; these strings share only tetrahedral corners.

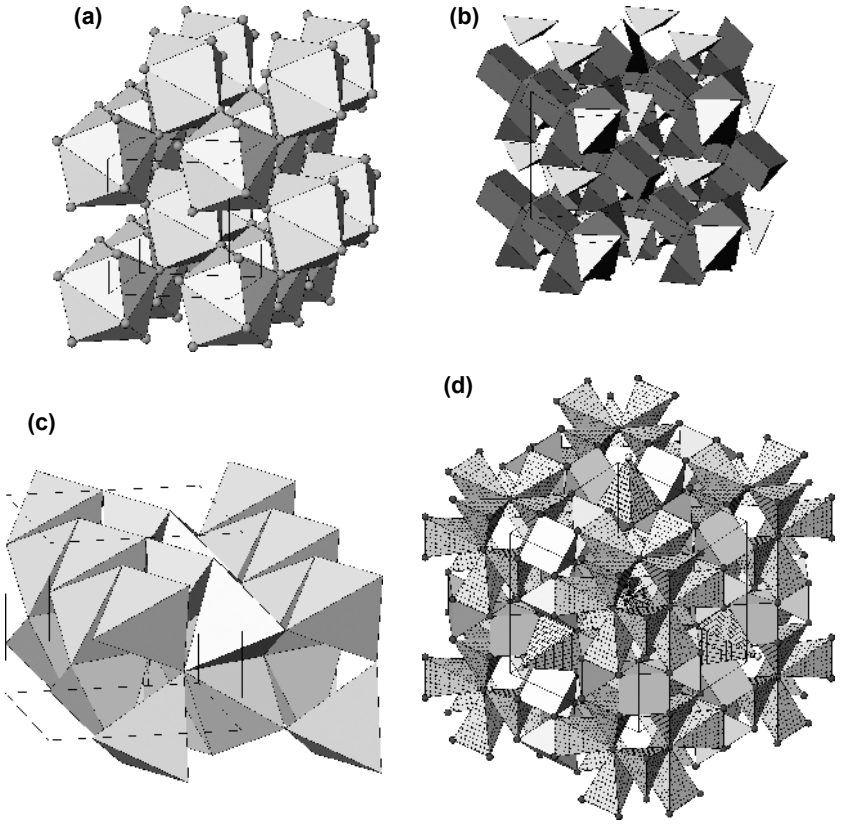

Figure 38. (a) Sulfur-centered bisdisphenoids (SPd_8) in the crystal structure of Pd_4S. Compare with Figure 36a. (b) Sulfur-centered coordination polyhedra in the crystal structure of $Pd_{16}S_7$. Tetrahedral clusters of trigonal coordination prisms (SPd_6) are interspersed by SPd_4 coordination tetrahedra. (c) PdS in terms of edge-sharing SPd_4 tetrahedra. Note the "propellers" of four tetrahedra. (d) S-centered coordination polyhedra in the crystal structure of $Rh_{17}S_{15}$. Cage-like configurations of SRh_4 coordination tetrahedra, two- and three-dimensional "iron crosses" of SRh_5 coordination pyramids. The latter also occur in pentlandite as $S(Fe,Ni)_5$.

In spite of similar unit cell parameters, the $Pd_{17}Se_{15}$ structure type is different from pentlandite; among the sulfur-centered polyhedra, however, three-dimensional "iron crosses" of six tall square coordination pyramids (M_5S) with a common S vertex (Fig. 38d) are prominent in both structure types.

The concept of anion-based coordination polyhedra has only rarely been applied to chalcogenides. It can bring quite a new insight into the crystal chemistry of these compounds.

IONIC CONDUCTORS AND THE CHALCOGENIDES OF Cu AND Ag

Ionic conductors are substances in which cations or anions become mobile above a transition temperature, and become "frozen" in fixed coordination polyhedra below this temperature. They dominate chalcogenide phase systems with copper and silver. They also occur among compounds with cations such as lithium, sodium, and other alkalis. This behaviour has been documented for many channel structures (see Makovicky 2005), some cage structures, and for many layer intercalates. A number of sulfosalts also belong to this category. In the present account we concentrate upon the sulfides and sulfosalts of Cu and Ag.

Compounds of copper. The Cu-S phase diagram has a number of phases belonging to this category, situated in the range Cu_2S-CuS (see Fleet 2006, this volume). Structure analyses exist for chalcocite Cu_2S (Evans 1979; Cava et al. 1981), djurleite $Cu_{1.934-1.965}S$ (Evans 1979) and anilite (Koto and Morimoto 1970). Furthermore, recent structural investigations have been published on high and low digenite, $Cu_{1.8}S$ (Will et al. 2002) and ample material has been published on high and low bornite (Cu_5FeS_4) and its solid solution with digenite (discussed among compounds with clusters of tetrahedra).

At temperatures above 103.5 °C (Roseboom 1966), chalcocite has a small hexagonal cell with symmetry $P6_3/mmc$ (Table 23). According to Buerger and Wuensch (1963) and Cava et al. (1981), its structure consists of an *hcp* arrangement of sulfur anions where copper is highly mobile, found primarily in triangular coordinations of the disordered cation substructure. Cu with anharmonic thermal motion occupies primarily the alternate triangular sites in the hexagonally packed (0002) layers (70% occupancy), and all triangular sites between two consecutive (0002) layers (20% occupancy). These occupancies should be understood as a fractional residence time. Below 103.5 °C, the Cu atoms become immobilized in the sites of a monoclinic $P2_1/c$ structure with 24 fully occupied Cu sites and 12 S sites in a cell (Table 23). The *c* axis is equal to 4*c* of the hexagonal (sub)cell, the *a* axis dips across the layers of the hexagonal close packing at an interval of $2c_{hex}$. The structures of the chalcocite – djurleite pair are built along closely related principles. The $P2_1/n$ cell of djurleite contains 62 Cu and 32 S atoms.

The situation in low-temperature chalcocite is illustrated well by the portion of it shown in Figure 39a. With the exception of two Cu atoms with close-to-linear coordination, the Cu atoms are in more or less regular triangular coordination. Only rarely do the Cu atoms deviate more substantially from the plane of the triangle defined by the sulfur ligands. Eight Cu atoms in a unit cell are in the triangles in the (0001) plane (the same for 20 Cu atoms in djurleite); the remaining Cu atoms are at the fixed ~1/3 and ~2/3 positions between two consecutive layers. Cu-Cu distances play an important role in the structure of chalcocite, the closest contacts being 2.52 Å (2.45 Å in djurleite). The most frequent Cu-Cu distances are about 2.77 Å; they are distributed symmetrically between 2.5 and 3.0 Å. Cu-S distances peak at 2.30 Å, the average triangular bond length. They are situated between 2.20 and 2.40 Å, whereas any tendencies towards tetrahedral coordination are very distorted.

Typical features of both structures are the empty coordination octahedra with 3-4 alternate triangular faces occupied by Cu in distinct combinations (Evans 1981). Exceptionally, two of these triangles share an edge. In an ideal octahedron (S-S distance of 3.95 Å), the triangular

Table 23. Copper and silver chalcogenides (ionic conductors).

Phase	Space Group	Lattice Parameters (Å,°)				Notes	Ref.
		a	*b*	*c*	Angle		
High-*T* Cu_2S	$P6_3/mmc$	3.985	3.985	6.806	120°	[a]	(1)
Low-*T* Cu_2S chalcocite	$P2_1/c$	15.246	11.884	13.494	β 116.35°	[b]	(2)
Digenite $Cu_{1.8}S$	$Fm\bar{3}m$	5.593	5.593	5.593	—	[c]	(3)
Djurleite $Cu_{1.96}S$	$P2_1/n$	26.897	15.745	13.565	β 90.13°	[d]	(2)
Anilite $Cu_{1.75}S$	$Pnma$	7.89	7.84	11.01	—	[e]	(4)
High-*T* Ag_2S	$Im\bar{3}m$	4.889	4.889	4.889	—	[f]	(5)
Low-*T* Ag_2S	$P2_1/n$	4.23	6.91	7.87	β 99.58°	[g]	(6)
High-*T* Ag_2Te	$Im\bar{3}m$	5.329	5.329	5.329	—	[h]	(7)
Intermediate-*T* Ag_2Te	$Fm\bar{3}m$	6.643	6.643	6.643	—	[i]	(7)
Low-*T* Ag_2Te	$P2_1/c$	8.164	4.468	8.977	β 124.16°	[j]	(8)
Stromeyerite CuAgS	$Cmc2_1$	4.059	6.617	7.967	—	[k]	(9)
Jalpaite Ag_3CuS_2	$I4_1/amd$	8.671	8.671	11.757	—	[l]	(10)

Notes: [a] 598 K; [b] Stable below 103.5 °C; [c] 673 K; [d] Ambient *T;* [e] under 75 °C; [f] 533K; [g] Stable below 177 °C; [h] 1123 K; [i] 723 K; [j] 295 K; [k] 298 K; [l] Ambient *T*

References: (1) Cava et al. 1981; (2) Evans 1979; (3) Will et al. 2002; (4) Koto and Morimoto 1970; (5) Cava et al. 1980; (6) Frueh 1958; (7) Schneider and Schulz 1993; (8) van der Lee and de Boer 1993; (9) Baker et al. 1991; (10) Baker et al. 1992

Cu-S distance is 2.28 Å, linear Cu-S distance is 1.98 Å, whereas Cu-Cu is 2.63 Å for alternate triangles and 3.23 Å across the volume of the octahedron. Thus, appreciable distortion of the sulfur framework is required in order to accommodate the Cu-Cu distances of about 2.77 Å, and the linear Cu-S distances especially (Evans 1981). Thus far, no principles have been defined for the long-range occupational patterns of triangles in these minerals; the two representations in Figures 39a-b illustrate well why this is so. The structure of chalcocite as well as that of djurleite is almost always multiply twinned with reference to their hexagonal substructure.

At Cu:S ratios less than 2:1, and above 435 °C (Roseboom 1966) for stoichiometric Cu_2S, a cubic phase, digenite (formally Cu_9S_5) exists, with a mobile copper array as in high chalcocite. As a point-like approximation to this mobile array, Will et al. (2002) found ~0.25 Cu in all tetrahedral sites, below 0.1 Cu in the octahedral positions of the F-centered cubic cell, and an envelope with a radius of about 0.9 Å of fractional ~0.03 sites around the tetrahedral site. These sites are at a distance of only 1.84 Å from the nearest S atom.

Anilite, Cu_7S_4 (Koto and Morimoto 1970) is based on *ccp* of sulfur atoms, its unit cell being $a\sqrt{2} \times a\sqrt{2} \times 2a$ of *ccp*. The structure contains rods composed of paired, edge-sharing tetrahedra of copper in an A-centered arrangement. They are actually rows of empty, edge-sharing octahedra with the tetrahedral interspaces occupied (Fig. 39c). The rest of the Cu atoms are present in triangular sites. Cu5 forms rows [010] of triangles, whereas Cu2 and Cu4 occupy three faces of empty coordination octahedra which are enclosed by four adjacent rows of paired tetrahedra. Triangularly coordinated Cu5 interconnects the empty octahedra with the filled tetrahedra of the tetrahedral rows.

An alternative description is that in terms of *ccp* layer stacking. The ABC sequence of layers $(011)_{anilite}$ is overprinted by a two-layer scheme of Cu occupancy, alternating the layers composed exclusively of triangular copper sites with the layers consisting of Cu tetrahedra and only occasional triangles. The latter are in parallel channels [100]. Anilite is stable only to 75 °C (Potter 1977). Obviously it does not survive mobilization of Cu, yielding digenite instead.

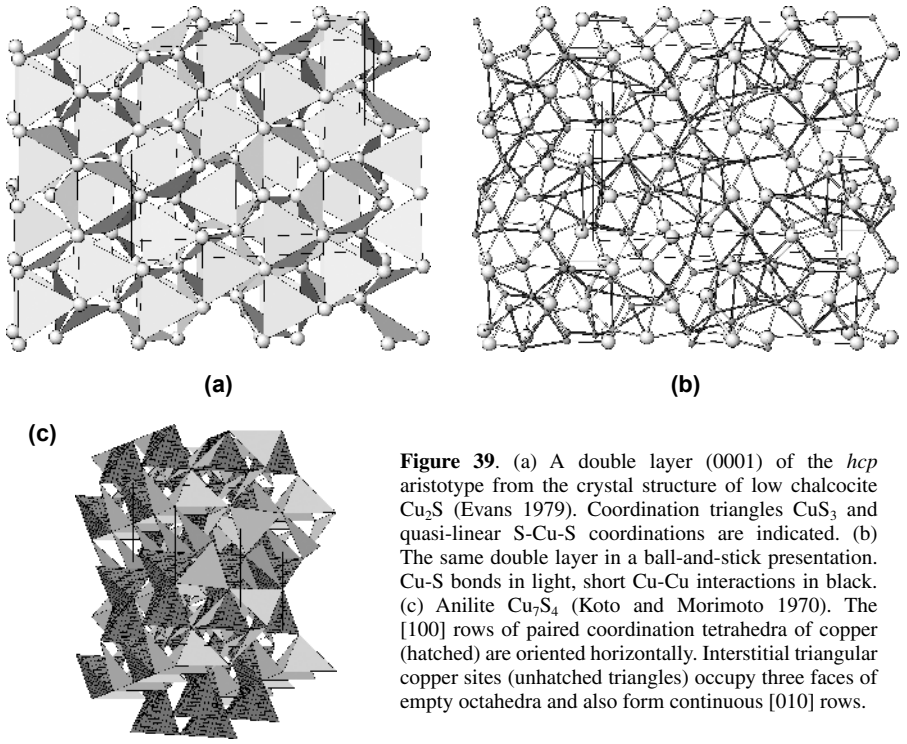

Figure 39. (a) A double layer (0001) of the *hcp* aristotype from the crystal structure of low chalcocite Cu_2S (Evans 1979). Coordination triangles CuS_3 and quasi-linear S-Cu-S coordinations are indicated. (b) The same double layer in a ball-and-stick presentation. Cu-S bonds in light, short Cu-Cu interactions in black. (c) Anilite Cu_7S_4 (Koto and Morimoto 1970). The [100] rows of paired coordination tetrahedra of copper (hatched) are oriented horizontally. Interstitial triangular copper sites (unhatched triangles) occupy three faces of empty octahedra and also form continuous [010] rows.

Among sulfosalts of copper, typical ionic conductors are found in the family of Cu_3XS_3 compounds (X = Sb,Bi; S = S,Se) (Table 24). These structures consist of an *hcp* array of anions which is twinned on $(11\bar{2}2)_{hcp}$ (Andersson and Hyde 1974). The thickness of *hcp* lamellae is $3d(11\bar{2}2)$, i.e., that of one S_6 octahedron. On the composition planes of the unit cell twinning, large trigonal coordination prisms are formed, occupied by the metalloid atom positioned close to one of the prism bases, i.e., in a pyramidal XS_3 coordination. Above the "freezing" temperature, this framework has symmetry *Pnma,* with Cu distributed (in sulfides) statistically over the available trigonal planar sites (Makovicky 1994; Pfitzner 1998). These are both the sites in the triangular walls shared by two tetrahedra and the sites of two kinds in the walls separating an octahedron and a tetrahedron. There are twice as many of these sites as the number of Cu atoms available, making these compounds eminently suitable for ionic conduction. In Cu_3SbSe_3 (Pfitzner 1995) a tetrahedral position straddling the mirror plane of the unit-cell twinning is occupied instead; yet another occupation scheme is found in the related Li_3AsS_3 (Seung et al. 1998).

In wittichenite, Cu_3BiS_3, every second row [001] of the triangles sandwiched between two tetrahedra is occupied by Cu in a continuous fashion (Fig. 40a). It is interspaced by 3D "rotors" composed of other types of occupied triangles. In the adjacent twin lamellae, these schemes alternate, related by 2_1 axes. Above the "freezing transformation" of 118 °C, this $P2_12_12_1$ polymorph has a precursor in the form of a modulated structure, with the **q** vector (parallel to c^*) changing from about 0.32 at the temperature of transformation to almost 0.5 at the point of fading out between 170° and 190 °C (Makovicky 1983) [1/**q** describes a periodicity of non-commensurate modulation in terms of the subcell periodicity in the given lattice direction]. The movement of satellites with temperature exhibits a change in behavior at

Table 24. Wittichenite homeotypes.

Mineral	Formula	Space Group	Lattice Parameters (Å,°)				Ref.
			a	*b*	*c*	β	
Wittichenite	Cu_3BiS_3	$P2_12_12_1$	7.72	10.4	6.72		[1]
Intermediate wittichenite	Cu_3BiS_3	*modulated*	7.66	10.5	6.72[(a)]		[2]
High wittichenite	Cu_3BiS_3[(2)]	*Pnma*	7.66	10.5	6.71[(b)]		[2]
Low skinnerite (γ)	Cu_3SbS_3	$P2_12_12_1$	7.88	10.2	6.62		[3][(c)]
Intermediate skinnerite (β)	Cu_3SbS_3	$P2_1/c$	7.81	10.2	13.27	90.29	[4][(d)]
High skinnerite (α)	Cu_3SbS_3	*Pnma*	7.81	10.3	6.59		[5]
Synth.	Cu_3SbSe_3[(e)]	*Pnma*	7.99	10.6	6.84		[6]
Synth.	Li_3AsS_3[(e)]	$Pna2_1$	8.05	9.82	6.63		[7]

Notes: (a) at 142 °C; (b) at 350 °C; (c) also Whitfield (1980); (d) also Pfitzner (1994), who gives transformation temperatures as –9 °C and +121 °C, respectively; (e) cation arrangements differ from the Cu_3BiS_3-Cu_3SbS_3 scheme.

References: [1] Kocman and Nuffield 1973; [2] Makovicky 1983; [2]; [3] Pfitzner 1994 [(c);] [4] Makovicky and Balić-Žunić 1995; [5] Pfitzner 1998; [6] Pfitzner 1995; [7] Seung et al. 1998

about 135 °C, close to the temperature of 150 °C given by Lugakov et al. (1975) as the onset of intense ionic conduction. Mizota et al. (1998) demonstrate a substantial decrease in resistivity of Cu_3BiS_3 at 100-115° but put the onset of ionic conduction at about 157 °C. The precursor has a substantial hysteresis both in the movement of satellites and in recovering the resistivity value that is appropriate for a given temperature. Several days are needed for a reequilibration from the reduced values of resistivity and larger values of the modulation **q** vector, which were inherited from the higher temperatures, on cooling. This suggests a heavily cooperative mechanism of ion movement in the structure. Models for the precursor structure have been proposed by Makovicky (1994).

Such a precursor has not been seen in Cu_3SbS_3 which has a phase transformation at 120 °C. In the ambient-temperature form of this compound, intermediate skinnerite, the [001] rows of tetrahedra are interrupted after two triangles, and shifted by *a*/2 to the alternate rows in the same twin lamella (Fig. 40b). The other Cu coordination triangles always occur as two opposing triangles in an empty octahedron. The Cu_3XS_3 structures actually are stackings of unit layers (001) of Cu-occupied triangles: the same layer-like enantiomorphs are related by a 2_1 axis perpendicular to them when they are stacked in wittichenite, whereas a two-layer pack of one enantiomorph is always followed by a two-layer pack of the opposite enantiomorph in intermediate skinnerite (Makovicky 1994). Low skinnerite, below –9 °C (Pfitzner 1994), does not have the (expected) symmetry $P2_1/n$, with single layers of enantiomorphs following one another, but it crystallizes in $P2_12_12_1$. The apparent reason is that the wittichenite structure offers the maximum number of structurally favoured short Cu-Cu distances, more than intermediate skinnerite, whereas the $P2_1/n$ form does not (Makovicky and Pfitzner, unpublished).

Another family of ionic conductors are the synthetic and natural copper-bismuth sulfides and selenides of the pavonite homologous series, typified by $Cu_{1.78}Bi_{4.73}Se_8$ (Makovicky et al. 2006). In this structure (Fig. 40c), the octahedral columns of the non-accretional layer contain three fractional copper sites, which add up to 1.5 Cu in one column period: the occupancy of the flattened tetrahedral sites in the upper and lower portions of the empty coordination octahedron is 0.31, that of the sideways positioned tetrahedral Cu is 0.26, whereas the tetrahedral sites between two adjacent octahedra contain 0.16 Cu each. Although

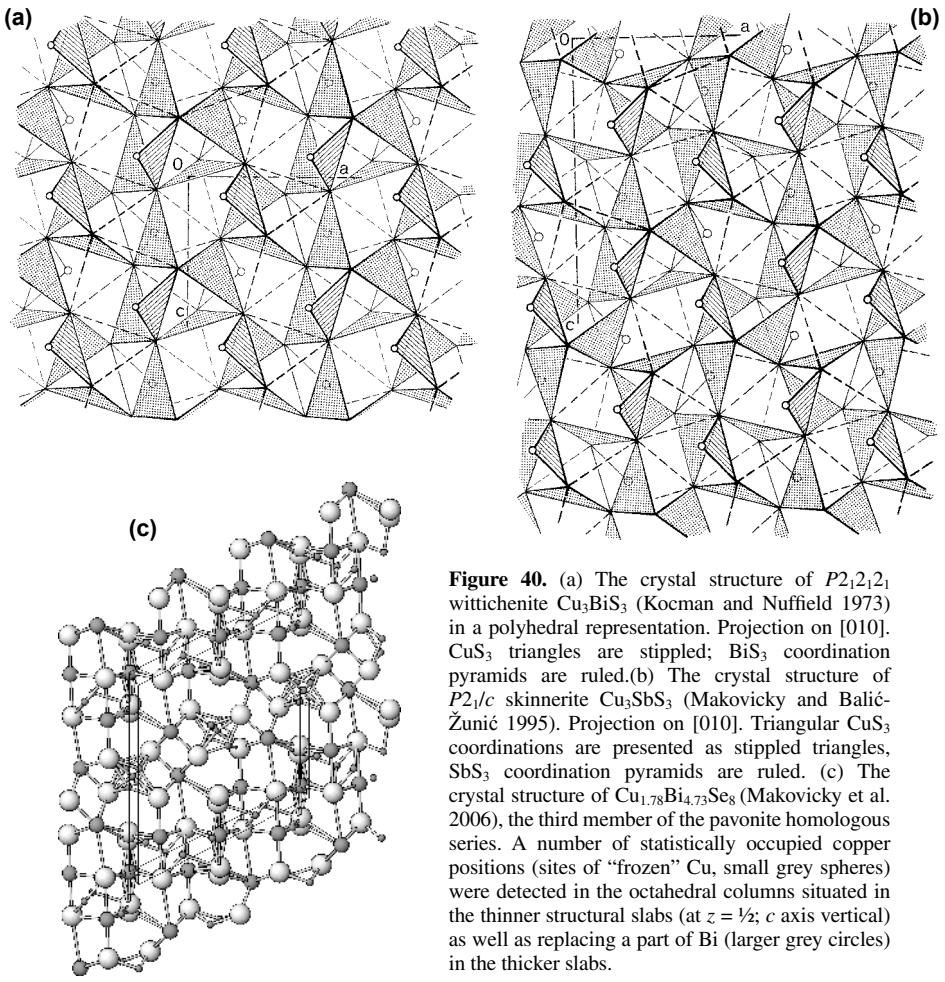

Figure 40. (a) The crystal structure of $P2_12_12_1$ wittichenite Cu_3BiS_3 (Kocman and Nuffield 1973) in a polyhedral representation. Projection on [010]. CuS_3 triangles are stippled; BiS_3 coordination pyramids are ruled.(b) The crystal structure of $P2_1/c$ skinnerite Cu_3SbS_3 (Makovicky and Balić-Žunić 1995). Projection on [010]. Triangular CuS_3 coordinations are presented as stippled triangles, SbS_3 coordination pyramids are ruled. (c) The crystal structure of $Cu_{1.78}Bi_{4.73}Se_8$ (Makovicky et al. 2006), the third member of the pavonite homologous series. A number of statistically occupied copper positions (sites of "frozen" Cu, small grey spheres) were detected in the octahedral columns situated in the thinner structural slabs (at $z = ½$; c axis vertical) as well as replacing a part of Bi (larger grey circles) in the thicker slabs.

no experimental confirmation is available as yet, the statistical character of Cu distribution along these columns suggests that they have been one-dimensional diffusion paths at the temperatures of formation. The statistically distributed fractional Cu in the accretional layer of Bi octahedra (site occupancies 0.02-0.09) must encounter much more hindrance when percolating through the framework of Bi octahedra. Olivier-Fourcade et al. (1983) prepared an ionic conductor $Li_{3x}Sb_{6-x}S_9$, a pavonite homologue $N = 4$ and Tomeoka et al. (1980) refined the $N = 3$ and 4 pavonite homologues in the system Cu-Bi-S, analogous to the above structure.

Compounds of silver. In the conducting state, the silver chalcogenides Ag_2S and Ag_2Se have body centered S frameworks in which the mobile Ag atoms reside preferentially at regular three-fold, slightly pyramidal sites. For Ag_2S (Cava et al. 1980), the three Ag-S distances are 2.73 Å; central angles are 126.9° and 2 × 101.5°). The Ag-Ag distances in the resulting "sodalite-like cage" of silver sites around a sulfur site (Fig. 41a) are not compatible with full occupancy, being 1.73 Å between all nearest neighbors, and 2.44 Å across the square faces of the cage. Occupancy is 33%. In high-temperature Ag_2Se (Oliveria et al. 1988), the corresponding Ag-Se distances are 2.82 Å, the Ag-Ag distances are 1.78 Å and 2.52 Å, respectively. The structure depicted is that above about 200 °C for Ag_2S, when practically

only the tetrahedral positions are occupied by silver atoms. Below this temperature, down to the temperature of a phase transformation at 177 °C, the octahedral positions centered between four such tetrahedral sites also show increasing occupancy. Fourier maps of high-*T* silver sulfide and selenide show continuous bands <100> of electron density, i.e., the preferred diffusion paths for silver. These are situated along the diameters of the square faces of the cuboctahedra; across the structure, these faces are strung along <100>. According to Wuensch (1993), diffusion in Ag_2S proceeds via crowded [100] second-nearest tetrahedral pairs and octahedral coordinations in a correlated, cooperative motion. The boundary with the other mode of ion conduction, diffusive hops between neighboring tetrahedral sites (such as in AgI), should lie at the $Ag_{1.5}X$ composition. The smooth distribution of Ag along its diffusion paths is a result of relaxation of the closely spaced tetrahedral dimers.

The highest temperature, *I*-centered polymorph of Ag_2Te (at about 1123 K) is isotypic, with distances Ag-Te = 2.98 Å, and Ag-Ag = 1.88 and 2.66 Å (Schneider and Schulz 1993). The intermediate "high" Ag_2Te polymorph (measured at 523-923 K) is F-centered and has Ag-Te distances of 2.65 Å and 2.84 Å. Ag forms a small cuboctahedron of sites, half-way between S atoms, with site-to-site distances equal to 1.12 and 1.58 Å, and in additional Ag sites at ¼ ¼ ¼ (Ag-Ag distances 1.95 and 2.13 Å); these distances might suggest diffusion paths for Ag. Distances from one cuboctahedron to an adjacent one are 2.47 Å, and less likely for direct diffusion. The low-temperature form of Ag_2Te (van der Lee and de Boer 1993) is composed of mackinawite-like layers (Ag-Te 2.88-3.02 Å) alternating with an openwork layer composed of elongated Ag tetrahedra (Ag-Te 2.84-3.03 Å); these share three edges with adjacent tetrahedra. All six edges of the tetrahedra in the mackinawite-like layer are shared with adjacent tetrahedra, two of these being below and above the layer (Fig. 41b). This leads to Ag-Ag distances between 2.91 and 3.13 Å.

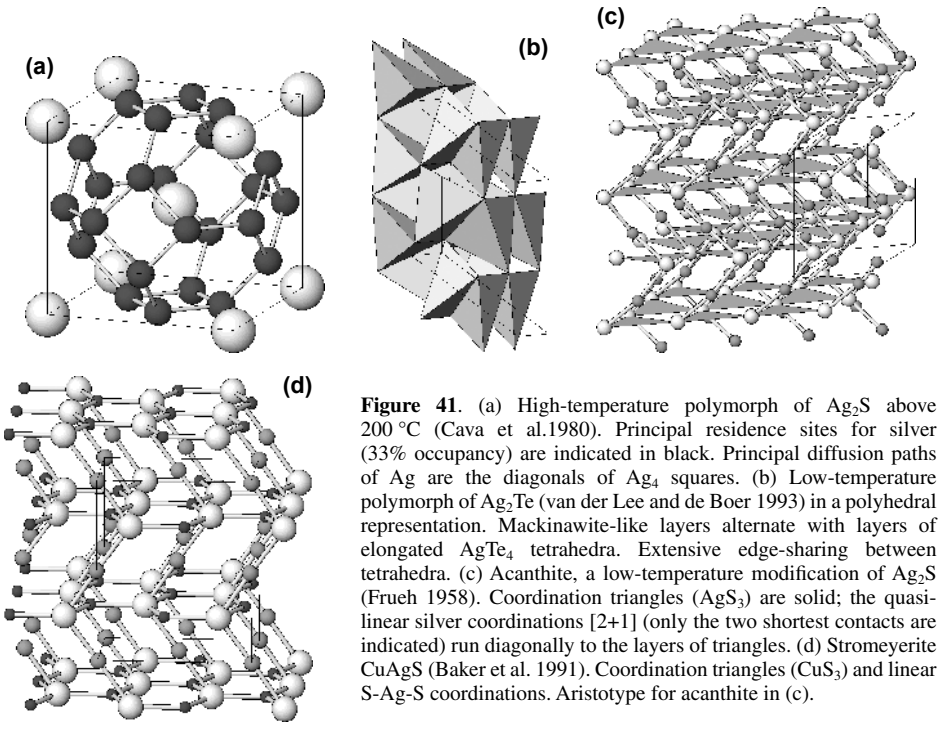

Figure 41. (a) High-temperature polymorph of Ag_2S above 200 °C (Cava et al.1980). Principal residence sites for silver (33% occupancy) are indicated in black. Principal diffusion paths of Ag are the diagonals of Ag_4 squares. (b) Low-temperature polymorph of Ag_2Te (van der Lee and de Boer 1993) in a polyhedral representation. Mackinawite-like layers alternate with layers of elongated $AgTe_4$ tetrahedra. Extensive edge-sharing between tetrahedra. (c) Acanthite, a low-temperature modification of Ag_2S (Frueh 1958). Coordination triangles (AgS_3) are solid; the quasi-linear silver coordinations [2+1] (only the two shortest contacts are indicated) run diagonally to the layers of triangles. (d) Stromeyerite CuAgS (Baker et al. 1991). Coordination triangles (CuS_3) and linear S-Ag-S coordinations. Aristotype for acanthite in (c).

The low-temperature form of Ag_2S, acanthite, consists of (010) layers which are distorted layers of hexagonally packed sulfur atoms, in which alternate triangles are occupied by Ag in trigonal coordination (Ag-S = 2.49, 2.57, and 2.60 Å). This coordination can also be interpreted as a very distorted tetrahedral coordination with the fourth bond of 2.98 Å out of the triangle plane (Fig. 41c). These planes are interconnected by quasi-linear Ag (S-Ag = 2.42 and 2.45 Å), with an additional distance equal to 2.92 Å. The only Ag-Ag interactions of interest are the isolated bonds at 2.94 Å between the two types of Ag; the network of other Ag-Ag interactions starts only at 3.05 Å. The *bcc* cell of the high-temperature form of Ag_2S becomes distorted in the low-temperature form into a pseudo-*bcc* cell with $a_1 = a_2 = 4.89$ Å, $a_3 = 4.76$ Å, $\alpha = 89.1°$, $\beta = 90.9°$, and $\gamma = 89.7°$ (Wuensch 1993). Adjustments between this state and the high-*T* cubic structure proceed first by change in the β angle of the low form, then by means of multiple twinning, followed by the transformation itself (Sadanaga and Sueno 1967).

The undistorted aristotype of acanthite is stromeyerite $CuAgS_2$ (Baker et al. 1991). This structure (Fig. 41d) consists of distorted hexagonal nets (001) of sulfur atoms, with alternate triangles occupied by Cu (2 × 2.25 Å and 2.34 Å). These nets are interconnected by linear S-Ag-S coordination units (2.44 and 2.45 Å). Ag-Ag distances are 3.88 and 3.89 Å whereas a zig-zag net of Ag-Cu distances in (010) planes of the structure are 2.88 Å and 3.45-3.52 Å. Another Cu-Ag sulfide, jalpaite, Ag_3CuS_2 (Baker et al. 1992) is essentially a structure based on linear coordination of both metals with the Cu-S distance equal to 2.18 Å and the Ag-S bonds equal to 2.50 and 2.57 Å. The Ag coordinations are of a quasi-tetrahedral (additional distances 2 × 2.94 Å) and linear type, respectively. In the interpretation based on these polyhedra, parallel and corner connected chains of edge-sharing Ag tetrahedra host linear Cu and Ag in interspaces. The structure is based on a distorted *I*-centered packing of sulfur.

The crystal structure of stephanite, Ag_5SbS_4 (Ribár and Nowacki 1970) can be treated as a distorted version of a unit-cell twinned *hcp* array, with the unit slabs only $1d_{11\bar{2}2}$ of *hcp* array thick, in comparison to wittichenite where they are $3d_{11\bar{2}2}$ thick. The trigonal coordination prisms on composition planes of unit cell twinning again contain Sb pyramids situated at a prism base, but these occur only in alternate [001] rows of prisms. The rows of prisms intervening in the *b* direction are occupied by three-fold coordinated Ag whereas the unit slabs themselves contain two distinct Ag sites, in 3-fold and 3+1 coordination, respectively. The polarity of the structure, space group $Cmc2_1$, is caused by the same orientation of all SbS_3 pyramids, in the $-c$ direction, throughout the entire structure.

In the case of Ag_3AsS_3, proustite, (Engel and Nowacki 1966), the basis of the structure is a rhombohedral arrangement of AsS_3 pyramids, stacked in continuous columns [001], and situated at the bases of trigonal coordination prisms preserving the same orientation of their As vertices (Fig. 42a). Silver is present in intervening trigonal channels [001], with a spiralling system of both S atoms and short S-Ag-S bonds (2.44 Å and 2.45 Å). Every silver atom has an additional S-Ag distance of 2.89 Å, i.e., a 2+1 coordination. The Ag-Ag distances in the channels are 3.25 Å, those between channels 3.48 Å, so there are no cation-cation interactions. A complete coordination polyhedron of Ag is a bipyramid with a rhomb-shaped cross-section in which the short, 2.45 Å, distances combine with long interactions (up to 3.61 Å). Three orientations of such pyramids intermesh in the silver-housing channels.

A remarkable low-temperature ionic conductor is pearceite $(Ag,Cu)_{16}(As,Sb)_2S_{11}$ (Bindi et al. 2006), refined in $P\bar{3}m1$, with $a = 7.388$ Å and $c = 11.888$ Å at room temperature and at 120 and 15 K. This structure consists of two alternating kinds of (0001) slabs, about 6 Å thick. One slab type, $(Ag,Cu)_6$ $(As,Sb)_2S_7$, has fully occupied trigonal pyramidal (As,Sb) sites, combined with trigonal planar Ag/Cu sites (average *M*-S=2.417 Å). These are fully occupied, with a certain amount of disorder present. The lone electron pairs of As/Sb point into the slab interior. The alternating types of slabs, Ag_9CuS_4, contain no semimetals, only a

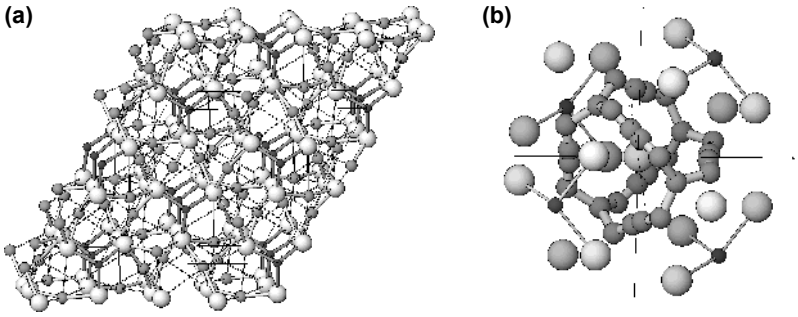

Figure 42. (a) Proustite Ag_3SbS_3 (Engel and Nowacki 1986) with spirals [001] of short S-Ag-S bonds and polar stacks of SbS_3 pyramids in the channels. Thin lines: long Ag-S interactions. (b) Argyrodite-like high-temperature Cu_7PSe_6 (Gaudin et al. 2000). A truncated tetrahedron of Cu diffusion paths with residence sites, surrounded by PSe_4 tetrahedra (partly shown) and additional Se atoms forming a cage which is centered by another Se atom.

linearly coordinated Cu site and mutually interconnected hexagonal anuli of highly smeared silver residence sites sandwiching the Cu position (Cu-Ag distance drops from 2.84 to 2.75 Å on temperature decrease). The Ag sites which are recognized display linear, trigonal and tetrahedral coordination with sulfur. There is a progressive individualization of fractional Ag sites from 300 K to 15 K, especially of the site interconnecting adjacent anuli, but the joint probability function still exhibits strong overlapping of neighbouring sites, i.e., a considerable mobility of Ag even at the lowest temperature measured.

The last example of silver-based ion conductors are the high-temperature phases of the argyrodite group, Ag_8MX_6, M=Ge, Sn, Si...., X=S, Se, Te (Gorochov 1968; Boucher et al. 1993). In the structures of Ag_8GeTe_6 and Ag_8SiTe_6 (Boucher et al. 1993), the M atoms are tetrahedrally coordinated by Te. Triangular walls of four isolated MTe$_4$ tetrahedra, and the combination of these tetrahedra with four independent Te atoms, form large cages with 24 triangular faces. Five faces meet at the corners of MTe$_4$ tetrahedra whereas six faces meet at each independent Te atom. The last Te atom centers the cavity and is surrounded by a truncated tetrahedron (Laves polyhedron) of three distinct Ag residence sites interconnected by clear diffusion paths: (a) the sites at the corners of the tetrahedral shape; (b) those at the long edges of the large tetrahedron, and (c) those above the short edges of the truncating faces. The short interconnections between the first type of residence sites in two adjacent cages serve as diffusion paths between the cages. This structure type is illustrated in Figure 42b using the new structure determination on another argyrodite-type compound, Cu_7PSe_6, by Gaudin et al. (2000).

LONE ELECTRON PAIR COMPOUNDS

Molecular arsenic sulfides

Most arsenic sulfides are typical molecular structures, with As_mS_n basket-like molecules. The lone electron pairs of all atoms in a molecule point outwards, into the intermolecular space. Thus, these molecules may be classified as inverted lone electron pair micelles. Molecules are held together by weak interactions of van der Waals character. The only non-molecular compound of this category, orpiment As_2S_3, and the As–Sb sulfides are discussed elsewhere.

The three-dimensional arrangement of the As_mS_n molecules is difficult to visualize. The As_4S_4 molecule of realgar (Fig. 43a, Table 25) with the ideal point-group symmetry $\bar{4}2m$, has covalent As-S bonds concentrated around the value of 2.24 Å and the As-As bonds of 2.57 Å.

Intermolecular distances start at 3.62 Å in the case of As-As interactions, and at 3.44 for the As-S interactions. Figure 44a shows the arrangement of As_4S_4 molecules in the structure, viewed along approximately [001].

The same molecule occurs in alacranite, β-As_4S_4 (Burns and Percival 2001); the interatomic distances are concentrated at 2.22 Å and 2.60 Å for the As-S and As-As interactions, respectively. For the columns of As_4S_4 molecules parallel to their $\bar{4}$-axes the stacking is similar to that of realgar. Configuration of the *pararealgar* molecule with the ideal point-group symmetry *m* is very different (Fig. 43b). It has one arsenic atom bound covalently to two As atoms at 2.48 Å and 2.53 Å and to one S atom at 2.19 Å; there are two further As atoms with one As-As and two As-S interactions, and the fourth As atom is bonded to three sulfurs. For the latter three As atoms the As-S distances are 2.23-2.26 Å. Columns of As_4S_4 molecules follow the direction of an approximate three-fold axis of the molecule, which runs through the triangle of As-As interactions (2.48 Å-2.53 Å-3.34 Å) at one pole of the molecule and the AsS_3 group at its opposing pole. This axis is perpendicular to the $(1\bar{1}1)$ layers of molecules in the structure.

Dimorphite, As_4S_3, is a subsulfide of arsenic; it occurs in two modifications, I and II. The As_4S_3 molecules (Fig. 43c) in both modifications have an As_3 triangle (As-As 2.44 Å) opposed by the AsS_3 group (As-S 2.22 Å); the remaining As-S bonds have a length equal to 2.20 Å. The three-fold axes of the molecules (ideal symmetry 3*m*) point sideways from their [010] zig-zag columns and are inclined to their [001] rows in dimorphite II; the same is true for the [010] and [110] rows in dimorphite I. The intermolecular As-As distances are 3.58 Å and the As-S distances 3.75 – 3.77 Å in the latter structure. The sulfur-rich member of the As-S family, uzonite, As_4S_5 (Whitfield 1973) contains two sulfur-bonded As atoms (As-S 2.23 – 2.27 Å) and an As-As pair (2.55 Å; its As-S bonds are 2.23-2.25 Å long) in an As_4S_5 molecule with

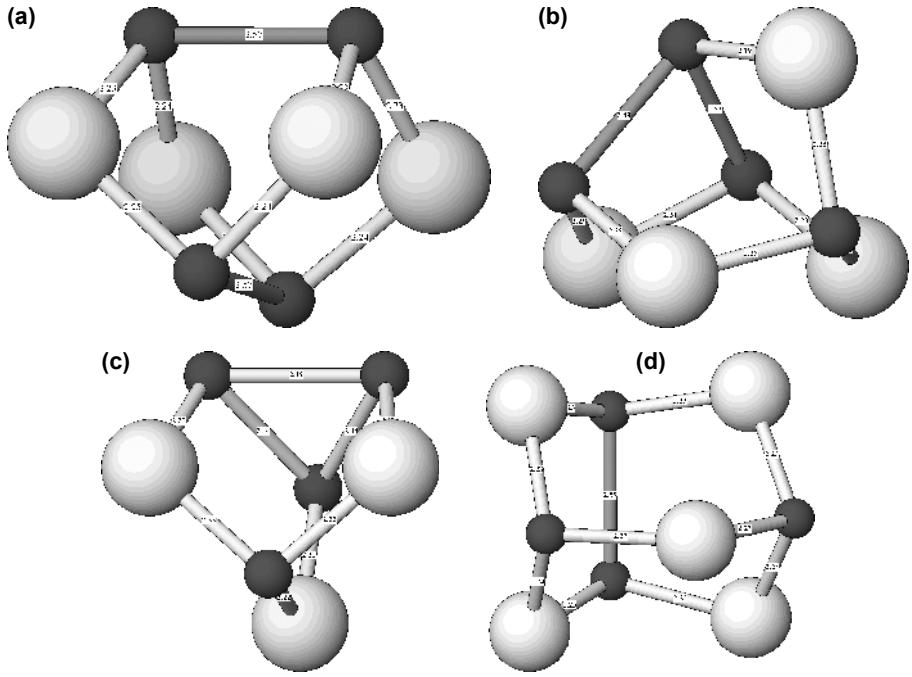

Figure 43. Molecules forming crystal structures of arsenic sulfides: (a) realgar, (b) pararealgar, (c) dimorphite, (d) uzonite. As: small dark spheres, S: large white spheres.

Table 25. Arsenic sulfides with molecular structures.

Mineral	Formula	Space Group	Lattice Parameters (Å,°)				Ref.
			a	*b*	*c*	β	
Realgar	α-As_4S_4	$P2_1/n$	9.325	13.571	6.587	106.38	[1]
Pararealgar	As_4S_4	$P2_1/c$	9.909	9.655	8.502	97.29	[2]
Alacranite	β-As_4S_4	$C2/c$	9.943	9.366	8.908	102.01	[3]*
Dimorphite I	α-As_4S_3	*Pnma*	9.12	7.99	10.10		[4]
Dimorphite II	β-As_4S_3	*Pnma*	11.21	9.90	6.58		[5]
Uzonite	As_4S_5	$P2_1/m$	7.98	8.10	7.14	101.0	[5]
Wakabayshilite	$[(As,Sb)_6S_9][As_4S_5]$	$Pna2_1$	25.262	14.563	6.492		[6]

Note: *high-temperature form: Pertlik (1994)
References: [1] Mullen and Nowacki 1972; [2] Bonazzi et al. 1995; [3] Burns and Percival 2001; [4] Whitfield 1970; [5] Whitfield 1973; [6] Bonazzi et al. 2005

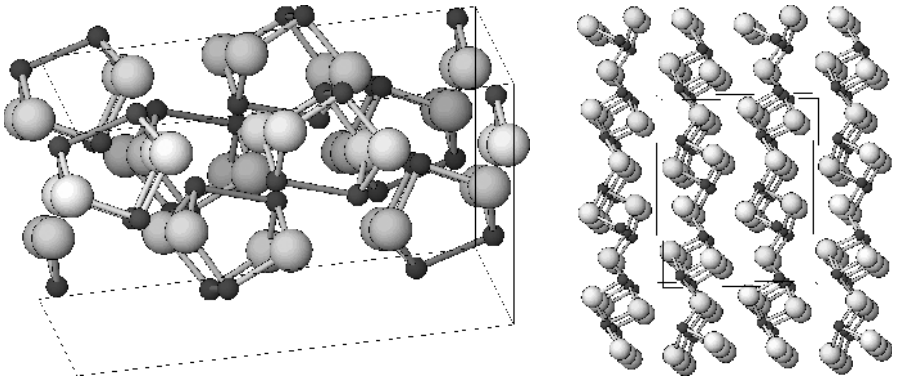

Figure 44. (a) Realgar AsS (Mullen and Nowacki 1972). Cage-like As_4S_4 molecules with lone electron pairs oriented into the intermolecular space. (b) Orpiment As_2S_3 (Mullen and Nowacki 1972). Layers (010) composed of edge-sharing As_2S_4 double chains. As: black spheres, S: large spheres. For OD description see text.

the ideal point-group symmetry *mm*2 (Fig. 43d). Only one mirror plane, that in the As-As dumbell, is preserved in the packing scheme of the molecules. The two-fold axis is nearly perpendicular to the [001] sequence of the molecules. Intermolecular As-As distances start at 3.74 Å; the As-S distances at 3.57 Å.

The remarkable light-induced degradation of realgar has been the subject of many investigations (summarized, e.g., in Kyono et al. 2005). It results in a formation of thin films and spherules of pararealgar on the surface of realgar crystals. Bonazzi et al. (2003) and Bindi et al. (2003) suggest an initial reaction $5As_4S_4+3O_2 \rightarrow 4As_4S_5+2As_2O_3$. The As_4S_5 molecules created by splitting one of the As-As bonds and inserting a sulfur atom are unstable and release another S atom giving a pararealgar molecule instead. According to Kyono et al. (2005), the resulting S radical is re-attached to another realgar molecule and produces an As_4S_5 molecule, repeating the reaction. This cycle is promoted by light and repeated during light exposure, even under low fugacities of oxygen.

An interesting plesiotype of the structures with As_mS_n cages is wakabayshilite, $[(As,Sb)_6S_9][As_4S_5]$ (Bonazzi et al. 2005). This structure contains: (a) hexagonally arranged $(As,Sb)_6S_9$ tubes, which look like a tube-like openwork of corner-connected $As_{0.8}Sb_{0.2}S_3$ pyramids (a tube with hexagonal symmetry, outward oriented As coordination pyramids and inner diameter, defined by S atoms, equal to 4.2 Å), and (b) columns [001] of stacked As_4S_5 cages filling space between the widely spaced tubes. Four out of six such columns have their As-As group oriented according to a six-fold rotation principle around the centering tube whereas two columns, on the opposite sides, break this orientation and conform with that valid for adjacent tubes. This arrangement results in ubiquitous twinning which caused a plethora of different interpretations in crystal structure studies before that of Bonazzi et al. (2005).

Ribbon-like arrangements

The crystal structure of diarsenic trisulfide, orpiment, is a layer-like structure with well expressed lone electron pairs of arsenic. However, as illustrated in Figure 44b, its (010) layers, separated by lone electron pair interspaces (planar micelles) with only very weak interactions, can be interpreted as composed of [001] double-columns of (very elongated) AsS_5 coordination pyramids, making it akin to the Sb and Bi-based structures with a much smaller lone electron eccentricity. The AsS_5 pyramids with elongated bases display three short bonds of 2.24-2.31 Å, with two very long distances (3.22-3.54 Å) in the bases, and distances of 3.48 Å, 3.67 Å or more across the interlayer space. Another interpretation of the (010) layer of orpiment is as an openwork of AsS_3 pyramids; the closest affinities are to the structure of As_2O_3 and the $(As,Sb)_6S_9$ tubes in wakabayshilite.

The structure of orpiment is a typical OD structure. If we follow the second (i.e., right-hand) (010) layer in the unit cell in Figure 44b, we see the double columns of As coordination pyramids which are interconnected via "hinges" of single S atoms. The configuration of the layer is mirror-symmetrical around these hinges. A corner of a double column of pyramids from both the layer below and the layer above protrudes into this symmetrical niche. However, they are not mirror-symmetrical themselves and inspection of Figure 44b shows that the layer below or above can, with equal probability, occur either in the orientation which is shown or in a reversed orientation, i.e., rotated by 180°. Configuration of a single layer pair will be the same in either case—this is the fundamental property of an OD structure. The observed structure has space group $P\,12_1/n1$; the polytype with every other layer rotated would have the space group $P112_1/b$.

Stibnite, Sb_2S_3, and bismuthinite, Bi_2S_3, are isotypic; their structures consist of ribbons of four MS_5 coordination pyramids which share edges (Figs. 3a and 45a). The condensed pyramids belong to two types: a pair of inner pyramids with less eccentric cation positions (Bi-S: 2.58 Å to the pyramid vertex and 2.74 Å, opposed by 2.97 Å, at the pyramid base), flanked by eccentric pyramids (2.69 Å to the vertex and 2.67 Å opposed by 3.06 Å at the base) which constitute margins of the ribbon. The ribbons form corrugated layers (010) via 3.03 Å Bi-S contacts interconnecting the bases of marginal pyramids. For antimony the bond scheme is similar but the latter contacts are longer than the distances in the pyramidal base. The lone electron pair of the inner Bi pyramid is accommodated in a standing trigonal coordination prism situated below its base (i.e., in the inter-ribbon space) (Bi-S 3.32 Å); that of the marginal pyramid is accommodated in the volume of a trigonal coordination prism below that pyramid and oriented at 90° to the 4 Å axis. In the latter case, Bi-S distances in the volume of the prism are 3.03 Å and 3. 40 Å. Behavior of lone electron pairs in Bi_2S_3 and Sb_2S_3 at high pressure was described by Lundegaard et al. (2003, 2005). The resulting space group is *Pbnm*.

Nearly isotypic are U_2S_3 and Dy_2S_3 but without lone electron pairs, and homeotypic is Sn_2S_3 in which the marginal pyramidal/lying prism coordinations are replaced by octahedra of Sn^{4+} whereas the central pyramids contain Sn^{2+} and resemble those of Sb^{3+}. In Sb_2S_2As,

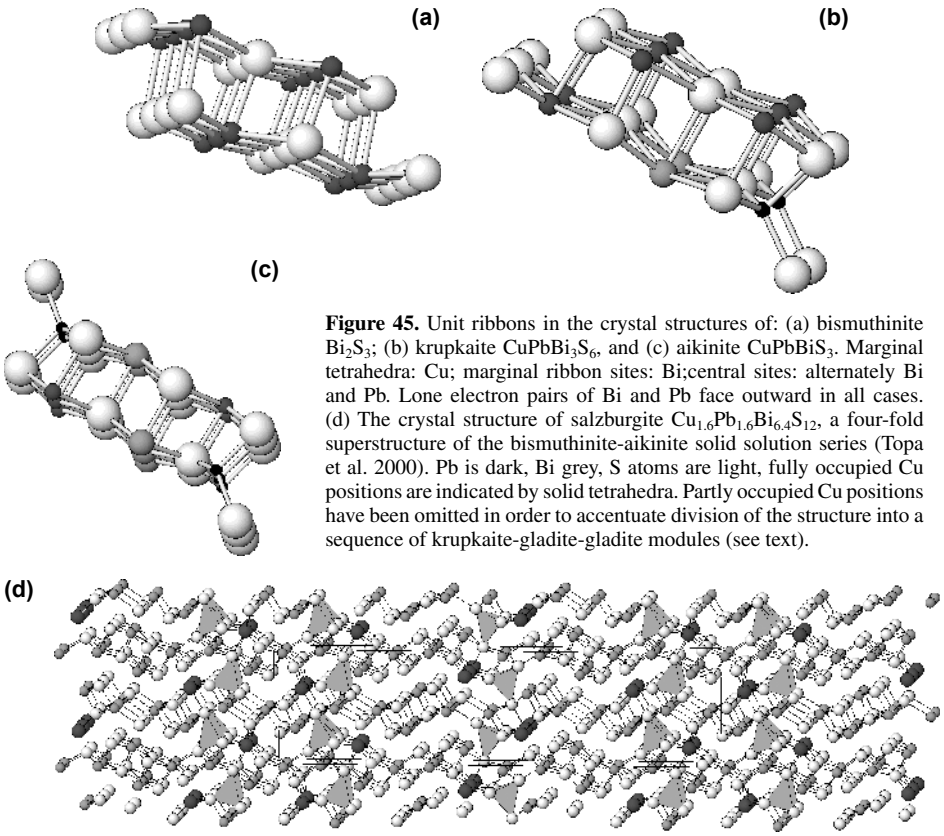

Figure 45. Unit ribbons in the crystal structures of: (a) bismuthinite Bi_2S_3; (b) krupkaite $CuPbBi_3S_6$, and (c) aikinite $CuPbBiS_3$. Marginal tetrahedra: Cu; marginal ribbon sites: Bi;central sites: alternately Bi and Pb. Lone electron pairs of Bi and Pb face outward in all cases. (d) The crystal structure of salzburgite $Cu_{1.6}Pb_{1.6}Bi_{6.4}S_{12}$, a four-fold superstructure of the bismuthinite-aikinite solid solution series (Topa et al. 2000). Pb is dark, Bi grey, S atoms are light, fully occupied Cu positions are indicated by solid tetrahedra. Partly occupied Cu positions have been omitted in order to accentuate division of the structure into a sequence of krupkaite-gladite-gladite modules (see text).

pääkkonnenite, (Bonazzi et al. 1995), the antimony and sulfur positions in the ribbons of this structure correspond to those in stibnite but the marginal sulfurs of stibnite are replaced by arsenic which is covalently bonded to Sb. The arsenic atoms from adjacent ribbons form covalent As-As pairs (2.47 Å) and the ribbons are arranged in layers (Fig. 3b) instead of the herringbone pattern of Sb_2S_3 (Fig. 3a). The resulting space group is *C*2/*m*. Although the overall configuration of the structure of kermesite Sb_2S_2O (Kupčík 1967; Bonazzi 1987; Ďurovič and Hybler 2006) is similar to pääkkonenite, the marginal Sb in the ribbons is coordinated primarily to oxygen whereas the central Sb is coordinated exclusively to sulfur.

The bismuthinite–aikinite series of sulfosalts

Stibnite is compositionally isolated, the only known solid solution is $(Sb,Bi)_2S_3$ (Kyono and Kimata 2004). Bismuthinite, Bi_2S_3, however, gives rise to an extensive solid solution series Bi_2S_3–$CuPbBiS_3$, which is continuous above ~300 °C (Springer 1971). At ambient temperatures, this series contains a number of derivatives with ordered structures, separated by exsolution gaps (Table 26). Some of them appear metastable, for example, salzburgite and paarite convert gradually into a gladite–krupkaite intergrowth (Topa et al. 2002). All ordered derivatives of the bismuthinite – aikinite solid solution series have the *a* and *c* axes in common (~4 Å and ~11.5 Å) whereas the *b* axis represents multiples of ~ 11.2 Å (Table 26). The space group is *Pmcn* for the end-members with *b*~11.2 Å and for the phases with *b* equal to odd multiples of 11.2 Å. It is $Pmc2_1$ for those with even multiples of *b* and for $CuPbBi_3S_6$, i.e., the central member of the series.

The crystal structures of this series are formed by ordered two-and-two combinations of three types of ribbons: bismuthinite-like ribbons, Bi_4S_6, krupkaite-like ribbons, $CuPbBi_3S_6$ and aikinite-like ribbons, $Cu_2Pb_2Bi_2S_6$ (Figs. 45a-c). They are named after the minerals in which they occur alone (Ohmasa and Nowacki 1970; Mumme et al. 1976). Thus, gladite $CuPbBi_5S_9$ is a 1:1 combination of bismuthinite- and krupkaite-like ribbons and hammarite is a corresponding combination of krupkaite- and aikinite-like ribbons. Ordered ribbon combinations (Fig. 45d) lead to a system of "supercells" arranged symmetrically around krupkaite, $CuPbBi_3S_6$, a phase half-way between bismuthinite and aikinite. In this sequence, the multiples of the bismuthinite-like subcell along the *b* direction are: 1 (= bismuthinite), 3, 3, 4, 5, 1 (= krupkaite), 5, 4, 3, 3, 1 (= aikinite).

For the entire series, substitution of a Bi position by Pb, connected with the occupation of an adjacent tetrahedral vacancy by Cu, involves the inner Bi sites of the ribbon and leaves the marginal Bi sites untouched. The tetrahedral vacancy involved is attached laterally to the ribbon (Figs. 45b-d). The filled tetrahedra (Cu sites) are organized into slightly warped (010) planes. Below the level of 100% substitution by Pb and Cu which results in the composition $Cu_2Pb_2Bi_2S_6$, some of the (010) planes in the structure are planes with all tetrahedra vacant. This leads to another way of looking at the ordered structures of the bismuthinite-aikinite series as a combination of three types of modules: (1) gladite-like modules (G) with copper-occupied planes 1½ subcells apart; (2) krupkaite-like modules (K) with such planes 1 subcell period apart; and (3) aikinite modules (A), with these planes ½ subcell period apart; in pekoite there may be a need for a still larger module.

One subcell spacing is equal to 11.2 Å. In their type structures, these modules occur in simple sequences (e.g., gladite is GGGG), but in the structures intermediate to these, 1:1, 1:2 or more complicated sequences of modules occur (Makovicky et al. 2001; Topa et al. 2002). Thus, in salzburgite (Fig. 45d) the sequence of modules is gladite-gladite-krupkaite, i.e., GGKGGK...; in paarite GKGK, in lindströmite KKAKKA, and in emilite KKAKAKKAKA... (Ferraris et al. 2004).

The majority of authors prefer ideal, simple stoichiometric formulae for the minerals of the bismuthinite–aikinite series., The *a* and *c* dimensions (as well as the subcell *b* dimensions) increase, however, parallel with the extent of Pb and Cu substitution so that a combination of two different modules of distinct types involves strain in the (010) planes

Table 26. Selected members of the bismuthinite-aikinite series.

Mineral	Formula	Lattice Parameters (Å)			Space Group	Ref.
		a	*b*	*c*		
Bismuthinite	Bi_2S_3	3.985	11.163	11.314	*Pmcn*	[1]
Gladite	$CuPbBi_5S_9$	4.004	33.575	11.48	*Pmcn*	[1]
Salzburgite	$Cu_{1.6}Pb_{1.6}Bi_{6.4}S_{12}$	4.007	44.81	11.513	$Pmc2_1$	[2]
Paarite	$Cu_{1.7}Pb_{1.7}Bi_{6.3}S_{12}$	4.007	55.998	11.512	*Pmcn*	[3]
Krupkaite	$CuPbBi_3S_6$	4.013	11.208	11.56	$Pmc2_1$	[1]
Lindströmite	$Cu_3Pb_3Bi_7S_{15}$	4.018	56.141	11.578	*Pmcn*	[1]
Emilite	$Cu_{10.7}Pb_{10.7}Bi_{21.3}S_{48}$	4.029	44.986	11.599	$Pmc2_1$	[4]
Hammarite	$Cu_2Pb_2Bi_4S_9$	4.025	33.773	11.595	*Pmcn*	[1]
Aikinite	$CuPbBiS_3$	4.042	11.339	11.652	*Pmcn*	[1]

References relate to the newest refinements of unit cell parameters.
References: [1] Topa et al. 2002; [2] Topa et al. 2000; [3] Makovicky et al. 2001; [4] Balić-Žunić et al. 2002

of "module composition." As might be expected, the strain becomes alleviated by a small fractional occupation of empty tetrahedral sites in the less-substituted set of modules and by a small number of Cu vacancies in the nominally full Cu sites. Both of these processes are accompanied by a corresponding shift in the amount of Pb in the relevant sites housing the large cations and cause, in some cases, deviations from simple stoichiometries. The possible degree of deviation from the ideal stoichiometry varies for different members of the series. For krupkaite, with 50% substitution, the amount of additional Cu and Pb substitution may reach 8 mol%, the undersubstitution in aikinite is quite common and may reach 17 mol%, hence even at 83% substitution there may be no signs of ordering (Topa et al. in prep.) or there may be only weak continuous streaks instead of superstructure reflections in the b^* direction of the reciprocal lattice (Ohmasa and Nowacki 1970).

The aikinite-bismuthinite series is just a member $N = 2$ of the meneghinite homologous series of sulfosalts (Makovicky 1989). In this series, the copper containing configurations on glide planes are identical for all members of the series, whereas the SnS-like slabs become broader with growing homologue order N. The structure of jaskolskiite $Cu_{0.2}Pb_{2.2}(Sb,Bi)_{1.8}S_5$ (Makovicky and Norrestam 1985) is a member with $N = 4$ and that of meneghinite $CuPb_{13}Sb_7S_{24}$ (Euler and Hellner 1960; Moëlo et al. 2002) is $N = 5$.

Layer-like structures

Herzenbergite. The crystal structure of SnS (herzenbergite) (Chattopadhayay et al. 1986) is a layered structure, with tightly-bonded double layers separated by spaces accommodating lone electron pairs of Sn^{2+}. The bonding scheme of Sn^{2+} is reminiscent of As^{3+} and Sb^{3+}, with three strong short bonds (Sn-S = 2.62-2.66 Å)(Fig. 46a), accompanied by two considerably longer, intralayer Sn-S distances (3.29 Å), and by still longer distances across the interlayer space (distances up to 3.6 Å are shown in Fig. 46a). The SnS_5 coordination pyramids with rectangular bases are illustrated in this figure.

SnS is one of the archetypes used by Makovicky (1985) for the definition and description of families of sulfosalts. Some references interpret it as a "distortion derivative" of the PbS archetype, although such an interpretation obscures the decisive role of stereochemically active lone electron pairs of Sn in this archetype. A modification of this motif is present in $TlSbS_2$ (Takéuchi 1997; Balić-Žunić and Makovicky 1995).

LARGE SULFOSALT FAMILIES

General features

According to the bond-valence concept, sulfosalts or, rather, chalcogenosalts are complex sulfides, selenides or tellurides containing a subset of cations with high valence, such as As^{3+}, Te^{4+}, Ge^{4+}, As^{5+}, and W^{6+} (Moëlo and Makovicky in press). Because the bulk of natural thioarsenates, thiostannates, thiotungstates, etc. are homeotypes of simple sulfides, the usual definition of sulfosalts is restricted to the compounds containing a subset of elements with elevated valence and, at the same time, with stereochemically active lone electron pairs. This restricted definition is a result of the defining influence of lone electron pair configurations upon the configuration of the resulting crystal structure.

Thus, sulfosalts are complex sulfides/selenides in which formally trivalent lone-electron pair metalloids As^{3+}, Sb^{3+} and/or Bi^{3+} are combined with different cations. In a half of natural sulfosalt species this cation is Pb^{2+}; otherwise Cu, Ag, Fe, Tl, Mn, Sn and other, less frequently occurring elements. Rare natural finds and a growing number of synthetic sulfosalts have enlarged the range of compositions to include sulfosalts of Li, Na, K, Rb, Cs, as well as those of alkaline earths and lanthanoids, and with a number of sulfosalts that contain $(NH_4)^+$ and

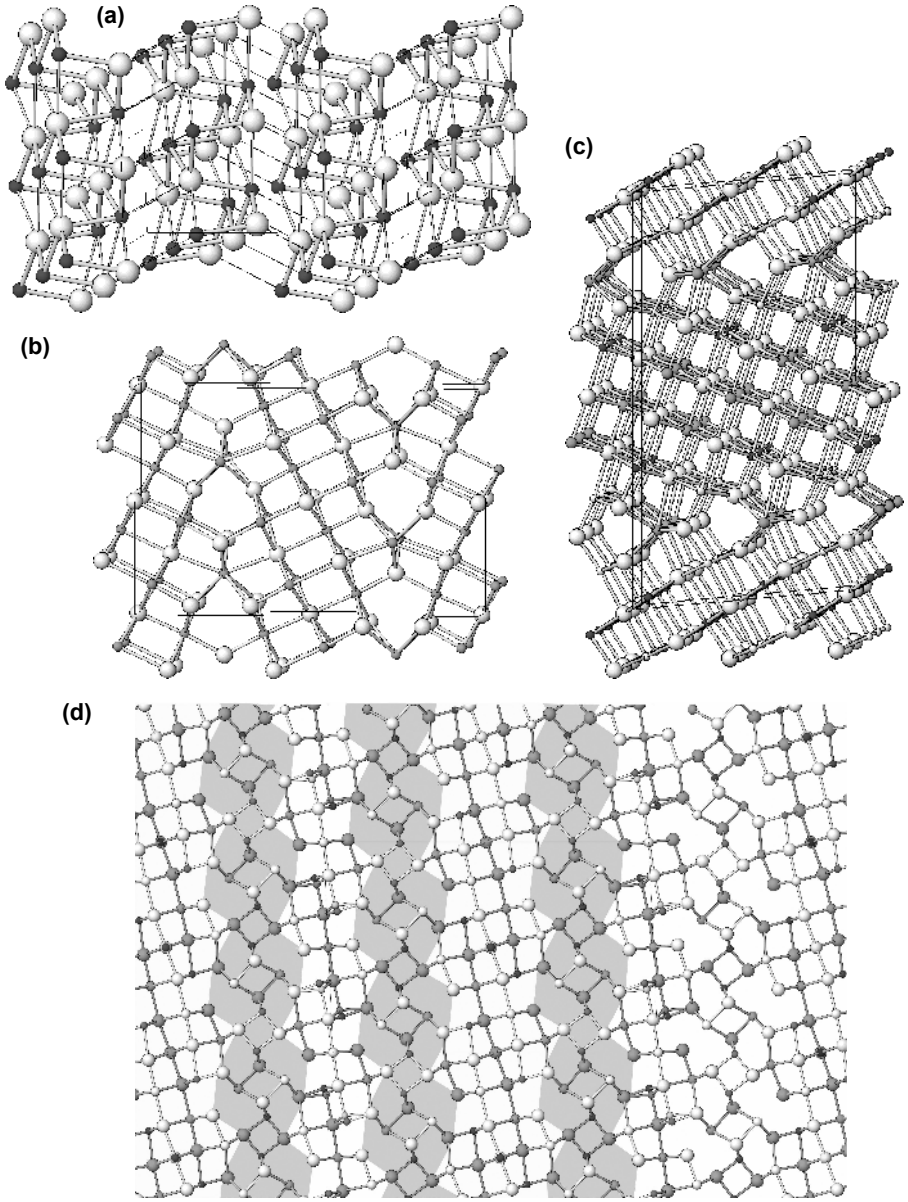

Figure 46. (a) An oblique edge-on view of a stack of double-layers in the structure of herzenbergite, SnS. Each Sn atom has three short Sn-S bonds (thick lines) and two longer bonds (thinner lines) inside the layer (i.e., forming coordination pyramids SnS_5), and longest distances (thin lines) across the lone electron pair interspace. (b) Lillianite, $Pb_3Bi_2S_6$ (Takagi and Takeuchi 1972). Pb and the mixed (Pb,Bi) positions are grey, S white. Number of octahedra in a diagonal edge-sharing chain across a unit slab (i.e., homologue order N) is four. (c) Vikingite $Pb_8Ag_5Bi_{13}S_{30}$ (Makovicky et al. 1992). White cations: Ag, dark cations: Bi, medium grey cations:Pb. Unit slabs are alternatively 4 and 7 octahedra wide when counted along diagonals. (d) Crystal structure of hodrushite $Cu_{7.6}Ag_{0.4}Fe_{0.4}Bi_{11.6}S_{22}$ (Topa et al. 2003), $N_{1,2}$ = 1,2 homologue of the cuprobismutite combinatorial series. Spheres in order of decreasing size indicate S, Bi (dark) and Cu. Note the PbS-like portions $(331)_{PbS}$ interleaved by thinner, Cu-Bi based layers (accentuated in grey). Shading of atoms indicates two height levels, 2 Å apart.

organic cations of various sizes. Li emulates Cu in sulfosalts (resulting in ionic conductivity); Na is a fairly small cation as also is Ca. Potassium can either be a "channel-building" element in sulfosalts, similar to Rb or Cs, or it can replace Pb^{2+} in the structures by means of coupled substitution, with Sb^{3+} (Bi^{3+}) or a lanthanoid ion replacing another Pb atom. In its channel- and interlayer-building role, K^+ also replaces Tl^+.

A more detailed outline of the crystal chemistry of sulfosalts is to be found in Makovicky (1989, 1997a) and Ferraris et al. (2004). However, it is important to mention the difference between the stereochemical activity of the lone electron pair (LEP) in As^{3+} and Sb^{3+} (a pronounced activity resulting in capped trigonal coordination prisms of these elements and an SnS-like archetypal configuration of structural units) and Bi^{3+} (a limited stereochemical activity of LEP, yielding octahedral, distorted octahedral as well as capped trigonal prismatic coordinations, and a PbS-like archetypal arrangement of atoms in structural blocks/layers). Other configurations occur in the structures with Cu or Ag as principal cations. Especially in these structures, when the concentration of metalloids (primarily As^{3+}, Sb^{3+}, and Te^{4+}) is low, the metalloids form MX_3 trigonal coordination pyramids, with a large space for the lone electron pair above the metalloid atom, away from the ligands. Pb^{2+} and Tl^+ have close to insignificant LEP activity and can, therefore, be replaced by alkali metals or alkaline earths.

As in the silicates, a large number of natural sulfosalts with very different crystal structures are formed from combinations of a small number of the same chemical elements in various proportions. Prominent examples are the combinations Pb-Bi-Cu-Ag-S and Tl-As-S. A very large proportion of sulfosalts are amenable to modular classification principles and form homologous series or plesiotypic series of various kinds and degrees of generalization. Several such families are described in this review; more complete listings are in Makovicky (1989, 1997a), Ferraris et al. (2004), as well as in Moëlo and Makovicky (in press). A number of other sulfosalts have already been discussed in the sections on layer-like structures, PbS-related or adamantane structures as well as on the ionic conductors.

Lillianite homologous series

The extensive accretional series of lillianite homologues (Makovicky and Karup-Møller 1977a, b) is produced by reflection twinning on a unit-cell level. These are sulfides with *ccp* anion arrays (portions of PbS archetype) in which all coordination octahedra are filled. These arrays are cut parallel to and twinned on $(311)_{PbS}$ with corresponding coordination changes on twin planes. The most prominent members of this series are Pb-Bi-Ag sulfosalts (Fig. 46b). The overlapping octahedra of the adjacent, mirror-related layers are replaced on planes of unit-cell twinning by bicapped trigonal coordination prisms PbS_{6+2}, with the Pb atoms positioned on the mirror planes (Otto and Strunz 1968; Takéuchi and Takagi 1974, etc.).

Distinct homologues differ in the thickness of the PbS-like layers, expressed as the number N of octahedra in the chain of octahedra that runs diagonally across an individual archetypal layer and is parallel to $[011]_{PbS}$ (Fig. 46b). A lillianite homologue is denoted as ${}^{N1,N2}L$ where N_1 and N_2 are the (not necessarily equal) values of N for the two alternating sets of layers (Fig. 46c). Its chemical formula is $Pb_{N-1-2x}Bi_{2+x}Ag_xS_{N+2}$ (Z = 4) where $N = (N_1 + N_2)/2$ and x is the coefficient of the Ag + Bi = 2Pb substitution in the coordination octahedra of the PbS-like layers. If the trigonal coordination prisms of Pb cannot be substituted by Ag and Bi (which is very close to the real situation), $x_{max} = (N - 2)/2$. This structure type is also quite frequently found outside the Pb-Bi-Ag compositional space, e.g., for a number of complex lanthanide sulfides; the general formula then becomes $M^{2+}{}_{N-1}M^{3+}{}_2S_{N+2}$. The rare instance of $TlSb_3S_5$ ($N = 3$) leads to the formula $M^{+}{}_{(N-1)/2}M^{3+}{}_{(N+3)/2}\ S_{N+2}$.

The existence of lillianite homologues (Table 27) depends on suitable sizes of coordination polyhedra (trigonal prisms vs. octahedra), satisfactory local valence balance and the feasibility of close-to-regular octahedral (i.e., *ccp* or PbS-like) arrays.The cases with $N = 1$

Table 27. Selected homologues of lillianite[4].

Compound	Homologue	Lattice Parameters (Å,°)				S.G.	Note	Ref.
$NdYbS_3$	$^{1,1}L$	*a* 12.55	*b* 9.44	*c* 3.85		$B22_12$		[1]
$UFeS_3$	$^{1,1}L$	*b* 11.63	*c* 8.72	*a* 3.80		*Cmcm*		[2]
$CuEu_2S_3$	$^{1,1}L$	*b* 12.86	*a* 10.35	*c* 3.95		*Pnam*	Cu tetrahedral	[3]
$MnEr_2S_4$[1]	$^{2,2}L$	*b* 12.60	*c* 12.75	*a* 3.79		$Cmc2_1$		[4]
$CrEr_2S_4$	$^{2,2}L$	*a* 12.56	*b* 12.48	*c* 7.54		$Pb2_1a$	*c'* = *c*/2	[5]
$FeHo_4S_7$	$^{1,2}L$	*a* 12.57	*c* 11.35	*b* 3.78	β 105.7	*C2/m*		[6]
$MnEr_4S_7$[1]	$^{1,2}L$	*a* 12.54	*c* 11.44	*b* 3.76	β 105.4	*C2/m*		[7]
$TlSb_3S_5$	$^{3,3}L$	*a* 7.23	*b* 15.55	*c* 8.95	β 113.6	$P2_1/c$	*c'* = *c*/2	[8]
$Pb_3Bi_2S_6$ (lillianite)	$^{4,4}L$	*a* 13.54	*b* 20.45	*c* 4.10		*Bbmm*	minor Ag	[9]
$Pb_3Bi_2S_6$ (xilingolite)	$^{4,4}L$	*a* 13.51	*c* 20.65	*b* 4.09	β 92.2	*C2/m*	cation ordering	[10]
$PbAgBi_3S_6$ (gustavite)	$^{4,4}L$	*a* 7.08	*b* 19.57	*c* 8.27	β 107.2	$P2_1/c$	*c'* = *c*/2	[11]
$Pb_8Ag_5Bi_{13}S_{30}$[2] (vikingite)	$^{4,7}L$	*a* 7.10	*c* 25.25	*b* 8.22	α 90.0; β 95.36; γ 106.8	$P\bar{1}$	*c'* = *c*/2	[12][13]
$Pb_6Sb_{11}Ag_3S_{24}$ (ramdohrite)	$^{4,4}L$	*b* 13.08	*a* 19.24	*c* 8.73	β 90.3	$P2_1/n$	*c'* = *c*/2	[14]
$AgMnPb_3Sb_5S_{12}$ (uchucchacuaite)	$^{4,4}L$	*a* 12.67	*b* 19.34	*c* 4.38[3]			pseudoorthorhomb.	[15]
$Pb_{18}Ag_{15}Sb_{47}S_{96}$ (andorite IV = quatrandorite)	$^{4,4}L$	*a* 13.04	*b* 19.18	*c* 17.07	γ 90.0	$P2_1/a$	*c'* = *c*/4	[16]
$Pb_{24}Ag_{24}Sb_{72}S_{144}$ (andorite VI = senandorite)	$^{4,4}L$	*a* 13.02	*b* 19.18	*c* 25.48		$Pn2_1a$	*c'* = *c*/6	[16][17]
$Pb_6Bi_2S_9$ (heyrovskyite)	$^{7,7}L$	*a* 13.71	*b* 31.21	*c* 4.13		*Bbmm*		[18]
$Pb_{5.92}Bi_{2.06}S_9$ (aschamalmite)	$^{7,7}L$	*a* 13.71	*c* 31.43	*b* 4.09	β 91.0	*C2/m*	cation ordering	[19]
$Pb_{3.36}Ag_{1.32}Bi_{3.32}S_9$ (Ag-Bi-heyrovskyite)	$^{7,7}L$	*b* 13.60	*c* 30.49	*a* 4.11		*Cmcm*		[20]
$Ag_7Pb_{10}Bi_{15}S_{36}$ (eskimoite)	$^{5,9}L$	*a* 13.46	*b* 30.19	*c* 4.10	β 93.4	*B2/m*		[12]
$Pb_4Ag_3Bi_5S_{13}$ (ourayite)	$^{11,11}L$	*a* 13.49	*b* 44.17	*c* 4.05		*Bbmm*		[22]

Notes: (1) Complex homologues $Mn_2Er_6S_{11}$ ($^{2,2,2,1}L$) and $Mn_3Er_8S_{15}$ ($^{2,2,1,2,2,1}L$) occur in this system (Landa-Canovas and Otero-Diaz 1992); the equivalent phases, MnY_2S_4, MnY_4S_7, and $Mn_2Y_6S_{11}$ occur in the MnS-Y_2S_3 system (Bakker and Hyde 1978). Random complex intergrowths ^4L-^7L occur in the PbS-Bi_2S_3-Ag_2S system ('schirmerite', Makovicky and Karup-Møller 1977b). (2) The 4Å subcell of vikingite has *a* 13.60 Å, *b* 4.11 Å, *c* 25.25 Å and β 95.6°, space group *C*2/*m*. (3) Determined from powder data. (4) Synthetic homologues $^{8,8}L$, $^{7,8}L$, $^{4,5}L$ were observed in the system Ag_2S-Bi_2S_3-PbS at high temperatures, by HRTEM (Skowron and Tilley 1990).

References: [1] Carré and Laruelle 1974; [2] Noël and Padiou 1976; [3] Lemoine et al. 1986; [4] Landa-Canovas and Otero-Diaz 1992; [5] Tomas and Guittard 1980; [6] Adolphe and Laruelle 1968; [7] Landa-Canovas and Otero-Diaz 1992; [8] Gostojić et al. 1982; [9] Takagi and Takéuchi 1972; [10] Berlepsch et al. 2002; [11] Harris and Chen 1975; [12] Makovicky and Karup-Møller 1977b; [13] Makovicky et al. 1992; [14] Makovicky and Mumme 1983; [15] Moëlo et al. 1984; [16] Moëlo et al. 1988; [17] Sawada et al. 1987; [18] Takéuchi and Takagi 1974; [19] Mumme et al. 1983; [20] Makovicky et al. 1991; [12] Makovicky and Karup-Møller 1977b; [22] Makovicky and Karup-Møller 1984

to 3 cannot accommodate lone electron pairs of Bi^{3+} or Sb^{3+} that enlarge selected volumes of individual layers while leaving the coordination pyramids (half-octahedra) of these elements unchanged. Therefore, $PbBi_2S_4$ is not a lillianite homologue, although about a half of its structure approximates the $N = 2$ configuration.

Sulfides with $N = 1$ to 3 present both the cases with ideal "aristotype" symmetry and those with subgroup symmetry (Table 27); the reduction of symmetry is caused either by distortions of coordination polyhedra or by the asymmetric position of cations in the trigonal coordination prisms. The tetrahedral voids on the mirror planes of unit cell twinning are occupied only in exceptional cases (Eu_2CuS_3,$^{1,1}L$). Bakker and Hyde (1978) found that the homologous pair MnY_2S_4 ($N = 2$) and "$MnYS_3$" ($N = 1$) (which occurs only as a layer in MnY_4S_7) form a combinatorial series that comprises MnY_4S_7 ($^{1,2}L$), $Mn_2Y_6S_{11}$ ($^{1,2,2}L$), $Mn_4Y_{10}S_{19}$($^{1,2,2,2,2}L$), etc.

Starting at $N = 4$ (although already at $N = 3$ for $TlSb_3S_5$, perhaps because of the very large size of the Tl^+ ion), the higher homologues allow more pronounced departures from the galena-like array, especially in the form of locally "inflated" interspaces that accommodate lone electron pairs of quasi-octahedral Bi or Sb (a common volume for lone electron pairs of several adjacent cations was named a lone electron pair micelle by Makovicky and Mumme 1983). Only $^{4,4}L$ (lillianite) and $^{7,7}L$ (heyrovskyite) are known for the Ag-free subsystem Pb-Bi-S. Reduction of symmetry from the usual orthorhombic to monoclinic, caused by different Pb/Bi ordering in the two mirror-related slabs, was observed for $^{4,4}L$ (xilingolite, Berlepsch et al. 2001) and $^{7,7}L$ (aschamalmite, Mumme and Makovicky unpublished). With the Ag + Bi = 2Pb substitution active in the octahedral layers, not only these combinations but also the cases $^{4,7}L$ (Fig. 46c), $^{4,8}L$, $^{5,9}L$ and $^{11,11}L$ (Makovicky and Karup-Møller 1977) are found (Table 27), as well as disordered combinations based on $N_1 = 4$ and $N_2 = 7$ in different proportions (ibid., Skowron and Tilley 1990). The structures with close-to-ideal PbS-like arrays and those with extensive lone electron pair micelles either do not mix as continuous solid solutions or they become separated by exsolution at low temperatures (e.g., the pair $Pb_3Bi_2S_6$-$PbAgBi_3S_6$ with $N = 4$).

A good match of coordination polyhedra in the octahedral layers of Pb-Ag-Bi sulfosalts results in an extensive accretional series. In the parallel system Pb-Ag-Sb-S, the size and shape mismatch of Pb, Ag and Sb coordination polyhedra appears serious; only members with $N = 4$ were found and they are known only for > 50% of (Ag + Sb) substitution for Pb. They form a string of intermediate (often mutually exsolved) phases with different spatial distribution of lone electron pair micelles in the structure and with different superperiods (2-, 4-, and 6-fold) of the 4 Å dimension. These superperiods result from complex distribution patterns of short and long Sb-S bonds in the walls of the lone electron pair micelles. For phases with substitution close to 50%, incorporation of smaller M^{2+} ions instead of a portion of octahedral Pb appears critical for the formation of viable unit layers; e.g., $AgPb_3MnSb_5S_{12}$ (Moëlo et al. 1984).

Symmetry and size of the trigonal prismatic site (its occupation by a symmetrically coordinated Pb atom or by an asymmetric, sideways oriented Bi configuration) is critical for the distinction between the lillianite and the pavonite homologous series in the Pb-Bi-Ag-Cu system (Makovicky et al. 1977; Makovicky 1981, 1989).

PAVONITE HOMOLOGOUS SERIES

The pavonite homologous series was defined by Makovicky et al. (1977) as an extensive series of complex sulfides in the Cu-Ag-(Pb)-Bi-S system. It has seen a vigorous growth in numbers of reported phases, the relatively new acquisitions being Cu-Bi selenides, sulfides of cadmium, lead and indium, as well as several hitherto unknown homologues.

Topology of the pavonite homologous series is similar to that of lillianite homologues with

$N_1 \neq N_2$, i.e., it is a case of contracted-set reflection twinning (Takeuchi 1997) and, to certain degree, of a heterochemical homologous series. In the pavonite homologues (Figs. 1a,b), all members have $N_1;N_2 = 1;N_{pav}$ where the order of pavonite homologue, N_{pav}, is 2 to 8, and possibly even higher (Table 28). The trigonal coordination prisms on the planes of contracted-set unit-cell twinning are distorted and are occupied by square-pyramidal Bi and its lone electron pair. Bi is displaced towards those prism caps that form a part of the thin $N = 1$ layers. The extensive PbS-like portions (those with N_2) contain quasi-octahedrally to octahedrally coordinated Bi combined with, or partly replaced by, Ag, Cu and some Pb, and occasionally Cd and In. The sole, skewed octahedron in the narrow portions ($N_1 = 1$) represents AgS_{2+4} or this octahedral column contains three- and four-coordinated Cu situated in the interior of the octahedra or in the tetrahedral spaces between them (see the description of $Cu_{1.78}Bi_{4.73}S_8$, Fig. 40c, in the section on ion conductors). Only for $N_{pav} = 2$ are these octahedra substantially occupied by Pb; in the cases with $N = 3$ they also accommodate Cd, Hg or Mn (Table 28).

The primarily synthetic Cu-Bi pavonite homologues exhibit a statistical substitution of Bi by copper in the thick layers. This copper is accommodated in the walls of, and adjacent to, the vacated Bi polyhedra (Fig. 40c). Synthetic phases (sulfides and selenides) with $N_{pav} = 3$ and 4 are constructed according to this principle. For natural phases with $N_{pav} = 4$, 5, and 8, this substitutional-and-interstitial solid solution exsolves into an intimate lamellar intergrowth of two phases with the same N_{pav}, one Cu-Pb poor and the other with a substantial substitution by Cu-Pb; the nature of the Cu-Pb rich phase is discussed further below. Natural pavonite homologues with $N_{pav} = 5$ and 7 prefer Ag in the isolated skewed octahedra but do not exclude Cu; the natural $N = 8$ homologue has mixed occupancy, and $N = 4$ is known both as a Cu-rich and as an Ag-rich variety (Table 28).

Sb alone does not form pavonite homologues because of its inability to assume near-regular octahedral coordination in the interior of the thicker slabs. The only exceptions are triclinic $Li_{3x}Sb_{6-x}S_9$ ($N = 4$) with large lone-electron pair micelles and partial Li for Sb substitution, and $MnSb_2S_4$ ($N = 3$), in which the central site of the accreting layer is formed by octahedral Mn.

Two ways of bridging the differences between the lillianite and pavonite accretional series have been observed. The first one is the "Phase V homologous series" investigated and summarized by Takéuchi (1997). We can describe this series, defined as $Pb_{1-x}Bi_{2x/3}S.\ 2Bi_2S_3$ by Takéuchi, as a combinatorial series of ordered intergrowths of lillianite ${}^{2,2}L$ and pavonite ${}^{1,2}L$ modules; the latter are present as the only component in the phase V-1 (Takéuchi et al. 1974). In this case, the lillianite and pavonite-like composition planes of unit-cell twinning are spatially separated, with varying alternation frequences. The second way has recently been observed in cupromakovickyite ($N_{1,2} = 1,4$) (Topa et al., in press.) and apparently relates also to cupropavonite ($N_{1,2} = 1,5$) and, possibly, other "cupro-" varieties. In "classical" pavonite homologues, the trigonal prisms, asymmetrically occupied by Bi, share edges of their caps across the thin, $N = 1$, layer, resulting in a column of paired Bi square pyramids. In the cupro-varieties, one Bi polyhedron from such a pair is exchanged with a symmetrically occupied trigonal prism hosting lead. This leads to an asymmetric occupation, by statistically distributed Cu atoms, of the adjacent octahedral column in the thin layer. The ordering pattern of these substitutions results in a doubled c parameter (Table 28).

CUPROBISMUTITE HOMOLOGOUS SERIES

Cuprobismutite homologues are copper-bismuth sulfosalts, with minor contents of Fe^{3+}, Pb and/or Ag. The crystal structures of the cuprobismutite homologous series (Fig. 46d) represent a regular 1:1 intergrowth, on a unit-cell scale, of two types of slabs: (a) $(331)_{PbS}$ slabs of a galena-like structure with two known thicknesses, typified by the layers in kupčíkite

Table 28. Selected pavonite homologues.

Mineral/Formula	Homologue	Lattice Parameters (Å)			β (°)	Space Group	Ref.
Synth. V-I $Pb_{1.46}Bi_{8.36}S_{14}$ (~ $PbBi_4S_7$)	^{2}P	*a* 13.25	*b* 4.03	*c* 12.04	105	*C2/m*	[1]
Synth. $CdBi_4S_7$	^{2}P	*a* 13.11	*b* 4.00	*c* 11.77	105.2	*C2/m*	[2]
Synth. $Cd_{2.8}Bi_{8.1}S_{15}$	^{2,3}P	*a* 13.11	*b* 3.99	*c* 24.71	97.8	*C2/m*	[2]
Synth. $Cd_2Bi_6S_{11}$	^{2,2,3}P	*a* 13.11	*b* 4.00	*c* 35.84	90.4	*C2/m*	[2]
Synth. $CdBi_2S_4$	^{3}P	*a* 13.10	*b* 3.98	*c* 14.61	116.3	*C2/m*	[2]
Synth. $Cu_{1.57}Bi_{4.57}S_8$	^{3}P	*a* 13.21	*b* 4.03	*c* 14.09	115.6	*C2/m*	[3][4]
Synth. $HgBi_2S_4$	^{3}P	*a* 14.17	*b* 4.06	*c* 13.99	118.3	*C2/m*	[5]
Synth. $Cu_{3.21}Bi_{4.79}S_9$	^{4}P	*a* 13.21	*b* 3.99	*c* 14.81	100.2	*C2/m*	[6]
Synth. $Cu_2Pb_{1.5}Bi_{4.5}S_9$	^{4}P	*a* 13.45	*b* 4.03	*c* 14.99	99.8	*C2/m*	[7]
Makovickyite $Cu_{1.12}Ag_{0.81}Pb_{0.27}Bi_{5.35}S_9$	^{4}P	*a* 13.37	*b* 4.05	*c* 14.71	99.5	*C2/m*	[8][9]
Cupromakovickyite $Cu_{1.85}Ag_{0.60}Pb_{0.70}Bi_{4.40}S_9$	^{4}P$^{(2)}$	*a* 13.40	*b* 4.01	*c* 29.93	100.07	*C2/m*	[10]
Ag-rich makovickyite $Cu_{0.11}Ag_{0.80}Pb_{0.86}Bi_{5.01}S_9$	^{4}P	*a* 13.83	*b* 4.04	*c* 14.72	97.50	*C2/m*	[8][9]
Synth. $Li_{3x}Sb_{6-x}S_9$ (x = 1/3)	^{4}P	*b* 6.68	*a* 4.09	*c* 14.70	(1)	$P\bar{1}$	[11]
Synth. $AgBi_3S_5$	^{5}P	*a* 13.31	*b* 4.04	*c* 16.42	94.0	*C2/m*	[12]
Pavonite $Cu_{0.27}Ag_{0.78}Pb_{0.33}Bi_{2.78}S_5$	^{5}P	*a* 13.42	*b* 3.99	*c* 16.39	94.3	*C2/m*	[13]
Cupropavonite $Cu_{0.9}Ag_{0.5}Pb_{0.6}Bi_{2.5}S_5$	^{5}P$^{(2)}$	*a* 13.45	*b* 4.02	*c* 33.06	93.5	*C2/m*	[13]
Benjaminite $Ag_3Bi_7S_{12}$	^{7}P	*a* 13.25	*b* 4.05	*c* 20.25	103.1	*C2/m*	[14]
Benjaminite $Cu_{0.5}Ag_{2.3}Pb_{0.4}Bi_{6.8}S_{12}$	^{7}P	*a* 13.30	*b* 4.07	*c* 20.21	103.3	*C2/m*	[15]
Mummeite $Cu_{0.58}Ag_{3.11}Pb_{1.10}Bi_{6.65}S_{13}$	^{8}P	*a* 13.47	*b* 4.06	*c* 21.63	92.9	*C2/m*	[16][8]

Notes: Pavonite homologues are denoted as ^{N}P where N is the order of the homologue as defined in the text. (1) α 96.84 β 90.28 γ 107.70. (2) Transitional between the pavonite and lillianite series.

References: [1] Takéuchi et al. 1974, 1979; [2] Choe et al. 1997; [3] Ohmasa and Nowacki 1973; [4] Tomeoka et al. 1980; [5] Mumme and Watts 1980; [6] Ohmasa 1973; [7] Mariolacos et al. (oral. comm.); [8] Mumme 1990; [9] Žák et al. 1994; [10] Topa et al. in prep.; [11] Olivier-Fourcade et al. 1983; [12] Makovicky et al. 1977; [13] Karup-Møller and Makovicky 1979; [14] Herbert and Mumme 1981; [15] Makovicky and Mumme 1979; [16] Karup-Møller and Makovicky 1992

(N = 1) and in cuprobismutite (N = 2) (Table 29), and (b) slabs composed of columns of paired BiS_5 pyramids and paired CuS_4 coordination tetrahedra (shaded in Fig. 46d), identical for all homologues.

The first kind of slab consists of regular BiS_6 octahedra, BiS_5 pyramids flanking them, and the fitting portions of the trigonal coordination bipyramids of Cu(Fe). In kupčíkite

(N = 1), coordination pyramids of Bi attach themselves to the opposite sides of the central Bi octahedron (Topa et al. 2003a). In cuprobismutite, N = 2, there are pairs of such pyramids attached; the inner one can be completed as a distorted octahedron, the outer one as a capped trigonal prism analogous to the sole pyramid in kupčíkite. Hodrushite (Fig. 46d) is a regular 1:1 combination of these two slab thicknesses, N = 1;2 (Kupčík and Makovicky 1968).

The regular coordination octahedron of Bi is typical for this homologous series. Pure Cu-Bi kupčikite requires some Cu^{2+} in the structure; but in natural samples this is accommodated by the presence of Fe^{3+} in some of the trigonal bipyramidal → distorted tetrahedral Cu positions, resulting in a composition $Cu_{3.4}Fe_{0.6}Bi_5S_{10}$ (Topa et al. 2003a). The N = 2 member has the opposite valence problem, solved by the substitution of some of the octahedral Bi by silver, $Cu_8AgBi_{13}S_{24}$ and also by its partial substitution by Pb (Topa et al. 2003b). In synthetic, admixture-free cuprobismutite, this problem is solved by extensive heterotopic substitution of Bi by Cu (Ozawa and Nowacki 1975). Owing to its N = 1;2 character, hodrushite (ideally $Cu_8Bi_{12}S_{22}$) displays all these substitutions, located in the appropriate slabs of the structure.

In the structures of $Cu_4Bi_4S_9$ (Takéuchi and Ozawa 1975; Bente and Kupčík 1984) and $Cu_4Bi_4Se_9$ (Makovicky et al. 2002), related to this homologous series, the thin galena-like portions contain paired Bi octahedra instead of the isolated ones whereas the intervening layers are more complicated than in the true cuprobismutite homologues. These structures contain covalently bonded *X*-*X* pairs. Another plesiotype is padčraite, $Cu_7((Cu,Ag)_{0.33}Pb_{1.33}Bi_{11.33})_{\Sigma 13}S_{22}$ (Mumme 1986; Topa and Makovicky in press). A complex modular description of this structure was offered by Mumme (1986); a different modular description was given by Topa and Makovicky (in press) as a regular 1:1 intergrowth of kupčikite-like slabs with thick slabs of a complex structure containing Bi_4S_6 ribbons and an independent, prismatic Pb site.

Rod-based sulfosalts

The plesiotype family of rod-based sulfosalts includes complex sulfides of Pb and Sb, Pb and Bi, Sn and Sb, as well as a number of synthetic sulfides of alkalis, alkaline earths and lanthanides combined with Sb or Bi. Minor elements, such as Cu, Ag, Fe or Mn, rarely also Sn^{4+}, are confined to specific roles or structures. Further references are Makovicky (1993), Ferraris et al. (2004), and Makovicky (2005).

Table 29. Cuprobismutite homologues and plesiotypes.

Mineral (Formula)	N1;N2	Lattice Parameters (Å,°)				Space Group	Ref.
Synth. ($Cu_4Bi_5S_{10}$)	1;1	*a* 17.54	*b* 3.93	*c* 12.85	β 108.0	*C*2/*m*	[1]
Kupčíkite ($Cu_{3.3}Fe_{0.7}Bi_5S_{10}$)	1;1	*a* 17.51	*b* 3.91	*c* 12.87	β 108.57	*C*2/*m*	[2]
Hodrushite[3] ($Cu_{8.12}Fe_{0.29}Bi_{11.54}S_{22}$)	1;2	*c* 17.58	*b* 3.94	*a* 27.21	β 92.15	*A*2/*m*	[3]
Synth.[1] ($Cu_{10.4}Bi_{12.6}S_{24}$)	2;2	*a* 17.52	*b* 3.93	*c* 15.26	β 100.2	*C*2/*m*	[4]
Cuprobismutite ($Cu_8AgBi_{13}S_{24}$)	2;2	*a* 17.65	*b* 3.93	*c* 15.24	β 100.5	*C*2/*m*	[5]
Synth. ($Cu_4Bi_4S_9$)	plesio[2]	*b* 11.66	*c* 3.97	*a* 31.68	—	*Pnam*	[6]
Synth. ($Cu_4Bi_4Se_9$)	plesio	*c* 12.20	*b* 4.12	*a* 32.69	—	*Pnma*	[7]
Paderaite ($Cu_{5.9}Ag_{1.3}Pb_{1.2}Bi_{11.2}S_{22}$)	plesio	*a* 28.44	*b* 3.90	*c* 17.55	β 106.0	$P2_1/m$	[8]

Notes: (1) Synthetic cuprobismutite (Ozawa and Nowacki 1975). (2) Plesiotypes of cuprobismutite homologues. (3) Hodrushite from Felbertal (Austria) is $Cu_{7.55}Ag_{0.39}Fe_{0.36}Bi_{11.58}S_{22.11}$ (Topa 2001).
References: [1] Mariolacos et al. 1975; [2] Topa et al. 2003; [3] Kodera et al. 1970; [4] Ozawa and Nowacki 1975; [5] Nuffield 1952; [6] Bente and Kupčík 1984; [7] Makovicky et al. 2002; [8] Mumme 1986

The rod-based sulfosalts (Figs. 47-49) contain rods of simpler configuration, based on a PbS or SnS archetype and generally with a lozenge-like cross section, which are several PbS/SnS subcells (i.e., cation polyhedra) wide and two or more (commonly four) atomic sheets thick. Their surfaces are alternately of a pseudotetragonal type (like the (100) surface of PbS) and of a (sheared or non-sheared) pseudohexagonal type (i.e., a hexagonal $(111)_{PbS}$ or a sheared-hexagonal $3^2{\cdot}4^2$ arrangement of anions) [the symbol of the sheared hexagonal net indicates that two triangular and two square mesh meet at each node]. Typically, the former surfaces face the latter in a complicated non-commensurate match across rod interfaces, so that the structure is not based on a single, continuous close-packed or sheared close-packed arrangement of anions.

The reader is asked to note that when we outline individual structural elements (layers, rods, blocks, ribbons) in these structures, we do not select only the groups based on strong bonds but we consider parts of the structure in their entirety. For example, a part of the structure based on the SnS archetype will contain both the tightly-bonded double-layers and the weakly-bonded interspaces (lone electron pair micelles) which are no less important for the entire configuration than the strongly bonded ones. Even if the tightly-bonded parts contribute most of the inner energy, these are common to many structures in a certain group of compounds and it is the weak interactions which determine the modular crystal chemistry of an individual compound. We draw boundaries between structural blocks (rods, etc.) on non-commensurate interfaces, i.e., between individual blocks of archetypal structure.

All rod-based structures show a distinct accumulation of Sb and Bi in the rod interiors, forming lone electron pair micelles, and of Pb and the above-mentioned large cations on the pseudotetragonal surfaces; the interiors of larger rods can contain mixed Pb-Sb and Sn-Sb positions. In synthetic products, the presence of univalent large cations is outweighed by the presence of trivalent cations, e.g., $KBi_{6.33}S_{10}$ (Kanatzidis et al. 1996) is homeotypic with $Pb_4Sb_4Se_{10}$ (Skowron and Brown 1990). These substitutions take place on rod surfaces (Makovicky 2005). The plesiotypic family of rod-based structures can be divided into four subfamilies according to the pattern which the rod-like elements compose as follows.

(a) Rod-layer structures (Table 30) in which rods are arranged in parallel rows and joined into layers via common polyhedra/atoms at their acute corners (Figs. 47a, 47b, and 48a). Their make-up will be explained in detail below using the example of dadsonite. Individual structures in this family differ in rod dimensions, number of rod types (one or two), and the modes of their interconnection (Makovicky 1993). This is not a homologous series but a more complicated, plesiotype, series; it contains only a very limited number of homologous pairs.

(b) Chess-board structures in which the rods form a chess-board pattern with non-commensurate interfaces. In the kobellite homologous series of Pb-Sb-Bi sulfides that belong to this category, the PbS-like rods can have complicated cross sections (Fig. 48b).

(c) Structures with a cyclic (six-fold) arrangement of rods; rod interfaces can either be of noncommensurate kind or they resemble contacts of archetype slabs in the lillianite series. An example is zinkenite (Fig. 49a). In the nearest lower homologue of zinckenite, $Bi_{0.67}Bi_{12}S_{18}Hal_2$, where *Hal* is either iodine or bromine, trigonal channels are formed which accommodate individual halogen anions and the lone electron pairs of Bi (Miehe and Kupčík 1971).

(d) Large-scale, doubly non-commensurate structures of a box-work type. They contain three types of rods, two of which form a box-work with pseudotetragonal surfaces, and the third one occurs inside the channels of this box-work and displays primarily pseudohexagonal surfaces (Table 31, Fig. 49b). Layer match problems encountered in several of these structures are mostly solved by incorporation of oxygen into the coordination polyhedra of selected Sb atoms; chlorine may participate as well.

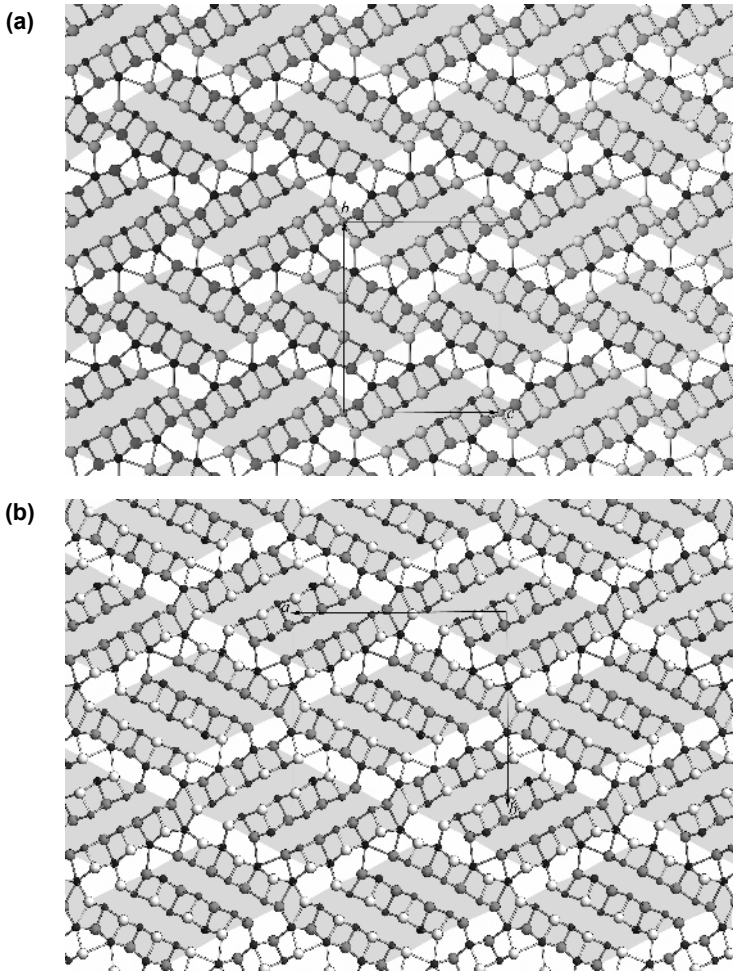

Figure 47. (a) Jamesonite $FePb_4Sb_6S_{14}$ (Matsushita and Ueda 2003). In order of decreasing size, spheres represent S, Pb (dark), Sb (dark), and Fe (light grey, situated in the octahedra joining adjacent rods in rod-layers). Rod-layers Type 2 of Makovicky (1993) are shaded, non-commensurate interlayer spaces are left unshaded. Dark and light spheres represent atoms at two levels, 2 Å apart. (b) Boulangerite (Skowron and Brown 1990). In order of decreasing size, spheres represent S, Pb, and Sb (as well as the mixed Sb-Pb sites). Heights of the light and dark spheres differ by 2 Å. Rod-layers of Type 1 (Makovicky 1993) are shaded, non-commensurate interspaces have been left unfilled.

The close similarity of rod types and identity of match modes found in these four categories justifies joining all these plesiotypic categories into a unique, higher plesiotype family. In all categories it is mostly only homologous *pairs* which are found because of their combined, accretional and variable-fit character. The pair $FePb_4Sb_6S_{14}$ (jamesonite)- $Pb_4Sb_4S_{11}$ or the pair $Ba_9Bi_{18}S_{36}$-$Ba_{12}Bi_{24}S_{48}$ are examples.

Case study: dadsonite

The crystal structure of the Pb-Sb sulfosalt dadsonite (Table 30; Makovicky et al. in press) can be used to highlight the majority of features exhibited by rod-based sulfosalts. Dadsonite was originally defined as $Pb_{11}Sb_{12}S_{29}$ (Jambor 1969) and later as $Pb_{23}Sb_{25}ClS_{60}$ (Moëlo 1979

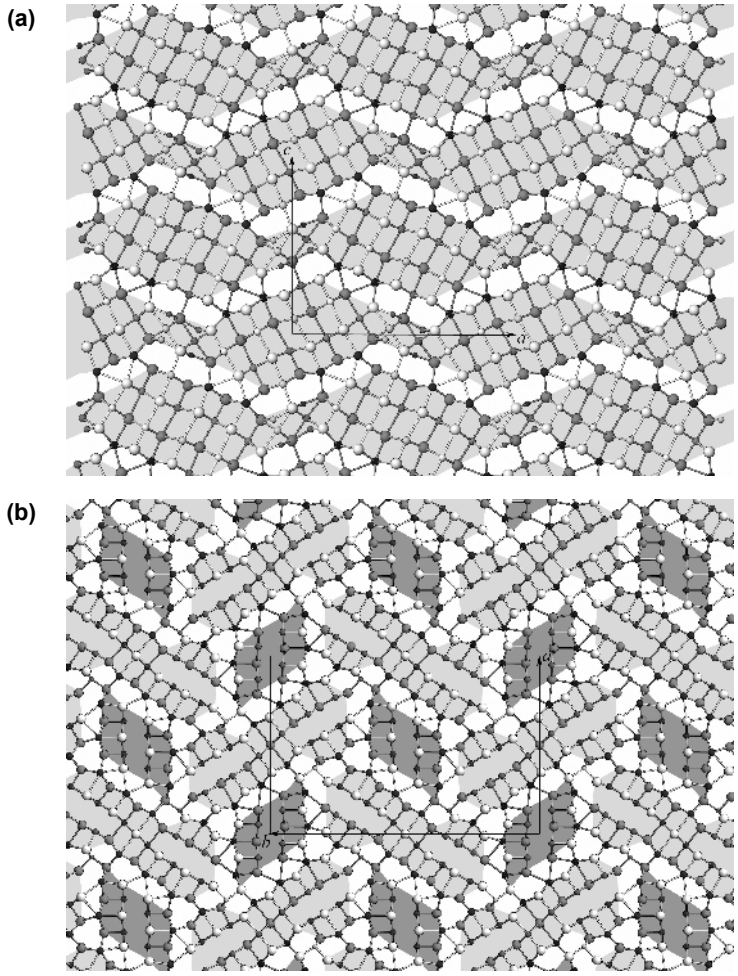

Figure 48. (a) Cosalite, Cu-and-Ag substituted $Pb_2Bi_2S_5$ (Topa et al. in prep.). Projection along the 4 Å axis (heights of light and dark spheres differ by 2 Å). In order of decreasing size, spheres represent S, (predominantly) Pb, (predominantly) Bi,otherwise Ag and Cu. Trigonal planar coordinations of Cu in cosalite were also found by Macíček (1986). Rod layers Type 3 of Makovicky (1993) (shaded) have rod interconnections consisting of two edge-sharing octahedra. Non-commensurate interspaces are uncoloured. (b) Kobellite, $(Cu,Fe)_2Pb_{12}(Bi,Sb)_{14}S_{35}$ (Miehe 1972). In order of decreasing size, spheres represent S, Pb, Sb or Bi, Cu and Fe. Light shading: Bi-enriched rods based on PbS archetype; dark shading: Sb-enriched rods based on SnS archetype. These are two pyramidal widths broad so that kobellite is a member of the series with $N = 2$.

and Cervelle et al. 1979).. The crystal structure of the 4 Å subcell of dadsonite was determined by Makovicky and Mumme (1984).

Rod-layers. The structure consists of rods of SnS-like arrangement, infinite along [001] of the SnS archetype. These rods, three coordination pyramids of Pb or Sb wide, and four combined sulfur-and-metal sheets thick, are organized into two alternating, distinct types of layers (shaded in Fig. 50a), the so-called rod-layers of Makovicky (1993). Their inner portions are occupied by square coordination pyramids of (primarily) Sb, which form the caps of the central row of "standing" trigonal coordination prisms hosting the lone electron pairs of Sb.

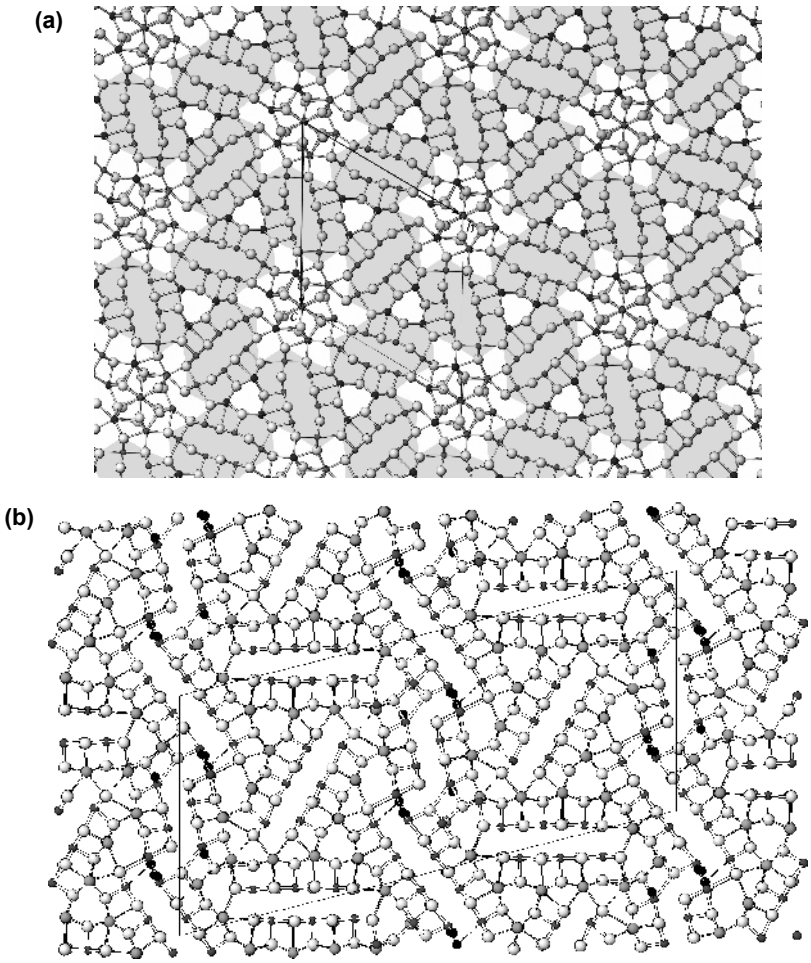

Figure 49. (a) Zinkenite $Pb_9Sb_{22}S_{42}$ (refinement by Topa, unpublished). In order of decreasing size, spheres are S, Pb and Sb. The SnS-based rods are shaded; triangular and hexagonal (Sb-filled) channels are left unshaded. (b) Scainiite $Pb_{14}Sb_{30}S_{54}O_5$ (Moëlo et al. 2000). *a* axis pointing to the right, *c* axis downward. Complex wavy layers (100) consisting of two types of amalgamated rods are interconnected by $N = 3$ rods at $z = 0$, forming a box-work arrangement that encloses another type of $N = 3$ rods at $z = ½$. Central portions of rods are occupied by Sb (dark), their surfaces primarily by Pb (grey). Oxygen is shown as small black circles situated very close to some Sb sites.

The outer surfaces consist of square coordination pyramids of Pb, forming parts of variously capped trigonal coordination prisms. The Pb prisms span the zigzag interspaces between adjacent rod layers. Each straight interval in these interspaces (left unshaded in Fig. 50a) represents a non-commensurate fit between the pseudotetragonal, Pb-rich surface (Q) of one rod and the purely anionic, sheared hexagonal $3^2{\cdot}4^2$ surface (H) of the opposing rod. The observed matches are 2Q:1½H and 2½Q:1½H in terms of a primitive pseudotetragonal and a centered orthohexagonal sub-mesh; they can be traced in Figure 50a. The match values found for the entire family of rod-based sulfosalts range from 1½Q:¾H to 4Q:2½H (Makovicky 1993). Coordinations spanning the interspaces in this family range from variously distorted capped trigonal prisms to occasional octahedra.

Table 30. Selected sulfosalts with rod-based layer structures.

Mineral	Formula	Layer Type	Rod Type	*N*	*N′*	Lattice Parameters[1] (Å, °)				Space Group	Ref.
Jamesonite	$FePb_4Sb_6S_{14}$	2	[001]SnS	3	4	*a* 15.57	*b* 18.98	*c* 4.03	β 91.8	$P2_1/a$	[1]
Boulangerite	$Pb_5Sb_4S_{11}$	1	[001]SnS	3	6	*b* 23.51	*a* 21.24	*c* 4.04	β 100.71	*Pbnm*[3]	[2]
						b 23.54	*a* 21.61	*c* 8.08		$P2_1/a$	
Synth.	$Sn_3Sb_2S_6$	4	[001]SnS	5	6	*c* 34.91	*a* 23.15	*b* 3.96	—	*Pbnm*	[3]
Robinsonite	$Pb_4Sb_6S_{13}$	1	[001]SnS	3	4	*b* 17.69	*a* 16.56	*c* 3.98	α 96.5; β 97.8; γ 91.1	*Pbnm*	[4]
		4	[001]SnS	2	4						
Synth.	$Sn_4Sb_6S_{13}$	1	[001]SnS	3	4	*a* 24.31[2]	*c* 23.49	*c* 3.92	β 94.05	*I*2/*m*	[5]
		4	[001]SnS	2	4						
Synth.	$Pb_{12.65}Sb_{11.35}S_{28.35}Cl_{2.65}$	1	[001]SnS	2	6	*c* 35.13	*a* 19.51	*b* 4.05	β 96.34	*I*2/*m*	[6]
		5	[001]SnS	2	4						
Dadsonite	$Pb_{23}Sb_{25}S_{60}Cl$	3	[001]SnS	3	4	*c* 17.39	b19.51	*a* 8.28	α 83.53; β 77.88; γ 89.22	$P\bar{1}$	[7]
		5	[001]SnS	3	4						
Synth.	$Pb_5Sb_6S_{14}$	6	[001]SnS	4	4	*a* 28.37[2]	*c* 22.04	*b* 4.02	α 89.59; β 92.28; γ 89.93	$I\bar{1}$	[8]
		4	[001]SnS	4	4						
Synth.	$Pb_7Sb_4S_{13}$	6	[001]SnS	4	6	*a* 23.67	*b* 25.55	*c* 4.00	—	*Pnam*	[9]
Cosalite	$Pb_2Bi_2S_5$[4]	3	[011]PbS	4	4	*b* 23.87	*a* 19.13	*c* 4.06	—	*Pbnm*	[10]
Synth.	$KBi_{6.33}S_{10}$	3	[011]PbS	4	4	*a* 24.05	*b* 19.44	*c* 4.10	—	*Pbnm*	[11]
Synth.	$Pb_4Sb_4Se_{10}$	3	[011]PbS	4	4	*a* 24.59	*b* 19.58	*c* 4.17	—	*Pbnm*	[12]
Synth.	$Ce_{1.25}Bi_{3.78}S_8$	4	[011]PbS	3	4	*c* 21.52	*a* 16.55	*b* 4.05	—	*Pbnm*	[13]
Synth.	$KLa_{1.28}Bi_{3.72}S_8$	4	[011]PbS	3	4	*c* 21.59	*a* 16.65	*b* 4.07	—	*Pbnm*	[14]
Moëloite	$Pb_6Sb_6S_{14}(S_3)$	10	[001]SnS	3	4	*c* 23.05	*a* 15.33	*b* 4.04	—	$P2_122_1$	[15]
Synth.	$BaBiSe_3$	10	[011]PbS	2	4	*a* 17.24	*b* 16.00	*c* 4.37	—	$P2_12_12_1$	[16]
Synth.	$SrBiSe_3$	10	[011]PbS	4	4	*a* 33.55	*b* 15.76	*c* 4.26	—	$P2_12_12_1$	[17]
Synth.	$Sr_6Sb_6S_{17}$	10	[001]PbS	3	4	*c* 22.87	*b* 15.35	*c* 8.29	—	$P2_12_12_1$	[18]

Notes: *N* denotes number of coordination polyhedra along, *N′* number of atom planes across the rod-like element.
[1] When not indicated otherwise, the first parameter (or the relevant vector *d*) is parallel to the periodicity of the rod-layer which has rods infinite along the 4 Å direction.; [2] Unit-cell vectors were selected diagonal to the direction and stacking of rod-layers.; [3] Presumed ordering variants for boulangerite. Structure refinements were published for $Pb_4Sb_6S_{13}$ in *P*1 (Petrova et al. 1978) and *I*2/*m* (Skowron and Brown 1990a) and for $Pb_5Sb_4S_{11}$ in *Pnam* (Skowron and Brown 1990b, Topa et al. in prep.).; [4] Variable amounts of substitution by Cu and Ag
References: [1] Niizeki and Buerger 1957*;* [2] Petrova et al. 1978; Mumme 1989*;* [3] Smith 1984; Parise et al. 1984*;* [4] Makovicky et al. 2004*;* [5] Jumas et al. 1980*;* [6] Kostov and Macíček 1995*;* [7] Makovicky, Topa and Mumme, in press*;* [8] Skowron et al. 1992 *;* [9] Skowron and Brown, written comm.*;* [10] Topa, pers. comm.*;* [11]Kanatzidis et al. 1996*;* [12] Skowron and Brown 1990c*;* [13] Ceolin et al. 1977*;* [14] Iordanidis et al. 1999*;* [15] Orlandi et al. 2002*;* [16] Volk et al. 1980*;* [17] Cook and Schäfer 1982*;* [18] Choi and Kanatzidis 2000

Table 31. Box-work type structures of complex sulfides.

Mineral	Formula	Lattice Parameters (Å,°)				Space Group	Ref.
Neyite	$Ag_2Cu_6Pb_{25}Bi_{26}S_{68}$	*a* 37.53	*b* 4.07	*c* 43.7	β 108.80	*C*2/*m*	[1]
Pillaite[1]	$Pb_9Sb_{10}S_{23}ClO_{0.5}$	*a* 49.49	*b* 4.13	*c* 21.83	β 99.62	*C*2/*m*	[2]
Scainiite[1]	$Pb_{14}Sb_{30}S_{54}O_5$	*a* 52.00	*b* 8.15	*c* 24.31	β 104.09	*C*2/*m*	[3]
Synth.	$Er_9La_{10}S_{27}$	*c* 21.83	*b* 3.94	*a* 29.71	β 122	*C*2/*m*	[4]

Notes: [1] Quasi-homologues; related to cyclically twinned structures of $Ba_{12}Bi_{24}S_{48}$ type
References: [1] Makovicky et al. 2001; [2] Meerschaut et al. 2001; [3] Moëlo et al. 2000; [4] Carré and Laruelle 1973.

The two rod-layers differ in the interconnection of the rods. Those at y = ½ in Figure 50a have rods interconnected via a single row of anions. These anions are underbonded, a site assumed by Cl in the structure. This layer is the rod-layer Type 5 of Makovicky (1993), also known from the structure of $Pb_{12.7}Sb_{11.4}S_{28.4}Cl_{2.7}$ (Kostov and Macíček 1995). The rod-layers at y = 0 have adjacent rods interconnected via a pair of standing, distorted monocapped coordination prisms of antimony. A similar interconnection in cosalite ~$Pb_2Bi_2S_5$ (Srikrishnan and Nowacki 1974) (Fig. 48a with a new interpretation of this structure portion) contains coordination octahedra. A different interconnection in boulangerite, $Pb_5Sb_4S_{11}$ (Type 1 layer) is shown in Figure 47b.

Ribbons of Sb coordination pyramids. The triple [100] ribbons of the square coordination pyramids of antimony in Type 3 layers are polar, with all short Sb-S bonds oriented in the +[100] direction. These ribbons are very similar to those in jamesonite (Niizeki and Buerger 1957). The approximate correspondence between the two consecutive Sb sites in each [100] row of pyramids means that Type 3 layer has, to a good approximation, two repetition periods within one ~8 Å long *a* period of the dadsonite lattice. The Type 5 layer at y = ½ has a completely different configuration. The triple ribbon of Sb pyramids (one of the pyramids being substituted by Pb) consists of trapezoidally distorted "square" coordination pyramids, with the pair of short distances in a base of the pyramid facing sideways. They have approximate mirror planes perpendicular to the ribbon extension. Sb sites form solitary SbS_3 groups of short bonds and one Sb_2S_4 pair. The non-crystallographic symmetry (i.e., in excess of the symmetry elements of the space group) in both layers is important for a potential order-disorder in the structure of dadsonite, discussed below.

The trapezoidally distorted bases of MX_5 coordination pyramids are a common configuration in sulfosalts, e.g., they occur for Sb in ramdohrite $Pb_6Sb_{11}Ag_3S_{24}$ (Makovicky and Mumme 1983), andorite $PbAgSb_3S_6$ (Sawada et al. 1987), zinkenite (Topa, unpublished), and for As in the sartorite group of Pb-As sulfosalts (Berlepsch et al. 2001). Partial substitution of Sb by Pb or a regular Sb-Pb alternation producing an ~8 Å periodicity occurs in, e.g., boulangerite $Pb_5Sb_4S_{11}$ and robinsonite $Pb_4Sb_6S_{13}$ (details in Mumme 1989 and Makovicky et al. 2004).

Coordination of Sb and its complications. There are two distinct types of coordination polyhedra of antimony in dadsonite. In the first group of polyhedra three short Sb-S bonds (2.42-2.59 Å) are combined with three-to-four long Sb-S distances, starting at 3.09 Å or even at 3.44 Å. Nearly all of these Sb atoms form typical [SbS_5] coordination pyramids with trapezoidal bases in the Type 5 layer. The two longest Sb-S distances span the space hosting lone electron pairs. The other set of polyhedra has three regularly increasing short empirical Sb-S distances, starting at 2.41-2.45 Å and increasing to 2.60-2.72 Å. These polyhedra contain split Sb sites, which in the unsplit refinement exhibited augmented U_{iso} values, distinctly elongated displacement ellipsoids, and also an average bond length atypical for Sb. Such split half-atoms will have a nearly equal bond length to the vertex of the [SbS_5] coordination pyramid in which they are situated (e.g., in a selected example it is 2.42 Å and 2.41 Å,

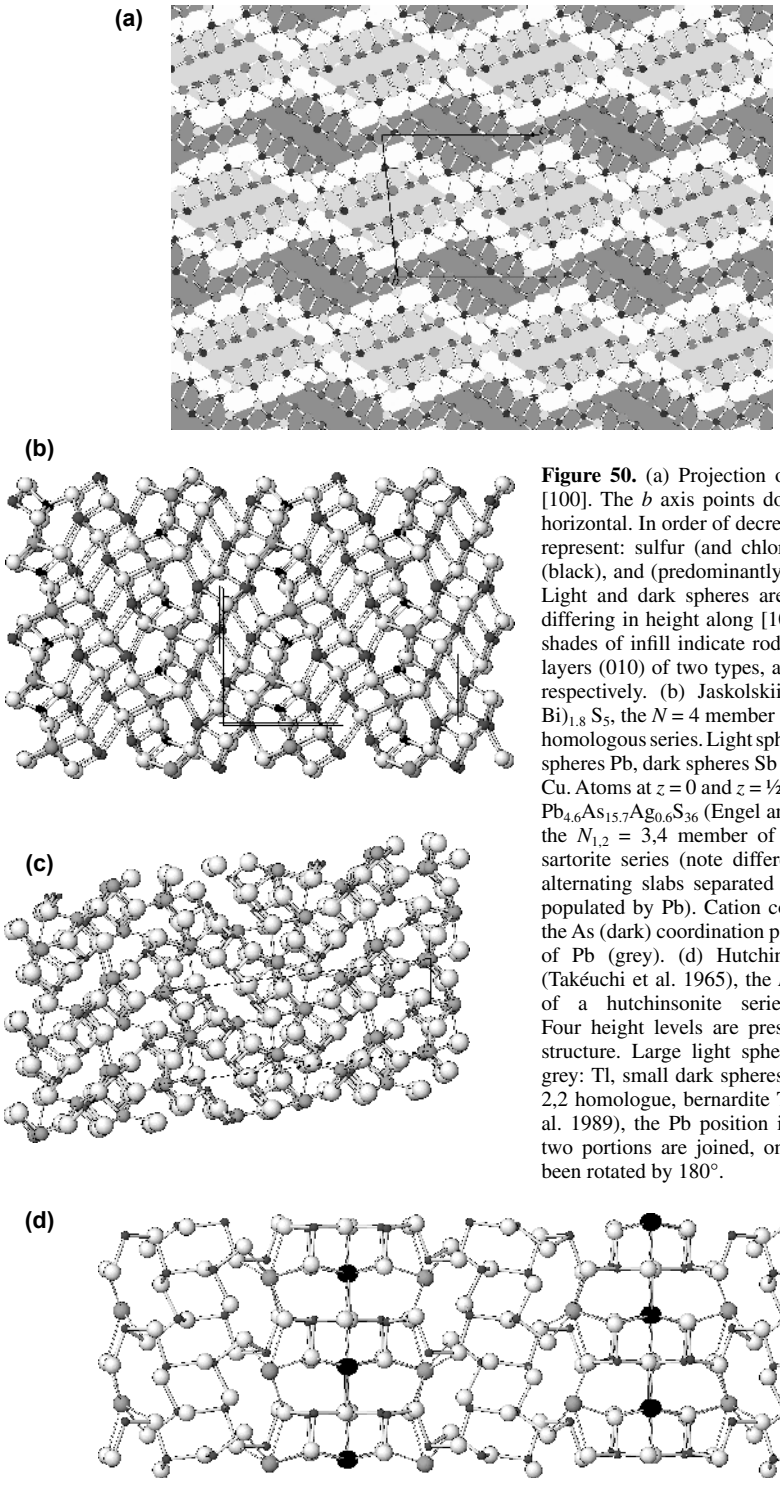

Figure 50. (a) Projection of dadsonite along [100]. The *b* axis points downward, *c* axis is horizontal. In order of decreasing size, spheres represent: sulfur (and chlorine) (white), lead (black), and (predominantly) antimony (grey). Light and dark spheres are strings of atoms differing in height along [100] by ~ 2 Å. Two shades of infill indicate rods constituting rod-layers (010) of two types, at $y = 0$ and $y = ½$, respectively. (b) Jaskolskiite $Cu_{0.2}Pb_{2.2}$ $(Sb, Bi)_{1.8}$ S_5, the $N = 4$ member of the meneghinite homologous series. Light spheres denote S, grey spheres Pb, dark spheres Sb and Bi; tetrahedral Cu. Atoms at $z = 0$ and $z = ½$. (c) Baumhauerite $Pb_{4.6}As_{15.7}Ag_{0.6}S_{36}$ (Engel and Nowacki 1969), the $N_{1,2} = 3{,}4$ member of the combinatorial sartorite series (note different thicknesses of alternating slabs separated by zig-zag planes populated by Pb). Cation count includes both the As (dark) coordination polyhedra and those of Pb (grey). (d) Hutchinsonite $TlPbAs_3S_9$ (Takéuchi et al. 1965), the $N_{1,2} = 2{,}3$ member of a hutchinsonite series of merotypes. Four height levels are present in the ~8.8 Å structure. Large light spheres: S, black: Pb, grey: Tl, small dark spheres: As. In the $N_{1,2} = 2{,}2$ homologue, bernardite $TlAs_5S_8$ (Pašava et al. 1989), the Pb position is missing and the two portions are joined, one of them having been rotated by 180°.

respectively). They will also have one more-or-less common, short Sb-S distance to one S atom in the square base of the pyramid (2.48 Å and 2.41 Å), and one long Sb-S distance that opposes this bond (3.18 Å and 3.28 Å, respectively). The other short Sb-S bond of each split Sb half-atom of antimony always overlaps the long Sb-S distance of its counterpart (2.70 Å and 2.69 Å, respectively, overlap with the distances 2.96-2.99 Å). Splitting of the two positions is never complete because also their S ligands are an average of two positions. The Sb-S bond distances should be investigated by means of a bond length hyperbola established for Sb by Berlepsch et al. (2001) ; the data for split positions will deviate from the normal hyperbolic trend. Data points belonging to the split/mixed cation sites also yield unrealistic bond valence values. Splitting of Sb sites inside a "square" coordination pyramid appears to be a fairly common and important phenomenon in the Pb-Sb sulfosalts; the same is true in the Pb-As sulfosalts of the sartorite group (Berlepsch et al. 2001).

Order-disorder phenomena. When we preserve the labelling of crystallographic axes used for the unit cell of dadsonite (Table 30), the Type 3_{SnS} layer has an ideal layer symmetry $P\bar{1}$ with the a' axis equal to one half of the a value of the unit cell. The Type 5 layer has an ideal layer symmetry $B2/m11$, with the c parameter doubled against the triclinic unit cell. After every Type 5 layer with its horizontal mirror planes, the triclinic stacking of layers ($\gamma = 89.2°$) can proceed in the $+\vec{a}$ or in the $-\vec{a}$ direction. Furthermore, the halved repetition period $a/2$ of the Type 3 layer means that the consecutive Type 5 layer can attach itself either at (practically) the same x height as the preceding Type 5 layer or it can attach itself at $(x + 0.5)$ instead. Both the double-periodicity of the Type 3 layer and the B2/m symmetry of the Type 5 layer are only approximate, violated to a small but always present extent. Therefore, we deal with a desymmetrized OD structure in which the OD phenomena are present only as an occasional twinning or antiphase-boundary event (Ďurovič 1979). Among sulfosalts, OD phenomena cause twinning in sinnerite $Cu_6As_4S_9$ (Makovicky and Skinner 1975), imhofite $Tl_3As_{7.66}S_{13}$ (Balić-Žunić and Makovicky 1993), gillulyite $Tl_2(As,Sb)_8S_{13}$ (Makovicky and Balić-Žunić 1999) as well as structural disorder in owyheeite $Ag_3Pb_{10}Sb_{11}S_{28}$ (Makovicky et al. 1998), vurroite $Pb_{20}Sn_2(Bi,As)_{22}S_{54}Cl_6$ (Pinto et al. in prep.) and diaphorite $Pb_2Ag_3Sb_3S_8$ (Armbruster et al. 2002).

8 Å superstructure vs. 4 Å substructure. Many lead-antimony sulfosalts exhibit a pronounced ~4 Å substructure, producing a subset of strong X-ray reflections, and an 8 Å superstructure which modifies the 4 Å submotif by ordered substitutions, occupation of alternative split positions in a coordination polyhedron or even vacancies, producing additional weak to very weak reflections. The intensity of the generally weak 8 Å reflections varies with the degree of modification present in the structure. Some sulfosalts, e.g., jamesonite $FePb_4Sb_6S_{14}$ (Niizeki and Buerger 1957) or robinsonite $Pb_4Sb_6S_{13}$ (Skowron and Brown 1990a) have only the 4 Å periodicity, confirmed by the latest refinements (e.g., Leone et al. 2003; Matsushita and Ueda 2003; Franzini et al. 1992; Makovicky et al. 2004). Others, like boulangerite $Pb_5Sb_4S_{11}$, might have both the ordered variants (Mumme 1986) and disordered (synthetic) variants (e.g., Petrova et al. 1978; Skowron and Brown 1990b) of the Pb-Sb substitution schemes. Finally, for zinkenite ~ $Pb_9Sb_{22}S_{42}$, both ordered and disordered 8 Å variants are known. The remarkable box-work oxy-sulfosalt structures from Bucca della Vena (Italy) show very weak 8 Å levels; they were found to be too weak to be further analyzed (e.g., scainiite $Pb_{14}Sb_{30}S_{54}O_5$, Moëlo et al. 2000).

Other sulfosalt families

Glide-plane twinned accretional series have coordination polyhedra on composition planes of adjacent slabs different from those in the slab interior. Such are the meneghinite series of sulfosalts of Cu, Pb, Sb or/and Bi (Fig. 50b; the bismuthinite-aikinite series dealt with above are $N = 2$ members of the meneghinite series) and the sartorite homologous series (sulfosalts of Pb and As). These respectively represent twinning of SnS-like arrays on $(501)_{SnS}$ and $(301)_{SnS}$ (Makovicky 1985).

Sartorite homologues. Members of the sartorite homologous series are Pb-As sulfosalts which can be obtained by a glide-plane type of unit cell twinning of a (modified) SnS like archetype on the planes $(301)_{SnS}$. A simplified formula of the series is $Pb_{4N-8}As_8S_{4N+4}$. The zigzag composition planes are occupied by tricapped coordination prisms of lead whereas the slabs by coordination pyramids of arsenic, replaced in central portions by Pb and also some Ag or Tl. The match problems expected between the As pyramids and the inserted multiple Pb polyhedra in the potential higher homologues of sartorite limit this series to combinations of $N = 3$ and $N = 4$ slabs in different proportions: $N = 3,3$; 3,4 (Fig. 50c); 3,4,4; 4,3,4,3,4,4,3,4,3,4; etc....; and, finally, 4,4; members with $N > 4$ would already have entire slabs of Pb polyhedra inserted into their SnS-based layers. Thus, the sartorite homologous series remains a combinatorial series. This is apparently valid also for its Ba-Sb analogs. This series has been treated in detail by Makovicky (1985), Berlepsch et al. (2001, 2003), Pring (2001) and Ferraris et al. (2004).

Axial unit-cell twins. The plagionite homologous series (Takéuchi 1997) consists of four Pb-Sb sulfosalts: füloppite $Pb_3Sb_8S_{15}$, plagionite $Pb_5Sb_8S_{17}$, heteromorphite $Pb_7Sb_8S_{19}$ and semseyite $Pb_9Sb_8S_{21}$. They differ from other Pb-Sb sulfosalts by not being rod-based structures. Instead, they consist of continuous slabs of SnS archetype (or $TlSbS_2$ archetype, Takeuchi 1997), cut diagonally and joined together on composition planes via the action of 2_1 axes. Takéuchi (1997) gives a detailed analysis and description of both the local and the modular aspects of this series; he used a distorted PbS archetype as a basis. Plagionite homologues form only a subset of all the known compounds in the system Pb-Sb-S, i.e., only those which have a restricted formula $Pb_{3+2x}Sb_8S_{15+2x}$ with $x = 0$, 1, 2 or 3 (Takéuchi 1997).

Hutchinsonite merotypes (Makovicky 1997) are a group of complex sulfides combining As or Sb with large uni- and divalent cations (Tl^+, Pb^{2+}, Na^+, Cs^+, NH_4^+, and others, including organic cations). The structures of these sulfosalts are regular 1:1 intergrowths of slabs (A) which can be described as $(010)_{SnS}$ cut-outs of different widths from the SnS-archetype, or as $(110)_{PbS}$ cut-outs from the PbS-archetype, with layers (B) of variable thickness and configuration. The (B) layers contain primarily MS_3 pyramids (M = As, Sb) with active lone electron pairs, mostly combined with coordination polyhedra of large (even of organic) cations. Slabs A and B share certain S atoms in common. In this family of merotypes the A slabs are built according to the common principles in all these structures, whereas the B slabs differ, being always adapted to the requirements of different large cations (Makovicky 1997).This series has been treated in detail by Ferraris et al. (2005) and only a single example will be given here.

The phases $TlPbAs_3S_9$ (hutchinsonite, *Pbca*, Takéuchi et al. 1965) - $TlAs_5S_8$ (bernardite, $P2_1/c$, $TlAs_5S_8$, Pašava et al. 1989) are examples of a pair of homologues. Both structures are composed of alternating slabs (A) of SnS-like configuration, with As, Tl ± Pb, and slabs (B) of a complex spiral configuration, accommodating only As with its active lone electron pairs (Fig. 50d). The similarity between the two structures, in nearly all coordination polyhedra and layer configurations, is striking. The only difference is that in bernardite the SnS-like slab is 2 coordination pyramids of As (As/Tl in the case of marginal pyramids) broad, i.e., a 2,2-homologue when considering the two faces of a tightly-bonded fragment in the SnS-like slab, whereas in hutchinsonite this tightly-bonded fragment is diagonally split, half of it rotated 180° about [010], and an additional Pb pyramid is inserted into only one face of the fragment. This operation defines it as a 2,3-homologue of the series(Fig. 50d). It is easy to imagine a 3,3-homologue with two Pb pyramids inserted. However, this has not been found, apparently because of the match problems between the large Pb polyhedra and the As pyramids.

ACKNOWLEDGMENTS

This paper profitted from the secretarial assistance of Mrs. Camilla Sarantaris and Mrs. Lisbeth Skjoldager; Dr. Dan Topa, Mrs Brita Munch and the deceased Mr. Ole Bang Berthelsen helped to edit the figures. Critical reading by the chief editor Prof. D.J. Vaughan and the kind assistance of Dr. J. J. Rosso improved this contribution and the patience and understanding of my wife created the necessary conditions for it. Partial support by the National Science Foundation project 21-03-0519 and the Carlsberg Foundation project ANS 1185/10 is gratefully acknowledged.

REFERENCES

Abrahams SC, Bernstein JL (1973) Piezoelectric nonlinear optic $CuGaS_2$ and $CuInS_2$ crystal structure: Sublattice distortion in A(I) B(III) C(VI)2 and A(II) B(IV) C(V)2 type chalcopyrites. J Chem Phys 59: 5415-5420

Abrahams SC, Bernstein JL (1974) Piezoelectric nonlinear optic $CuGaSe_2$ and CdGe As_2: Crystal structure, microhardness, and sublattice distortion. J Chem Phys 61:1140-1146

Adenis C, Olivier-Fourcade J, Jumas JC, Philippot E (1986) Etude structurale de $In_2Sn_3S_7$ par spectrometrie moessbauer de 119Sn et diffraction des rayons X. Rev Chimie minerale 23:7335-745

Adolphe C, Laruelle P (1968) Structure cristalline de $FeHo_4S_7$ et de certains composés isotypes. Bull Soc Franc Minér Crist 91:219-232

Agrawal BK, Yadav PS, Agrawal S. (1994) Ab initio calculation of the electronic, structural and dynamical properties of Zn-based semiconductors. Phys Rev B – Cond Matt 50:14881-14887

Andersson S, Åström A, Galy J, Meunier G (1973) Simple calculations of bond lengths and bond angles in certain oxides, fluorides and oxide fluorides of Sb^{3+}, Te^{4+} and Pb^{2+}. J Solid State Chem 6:187-190

Andersson S and Hyde BG (1974) Twinning on the unit cell level as a structure-building operation in the solid state. J Solid State Chem 9:92-101

Andresen AF, Leciejewicz J (1963) A neutron diffraction study of Fe_7Se_8. J Phys (Paris) 25:574-578

Andresen AF, van Laar R (1970) The magnetic structure of Fe_3Se_4. Acta Chim Scand 24:2435-3439

Angel RJ, Price GD, Yeomans J (1985) The energetics of polytypic structures: Further applications of the ANNNI model. Acta Cryst B41:310-319

Armbruster T, Hummel W (1987) (Sb, Bi, Pb) ordering in sulfosalts: Crystal-structure refinement of a Bi-rich izoklakeite. Am Mineral 72:821-831

Armbruster T, Makovicky E, Berlepsch P, Sejkora J (2003) Crystal structure, cation ordering and polytypic character of diaphorite $Pb_2Ag_3Sb_3S_8$, a PbS based structure. Eur J Mineral 15:137-146

Aurivilius B (1983) The crystal structures of two forms of $BaBi_2S_4$. Acta Chem Scand A37:399-407

Avilov AS, Imamov RM, Pinsker ZG (1971) Electron diffraction study of the Cu_2TlSe_2 phase. Kristallografiya 16:635-636

Baker CL, Lincoln FJ, Johnson AWS (1991) A low-temperature structural phase transformation in CuAgS. Acta Cryst 47:891-899

Baker CL, Lincoln FJ, Johnson AWS (1992) Crystal structure determination of Ag_3CuS_2 from powder X-ray diffraction. Australian J Chem 45:1441-1449

Bakker M, Hyde BG (1978) A preliminary electron microscope study of chemical twinning in the system MnS + Y_2S_3, an analog of the mineral system PbS + Bi_2S_3 (galena + bismuthinite). Phil. Mag A38:615-628

Balić-Žunić T, Makovicky E (1993) Contributions to the crystal chemistry of thallium sulphosalts. I. The O-D nature of imhofite. N Jahrb Mineral Abh 165:317-330

Balić-Žunić T, Topa D, Makovicky E (2002) The crystal structure of emilite, $Cu_{10.7}Pb_{10.7}Bi_{21.3}S_{48}$, the second 45 Å derivative of the bismuthinite-aikinite solid-solution series. Can Mineral 40:239-245

Balić-Žunić T, Makovicky E, Moelo Y (1995) Contributions to the crystal chemistry of thallium sulphosalts. III. The Crystal structure of lorandite $TlAsS_2$ and its relation to weissbergite $TlSbS_2$. N Jahrb Mineral Abh 168:213-235

Balić-Žunić T, Mariolacos K, Friese K, Makovicky E (2005) Structure of a synthetic halogen sulfosalt $Cu_3Bi_2S_3I_3$. Acta Cryst B 61:239-245

Baronett A (1997) Equilibrium and kinetic processes for polytype and polysome generation. EMU Notes in Mineralogy 1:119-152

Bayliss P. (1968) The crystal structure of disordered gersdorffite. Am Mineral 53:290-293

Bayliss P (1991) Crystal chemistry and crystallography of some minerals in the tetradymite group. Am Mineral 76:257-265

Belov NV, Godovikov AA, Bakakin VV (1982) Ocherki po Teoreticheskoy Mineralogii (Essays on Theoretical Mineralogy). Publ House Nauka, Moscow

Belov NV (1976) Ocherki po strukturnoy mineralogii (Essays on Structural mineralogy). Publ House Nedra, Moscow

Bente K, Kupčík V (1984) Redetermination and refinement of the structure of tetrabismuth tetracopper enneasulphide, $Cu_4Bi_4S_9$. Acta Cryst C40:1985-1986

Bergerhoff G, Berndt M, Brandenburg K, Degen T (1999) Concerning inorganic crystal structure types. Acta Crystallogr B55:147-156

Berger R. (1987) A phase-analytical study of the Tl-Cu-Se system. J of Solid State Chem 70:65-70

Berger R. (1989) Synthesis und characterization of a layered metal $TlCu_2S_2$. J Less-Common Metals 147: 141-148

Berger R, Eriksson L (1990) Crystal structure and properties of $TlCu_6S_4$. J Less-Common Metals 161:165-173

Berger R, Eriksson L (1990) Crystal structure refinement of monoclinic $TlCu_3Se_2$. J of Less-Common Metals 161:101-108

Berger R, Eriksson L, Meerschaut A (1990) The crystal structure of $TlCu_5Se_3$. J Solid State Chem 87:283-288

Berger R, Meerschaut A (1988) The crystal structure of $Tl_5Cu_{14}Se_{10}$. Eur Solid State Inorg Chem 25:279-288

Berger RA, Sobott RJ (1987) Characterization of $TlCu_7S_4$, a crookesite analog. Mh für Chem und verw Teile anderer Wissenschaften 118:967-972

Berger R, Tergenius L-E, Noren L, Eriksson L (1995) The crystal structure of room-temperature synthesized orthorhombic $TlCu_4Se_3$ from direct methods on X-ray powder data. J Alloys Comp 224:171-176

Berger R, van Bruggen CF (1984) $TlCu_2Se_2$: A p-type metal with a layer structure. J Less-Common Metals 99:113-123

Berlepsch P, Armbruster T, Makovicky E, Hejny C, Topa D, Graeser S (2001) The crystal structure of (001) twinned xilingolite, $Pb_3Bi_2S_6$, from Mittal-Hohtenn, Valais, Switzerland. Can Mineral 39:1653-1663

Berlepsch P, Armbruster T, Makovicky E, Topa D (2003) Another step toward understanding the true nature of sartorite: Determination and refinement of a ninefold superstructure. Am Mineral 88:450-461

Berlepsch P, Armbruster T, Topa D (2003) Structural and chemical variation in rathite, $Pb_8Pb_{4-x}(Tl_2As_2)_x(Ag_2As_2)As_{16}S_{40}$: modulations of a parent structure. Z Kristallogr 217:581-590

Berlepsch P, Makovicky E, Balić-Žunić T (2001) Crystal chemistry of sartorite homologues and related sulfosalts. N Jahrb Mineral Abh 176:45-66

Berlepsch P, Makovicky E and Balić-Žunić T (2001) Crystal chemistry of meneghinite homologues and related sulfosalts. N Jahrb Mineral Mh 2001:115-135

Berlepsch P, Miletich R, Makovicky E, Balić-Žunić T, Topa D (2001) The crystal structure of synthetic $Rb_2Sb_8S_{12}(S_2).2(H_2O)$ a new member of the hutchinsonite family of merotypes. Z Kristallogr 216:272-277

Berner RA (1962) Tetragonal iron sulfide. Science, 137:669-669

Bernert T, Pfitzner A (2005) $Cu_2MnM^{IV}S_4$ (M^{IV} = Si, Ge, Sn)-analysis of crystal structures and tetrahedra volumes of normal tetrahedral compounds. Z Kristallogr 220:968-972

Bernstein LR, Reichel DG, Merlino S (1989) Renierite crystal structure refined from Rietveld analysis of powder neutron-diffraction data. Am Mineral 74:1177-1181

Bichon J, Davot M, Rouxel J (1973) Systematique structurale pour les series d'intercalaires M_xTiS_2 (M = Li, Na, K, Rb, Cs). Comptes Rendus Acad Sci, Ser C, Sci Chim 276:1283-1286

Bindi L, Popova V, Bonazzi P (2003) Uzonite, As_4S_5, from the type locality: single-crystal X-ray study and effects of exposure to light. Can Mineral 41:1463-1468

Bindi L, Cipriani C (2004) The crystal structure of skippenite, Bi_2Se_2Te, from the Kochkar deposit, southern Urals, Russian Federation Can Miner 42:835-840

Bindi L, Evain M, Menchetti S (2006) Temperature dependence of the silver distribution in the crystal structure of natural pearceite, $(Ag, Cu)_{16}$ $(As, Sb)_2$ S_{11}. Acta Crystallogr 62:212-219

Boller H (1978) Faserförmige Erdalkali–thioferrate. Mh Chem 109:975-985

Boller H, Sing M (1997) On the formation and thermal stability of $NH_4Cu_7S_4$ and $NH_4Cu_4S_3$. Topotactic decomposition of $NH_4Cu_7S_4$. Solid State Ionics 101: 1287-1291

Bonazzi P, Borrini D, Mazzi F, Olmi F (1995) Crystal structure and twinning of Sb_2 AsS_2, the synthetic analog of pääkkönenite. Am Mineral 80:1054-1058

Bonazzi P, Menchetti S, Sabelli C (1987) Structure refinement of kermesite: Symmetry, twinning, and comparison with stibnite. N Jahrb Mineral Mh 1987:557-567

Bonazzi P, Bindi L, Bernardini GP, Menchetti S (2003) A model for the mechanism of incorporation of Cu, Fe and Zn in the stannite – këtserite series, Cu_2FeSnS_4 – Cu_2ZnSnS_4. Can Mineral 41: 639-647

Bonazzi P, Bindi L, Olmi F, Menchetti S (2003) How many alacranites do exist? A structural study of non-stoichiometric As_8S_{9-x} crystals. Eur J Mineral 15:283-288

Bonazzi P, Lampronti GI, Bindi L, Zanardi S (2005) Wakabayshilite, $[(As,Sb)_6S_9][As_4S_5]$: Crystal structure, pseudosymmetry, twinning, and revised chemical formula. Am Mineral 90:108-1114

Bonazzi P, Menchetti S, Pratesi G (1995). The crystal structure of pararealgar. Am Mineral 80:400-403

Boucher F, Evain M, Brec R (1993) Distribution and ionic diffusion path of silver in gamma-Ag_8GeTe_6: a temperature dependent anharmonic single crystal structure study. J Solid State Chem 107:332-346

Bouwmeester HJM, Dekker EJP, Bronsema KD, Haange RJ, Wiegers GA (1982) Structures and phase relations of compounds Na_xTiS_2 and Na_xTiSe_2. Rev Chim Minérale 19:333-342

Brandt G, Raeuber A, Schneider J (1973) ESR and X-ray analysis of the ternary semiconductors $CoAlS_3$,$CuInS_2$, $AgGaS_2$. J Solid State Chem12:481-483

Brese NE, Squattrito PJ, Ibers JA (1985) Reinvestigation of the structure of PdS. Acta Crystallogr C41:1829-1830

Breskovska V, Tarkian M (1994) Compositional variations in Bi-bearing fahlores. N Jb Miner Mh 1994:230-240

Bronger W, Böttcher P (1972) Über Thiomanganate und - kobaltate der schweren Alkalimetalle: $Rb_2Mn_3S_4$, $Cs_2Mn_3S_4$, $Rb_2Co_3S_4$, $Cs_2Co_3S_4$. Z anorg allg Chem 390:1-96

Bronger W, Kyas A, Muller P (1987) The antiferromagnetic structures of $KFeS_2$, $RbFeS_2$, $KFeSe_2$ and $RbFeSe_2$ and the correlation between magnetic moments and crystal field calculations. J Solid State Chem 70: 262-270

Bronger W, Genin HS, Mueller P (1999) K_3FeSe_3 und $K_3Fe_2Se_4$. Zwei neue Verbindungen im System K/Fe/Se. Z anorg allg Chem 625:274-278

Bronger W, Müller P (1980) Low-spin Anordnungen in Tetraederstrukturen von Eisensulfiden: Untersuchungen zum System $CsGa_{1-x}Fe_xS_2$. J Less-Common Metals 70:253-262

Bronger W, Ruschewitz V, Müller P (1995) New ternary iron sulphides $A_3Fe_2S_4$(A = K, Rb, Cs): syntheses and crystal structures. J Alloys Compounds 218:22-27

Bronsema KD, de Boer JL, Jellinek F (1986) On the structure of molybdenum diselenide and disulfide. Z anorg allg Chem 540:15-17

Brostigen G, Kjekshus A, Romming C (1973) Compounds with the marcasite type crystal structure VIII, Redetermination of the prototype. Acta Chem Scand 27:2791-2796, Acta Chem Scand 24:1925-1940

Brouwer R, Jellinek F (1979) Modulation of the intergrowth structures of $A_{1-p}Cr_2X_{4-p}$ (A = Ba, Sr, Eu, Pb; x = S, Se; $p \approx 0.29$). Am Inst Phys Conf Proceedings 53:114-116

Brown DB, Zubieta J, Vella PA, Wrobleski JT, Watt T, Hatfield WE, Day P (1980) Solid-State and Electronic Properties of a Mixed-Valence Two-Dimensional Metal, KCu_4S_3. Inorg Chem 19:1945-1950

Buerger MJ, Wuensch BJ (1963) Distribution of atoms in high chalcocite, Cu_2S. Science 141:276-277

Burns PC, Percival JB (2001) Alacranite As_4S_4: a new occurrence, new formula and determination of the crystal structure. Can Mineral 39:809-818

Burr GL, Young VG Jr, McKelvy MJ, Glaunsinger WS, von Dreele RB (1990) A structural investigation of $Ag_{0.167}TiS_2$ by time-of-flight neutron powder diffraction. J Solid State Chem 84:355-364

Burschka C (1980) $CsCu_4S_3$ und $CsCu_3S_2$: Sulfide mit tetraedrisch und linear koordiniertem Kupfer. Z anorg allg Chem 463:65-71

Busch G, Froehlich C, Hullinger F (1961) Struktur, elektrische und thermoelektrische Eigenschaften von $SnSe_2$. Helvet Phys Acta 34:359-368

Cabri LJ, Hall SR, Szymanski JT, Stewart JM (1973) On the transformation of cubanite. Can Mineral 12: 33-38

Cario L, Meerschaut A, Moëlo Y, Nader A, Rouxel J (1997) Structure determination and electrical properties of a new misfit layer compound $(SmS)_{1.25}$ TiS_2. Eur J Solid State Inorg Chem 34:913-924

Carré D, Laruelle P (1973) Structure cristalline du sulfure d'erbium et de lanthane, $Er_9La_{10}S_{27}$. Acta Crystallogr B29:70-73

Carré D, Laruelle P (1974) Structure cristalline du sulfure de néodyme et d'ytterbium, $NdYbS_3$. Acta Crystallogr B30:952-954

Cava RJ, Reidinger F, Wuensch BJ (1980) Single-crystal neutron diffraction study of the fast-ion conductor beta-Ag_2 S between 186 and 325 C. J Solid State Chem 31:69-80

Cava RJ, Reidinger F, Wuensch BJ (1981) Mobile ion distribution and anharmonic thermal motion in fast ion conducting Cu_2S. Solid State Ionics 5:501-504

Chattopadhyay TK, von Schnering HG, Stansfield RFD, McIntyre GJ (1992) X-ray and neutron diffraction study of the crystal structure of MnS_2. Z Kristallogr 199:13-24

Chattopadhyay TK, Pannetier J, von Schnerring HG (1986) Neutron diffraction study of the structural phase transition in SnS. J Phys Chem Solids 47:879-885

Ceolin R, Tofoli P, Khodadad P, Rodier N (1977) Structure cristalline du sulfure mixte de cerium et de bismuth $Ce_{1.25}Bi_{3.78}S_8$. Acta Crystal B33:2804-2806

Cervelle BD, Cesbron FP, Sichère MC (1979) La chalcostibite et la dadsonite de Saint-Pons, Alpes de Haute Provence, France. Can Mineral 17:601-605

Charnock JM, Garner CD, Pattrick RAD, Vaughan DJ (1989) EXAFS and Mössbauer spectroscopic study of Fe-bearing tetrahedrites. Miner Mag 53:193-199

Chen BH, Eichhorn BW, Peng JL, Greene RL (1993) Superconductivity in the A_xNbS_2 intercalation compounds (A = Cs, Rb). J Solid State Chem 103:307-313

Chen TT, Szymanski JT (1981) The structure and chemistry of galkhaite, a mercury sulfide containing Cs and Tl. Can Mineral 19:571-581

Chen X-A, Wada H, Sato A (1999) Preparation, crystal structure and electrical properties of Cu_4SnS_6. Mater Res Bull 34:239-247

Chevrel R (1992) Cluster Solid State Chemistry: a frontier discipline between metallurgy and molecular chemistry. Parthé Eeditor Modern Perspectives in Inorganic Crystal Chemistry. NATO ASI Series C382: 17-26

Choe W, Lee S, O'Connel P, Covey A (1997) Synthesis and structure of new Cd-Bi-S homologous series: a study in intergrowth and the control of twinning patterns. Chem Mater 9:2025-2030

Choi K-S, Kanatzidis MG (2000) Sulfosalts with alkaline earth metals. Centrosymmetric vs acentric interplay in $Ba_3Sb_{4.66}S_{10}$ and $Ba_{2.62}Pb_{1.38}Sb_4S_{10}$ based on the Ba/Pb/Sb ratio. Phases related to the arsenosulfide minerals of the rathite group and the novel polysulfide $Sr_6Sb_6S_{17}$. Inorg Chem 39:5655-5662

Clark R, Brown GE (1980) Crystal structure of rasvumite, KFe_2S_3. Am Mineral 65:477-482

Conde C, Manolikas C, Van Dyck D, Delavignette P, Van Landuyt J, Amelinckx S (1978) Electron microscopic study of digenite-related phases ($Cu_{2-x}S$). Mater Res Bull 13:1055- 1063

Cook R, Schaefer H (1982) Darstellung und Kristallstrukur von $SrBiSe_3$. Rev chimie Minerale 19:19-27

Cook NJ, Ciobanu CL, Wagner T, Stanley CL (in press) Minerals of the system (Pb)-Bi-Te-Se-S related to the tetradymite archetype**:** Review of classification and compositional variation. Can Mineral in press

Cordier G, Cook R, Schäfer H (1980) Isolierte Selenoantimonat (III) anionen in $Ba_4Sb_4Se_{11}$. Revue Chim Miner 17:1-6

Craig DC, Stephenson NC (1965) The crystal structure of lautite, CuAsS. Acta Crystallogr 19:543-547

Daams JLC, Villars P (1993) Atomic environment classification of the rhombohedral "intermetallic" structure types. J Alloys Compd 201:11-16

de Boer JL, Meetsma A (1991) Structures of misfit layer compounds $(LaS)_{1.13}TaS_2$ "$LaTaS_3$" and $(CeS)_{1.15}TaS_2$ "$CeTaS_3$." Acta Crystallogr C47:924-930

di Benedetto F, Bernardini GP, Borrini D, Emiliani C, Cipriani C, Danti C, Caneschi A, Gatteschi D, Romanelli M (2002) Crystal chemistry of tetrahedrite solid solution: EPR and magnetic investigations. Can Mineral 40:837-847

di Benedetto F, Bernardini GP, Cipriani C, Emiliani C, Gatteschi D, Romanelli M (2003) The distribution of Cu(II) and the magnetic properties of the synthetic analog of tetrahedrite: $Cu_{12}Sb_4S_{13}$. Phys Chem Min 32:155-164

Dickinson RG, Friauf JB (1924) The crystal structure of tetragonal lead monoxide. J Am Chem Soc 46:2457-2462

Digiuseppe M, Steger J, Wold A, Kostiner E (1974) Preparation and characterization of the system $CuGa_{1-x}Fe_xS_2$. Inorg Chem 13:1828-1831

Ding Y, Veblen DR, Prewitt CT (2005) High-resolution transmission electron microscopy (HRTEM) study of the 4a and 6a superstructure of bornite Cu_5FeS_4. Am Mineral 90:1256-1264

Ding Y, Veblen DR, Prewitt CT (2005) Possible Fe/Cu ordering schemes in the 2a superstructure of bornite (Cu_5FeS_4). Am Mineral 90:1265-1269

Divjaković V, Nowacki W (1976) Die Kristallstruktur von Imhofit, $Tl_{5.6}As_{15}S_{25.3}$. Z Kristallogr 144:323-333

Dmitrieva MT, Ilyukhin VV, Bokii GB (1979) Close packing and cation arrangement in the djerfisherite structure. Kristallografiya 24:1193-1197

Dmitrieva MT, Yefremov VA, Kovalenker VA (1987) Crystal structure of As goldfieldite Dokl Acad Sci USSR, Earth Sci Sect 297:141-144

Dobrovolskaya MG, Tsepin AI, Evstigneyeva TL, Vyaltsov LN, Zaozerina AO (1981) Murunskite, $K_2Cu_3FeS_4$, a new sulfide of potassium, copper and iron. Zap Vses Mineral Obshch 110:468-473

Donnay G, Donnay JDH, Elliott N, Hastings JM (1958) Symmetry of magnetic structures: Magnetic structure of chalcopyrite. Phys Rev 112:1917-1923

Dornberger-Schiff K, Hoehne E (1959) Die Kristallstruktur des Betechtinit $Pb_2(CuFe)_{21}S_{15}$. Acta Crystallogr 12:646-651

Dornberger-Schiff K (1966) Lehrgang über OD-Strukturen. Akademie-Verlag, Berlin.

Dubost V, Balić-Žunić T, Makovicky E (in press) The crystal structure of $Ni_{10}Pd_7S_{15}$. Can Miner in press

Ďurovič S (1979) Desymmetrization of OD structures. Kristall und Technik 14:1047-1053

Ďurovič S (1992) Layer stacking in general polytypic structures. International Tables for X-ray Crystallography, Vol. C, chapter 9.2.2., 667-680. Kluwer Acad. Publ.

Ďurovič S, Hybler J (2006) OD Structures in crystallography – basic concepts and suggestions for practice. Z Kristallogr 221:63-76

Effenberger H, Pertlik F (1981) Ein Beitrag zur Kristallstruktur von α-CuSe (Klockmannit). N Jahrb Mineral Mh 1981:197-205
Effenberger H, Paar WH, Topa D, Culetto FJ, Giester G (1999) Toward the crystal structure of nagyagite (Pb (Pb, Sb) S_2) (Au,Te)). Am Mineral 84:669-676
Effenberger H, Culetto FJ, Topa D, Paar WH (2000) The crystal structure of synthetic buckhornite (Pb_2BiS_3) ($AuTe_2$). Z Kristallogr 215:10-16
Emsley J (1994) The Elements, 2nd ed. Oxford Univ Press
Engel P, Nowacki W (1969) Die Kristallstruktur von Baumhauerit. Z Kristallogr 129:178-202
Engel P, Nowacki W (1966) Die Verfeinerung der Kristallstruktur von Proustit, Ag_3AsS_3 und Pyrargyrit, Ag_3SbS_3. N Jahrb Mineral, Mh 1966:181-184
Eppinga R, Wiegers GA (1977) The crystal structure of the intercalates $SnTaS_2$ and $SnNbS_2$. Mater Res Bull 12:1057-1062
Eppinga R, Wiegers GA (1980) A generalized scheme for niobium and tantalum dichalcogenides intercalated with post-transition elements. Physica B and C (Netherland) 99:121-127
Eriksson L, Werner P-E, Berger R, Meerschaut A (1991) Structure refinement of $TlCu_7Se_4$ from X-ray powder profile data. J Solid State Chem 90:61-68
Euler R, Hellner E (1960) Ueber komplex zusammengesetzte sulfidische Erze VI. zur Kristallstruktur des Meneghinits $CuPb_{13}Sb_7S_{24}$ 113:345-372
Evans HT Jr (1979) The crystal structures of low chalcocite and djurleite. Z Kristallogr 150:299-320
Evans HT Jr, Allmann R (1968) The crystal structure and crystal chemistry of valleriite. Z Kristallogr 127: 73-93
Evans HT Jr, Konnert JA (1976) Crystal structure refinement of covellite. Am Mineral 61:996-1000
Evans HT Jr, Clark JR (1981) The crystal structure of bartonite, a potassium iron sulfide, and its relationship to pentlandite and djerfisherite. Am Mineral 66:376-384
Evstigneeva TL, Kabalov YuK (2001) Crystal structure of the cubic modification of Cu_2FeSnS_4. Kristallografiya 46:418-422 (in Russian)
Fei Y, Prewitt CT, Frost DJ, Parise JB, Brister K (1998) Structures of FeS polymorphs at high pressure and temperature. Rev High Pressure Sci Technol 7:55-58
Ferraris G, Makovicky E, Merlino S (2004) Crystallography of Modular Materials. IUCr Monographs on Crystallography 15. Oxford Sci Publ
Feutelais Y, Legendre B, Rodier N, Agafonov V (1993) A study of phases in the bismuth – tellurium system. Materials Res Bull 28:591-596
Fleet ME (1972) The crystal structure of pararammelsbergite $NiAs_2$. Am Mineral 57:1-9
Fleet ME (1973) The crystal structure of maucherite. Am Mineral 58:203-210
Fleet ME (1987) Structure of godlevskite Ni_9S_8. Acta Crystallogr 43:2255-2257
Fleet ME (1970) Structural aspects of the marcasite-pyrite transformation. Can Mineral 10:224-231
Fleet ME (1970) Refinement of the crystal structure of cubanite and polymorphism of $CuFe_2S_3$. Z Kristallog 132:276-287
Fleet ME (2006) Phase equilibria at high temperatures. Rev Mineral Geochem 61:365-419
Fleet ME, Burns PC (1990) Structure and twinning of cobaltite. Can Mineral 28:719-723
Foecker AJ, Jeitschko W (2001) The atomic order of the pnictogen and chalcogen atoms in equiatomic ternary compounds TPnCh (T=Ni, Pd; Pn=P, Sb ; Ch=S, Se,Te). J Solid State Chem 162:69-78
Foit FF, Robinson PD, Wilson JR (1995) The crystal structure of gillulyite, Tl_2 $(As, Sb)_8$ S_{13}, from the Mercur gold deposit, Tooele County, Utah, U.S.A. Am Mineral 80:394-399
Frank-Kamenetskaya OV, Rozhdenstvenskaya IV, Yanulova LA (2002) New data on the crystal structures of colusites and arsenosulvanites. J Struct Chem (USSR) 43:89-100
Franzini M, Orlandi P, Paserp M (1992) Morphological, chemical and structural study of robinsonite ($Pb_4Sb_6S_{13}$) from Alpi Apuane, Italy. Acta Volcanologica 2:231-235
Frueh AJ Jr (1950) Disorder in the mineral bornite Cu_5FeS_4. Am Mineral 35:185-192
Frueh AJ jr. (1958) The crystallography of silver sulfide Ag_2S. Z Kristallogr 110:136-144
Fuess H, Kratz T, Töpel-Schadt J, Miehe G (1987) Crystal structure refinement and electron microscopy of arsenopyrite. Z Kristallogr 179:335-346
Furubayashi T, Matsumoto T, Hagino T, Nagata S (1994) Structural and magnetic properties of metal-insulator transition in thiospinel $CuIr_2S_4$. J Phys Soc Japan 63:3333-3339
Furuseth S (1992) Structural properties of the $Ti_{1-x}S_2$ phase. J Alloys Comp 178:211-215
Furuseth S, Selte K, Kjekhus A (1965) Redetermined crystal structures of $NiTe_2$, PtS_2, $PtTe_2$. 19:257-258
Gaines RV, Skinner HCW, Foord EE, Mason B, Rosenzweig A (1997) Dana's New Mineralogy, 8th Ed. John Wiley and Sons
Garin J, Parthe E, Oswald HR (1972) The crystal structure of Cu_3PSe_4 and other ternary normal tetrahedral structure compounds with composition 13 5 64. Acta Crystallogr B 28:3672-3674

Gastaldi L, Simeone MG, Viticoli S (1985) Cation ordering and crystal structures in AGa_2X_4 compounds ($CoGa_2S_4$, $CdGa_2S_4$, $CdGa_2Se_4$, $HgGa_2Se_4$, $HgGa_2Te_4$). Solid State Comm 55:605-607

Gattow G (1957) Die Kristallstruktur von $NH_4Cu_7S_4$. Acta Crystallogr 10:549-553

Gaudin E, Jobic S, Evain M, Brec R, Rouxel J (1995) Charge balance in some $Bi_x Se_y$ phases through atomic structure determination and band structure calculations. Mater Res Bull 30:549-561

Gaudin E, Brocher F, Patricek V, Taulelle F, Evain M (2000) Structures and phase transition of the A_7 P Se_6 (A=Ag, Cu) argyrodite-type ionic conductors. II. beta-and gamma –Cu_7PSe_6. Acta Crystallogr B56:402-408

Gelabert MC, Ho MH, Malik A-S, DiSalvo FJ, Deniard P (1997) Structure and properties of $Ba_6Ni_{25}S_{27}$. Chem Eur J 3:1884-1889

Geller S (1962a) The crystal structure of $Pd_{17}Se_{15}$. Acta Crystallogr 15:713-721

Geller S (1962b) The crystal structure of the superconductor $Rh_{17}S_{15}$. Acta Crystallogr 15:1198-1201

Giese RF, Kerr DF (1965) The crystal structure of ordered and disordered cobaltite. Am Mineral 50:1002-1014

Ginderow D (1978) Structures cristallines de $Pb_4In_9S_{17}$ et $Pb_3In_{6.67}S_{13}$. Acta Crystallogr B34:1804-1811

Gorochov O (1968) Les composés Ag_8MX_6 (M=Si,Ge,Sn et X= S,Se,Te). Bull Soc Chim France 1968:2263-2275

Gostojić M, Nowacki W, Engel P (1982) The crystal structure of synthetic $TlSb_3S_5$, Z Kristallogr 159:217-224

Gotoh Y, Akimoto J, Goto M, Oosawa Y, Onoda M (1995) The layered composite crystal structure of the ternay sulfide $(BiS)_{1.11}NbS_2$. J Solid State Chem 116:61-67

Graham AR, Thompson RM, Berry LG (1953) Studies of mineral sulphosalts: XVII -Cannizzarite. Am Mineral 38:536-544

Grey IE (1975) The structure of $Ba_5Fe_9S_{18}$. Acta Crystallogr B31:45-48

Grguric BA, Putnis A (1998) Compositional controls on phase-transition temperatures in bornite: a differential scanning calorimetry study. Can Mineral 36:215-227

Grice JD, Ferguson RB (1974) Crystal structure refinement of millerite (beta-NiS). Can Mineral 12:248-252

Grice JD, Ferguson RB (1989) The crystal structure of arsenohauchecornite. Can Mineral 27:137-142

Grønvold F, Haraldsen H, Kjekshus A, (1960) On the sulfides, selenides and tellurides of platinum. Acta Chem Scand 14:1879-1893

Grønvold F, Rost E (1957) The crystal structures of $PdSe_2$ and PdS_2. Acta Crystallogr 10:329-331

Grønvold F, Rost E (1962) The crystal structures of Pd_4Se and Pd_4S. Acta Crystallogr 15:11-13

Guinier A, Bokij GB, Boll-Dornberger K, Cowley JM, Ďurovič S, Jagodzinski M, Krishna P et al (1984) Nomenclature of polytype structures. Report of the IUCr Ad-hoc Committee on the Nomenclature of Disordered, Modulated and Polytype Structures. Acta Crystallogr A40:399-404

Guenter JR, Oswald (1968) Neue polytype Form von Zinn (IV)-Sulfid. Naturwissen-schaften 55:177

Hall AJ (1972) Substitution of Cu by Zn, Fe and Ag in synthetic tetrahedrite. Bull Soc franç Minér Crist 99: 152-158

Hall SR, Gabe EJ (1972) The crystal structure of talnakhite $Cu_{18}Fe_{16}S_{32}$. Am Mineral 57:368-380

Hall SR, Rowland JF (1973) The crystal structure of synthetic mooihoekite, $Cu_9Fe_9S_{16}$. Acta Crystallogr B29: 2365-2372

Hall SR, Stewart JM (1973) The crystal structure of argentian pentlandite $(Fe\ Ni)_8AgS_8$, compared with the refined structure of pentlandite $(Fe\ Ni)_9S_8$.Can Mineral 12:61-65

Hall SR, Stewart JM (1973) The crystal structure refinement og chalcopyrite, $CuFeS_2$. Acta Crystallogr 1329: 579-585

Hall SR, Szymanski JT, Stewart JM (1978) Kesterite, $Cu_2(Zn,Fe)SnS_4$, and stannite, $Cu_2(Fe,Zn)SnS_4$, structurally similar but distinct minerals. Can Mineral 16: 131-137

Hallak H, Lee P (1983) Lithium ordering in Li_xTiS_2: a superlattice structure for $Li_{0.33}TiS_2$. Solid State Comm 47:503-505

Harker D (1934) The crystal structure of the mineral tetradymite Bi_2Te_2S. Z Kristallogr 89:175-181

Harris DC, Chen TT (1975) Gustavite - two Canadian occurrences. Can Mineral 13:411-414.

Harris DC, Roberts AC, Thorpe RI, Criddle AJ, Stanley CJ (1984) Kiddcreekite, a new mineral species from the Kidd Creek Mine, Timmins, Ontario and from the Campbell orebody, Bisbee, Arizona. Can Mineral 22:227-232

Hazen RM, Finger LW (1978) The crystal structures and compressibilities of layer minerals at high pressure. I. SnS_2, berndtite. Am Mineral 63:289-292

Henriksen RB, Makovicky E, Stipp SLS, Nissen C, Eggleston CM (2002) Atomic-scale observations of franckeite surface morphology. Am Mineral 87:1273-1278

Herbert HK, Mumme WG (1981) Unsubstituted benjaminite from the A W Mine, NSW: a discussion of metal substitutions and stability. N Jahrb Mineral Mh 1981:69-80

Hill RJ, Craig JR, Gibbs GV (1978) Cation ordering in the tetrahedral sites of the thiospinel $FeIn_2S_4$ (indite). J Phys Chem Solids 39:1105-1111

Hoistad LM, Meerschaut A, Bonneau P, Rouxel J (1995) Structure determination of a trilayer misfit compound $(Gd_\varepsilon\ Sn_{1-\varepsilon}S)_{1.16}(NbS_2)_3$. J Solid State Chem 114:435-441

Hoggins J, Steinfink H (1977) Compounds in the infinitely adaptive series $Ba_P(Fe_2S_4)_Q$: $Ba_9(Fe_2S_4)_8$. Acta Crystallogr B33:673-678

Horiuchi H, Akaogi M, Sawamoto H (1982) Crystal structure studies on spinel-related phases. *In:* High-presssure Research in Geophysics. Akimoto S, Manghnani MH (eds) Reidel Publ Co, p 391-403

Hong HYP, Steinfink H (1972) The crystal chemistry of phases in the Ba-Fe-S and Se systems. J Solid State Chem 5:93-104

Huan G, Greenblatt M (1989) Antiferromagnetic-to-ferromagnetic transition in metallic $Tl_{1-x}K_xCo_2Se_2$ ($0 \le x \le 1.0$) with $ThCr_2Si_2$-type structure. J Less-Common Metals 156:247-257

Huhma M, Vuorelainem Y, Häkli TA, Papunen H (1973) Haapalaite, a new nickel-iron sulphide of the valleriite type from East Finland. Bull geol Soc Finland 45:103-106

Hulliger F (1963) Marcasite-type semiconductors. Nature 198:1081-1082

Hulliger F (1968) Crystal chemistry of chalcogenides and pnictides of the transition elements. Struct Bonding 4:83-229

Hyde BG, Bagshaw AN, Andersson S, O'Keeffe MO (1974) Some defect structures in crystalline solids. Ann Rev Mat Sci 4:43-92

Iitaka Y, Nowacki W (1962) A redetermination of the crystal structure of galenobismutite, $PbBi_2S_4$. Acta Crystallogr 15: 691-698

Ijaali I, Ibers JA (2001) Crystal structure of palladium selenide, PdSe. Z Kristallogr New Cryst St, 216: 485-486

Ioffe PA, Tsemekham LSh, Parshukova LN, Bobkovskii AG (1985) The chemical state of the iron atoms in FeS_2, FeAsS and $FeAs_2$. Russian J Inorg Chem 30:1566-1567.

Iordanidis L, Schindler JL, Kannewurf CR, Kanatzidis MG (1999) $ALn_{1\pm x}Bi_{4\pm x}S_8$ (A = K, Rb; Ln = La, Ce, Pr, Nd): New semiconducting quaternary bismuth sulfides. J Solid State Chem 143:151-162

Ito T, Nowacki W (1974) The crystal structure of freieslebenite, $PbAgSbS_3$. Z Kristallogr 139:85-102

Jambor JL (1969) Dadsonite (minerals Q and QM), a new lead sulphantimonide. Mineral Mag 37:437-441

Jellinek F (1957) The structure of chromium sulfides. Acta Crystallogr 10:620-628

Jellinek F (1968) Sulphides. *In:* Inorganic Sulphur Chemistry. Nicless G (ed) Elsevier, p 669-747

Jellinek F, Brauer G, Mueller H (1960) Molybdenum and niobium sulphides. Nature 185:376-377

Jellinek F (1962) The system tantalum-sulfur. J Less-Common Metals 4:9-15

Jobic S, Le Boterf, P, Brec R, Ouvrard G (1994) Structural determination and magnetic properties of a new mixed valence tin chromium selenide: $Cr_2Sn_3Se_7$. J. Alloys Comp 205:139-145

Jobic S, Bodenan F, Ouvrard G, Elkaim E, Lauriat JP (1995) Structural determination and magnetic properties of a new orthorhobic chromium seleno stannate $Cr_2Sn_3Se_7$.J Solid State Chem 155:165-173

Johan Z, Kvaček M (1971) La bukovite Cu_{3+x} Tl Fe Se_{4-x}, une nouvelle espèce minerale. Bull Soc fr Minéral 94:529-533

Johnson ML, Burnham CW (1985) Crystal structure refinement of an arsenic bearing argentian tetrahedrite. Am Mineral 70:165-170

Johnson NE, Craig JR, Rimstidt JD (1987) Substitutional effects on the cell dimension of tetrahedrite. Can Miner 25:237-244

Julien-Pouzol M, Jaulmes S, Laruelle P (1979) Structure cristalline du sulfure de bismuth et thallium $Tl_4Bi_2S_5$. Acta Crystallogr B35:1313-1315

Jumas JC, Olivier-Fourcade J, Philippot E, Maurin M (1980) Sur le système SnS-Sb_2S_3: Etude structurale de $Sn_4Sb_6S_{13}$. Acta Crystallogr B36:2940-2945

Jumas JC, Philippot E, Maurin M (1979) Structure du rhodostannite synthetique. Acta Crystallogr 35:2195-2197

Kalbskopf R (1972) Strukturverfeinerung des Freibergits. Tschermaks Mineral Petrogr Mitt 18:147-155

Kalbskopf R (1974) Synthese und Kristallstruktur von $Cu_{12-x}Te_4S_{13}$, dem Tellur-Endglied der Fahlerze. TMPM Tschermaks Mineral Petrogr Mitt 21:1-10

Kalbskopf R (1971) Die Koordination des Quecksilbers im Schwazit. Tschermaks Mineral Petrogr Mitt 16: 173-175

Kanatzidis MG, McCarthy TJ, Tanzer TA, Chen L-H, Iordanidis L, Hogan T, Kannewurf CR, Uher C, Chen B (1996) Synthesis and thermoelectric properties of the new ternary bismuth sulfides $KBi_{6.33}S_{10}$ and $K_2Bi_8S_{13}$. Chem Materials 8:1465-1474

Kanatzidis MG (1990) Molten alkali-metal polychalcogenides as reagents and solvents for the synthesis of new chalcogenide materials. Chem Materials 2:353-363

Kanazawa Y, Koto K, Morimoto N (1978) Bornite (Cu_5FeS_4): Stability and crystal structure of the intermediate form. Can Mineral 16:397-404

Kaplunnik LN, Pobedimskaya EA, Belov NV (1980) The crystal structure of schwazite ($Cu_{4.4}Hg_{1.6}$) $Cu_6Sb_4S_{12}$. 253:105-107

Karanovic Lj, Cvetkovic Lj, Poleti D, Balić-Žunić T, Makovicky E (2002) Crystal and absolute structure of enargite from Bor (Serbia). N Jahrb Mineral Mh 2002:241-253

Karanović L, Cvetković L, Poleti D, Balić-Žunić T, Makovicky E(2003) Structural and optical properies of schwazite from Dragodol (Serbia). N Jb Miner Mh 2003:503-520

Karup-Møller S, Makovicky E (1979) On pavonite, cupropavonite, benjaminite and "oversubstituted" gustavite. Bull Minéral 102:351-367

Karup-Møller S, Makovicky E (1979) Topotactic replacement of niccolite by rammelsbergite; new data on alloclasite, $Co_{0.56}Ni_{0.45}Fe_{0.01}As_{1.18}S_{0.80}$. N Jb Miner Abh 136:310-325

Karup-Møller S, Makovicky E (1992) Mummeite - A new member of the pavonite homologous series from Alaska Mine, Colorado. N Jahrb Mineral Mh 1992:555-576

Karup-Møller S, Makovicky E (1995) The phase system Fe-Ni-S at 725 °C. N Jb Min Mh 1995:1-10

Karup-Møller S, Makovicky E (1999) Exploratory studies of element substitutions in synthetic tetrahedrite. Part II. Selenium and tellurium as anions in Zn-Fe tetrahedrites. N Jb Miner Mh 1999:385-399

Karup-Møller S, Makovicky E (2003) Exploratory studies of element substitutions in synthetic tetrahedrite Part V. Mercurian tetrahedrite. N Jb Miner Abh 179:73-83

Karup-Møller S, Makovicky E (2004) Exploratory studies of the solubility of minor elements in tetrahedrite VI. Zinc and the combined zinc-mercury and iron-mercury substitutions. N Jb Miner Mh 2004:508-524

Kato K, Kawada I, Takahashi T (1977) Die Kristallstruktur von $LaCrS_3$. Acta Crystallogr B33:3437-3493

Kawada I and Hellner E (1971) Dei Kristallstruktur der Pseudozell (subcell) von Andorit VI (Ramdohrit). N Jahrb Mineral Mh 1971:551-560

Keller-Besrest F, Collin G (1983) Structure and planar faults in the defective NiAs-type compound 3c, Fe_7S_8. Acta Crystallogr B39:296-303

Keller-Besrest F, Collin G (1990) Structural aspects of the alpha transitition in stoichiometric FeS. Identification of the high-temperature phase. J Solid State Chem 84:194-210

Kim S-J, Kim WC, Kim CS (2002) Neutron diffraction and Mössbauer studies on $Fe_{1-x}Cr_2S_4$ (x=0.0, 0.04,.0.08). J Appl Phys 91:7935-7937

King HEjr, Prewitt CT (1982) High-pressure and high-temperature polymorpism of iron sulfide. Acta Crystallogr B38:1877-1887

Kissin SA (1974) Phase relations in a portion of the Fe-S system. PhD Dissertation, Univ Toronto

Kjekshus A, Peterzons PG, Rakke T, Andresen AF (1979) Compounds with the marcasite type crystal structure. XIII. Structural and magnetic properties of $Cr_tFe_{1-t}As_2$, $Cr_tFe_{1-t}Sb_2$, $Fe_{1-t}Ni_tAs_2$ and $Fe_{1-t}Ni_tSb_2$. Acta Chem Scand A33:469-480

Kjekshus A, Rakke T (1979) Structural transformations in $Co_tNi_{1-t}As_2$, $NiAs_{2-x}S_x$, $NiAs_{2-x}Se_x$, and $CoAs_{1-x}Se_{1+x}$. Acta Chem Scand A33:609-615

Klepp KO (1993) $Tl_2Pt_5S_6$ - a new thioplatinate with a channel-type structure. J Alloys Comp 196:25-28

Klepp KO, Boller H (1978) Ternäre Thallium-Übergangsmetall-Chalkogenide mit $ThCr_2Si_2$ Struktur. Mh Chemie 109:1049-1057

Klepp KO, Boller H, Völlenkle H (1980) Neue Verbindungen mit KCu_4S_3-Struktur. Mh Chemie 111:727-733

Klepp KO, Boller H (1981) $Na_3Fe_2S_4$ ein Thioferrat mit gemischt valenter (FeS_2) – kette. Mh Chemie und verw Teile anderer Wiss 112:83-89

Klepp KO, Pantschov S, Boller H (2000) Crystal structure of mixed-valent trirubidium tetraselenidoferrate $Rb_3Fe_2Se_4$. Z Kristallogr – New cryst struct 215:5-6

Klünder-Hansen M, Makovicky E, Karup-Møller S (2003) Exploratory studies on substitutions in tetrahedrite-tennantite solid solution. Part IV. Substitution of germanium and tin. N Jb Miner Abh 179:43-71

Klünder-Hansen M, Karup-Møller S, Makovicky E (2003) Exploratory studies on substitutions in tetrahedrite-tennantite solid solution. Part III. The solubility of bismuth in tetrahedrite –tennantite containing iron and zinc. N Jb Miner Mh 2003: 153-175

Knop O, Reid KIG, Sutarno R, Nakagawa Y (1968) Chalkogenides of the transition elements VI X-Ray neutron and magnetic investigation of the spinels Co_3O_4, $NiCo_2O_4$, Co_3S_4, $NiCo_2S_4$. Can J Chem 46:3463-3476

Kocman V, Nuffield EW (1973) The crystal structure of wittichenite, Cu_3BiS_3. Acta Crystallogr B29:2528-2535

Kocman V, Nuffield EW (1974) Crystal structure of antimonian hauchecornite from Westphalia. Can Mineral 12:269-274

Koděra M, Kupčik V, Makovicky E (1970) Hodrushite - a new sulphosalt. Mineral Mag 37:641-648

Konnert JA, Evans HT jr. (1980) The crystal structure of erdite $NaFeS_2$ $(H_2O)_2$. Am Mineral 65:516-521

Konopka D, Kozlowska I, Chelkowski A (1973) X-ray investigations of spinel structure compounds of the $HgCr_2$ $(Se_x$ $S_{1-x})_4$ type. Phys Lett A44:289-290

Kostov VV, Macíček J (1995) Crystal structure of synthetic $Pb_{12.65}Sb_{11.35}S_{28.35}Cl_{2.65}$ - A new view of the crystal chemistry of chlorine-bearing lead-antimony sulphosalts. Eur Mineral 7:1007-1018

Kostov I, Minčeva Stefanova J (1982) Sulphide Minerals. Crystal Chemistry, Parageneses and Systematics. E.Schweizerbartsche Verlagsbuchhandlung.
Koto K, Morimoto N (1975) Superstructure investigation of bornite Cu_5FeS_4 by the modified partial Patterson function. Acta Crystallogr B31:2268-2273
Koto K, Morimoto N (1970) The crystal structure of anilite. Acta Crystallogr 26:915-924
Koto K, Morimoto N, Gyobu A (1975) The superstructure of the intermediate pyrrhotite. I. Partially disordered distribution of metal vacancy in the 6C type, $Fe_{11}S_{12}$. Acta Crystallogr B31:2759-2769
Kovalenker VA, Laputina IP, Yevstigneyeva TL, Izoitko VM (1976) Thalcusite, $Cu_{3-x}\,Tl_2\,Fe_{1-x}\,S_4$, a new sulfide of thallium from copper – nickel ores of the Talnakh Deposit. Zap Vsez Min Obshch 105:202-206
Krämer V (1980) Structure of bismuth indium sulphide $Bi_3In_5S_{12}$. Acta Crystallogr B 36:1922-1923
Krämer V (1983) Lead indium bismuth chalcogenides III. Structure of $Pb_4In_2Bi_4S_{13}$. Acta Crystallogr C42: 1089-1091
Krämer V, Reis I (1986) Lead indium bismuth chalcogenides. II. Structure of $Pb_4In_3Bi_7S_{18}$. Acta Crystallogr C42:249-251
Kudoh Y, Takeuchi Y (1976) The superstructure of stannoidite. Z Kristallogr 144:145-160
Kupčík V (1967) Die Kristallstruktur des Kermesits, Sb_2S_2O. Naturwissenschaften 54:114-115
Kupčík V, Makovicky E (1968) Die Kristallstruktur des Minerals (Pb, Ag, Bi) $Cu_3Bi_5S_{11}$. N Jahrb Mineral Mh 236-237.
Kupčík V, Steins M (1991) Verfeinerung der Kristallstruktur von Gustavit $Pb_{1.5}Ag_{0.9}Bi_{2.5}Sb_{0.1}S_6$. Berichte Deutsch Mineral Gesellschaft 1990/2. 151
Kusawake T, Takahashi Y, Oshima K-I (2000) Structural analysis of the layered compounds Cu_xTiS_2. Molec Cryst Liquid Cryst 341:93-98
Kutoglu A, Allmann R (1972) Strukturverfeinerung des Patronits, $V(S_2)_2$. N Jahrb Mineral Mh 1972:339-345
Kyono A, Kimata M, Matsuhisa M, Miyashita Y, Okamoto K (2002) Low-temperature crystal structures of stibnite implying orbital overlap of Sb $5is^2$ inert pair electrons. Phys Chem Mineral 29:254-260
Kyono A, Kimata M (2004) Structural variations induced by difference of the inert pair effect in the stibnite – bismuthinite solid solution series $(Sb,Bi)_2S_3$. Am Mineral 89:932-940
Kyono A, Kimata M, Hatta T (2005) Light-induced degradation dynamics in realgar: in situ-structural investigation using single-crystal X-ray diffraction study and X-ray photoelectron spectroscopy. Am Mineral 90:1563-1570
Lafond A, Deudon C, Meerschaut A, Palvadeau P, Moelo Y, Briggs A (1999) Structure determination and physical properties of the misfit layered compound $Pb_2FeS_3\,0.58\,NbS_2$. J Solid State Chem142:461-469
Landa-Canovas A R, Otero-Diaz L C (1992) A trasmission electron microscopy study of the MnS-Er_2S_3 System. Austral J Chem 45:1473-1487
Lavina B, Salviulo G, Della Giusta A (2002) Cation distribution and structure modelling of spinel solid solutions. Phys Chem Mineral 29:10-18
le Blanc A, Rouxel J (1972) Sur les types structuraux des composés intercalaires $MSnS_2$ (M = Li, Na, K, Rb). Comptes Rendus Acad Sci, Serie C, Sci Chimi 274:786-788
Lemoine P, Carré D, Guittard M (1986) Structure de sulfure d'europium et de cuivre Eu_2CuS_3. Acta Crystallogr 42: 390-391
Lemoine P, Carré D, Guittard M (1986) Structure du sulfure d'europium et de bismuth $Eu_{1.1}Bi_2S_4$. Acta Crystallogr C42:259-261
le Nagard N, Gorochov O, Collin G (1974) Structure cristalline et proprietes physiques de Cu_xTiS_2. Materials Res Bull 10:1287-1296
Lennie AR, Redfern SAT, Schofield PF, Vaughan DJ (1995) Synthesis and Rietveld crystal structure refinement of mackinawite, tetragonal FeS. Mineral Mag 59:677-683.
Leon M, Merino JM, de Vidales JLM (1992) Crystal structure of synthesized $CuGaTe_2$ determined by X-ray powder diffraction using the Rietveld method. J Materials Sci 27:4495-4500
Léone P, Le Leuch L-M, Palvadeau P, Molinié P, Moëlo Y (2003) Single crystal structures and magnetic properties of two iron- or manganese-lead-antimony sulfides: $MPb_4Sb_6S_{14}$(M:Fe,Mn). Solid State Sci 5: 771-776
Lima-de-Faria J, Hellner E, Liebau F, Makovicky E, Parthé E (1990) Nomenclature of inorganic structure types. Report of the IUCr Commission on Crystallographic Nomenclature, Subcommittee on the Nomenclature of Inorganic Structure Types. Acta Crystallogr A46:1-11
Llanos J, Tapia M, Mujica C, Oro-Sole J, Gomez-Romero P (2000) A new structural modification of stannite. Bol Soc Chilena Quimica 45:605-609
Luedecke J, van Smaalen S, Spijkerman A, de Boer JL, Wiegers GA (1999) Commensurately modulated structure of 4Hb- (Ta Se2) determined by X-ray crystal structure refinement. Phys Rev, Serie 3. B - Condensed Matter 59:6063-6071
Lugakov NF, Movchanskiy EA, Pokrovskiy II (1975) Self-diffusion of copper and ion conductivity in Cu_3BiS_3. Izv Akad Nauk BSSR, Ser Khim 3:42-44

Lundegaard LF, Miletich R, Balić-Žunić T, Makovicky E (2003) Equation of state and crystal structure of Sb_2S_3 between 0 and 10 GPa. Phys Chem Min 30:463-468

Lundegaard LF, Makovicky E, Boffa-Ballaran T, Balić-Žunić T (2005) Crystal structure and cation lone electron pair activity of Bi_2S_3 between 0 and 10 GPa. Phys Chem Min 32:578-584

Lundqvist D (1947) X-ray studies on the binary system Ni-S. Arkiv foer Kemi, Mineral Geol 24:1-12

Lutz HD, Jung M, Waeschenbach G (1987) Kristallstrukturen des Loellingits $FeAs_2$ und des Pyrits $RuTe_2$. Z anorg allg Chem 554:87-91

Lyman PS, Prewitt CT (1984) Room- and high-pressure crystal chemistry of CoAs and FeAs. Acta Crystallogr B40:14-20

Machatschki F (1928) Formel und Kristallstruktur des Tetraedrites. Norsk Geol Tidsskr 10:23

Machatschki F (1928) Praezisionmessungen der gitterkonstanten verschiedener Fahlerze Formel und Struktur derselben. Z Kristallogr 68:204-222

Maciček J (1986) The crystal chemistry of cosalite. Coll Abstr Xth Eur Cryst Meeting Wroclaw, 260

Makeyev AB, Evstigneeva TL, Troneva NV, Vyalsov LN, Gorshkov AI, Trubkin NV (1984) Yushkinite $V_{1-x}S.n[(Mg, Al)(OH)_2]$ – a new mineral. Mineral Zhurnal 6:91-97

Makovicky E (1976) Crystallography of cylindrite. I. Crystal lattices of cylindrite and incaite. N Jahrb Mineral Abh 126:304-326

Makovicky E (1981) The building principles and classification of bismuth-lead sulphosalts and related compounds. Fortschr Mineral 59:137-190

Makovicky E (1985) The building principles and classification of sulphosalts based on the SnS archetype. Fortschr Mineral 63:45-89

Makovicky E (1989) Modular classification of sulphosalts - current status. Definition and application of homologous series. N Jahrb Mineral Abh 160:269-297

Makovicky E (1993) Rod-based sulphosalt structures devided from the SnS and PbS archetype. Eur J Mineral 5:545-591

Makovicky E (1994) Polymorphism in Cu_3SbS_3 and Cu_3BiS_3: The ordering schemes for copper atoms and electron microscope observations. N Jahrb Mineral Abh 168:185-212

Makovicky E (1997a) Modular crystal chemistry of sulphosalts and other complex sulphides. Europ Mineral Union Notes Mineral 1:237-271

Makovicky E (1997b) Modularity - different types and approaches. Europ Mineral Union Notes Mineral 1: 315-343

Makovicky E, Balić-Žunić T (1993) Contributions to the crystal chemistry of thallium sulphosalts. II. $TlSb_3S_5$ - the missing link of the lillianite homologous series. N Jahrb Mineral Abh 165:331-344

Makovicky E, Balić-Žunić T (1995) The crystal structure of skinnerite, $P2_1/c$-Cu_3SbS_3, from powder data. Can Mineral 33:655-663

Makovicky E, Balić-Žunić T(1999) Gillulyite $Tl_2(As, Sb)_8S_{13}$: Reinterpretation of the crystal structure and order-disorder phenomena. Am Mineral 84:400-406

Makovicky E, Balić-Žunić T, Topa D (2001) The crystal structure of neyite, $Ag_2Cu_6Pb_{25}Bi_{26}S_{68}$. Can Mineral 39:1365-1376

Makovicky E (2002) Experimental studies of palladium containing systems and compounds. Bol Soc Españ Miner 25:5-37

Makovicky E (2005) Micro and mesoporous sulfide and selenide structures. Rev Mineral Geochem 57:403-433

Makovicky E, Mumme WG, Topa D (in press) The crystal structure of dadsonite. Can Mineral, in press

Makovicky E, Balić-Žunić T, Karanović L, Poleti D, Pršek J (2004) Structure refinement of natural robinsonite, $Pb_4Sb_6S_{13}$: Cation distribution and modular description. N Jahrb Mineral 2004:49-67

Makovicky E, Forcher K, Lottermoser W, Amthauer D (1990) The role of Fe^{2+} and Fe^{3+} in synthetic Fe-substituted tetrahedrite. Miner Petrol 43:73-81

Makovicky E, Hyde BG (1981) Non-commensurate (misfit) layer structures. Struct Bonding 46:101-170

Makovicky E, Hyde BG (1992) Incommensurate, two-layer structures with complex crystal chemistry: minerals and related synthetics. *In*: Incommensurate Misfit Sandwiched Layered Compounds. Meerschaut A (ed) Materials Sci Forum 100-101:1-100 Trans. Tech Publ. Ltd.

Makovicky E, Karanović L, Poleti D, Balić-Žunić T (2005) Crystal structure of copper-rich unsubstituted tennantite, $Cu_{12.5}As_4S_{13}$. Can Miner 43:679-688

Makovicky E, Johan Z, Karup-Møller S (1980) New data on bukovite, thalcusite, chalcothallite and rohaite. N Jahrb Mineral Abh 138:122-146

Makovicky E, Karup-Møller S (1977 a) Chemistry and crystallography of the lillianite homologous series. I. General properties and definitions. N Jahrb Mineral Abh 130:264-287

Makovicky E, Karup-Møller S (1977 b) Chemistry and crystallography of the lillianite homologous series. Part II: Definition of new minerals: eskimoite, vikingite, ourayite and treasurite. Redefintion of schirmerite and new data on the lillianite - gustavite solid solution series. N Jahrb Mineral Abh 131:56-82

Makovicky E, Karup-Møller S (1984) Ourayite from Ivigtut, Greenland. Can Mineral 22:565-575
Makovicky E, Karup-Møller S (1994) Exploratory studies on substitution of minor elements in synthetic tetrahedrite. Part I. Substitution by Fe, Zn, Co, Ni, Mn, Cr, V and Pb. Unit-cell parameter changes on substitution and the structural role of "Cu^{2+}." N Jb Miner Abh 167:89-123
Makovicky E, Leonardsen E, Moëlo Y (1994) The crystallography of lengenbachite, a mineral with the non-commensurate layer structure. N Jahrb Mineral Abh 166:169-191
Makovicky E, Mumme WG, Watts JA (1977) The crystal structure of synthetic pavonite, $AgBi_3S_5$ and the definition of the pavonite homologous series. Can Mineral 15:339-348
Makovicky E, Mumme WG (1979) The crystal structure of benjaminite $Cu_{0.50}Pb_{0.40}Ag_{2.30}Bi_{6.80}S_{12}$. Can Mineral 17:607-618
Makovicky E, Mumme WG (1983) The crystal structure of ramdohrite, $Pb_6Sb_{11}Ag_3S_{24}$ and its implications for the andorite group and zinckenite. N Jahrb Mineral Abh 147:58-79
Makovicky E, Mumme WG (1984) The crystal structures of izoklakeite, dadsonite and jaskolskiite. 15th Int. Congr Crystallog., Coll Abstr, Hamburg: C-246
Makovicky E, Mumme WG (1986) The crystal structure of isoklakeite, $Pb_{51.3}Sb_{20.4}Bi_{19.5}Ag_{1.2}Cu_{2.9}Fe_{0.7}S_{11.4}$. The kobellite homologous series and its derivatives. N Jahrb Mineral Abh 153:121-148
Makovicky E, Mumme WG, Hoskins BF (1991) The crystal structure of Ag-Bi bearing heyrovskyite. Can Mineral 29:553-558
Makovicky E, Mumme WG, Madsen IC (1992) The crystal structure of vikingite. N Jahrb Mineral Mh 454-468
Makovicky E, Norrestam R (1985) The crystal structure of jaskolskiite, $Cu_x\ Pb_{2+x}\ (Sb, Bi)_{2-x}\ S_5$ ($x \approx 0.2$), a member of the meneghinite homologous series. Z Kristallogr 171:179-194
Makovicky E, Skinner BJ (1975) Studies of the sulfosalts of copper. IV. Structure and twinning of sinnerite, $Cu_6As_4S_9$. Am Mineral 60:998-1012
Makovicky E, Skinner BJ (1979) Studies of the sulfosalts of copper. VII. Crystal structures of the exsolution products $Cu_{12.3}Sb_4S_{13}$ and $Cu_{13.8}Sb_4S_{13}$ of unsubstituted synthetic tetrahedrite. Can Miner 17:619-634
Makovicky E (1993) Rod-based sulphosalt structures derived from the SnS and PbS archetype. Eur J Miner 5:545-591
Makovicky E (1983) The phase transformations and thermal expansion of the solid electrolyte Cu_3BiS_3 between 25 and 300 °C. J Solid State Chem 49:85-92
Makovicky E, Søtofte I, Karup-Møller S (2002): The crystal structure of $Cu_4Bi_4Se_9$. Z Kristallogr 217:597-604
Makovicky E, Søtofte I, Karup-Møller S (2006) The crystal structure of $Cu_{1.78}Bi_{4.73}S_8$, an N=3 pavonite homologue with a Cu-for-Bi substitution. Z Kristallogr 221:122-127
Makovicky E, Tippelt G, Forcher K, Lottermoser W, Karup-Møller S, Amthauer G (2003) Mössbauer study of Fe-bearing synthetic tennantite. Can Mineral 41:1125-1134
Makovicky E, Topa D, Balić-Žunić T (2001) The crystal structure of paarite, the newly discovered 56 Å derivative of the bismuthinite-aikinite solid-solution series. Can Mineral 39:1377-1382
Mardix S (1986) Polytypism: A controlled thermodynamic phenomenon. Phys Rev Ser 3B Cond Matter 33: 8677-8684
Mariolacos K, Kupčík V, Ohmasa M, Miehe G (1975) The crystal structure of $Cu_4Bi_5S_{10}$ and its relation to the structures of hodrushite and cuprobismutite. Acta Crystallogr B31:703-708
Marumo F (1967) The crystal structure of nowackiite, $Cu_6Zn_3As_4S_{12}$. Z Kristallogr 124:352-368
Marumo F, Nowacki W (1967) A refinement of the crystal structure of luzonite, Cu_3AsS_4. Z Kristallogr 124: 1-8
Matković P, El-Boragy, M, Schubert K (1976) Kristallstruktur von $Pd_{16}S_7$. J Less Common Metal, 50:65-176
Matsushita Y, Ueda Y (2003) Structure and physical properties of 1D magnetic chalcogenide, jamesonite $FePb_4Sb_6S_{14}$. Inorg Chem 42:7830-7838
Matsushita Y (2005) Chalcogenide structure data base version 4.3M. (downloadable database)
Matzat E (1972) Die Kristallstruktur des Wittichenits, Cu_3BiS_3. Tschermaks Mineral-Petrogr Mitt 18:312-316
Matzat E (1979) Cannizzarite. Acta Crystallogr B35:133-136
Matsushita Y, Takéuchi Y (1994) Refinement of the crystal structure of hutchinsonite, $TlPbAs_5S_9$. Z Kristallogr 209:475-478
McCammon C, Zhang J, Hazen RM, Finger LW (1992) High-pressure crystal chemistry of cubanite, $CuFe_2S_3$. Am Mineral 77:937-944
McKelvy MJ, Wiegers GA, Dunn JM, Young VG Jr, Glaunsinger W.S. (1990): Structural investigation of the ammonnium intercalates of titanium and niobium disulfides. Solid State Ionics 38:163-170
Meerschaut A, Deudon C (2001) Crystal structure studies of the 3R-$Nb_{1.09}S_2$ and the 2H-$NbSe_2$ compounds: correlation between nonstoichiometry and stacking type (= polytypism). Mater Res Bull 36:1721-1727

Meerschaut A, Guemas L, Auriel C, Rouxel J (1990) Preparation structure determination and transport properties of a new misfit layer compound $PbS_{1.14}(NbS_2)_2$. Eur J Solid State Inorg Chem 27:557-570

Meerschaut A, Palvadeau P, Moëlo Y, Orlandi P (2001) Lead-antimony sulfosalts from Tuscany (Italy). IV. Crystal structure of pillaite, $Pb_9Sb_{10}S_{23}ClO_{0.5}$, an expanded monoclinic derivative of hexagonal $Bi(Bi_2S_3)_9I_3$, from the zinkenite group. Eur J Mineral 13:779-790

Meetsma A, Wiegers GA, Haange RJ, de Boer JL (1990) Structure of 2H-TaS_2. Acta Crystallogr C46:1598-1599

Megaw HD (1973) Crystal Structures: A Working Approach. W.B. Saunders Co.

Merlino S (1988) Average and real structures in minerals. Z Kristallogr 185:13-14

Merlino S, Pasero M (1997) Polysomatic approach in the crystal chemical study of minerals. EMU Notes Mineral 1:297-312

Miehe G (1971) Crystal structure of kobellite. Nature Phys Sci 231:133-134

Miehe G, Kupčík V (1971) Die Kristallstruktur des $Bi(Bi_2S_3)_9J_3$. Naturwiss 58:219-220

Mizota T, Inove A, Yamada T, Nakatsuka A, Nakayama N (1998) Ionic conduction and thermal nature of synthetic Cu_3BiS_3. Min J (Japan) 20:81-90

Moëlo Y, Palvadeau P, Meisser N, Meerschaut A (2002) Structure cristalline d'une meneghinite naturelle pauvre en cuivre $Cu_{0.58}Pb_{12.72}(Sb_{7.04}Bi_{0.24})S_{24}$. Comptes Rendus Geosci 334:529-536

Moëlo Y (1979) Quaternary compounds in the system Pb-Sb-S-Cl: dadsonite and synthetic phases. Can Mineral 17:595-600

Moëlo Y (1983) Contribution à l'étude des conditions naturelles de formation des sulfures complexes d'antimoine et plomb (sulfosels de Pb/Sb). Signification métallogènique. Série "Documents du B.R.G.M.," Orléans 55 : 624 p

Moëlo Y, Makovicky E, Karup-Møller S (1988) Sulfures complexes plombo-argentifères: Minéralogie et cristallochimie de la série andorite-fizelyite $(Pb, Mn,Fe, Cd,Sn)_{3-2x}(Ag,Cu)_x(Sb,Bi,As)_{2+x}(S,Se)_6$. Documents BRGM (Orlèans) 167:107 pp

Moëlo Y, Makovicky E, Karup-Møller S, Corvelle B, Maurel C (1990) La lévyclaudite, $Pb_8Sn_7Cu_3(Bi,Sb)_3S_{28}$, une nouvelle espèce à structure incommensurable, de la série de la cylindrite. Eur J Mineral 2:711-723

Moëlo Y, Meerschaut A, Rouxel J, Auriel C (1995) Precise analytical characterization of incommensurate sandwiched layered compounds $[(Pb,Sn)S]_{1+x}[(Nb,Ti)S_2]_m$ ($0.08<x<0.28$), m=1-3). Role of cationic coupling on the properties and the structural modulation. Chem Mater 7:1759-1771

Moëlo Y, Meerschaut A, Orlandi P, Palvadeau P (2000) Lead-antimony sulfosalts from Tuscany (Italy): II-Crystal structure of scainiite, $Pb_{14}Sb_{30}S_{54}O_5$, an expanded monoclinic derivative of $Ba_{12}Bi_{24}S_{48}$ hexagonal sub-type (zinkenite group). Eur J Mineral 12:835-846

Moëlo Y, Oudin E, Picot P, Caye R (1984) L'uchucchacuaite, $AgMnPb_3Sb_5S_{12}$, une nouvelle espèce minérale de la série de l'andorite. Bull Minéral 107:597-604

Moëlo Y, Makovicky E (in press) Revision of sulfosalt definition and nomenclature. Report COM IMA

Morimoto N, Kullerud G (1961) Polymorphism in bornite. Am Mineral 46:1270-1282

Morimoto N (1964) Structures of two polymorphic forms of Cu_5FeS_4. Acta Crystallogr 17:351-360

Morimoto N, Koto K (1970) Phase relations of the Cu-S system at low temperatures: stability of anilite. Am Mineral 55:106-117

Morosin B (1974) Structure refinement on NbS_2. Acta Crystallogr B30:551-552

Mujica C, Carvajal G, Llanos J, Wittke O (1998) Redetermination of the crystal structure of copper (I) tetrathiovanadate (sulvanite), Cu_3VS_4. Z Kristallogr – New Crystal Struct 213:p 12

Mujica C, Paez J, Llanos J (1994) Synthesis and crystal structure of layered chalcogenides $KCuFeS_2$ and $KCuFeS_2$. Mater Res Bull 29:263-268

Mullen DJE, Nowacki W (1972) Refinement og the crystal structures of realgar AsS and orpiment As_2S_3. Z Kristallogr 136:48-65

Müller U (1996) Anorganische Strukturchemie. B.G. Teubner

Mumme WG (1975) Junoite, $Cu_2Pb_3Bi_8(S,Se)_{16}$, a new sulfosalt from Tennant Creek, Australia: Its crystal structure, and relationship with other bismuth sulfosalts. Am Mineral 60:548-558

Mumme WG (1980) Weibullite, $Ag_{0.32}Pb_{5.02}Bi_{8.55}Se_{6.08}S_{11.92}$ from Falun, Sweden. A higher homologue of galenobismutite. Can Mineral 18:1-18

Mumme WG (1980c) The crystal structure of nordströmite, $CuPb_3Bi_7(S,Se)_{14}$ from Falun, Sweden: A member of the junoite homologous series. Can Mineral 18:343-352

Mumme WG (1986) The crystal structure of paderaite, a mineral of the cuprobismutite series. Can Mineral 24:513-521

Mumme WG (1989) The crystal structure of $Pb_{5.05}(Sb_{3.75}Bi_{0.28})Se_{10.72}Se_{0.28}$: boulangerite of near ideal composition. N Jahrb Mineral Mh 1989:498-512

Mumme WG (1990) A note on the occurrence, composition and crystal structures of pavonite homologous series members ^{4}P, ^{6}P, and ^{8}P. N Jahrb Mineral Mh 1990:193-204

Mumme WG, Niedermayr G, Kelly PR, Paar WH (1983) Aschamalmite, $Pb_{5.92}Bi_{2.06}S_9$, from Untersulzbach Valley in Salzburg, Austria - "monoclinic heyrovskyite." N Jahrb Mineral Mh 1983:433-444

Mumme WG, Watts JA (1980) $HgBi_2S_4$: Crystal structure and relationship with the pavonite homologous series. Acta Crystallogr B 36:1300-1304

Mumme WG, Welin E, Wuensch BJ (1976) Crystal chemistry and proposed nomenclature for sulfosalts in the system bismuthinite-aikinite (Bi_2S_3-$CuPbBiS_3$). Am Mineral 61:15-20

Nakajima S (1963) The crystal structure of $Bi_2Te_{3-x}Se_x$. J Phys Chem Solids 24:479-485

Nakayama N, Kosuge K, Kachi S (1981) Studies on the compounds in Ba-Fe-S system (III). Phase relations of $Ba_{1+x}Fe_2S_4$ with infinitely adaptive structure. J Solid State Chem 36:9-19

Navrotsky A(1994) Physics and Chemistry of Earth Materials. Cambridge Univ Press

Niizeki W, Buerger MJ (1957) The crystal structure of jamesonite, $FePb_4Sb_6S_{14}$. Z Kristallogr 109:161-183

Noël H, Padiou J (1976) Structure cristalline de $FeUS_3$. Acta Crystallogr B32:1593-1595

Nowack E, Schwarzenbach D, Hahn T (1991) Charge densities in CoS_2 and NiS_2 pyrite structure. Acta Crystallogr B47:650-659

Nowacki W (1982) Isotypy in aktashite $Cu_3Hg_3As_4S_{12}$ and nowackiite $Cu_6Zn_3As_4S_{12}$. Kristallografiya 27: 49-50

Nuffield EW (1952) Studies of mineral sulpho-salts: XVI-cuprobismutite. Am Mineral 37:447-452

Nuffield EW (1980) Cupropavonite from Hall's Valley, Park Country, Colorado. Can Mineral 18:181-184

O'Keefe M, Hyde BG (1996) Crystal Structures. I. Patterns and Symmetry. Mineralogical Society of America

Ohmasa M (1973) The crystal structure of $Cu_{2+x}Bi_{6-x}S_9$ (x = 1.21). N Jahrb Mineral Mh 1973:227-233

Ohmasa M, Nowacki W (1970) A redetermination of the crystal structure of aikinite [$BiS_2|S|Cu^{IV}Pb^{VIII}$]. Z Kristallogr 137:422-432

Ohmasa M, Nowacki (1973) The crystal structure of synthetic $CuBi_5S_8$. Z Kristallogr 137:422-432

Oledzka M, Lee J-G, Ramanujacheri KV, Greenblatt M (1996) Synthesis and characterization of quaternary sulfides with $ThCr_2Si_2$-type structures: $KCo_{2-x}Cu_xS_2$ (0.5 L × L 1.5) and $ACoCuS_2$ (A = K, Rb, Cs). J Solid State Chem 127:151-160

Oliveria M, McMullan RK, Wuensch BJ (1988) Single crystal neutron diffraction analysis of cation distribution in the high-temperature phases alpha-$Cu_{2-x}S$, alpha-$Cu_{2-x}Se$ and alpha Ag_2Se. Solid State Ionics 28-30: 1332-1337

Olivier-Fourcade J, Maurin M, Philippot E (1983) Étude cristallochimique du système Li_2S-Sb_2S_3. Revue Chim Minérale 20:196-217

Omloo WP, Jellinek F(1970) Intercalation compounds of alkali metals with niobium and tantalum dichalcogenides. J Less-Common Metals 20:121-129

Onoda M, Kato K, Gotoh Y, Oosawa Y (1990) Structure of the incommensurate composite crystal $PbS_{1.12}VS_2$. Acta Crystallogr 46:487-492

Organova NI, Drits VA, Dmitrik AL (1972) Strutural study of tochilinite Part I The isometric variety. Kristallografiya 17:761-767

Organova NI, Drits VA, Dmitrik AL (1973) Strutural study of tochilinite PartII Acicular variety. Unusual diffraction patterns. Kristallografiya 18:966-972

Organova NI, Drits VA, Dmitrik AL (1974) Selected area diffraction study of a type II valleriite like mineral. Am Mineral 59:190-200

Organova NI (1989) Crystal Chemistry of Incommensurate and Modulated Mixed-layer Minerals. Nauka, Moscow

Orlandi P, Meerschaut A, Palvadeau P, Merlino S (2002) Lead-antimony sulfosalts from Tuscany (Italy). V. Definition and crystal structure of moëloite, $Pb_6Sb_6S_{14}(S_3)$, a new mineral from the Ceragiola marble quarry. Eur J Mineral 14:599-606

Otto HH, Strunz H (1968) Zur Kristallchemie synthetischer Blei-Wismut-Spiessglanze, N Jahrb Mineral Abh 108:1-19

Ozawa T, Nowacki W (1975) The crystal structure of, and the bismuth-copper distribution in synthetic cuprobismutite. Z Kristallogr 142:161-176

Ozawa T, Tachikawa O (1996) A transmission electron microscope observation of 138 Å period in Pb-As-S sulfosalts. Mineral J 18:97-101

Ozawa T, Takéuchi Y (1993) X-ray and electron diffraction study of sartorite - A periodic antiphase boundary structure and polymorphism. Mineral J 16:358-370

Paar WH, Topa D, Makovicky E, Culetto FY (2005) Milotaite, PbSbSe, a new palladium mineral species from Předbořice, Ccech Republic. Can Mineral 43:689-694

Parise JB (1980) Structure of Heazlewoodite Ni_3S_2. Acta Crystallogr 36:1179-1180

Parise JB, Smith PPK, Howard CJ (1984) Crystal structure refinement of $Sn_3Sb_2S_6$ by high-resolution neutron powder diffraction. Mater Res Bull 19:503-508

Parthé E (1990) Elements of Inorganic Structural Chemistry, A Course on Selected Topics. Publ K Sutter Parthé, Petit-Lancy

Pašava J, Pertlik F, Stumpfl EF, Zemann J (1989) Bernardite, a new thallium arsenic sulphosalt from Allchar, Macedonia, with a determination of the crystal structure. Mineral Mag 53:531-538

Pattrick RAD, Hall AJ (1983) Silver substitution into synthetic zinc, cadmium and iron tetrahedrites Mineral Mag 47:441-450

Pauling L(1927) Electronic polarizabilities. Proc Roy Soc (London) A114:181

Pauling L, Neumann EW (1934) The crystal structure of binnite $(Cu,Fe)_{12}As_4S_{13}$, and the chemical composition and structure of minerals of the tetrahedrite group. Z Kristallogr 88:54-62

Pertlik F (1984) Kristallchemie natuerlicher Telluride I Verfeinerung der Kristallstruktur des Sylvanits $AuAgTe_4$.TMPM. Tscher Mineral Petrogr Mitt 33:203-212

Pertlik F (1984) Crystal chemistry of natural tellurides II Redetermination of the crystal structure of Krennerite $Au_{1-x}Ag_x Te_2$ with *x* about 0.2. v TMPM. Tscher Mineral Petrogr Mitt 33:253-262

Pertlik F (1994) Kristallstrukturbestimmung der monoklinen Hochtemperaturmodi-fikation von AsS (alpha-AsS), Oesterreische Akad Wiss, Math-Naturwiss Klasse, Sitzungsberichte 131:3-5

Peters J, Krebs B (1982) Silicon disulphide and silicon diselenide: A reinvestigation. Acta Crystallogr B38: 1270-1272

Peterson RC, Miller I (1986) Crystal structure and cation distribution in freibergite and tetrahedrite. Min Magazine 50:717-721

Petkov V, Billinge SJL, Larson P, Mahanti SD, Vogt T, Rangan KK, Kanatzidis MG (2002) Structure of nanocrystalline materials using atomic pair distribution function analysis: Study of $LiMoS_2$. Phys Rev 3B Cond Matt 65:0921051-0921054

Petřiček V, Cisařová I, de Boer JL, Zhou W, Meetsma A, Wiegers A, van Smaalen S (1993) The modulated structure of the commensurate misfit-layer $(BiSe)_{1.09}$ $TaSe_2$. Acta Crystallogr B49:258-266

Petrova IV, Kaplunnik LN, Bortnikov NS, Pobedimskaya YeA, Belov NV (1978) The crystal structure of synthetic robinsonite. Dokl Akad Nauk SSSR 241:88-90

Petrova IV, Bortnikov NS, Pobedimskaya Ye A, Belov NV (1979) The crystal structure of a new synthetic Pb,Sb-sulphosalt. Dokl Akad Nauk SSSR 244:607-609

Petrova IV, Pobedimskaya EA, Brygzgalov IA (1988) Crystal structure of miharaite $Cu_4FePbBiS_6$. Dokl Akad NaukSSSR 299:123-127- Soviet Physics Doklady 33:157-159

Petrova I V, Kuznetsov A I, Belokoneva Ye L, Simonov M A, Pobedimskaya Ye A, Belov NV (1978) On the crystal structure of boulangerite (in Russ.). Dokl Akad Nauk SSSR 242:337-340

Pfitzner A (1994) Cu_3SbS_3: Zur Kristallstruktur und Polymorphie. Z anorg allg Chemie 620:1992-1997

Pfitzner A (1995) Cu_3SbSe_3: Synthese und Kristallstruktur. Z anorg allg Chemie 621: 685-688

Pfitzner A (1997) Die Präparative Anvendung der Kupfer (I)-halogenid-Matrix zur Synthese neuer Materialen. Habilitationschrift Universität Siegen.

Pfitzner A (1998) Disorder of Cu^+ in Cu_3SbS_3: Structural investigations of the high- and low-temperature modification. Z Kristallogr 213:228-236

Pfitzner A, Bernert T (2004) The system Cu_3AsS_4-Cu_3SbS_4 and investigations on normal tetrahedral structures. Z Kristallogr 219:20-26

Pfitzner A, Evain M, Petříček V (1997) $Cu_{12}Sb_4S_{13}$ a temperature-dependent structure investigation. Acta Crystallogr 53:337-345

Pfitzner A, Reiser S (2002) Refinement of the crystal structures of Cu_3PS_4 and Cu_3SbS_4 and a comment on normal tetrahedral structures. Z Kristallogr 217:51-54

Pickardt J, Reuter B, Riedel E, Soechtig J (1975) On the formation of $FeSe_2$ single crystals by chemical transport reactions. J Solid State Chem 15:366-368

Pierce L, Buseck PR (1978) Superstructuring in the bornite-digenite series: a high resolution electron microscopy study. Am Mineral 63:1-16

Pocha R, Johrendt D (2002) Kristallstrukturen und elektronische Eigenschaften von $Ge_{1/3}NbS_2$ und $Ge_{1/4}NbS_2$. Z Naturforsch B. Anorg Org Chemie 57:1367-1374

Pohl D, Liessmann W, Okrugin VM (1996) Rietveld analysis of selenium-bearing goldfieldites. N Jahrb Mineral. Mh 1996:1-8

Portheine JC, Nowacki W (1975) Refinement of the crystal structure of zinckenite, $Pb_6Sb_{14}S_{27}$. Z Kristallogr 141:79-96

Potter RW (1977) An electrochemical investigation of the system Cu-S. Econ Geol 72:1524-1542

Povarennykh AS (1963) Grundsätze einer kristallchemischen Klassifikation der Sulfide. Geologie 12:377-400

Pratt JL, Bayliss P (1980) Crystal structure refinement of a cobaltian ullmannite. Am Mineral 65:154-156

Prewitt CT, Rajamani V (1974) Electron interaction and chemical bonding in sulfides. In: Sulfide Mineralogy, MSA Short Course Notes 1. Ribbe P (ed) Mineral Soc Am, p 1-41

Pring A (1990) Disordered intergrowths in lead-arsenic sulfide minerals and the paragenesis of the sartorite-group minerals. Am Mineral 75:289-294

Pring A (2001) The crystal chemistry of the sartorite group minerals from Lengenbach, Binntal, Switzerland - a HRTEM study. Schweiz Mineral-Petrogr Mitt 81:69-87

Pring A, Graeser S (1994) Polytypism in baumhauerite. Am Mineral 79:302-307
Pring A, Jercher M, Makovicky E (1999) Disorder and compositional variation in the lillianite homologous series. Mineral Mag 63:(6) 917-926
Pring A, Williams T, Withers R (1993) Structural modulation in sartorite: An electron microscope study. Am Mineral 78:619-626
Putnis A, Grace J (1976) The transformation behavior of bornite. Contrib Mineral Petrol 55:311-315
Putz H, Paar WH, Topa D, Makovicky E, Roberts AC (in press): Catamarcaite, Cu_6GeWS, a new germanium – tungsten sulfide from Capillitas, Catamaren, Argentina: description, paragenesis and crystal structure. Can Mineral in press.
Rabu P, Meerschaut A, Rouxel J, Wiegers GA (1990) The crystal structure of the misfit layer compound $(YS)_{1.23}NbS_2$. J Solid State Chem 88:451-458
Rad HD, Hoppe R (1978) Über thiotitanate (IV): Synthese und Struktur von $Cs_2(TiS_3)$. Z Naturforschung B33: 1184-1185
Rajamani V, Prewitt CT (1975) Refinement of the structure of Co_9S_8. Can Mineral 13:75-78
Ramdohr P, Strunz H (1978) Klockmanns Lehrbuch der Mineralogie, 16th edition. Ferdinand Enke Verlag
Ramirez R, Mujica C, Buljan A & Llanos J (2001) A family of new compounds derived from chalcopyrite. Common patterns in their electronic and crystal structures. Bol Soc Chilena Química 46:235-245
Reithmayer K, Steurer W, Schulz H, de Boer JL (1993) High-pressure single-crystal structure study on calaverite $AuTe_2$. Acta Crystallogr 49:6-11
Remmert P, Fischer E, Hummel HV (1994) Phasenuntersuchungen im System 2Ha-TaS_2-2Hc-MoS_2. Z Naturforsch B, Anorg Org Chemie 49:1175-1178
Ribar B, Nowacki W (1970) Die Kristallstruktur von Stephanit. Acta Crystallogr 26:201-207
Řidkošil T, Skala R, Johan Z, Srein V (2001) Telluronevskite Bi_3TeSe_2 a new mineral. Eur J Mineral 13:177-185
Riedel E, Karl R, Rackwitz R (1981) Moesbauer studies of thiospinels V system $Cu_{1-x}Fe_xMe_2S_4$ Me=Cr, Rh and $Cu_{1-x}Fe_xCr_2(S_{.7}Se_{.3})_4$. J Solid State Chem 40:255-265
Riedel E, Karl R (1980) Moesbauer studies of thiospinels I The system $FeCr_2S_4$- Fe Rh_2S_4. J Solid State Chem 35:77-82
Riedel E, Pickardt J, Soechtig J (1976) Roentgenographische Untersuchung des Spinellsystems $CuRh_2$ $(S_{1-x}Se_x)_4$. Z Anorg Allg Chem 419:63-66
Riekel C, Reznik HG, Schoellhorn R, Wright CJ (1979) Neutron diffraction study on formation and structure of D_xTaS_2 and H_xNbS_2. J Chem Physics 70:5203-5212
Robert JL, Makovicky E (1984) Cristallochimie Minérale. Encyclop Univer Paris: 747-753
Roseboom EH (1966) An investigation of the system Cu-S and some natural copper sulfides between 25° and 700 °C. Econ Geol 61:641-672
Ross V (1957) Geochemistry, crystal structure and mineralogy of the sulfides. Econ Geol 52:755-774
Rost E, Vestersjö E (1968) The crystal structure of the high temperature phase Pd_3S. Acta Chem Scand 22: 819-826
Rouxel J (1991) Des solides à moins de trois dimensions. Pour la Science 165:64-73
Rouxel J, Moëlo Y, Lafond A, DiSalvo FJ, Meerschaut A, Roesky R (1994) Role of vacancies in misfit layered compounds: The case of gadolinium chromium sulfide compound. Inorg Chem 33:3358-3363
Rowland JF, Hall SR (1975) Haycockite, $Cu_4Fe_5S_8$: a superstructure in the chalcopyrite series. Acta Crystallogr B 57:689-708
Rudashevski NS, Karpenkov AM, Shipova GS, Shishkin NN, Ryabkin VA (1979) Thalfenisite, the thallium analog of djerfisherite. Vses Mineralog Obsch Zapiski 108:696-701 (in Russ.)
Ruedorff W, Schwarz HG, Walter MC (1952) Strukturuntersuchungen an Alkalithiocupraten. Z Anorg Allg Chemie 269:141-152
Saeki M, Onoda M (1987) Preparation of molybdenum intercalated tantalum disulphide Mo_xTaS_2. Chem Lett 1987:1353-1356
Sawada H, Kawada I, Hellner E, Tokonami M (1987) The crystal structure of senandorite (andorite VI): $PbAgSb_3S_6$. Z Kristallogr 180:141-150
Schils H, Bronger W (1979) Ternäre Selenide des Kupfers. Z anorg allg Chemie 456:187-193
Schleid T (1990) Das System Na_zGdClH_x/S. II Einkristalle von Gd_2S_3 im U_2S_3-Typ. Zeitschrift für Anorgan Allgemeine Chemie 590:111-119
Schleid T, Lauxmann P, Schneck C (1999) Roentgenographische Einkristalluntersuchungen an alpha-HgS (zinnober). Z Kristallogr 16:95-95
Schneider J, Schultz H (1993) X-ray powder diffraction of Ag_2Te at temperatures up to 1123K. Z Kristallogr 203:1-15
Schoenfeld B, Huang JJ, Moss SC (1983) Anisotropic mean-square displacement (MSD) in single crystals of 2H- and 3R-MoS_2. Acta Crystallogr B39:404-407

Schutte WJ, de Boer JL, Jellinek F (1987) Crystal structures of tungsten disulfide and diselenide. J Solid State Chem 70:207-209

Scott JD (1974) Experimental methods in sulfide synthesis *In:* Sulfide Mineralogy, MSA short Course Notes 1. Ribbe P (ed) Mineral Soc Am, p. S1-S38

Scott JD, Nowacki W (1976) The crystal structure of alloclasite, CoAsS, and the alloclasite-cobaltite transformation. Can Mineral 14:561-566

Seung DY, Gravereau P, Trut L, Levasseur A (1988) Li_3AsS_3. Acta Crystallogr C54: 900-902

Shamrai VF, Leitus GM, Meshcheryakov VN, Faustov NI (1986) Study of the ternary chalcogenides of layer structure. Izv Akad Nauk SSSR, Metally 1986:213-219

Shannon RD (1981) Bond distances in sulfides and a preliminary table of sulfide crystal radii. Struct Bond Crystals 2:53-70

Shelimova LE, Karpinski OG, Svechnikova TE, Avilov ES, Kretova MA, Zemskov VS (2004) Synthesis and structure of layered compounds in the PbTe-Bi_2 Te_3 and PbTe-Sb_2Te_3 systems. Neorg Mat 40:1440-1447

Shimazaki H, Ozawa T (1978) Tsumoite, Bi Te, a new mineral from Tsumo mine, Japan. Am Mineral 63: 1162-1165

Skinner BJ, Erd RC, Grimaldi FS (1964) Greigite the thio-spinel of iron; a new mineral. Am Mineral 49:543-555

Skowron A, Brown ID, Tilley RJD (1992) A single-crystal X-ray and high resolution microscope study of $Pb_5Sb_6S_{14}$. J Solid State Chem 97:199-211

Skowron A, Brown ID (1990a) Refinement of the structure of robinsonite, $Pb_4Sb_6S_{13}$. Acta Crystallogr C46: 527-531

Skowron A, Brown ID (1990b) Refinement of the structure of boulangerite, $Pb_5Sb_4S_{11}$. Acta Crystallogr C46: 531-534

Skowron A, Brown ID (1990c) Structure of antimony lead selenide, $Pb_4Sb_4Se_{10}$, a selenium analog of cosalite. Acta Crystallogr C46:2287-2291

Skowron A, Tilley RJD (1990) Chemically twinned phases in the Ag_2S-PbS-Bi_2S_3 system. Part 1. Electron microscope study. J Solid State Chem 85:235-250

Smith PPK (1984) Structure determination of diantimony tritin hexasulphide, $Sn_3Sb_2S_6$, by high-resolution transmission electron microscopy. Acta Crystallogr C40:581-584

Spijkerman A, de Boer JL, Meetsma A, Wiegers GA, van Smaalen S (1997) X-ray crystal structure refinement of the nearly commensurate phase of 1T-(TaS_2) in (3+2) dimensional superspace. Phys Rev 3B - Cond Matter 56:13757-13767

Springer G (1971) The synthetic solid-solution series Bi_2S_3-$BiCuPbS_3$ (bismuthinite-aikinite). N Jb Miner Mh 1971:13-24

Spry PG, Merlino S, Wang S, Zhang XM, Buseck PR (1994) New occurrences and refined crystal chemistry of colusite, with comparisons to arsenosulvanite. Am Mineral 79:750-762

Srikrishnan T, Nowacki, W (1974) A redetermination of the crystal structure of cosalite, $Pb_2Bi_2S_5$. Z Kristallogr 140:114-136

Srikrishnan T, Nowacki W (1975) A redetermination of the crystal structure of livingstonite $HgSb_4S_8$. Z. Kristallogr 141:174-192

Stasova MM (1968) The crystal structure of bismuthum selenide Bi_4Se_3. Izvestiya Akad Nauk SSSR Neorg Materialy 4:28-31

Stoll P, Näther C, Jess I, Bensch W (1999) KCu_4Se_3. Acta Crystallogr C55:286-288.

Strunz H, Nickel EH (2001) Strunz Mineralogical Tables. E. Schweizerbart'sche Verlagsbuchhandlung

Sugaki A, Shima H, Kitakaze A, Mizota T (1981) Hydrothermal synthesis of nukundamite and its crystal structure. Am Mineral 66:398-402

Szymanski JT (1995) The crystal structure of owensite $(Ba,Pb)_6(Cu,Fe,Ni)_{25}S_{27}$, a new member of the djerfisherite group. Can Mineral 33:671-677

Szymanski JT (1974) The crystal structure of high-temperature $CuFe_2S_3$. Z Kristallogr 140:240-248

Szymanski JT (1976) The crystal structure of mawsonite, $Cu_6Fe_2SnS_8$. Can Mineral 3:79-86

Szymanski JT (1978) The crystal structure of černyite, Cu_2CdSnS_4, a cadmium analog of Stannite. Can Mineral 16:147-151

Szymanski JT (1979) The crystal structure of platarsite, $Pt(As,S)_2$, and a comparison with sperrylite, $PtAs_2$. Can Mineral 17:117-123

Takagi J, Takeuchi Y (1972) The crystal structure of lillianite. Acta Crystallogr B 28:649-651

Takeuchi Y (1957) The absolute structure of ullmannite NiSbS. Mineral J 2:90-102

Takeuchi Y, Ozawa T (1975) The structure of $Cu_4Bi_4S_9$ and its relation to the structures of covellite CuS and bismuthinite Bi_2S_3. Z Kristallogr 141:217-232

Takeuchi Y (1970) On the crystal chemistry of sulphides and sulphosalts. *In*: Volcanism and Ore Deposits. Tstsumi T (ed), Univ of Tokyo Press, p. 395-420

Takéuchi Y (1997) Tropochemical cell-twinning. Terra Scientific Publishing Co

Takeuchi Y, Ghose S, Nowacki W (1965) The crystal structure of hutchinsonite, $(Tl,Pb)_2\ As_5S_9$. Z Kristallogr 121:321-348

Takeuchi Y, Ozawa T, Takagi J (1974) Structural characterization of the high-temperature phase V on the PbS - Bi_2S_3 join. Z Kristallogr 140:249-272

Takeuchi Y, Ozawa T, Takagi J (1979) Tropochemical cell-twinning and the 60 Å structure of phase V in the PbS - Bi_2S_3 system. Z Kristallogr 150:75-84

Takeuchi Y, Takagi I (1974) The crystal structure of heyrovskyite (6PbS-Bi_2S_3). Proc Japan Acad 50:75-79

Talybov AG, Vainshtein BK (1962) An electron diffraction study of the second superlattice in Pb Bi_4 Te_7. Kristallografiya 7:43-50

Tani B, Mrazek F, Faber J jr; Hitterman RL (1986) Neutron diffraction study of electrochemically synthesized djerfisherite. J Electrochemi Soci 133:2644-2649

Tettenhorst RT, Corbato CE (1984) Crystal structure of germanite, $Cu_{26}Ge_4Fe_4S_{32}$, determined by powder X-ray diffraction. Am Mineral 69:943-947

Thompson JB Jr. (1978) Biopyriboles and polysomatic series. Am Mineral 58:239-249

Tokonami M, Nishiguchi K, Morimoto N (1972) Crystal structure of a monoclinic pyrrhotite (Fe_7S_8). Am Mineral 57:1066-1080

Tomas A, Guittard M (1980) Cristallochimie des sulfures mixtes de chrome et d'erbium. Mater Res Bull 15: 1547-1556

Tomeoka K, Ohmasa M, Sadanaga R (1980) Crystal chemical studies on some compounds in the copper-bismuth sulfide (Cu_2S-Bi_2S_3) system. Mineral J 10:57-70

Tomeoka K, Buseck PR (1985) Indicators of aqueous alteration in CM carbonaceous chondrites: Microtextures of a layered mineral containing Fe,S,O and Ni. Geochem Cosmochim Acta 49:2149-2164

Topa D (2001) Mineralogy, Crystal Structure and Crystal chemistry of the Bismuthinite- Aikinite Series from Felbertal, Austria. Ph D Tesis, Inst Mineral Univ Salzburg, Austria.

Topa D, Balić-Žunić T, Makovicky E (2000) The crystal structure of $Cu_{1.6}Pb_{1.6}Bi_{6.4}S_{12}$, a new 44.8 Å derivative of the bismuthinite-aikinite solid-solution series. Can Mineral 38:611-616

Topa D, Makovicky E, Balić-Žunić T, Berlepsch P (2000) The crystal structure of $Cu_2Pb_6Bi_8S_{19}$. Eur J Mineral 12:825-833

Topa D, Makovicky E, Criddle A, Paar WH, Balić-Žunić T (2001) Felbertalite, $Cu_2Pb_6Bi_8S_{19}$, a new mineral species from Felbertal, Salzburg Province, Austria. Eur J Mineral 13:961-972

Topa D, Makovicky E, Balić-Žunić T (2002) The structural role of excess Cu and Pb in gladite and krupkaite based on new refinements of their structure. Can Mineral 40:1147-1159

Topa, D., Makovicky, E. and Paar, W.H. (2002): Composition ranges and exsolution pairs for the members of the bismuthinite-aikinite series from Felbertal, Austria. Can Mineral 40:549-869

Topa D, Makovicky E, Balić-Žunić T, Paar WH (2003) Kupčíkite, a new Cu-Bi sulfosalt from Felbertal, Austria and its crystal structure. Can Mineral 41:1155-1166

Topa D, Makovicky E, Balić-Žunić T (in press) The crystal structure of jaguéite, $Cu_2Pd_3Se_4$ and chrisstanleyite, $Ag_2Pd_3Se_4$. Can Miner in press

Topa D, Makovicky E (in press) The crystal structure of paderaite Cu_7 $(X_{0.33}Pb_{1.32}Bi_{11.33})$ S_{11}, with x = Cu or Ag. Can Mineral, in press

Tossell JA, Vaughan DJ, Burdett JK (1981) Pyrite, marcasite and arsenopyrite type minerals: Crystal chemical and structural principles. Phys Chem Minerals 7:177-184

Towle LC, Oberbeck V, Brown BE, Stajdohar RE (1966) Molybdenum diselenide: rhombohedral high pressure - high temperature polymorph. Science 154:895-896

Trudu AG, Kittel U (1998) Crystallography, mineral chemistry and chemical nomenclature of goldfieldite, the tellurian member og the tetrahedrite solid-solution series. Can Mineral 36:1115-1137

Uda M (1968) Synthesis of magnetic Fe_3S_4. Scientific Papers of the Institute of Phys Chem Research 62:14-23

Uda M (1968) The structure og tetragonal FeS. Z Anorg Allg Chem 361:94-98

Van der Lee A, de Boer JL (1993) Redetermination of the structure of hessite, Ag_2Te-III. Acta Crystallogr C49: 1444-1446

Van Dyck D, Conde C, Amelinckx S (1979) The diffraction pattern of crystals presenting a digenite type of disorder I. Phys Status Solidi 56:327-334

Van Dyck D, Conde-Amiano C, Amelickx S (1980) The diffraction pattern of crystals presenting a digenite type of disorder II. Phys Status Solidi 58:451-468

van Laar V (1967) Ferrimagnetic and anti-ferromagnetic structures of Cr_5S_6. Phys Rev 156:654-662

van Smaalen S (1995) Incommensurate crystal structures. Cryst Rev 4, 79-202

Vaughan DJ, Burns RG (1972) Mössbauer spectroscopy and bonding in sulfide minerals containing four-coordinated iron. Proc 24th Int Geol Congr 14:156-167

Vaughan DJ, Wright KV (1998) Crystal chemistry of ore minerals. *In:* Modern Approaches to Ore and Environmental Mineralogy. Cabri LJ, Vaughan DJ (eds) Min Soc Canada Short Course Ser 27:75-109

Vaughan DJ, Craig JR (1978) Mineral Chemistry of Metal Sulfides. Cambridge Univ Press
Vaughan DJ, Craig JR (1985) The crystal chemistry of iron-nickel spinels. Am Mineral 70:1036-1043
Vaughan DJ, Rosso KM (2006) Chemical bonding in sulfide minerals. Rev Mineral Geochem 61:231-264
Vaqueiro P, Kosidowski ML, Powell AV (2002) Structural distortions of the metal dichalcogenide units in AMo_2S_4 (A = V, Cr, Fe, Co) and magnetic and electrical properties. Chem Mater 14:1201-1209
Volk K, Cordier G, Cook R, Schäfer H (1980) $BaSbTe_3$ und $BaBiSe_3$. Verbindungen mit BiSe-bzw. SbTe-Schichtverbänden. Z Naturforsch 35B: 136-140
Volk K, Schäfer H (1979) $Cs_2Sb_8S_{13}$, ein neuer Formel- und Strukturtyp bei Thioantimoniten. Z Naturforsch 34b: 1637-1640
Wagner T, Monecke T (2005) Germanium-bearing colusite from the Waterloo volcanic-rock- hosted massive sulfide deposit, Australia: Crystal chemistry and formation of colusite-group minerals. Can Mineral 43: 655-669
Wang X (1989) Transmission electron microscope study of the minerals of the franckeite family. PhD Thesis (in Chinese). Chinese Geological University,
Waychunas GA (1991) Crystal chemistry of oxides and oxyhydroxides. Reviews Mineral 25:11-61
Whitfield HJ (1980) Polymorphism in skinnerite, Cu_3SbS_3. Solid State Comm 33:747-748
Whitfield HJ (1981): The crystal structure of hcc-CuAsSe. J Solid State Chem 39:209-214
Whitfield HJ (1970) The crystal structure of tetraarsenic trisulfide. J Chem Soc A Inorg Phys Theor Chem 1970:1800-1803
Whitfield HJ (1973) Crystal structure of the beta-form of tetraarsenic trisulphide. J Chem Soc Dalton Trans Inorg Chem 1973:1737-1738
Wiegers GA, Meerschaut A (1992) Structures of misfit layer compounds $(MS)_nTS_2$ (M=Sn, Pb, Bi, rare earth metals; T=Nb,Ta, Ti, V, Cr; 1.08<n<1.23). J Alloys Comp 178:351-368
Wiegers GA, Meetsma A, Haange RJ, de Boer JL (1990) Structure, electrical transport and magnetic properties of the misfit layer compound $SmS_{1.19}TaS_2$ ($SmTaS_3$). J Less-Common Metals 168:347-359
Wiegers GA, Meetsma A, Haange RJ, van Smaalen S, de Boer JL, Meerschaut A, Rabu P, Rouxel J (1990) The incommensurate misfit layer structure of $PbS_{1.14}NbS_2$ ($PbNbS_3$) and $LaS_{1.14}NbS_2$ ($LaNbS_3$) an x-ray diffraction study. Acta Crystallogr 46:324-332
Will G, Hinze E, Abdel RAM, (2002) Crystal structure analysis and refinement of digenite ($Cu_{1.8}S$) in the temperature range 20 to 500 C under controlled sulfur partial pressure. Eur J Mineral 14:591-598
Will G, Lauterjung J, Schmitz H, Hinze E (1984) The bulk moduli of 3d-transition element pyrites measured with synchrotron radiation in a new belt-type apparatus. Mater Res Soc Symp Proc 22:49-52
Williamson DP, Grimes NW (1974 +1973) An X-ray diffraction investigation of sulphide spinels. J Phys D Appl Phys 7:1-6 Mater Res Bull 8:973-982
Wilson JA, Di Salvo FJ, Mahajan S (1975) Charge-density waves and superlattices in the metallic layered transition metal dichalcogenides. Adv Phys 24:117-200
Wintenberger M (1979) Etude de la structure cristallographique et magnetique de Cu_2FeGeS_4 et remarque sur la structure magnetique de Cu_2MnSnS_4. Mater Res Bull 14:1195-1202
Wittlinger J, Werner S, Schultz H (1997) On the amorphisation of $ZnCr_2S_4$ spinel under high pressure x-ray diffraction studies. Phys Chem Mineral 24:597-600
Wolf M, Hunger H-J, Bewilogua K (1981) Potosiit - ein neues Mineral der Kylindrit-Franckeit-Gruppe. Freiberg Forsch Hefte C364:113-133
Wuensch BJ (1964) The crystal structure of tetrahedrite, $Cu_{12}Sb_4S_{13}$. Z Kristallogr 119:437-453
Wuensch BJ, Takeuchi Y, Nowacki W (1964) Refinement of the crystal structure of binnite, $Cu_{12}As_4S_{13}$. Z Kristallogr 123:1-20
Wuensch BJ (1993) Cation distributions, bonding and transport behavious in silver and copper fast-ion conductors with simple anion packings. Mat Sci Eng B18:186-200
Xu YN, Ching WY (1993) Electronic, optical, and structural properties of some wurtzite crystals. Phys Rev Cond Matter 48:4335-4351
Yajima J, Okta E, Kanazawa Y (1991) Toyohaite, $Ag_2 FeSn_3S_8$, a new mineral. Mineral J (Japan) 15:222-232
Yakovenchuk VN, Pakhomovsky YA, Men'shikov YP, Ivanyuk GYu, Krivorichev SV, Burns PC (2003) Chlorbartonite, $K_6Fe_{24}S_{26}$(Cl,S) a new mineral species from a hydrothermal vein in the Khikina massif, Kola Peninsula, Russia: description and crystal structure. Can Mineral 41:503-511.
Yund RA (1962) Phase relations in the system Ni-As. Econ. Geology 56:1273-1296
Žák L, Frýda J, Mumme WG, Paar WM (1994) Makovickyite, $Ag_{1.5}Bi_{5.5}S_9$, from Baita Bihorului, Romania: The ^{4}P natural mineral member of the pavonite series. N Jahrb Mineral Abh 168:147-169
Zaritskii VN, Sadykov RA, Kostyuk YaI, Sizov RA, Aminov TG, Gubaidullin RK, Safin ShR (1986) Superlattice and cation distribution in the Fe_{1-x} Cu_x Cr_2S_4 system. Fiz Tverd Tela Solid State Physics 28: 3293-3298
Zhang X, Kanatzidis MG, Hogan T, Kannewurf CR(1996) $NaCu_4S_4$, a simple new low-dimensional, metallic copper polychalcogenide, structurally related to CuS. J Am Chem Soc 118:693-694

Zhukova TB, Zaslavskii AI (1972) Crystal structures of the compounds $PbBi_4Te_7$ $PbBi_2T_4$ $SnBi_4Te_7$ $SnBi_2Te_4$ $SnSb_2Te_4$ and $GeBi_4Te_7$. Kristallografiya 16:918-922.

Zhuze VP, Sergeeva VM, Strum EL (1958) New semiconductor compounds. Zh Tekhn Fiziki 3:208-211

Zolensky ME (1984) Hydrothermal alteration of CM carbonaceous chondrites: Implications of the identification of tochilinite as one type of meteoritic PCP. Meteoritics 19:346-347